ISBN 978-82-471-4140-3 (printed ver.)
ISBN 978-82-471-4154-0 (electronic ver.)
ISSN 1503-8181

Theses at NTNU, 2007:188

Kari Unneland

Identification and Order Reduction of Radiation Force Models of Marine Structures

NTNU
Norwegian University of
Science and Technology
Thesis for the degree of
philosophiae doctor
Faculty of Information Technology, Mathematics and
Electrical Engineering
Department of Engineering Cybernetics

NTNU
Det skapende universitet

Theses at NTNU, 2007:188

NTNU

NTNU
Det skapende universitet

Kari Unneland

Identification and Order Reduction of Radiation Force Models of Marine Structures

Thesis for the degree of philosophiae doctor

Trondheim, December 2007

Norwegian University of
Science and Technology
Faculty of Information Technology, Mathematics and Electrical Engineering
Department of Engineering Cybernetics

NTNU

Norwegian University of
Science and Technology

NTNU
Norwegian University of Science and Technology

Thesis for the degree of philosophiae doctor

Faculty of Information Technology, Mathematics and Electrical Engineering
Department of Engineering Cybernetics

ISBN 978-82-471-4140-3 (printed ver.)
ISBN 978-82-471-4154-0 (electronic ver.)
ISSN 1503-8181

ITK-report 2007-8-W

Theses at NTNU, 2007:188

Printed by Tapir Uttrykk

Abstract

This thesis addresses parametric time-domain modeling of radiation forces in marine applications based on hydrodynamic computations, intended for use in control and observer design for vessels. Marine applications where it is of interest to accurately model the radiation forces include dynamically positioned offshore vessels, moored floating structures and wave power plants. The radiation forces of marine structures describe interactions between the floating body and the surrounding fluid. These radiation forces appear as a consequence of the change in the momentum of the fluid and the waves generated due to the motion of the body in the fluid. In the frequency domain the forces are proportional to the accelerations and velocities of the body. The term proportional to the acceleration is referred to as the added mass, and the term proportional to the velocities is referred to as the damping. Both the added mass and damping parameters are dependent on the frequency of motion.

Several methods exist for obtaining the frequency dependent added mass and damping parameters. One can either do full-scale experiments, model testing, use scaled data sets from existing tests or use numerical hydrodynamic software. As both full-scale and model-scale experiments are expensive and time consuming, using numerical simulations in the design phase gives flexibility. Also, as hydrodynamic software is becoming more accurate and reliable, it represents an economically sound alternative to experiments. Inspired by this, the frequency dependent added mass and damping parameters will be obtained from hydrodynamic software.

The radiation forces are hydrodynamical forces, and the theory has been developed by hydrodynamicists. As control systems become more common in marine applications there is a need for analyzing the radiation forces from a control theoretical perspective. The properties of the frequency dependent added mass and damping parameters are used to show stability and passivity of the radiation forces. In addition the frequency dependent added mass and damping parameters are used to investigate the structure of the parametric radiation forces model.

The impulse response of the radiation forces can be obtained either from the frequency dependent added mass parameters or from the frequency dependent damping parameters, whereas the frequency response of the radiation forces are obtained as a combination of both types of parameters. Given the impulse and frequency responses of the radiation forces both time domain and frequency domain identification can be used to obtain parametric models. Both approaches are applied and compared. Existing algorithms in the time domain and in the frequency domain are proposed for this use. The methods can ensure stable systems, but passivity might not be preserved, and it is of interest to investigate how often this occurs. It is important that the identified models are passive in order to avoid nonphysical behavior when used in simulations.

The identification schemes allow to either identify a low order model or identify a high order model followed by model reduction. For a horizontal 3 degree of freedom (DOF) vessel model there are 9 modes which can be identified representing a 3×3 multi-input multi-output (MIMO) system. Three different approaches for identification are proposed; identification of each mode as a single-input single-output (SISO) system; MIMO identification of the overall system; identification of each mode as a SISO system with reduction of the overall system as a MIMO system.

For model reduction, the focus in this thesis is on balanced truncation methods which are well suited for systems of moderate size. A review of existing methods is given, where the focus is on passivity preserving algorithms. A new scheme for positive real balanced truncation is proposed. The scheme is numerical efficient and shows good accuracy. Further, it is shown that this result can be extended and an algorithm for positive real frequency weighted truncation is suggested.

Two case studies are presented. First the modeling of a 3-DOF vessel model where the frequency dependent added mass and damping parameters are obtained by the use of the hydrodynamic software WAMIT. Subsequently a lateral vessel model is obtained where the frequency dependent added mass and damping parameters are obtained by using the hydrodynamic software VERES. The proposed modeling approaches are compared in terms of model order estimates, accuracy of fit, the use of available information, ease of use and generation of positive real systems. It is shown that combining identification and model reduction offers flexibility in the choice of model complexity and accuracy.

Acknowledgments

This thesis presents the main results of my research as a doctoral student at the Department of Engineering Cybernetics, NTNU, from January 2004 through March 2007, under the supervision of Professor Olav Egeland and Dr. Tristan Perez, and partly as a Marie Curie Fellow, from October 2005 through June 2006, at the Department of Mathematical Engineering at the Catholic University of Louvain (UCL) under the guidance of Professor Paul Van Dooren. My funding has also been supported by the Research Council of Norway through the Centre for Ships and Ocean Structures a Centre of Excellence at NTNU directed by Professor Torgeir Moan.

Thanks to my supervisor Professor Olav Egeland for giving me the opportunity to do the research reported in this thesis, and for providing me with good and stimulating working conditions for doing research. I should also like to thank Dr. Tristan Perez for his invaluable advice and interesting discussions which should not be underestimated. Further, I am very grateful to Professor Paul Van Dooren for accepting my ten-month academic visit to UCL and introducing me to valuable topics in model reduction.

My thesis depends upon research previously done by Erlend Kristiansen. I am thankful for the introduction he gave me to his work as I was getting started. Thanks to Professor Thor I. Fossen and to Giovanna Fanizza for cooperation on publications and good advice on my research. Special thanks to Professor Anders Lindquist for inviting me to the Royal Institute of Technology (KTH) and introducing me to Giovanna Fanizza. I am also very grateful to Professor Johannes Falnes for valuable advices on my thesis. I would also like to thank the staff Tove K.B. Johnsen and Sigrid B. Wold for fixing administrative matters. I acknowledge the assistance from Stewart Clark, English language advisor at NTNU in editing this thesis.

A special thanks to my former office mate Andrew Ross for all the helpful discussions, coffee breaks and mess in the office. I would like to thank my former colleagues from Centre for Ships and Ocean Structures, Department of Marine Technology, Department of Engineering Cybernetics and Department of Mathematical Engineering (UCL) for making a good working and social

environment. Special thanks also go to Per Ivar Barth Berntsen, Turker Biyikoglu, Morten Breivik, Clementina Dellomonaco, Damien Franois, Svein Hovland, Ivar Ihle, David Kristiansen, Trygve Kristiansen, Ljubisa Miskovic, Sergey Nazin, Hynek Prochazka, Jon Refsnes, Anne Marthine Rustad, Eivind Ruth, Reza Taghipour and Anders Wroldsen.

I would also like to thank my colleagues at StatoilHydro for being understanding and supportive while I finished this thesis. Thanks to Borghild, Ellen, Guro, Hilde, Ingrid, Jorunn, Linda, Martha, Marvel, Sigrun, Siv and Synnøve for friendship and fun during this period. Thanks to Mum, Dad and Tord for support in all matters. Finally, dear Trygve, THANKS!

Trondheim, Norway
November 2007 KARI UNNELAND

Contents

Chapter 1

Introduction

1.1 Motivation

This thesis discusses low order parametric modeling of radiation forces. The radiation forces describe the radiative interaction of a floating body with the surrounding fluid in the absence of incident waves. In the frequency domain the forces are proportional to the velocities and accelerations of the floating body, and are accordingly split in added mass and damping forces. This thesis will address the modeling of floating bodies at zero speed with arbitrary motion, not necessarily sinusoidal. Under these conditions the added mass and damping forces are dependent on the frequencies of excitation.

Several methods exist for obtaining the frequency dependent added mass and damping parameters for floating bodies. One can either do full-scale experiments, model testing, use scaled data sets from existing tests or use numerical hydrodynamical software (Lewandowski, 2004; Faltinsen, 1990). Both full-scale or model-scale experiments are expensive and time consuming as advanced testing facilities are required. Obtaining the model data by use of hydrodynamic software offers flexibility in the design phase as one can avoid costly trial and error testing with either full-scale or scaled models. This is illustrated in Figure 1.1. As the hydrodynamical software is becoming more accurate and reliable it represents an economically sound alternative to experiments. Inspired by this, the frequency dependent added mass and damping parameters in this thesis will be obtained from hydrodynamical software. Examples of hydrodynamical software which is possible to use for

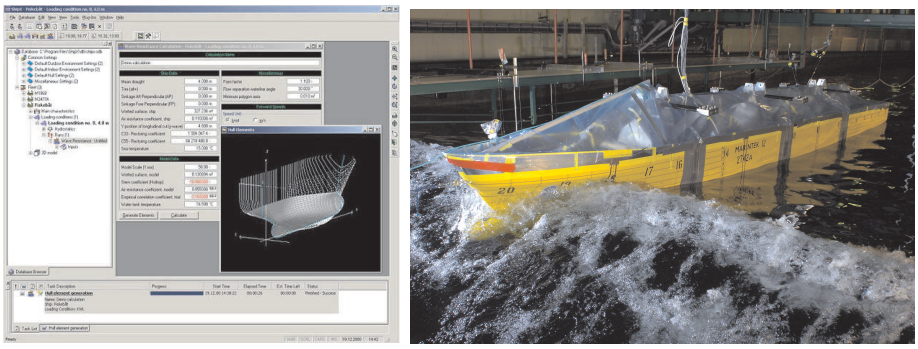

Figure 1.1: Obtaining the vessel model data by use of hydrodynamic software (courtesy of Marintek, www.marintek.no) or by use of towing tank experiments (courtesy of CeSOS, www.cesos.ntnu.no).

this purpose are WAMIT[1] , Veres[2] and Seaway[3].

The easiest way of obtaining the models of the radiation forces is to neglect the frequency dependence and approximate the added mass and damping parameters by constant matrices, discarding parts of the dynamics. The impulse response of the radiation forces can be obtained either from the frequency dependent added mass parameters or from the frequency dependent damping parameters. The frequency response can be obtained as a combination of the frequency dependent added mass and damping parameters. Hence, time domain or frequency domain identification methods can be used to obtain state-space models in the time domain or rational transfer functions in the frequency domain to represent the radiation forces. Since the models are intended for use in control system design and marine systems simulators these formulations are attractive.

In this thesis different approaches for modeling the radiation forces will be investigated in order to obtain accurate and efficient models in an economically sound way for use in simulators and control design. Several applications exist where this is of interest and some examples are given below.

Dynamic Positioning (DP)

Dynamic positioning is a term used for control systems where the aim is to automatically maintain a vessel's position and heading by the use of actu-

[1] www.wamit.com
[2] www.marintek.no
[3] www.shipmotions.nl

ators such as propellers or thrusters. This type of system is usually used in low-speed applications for station keeping. DP systems were introduced in the 1960s, and today DP systems are common in the offshore industry. A useful historical overview of the development of this type of system and different applications is given in Fossen (2002). Examples of vessels where DP systems can be used, are floating offshore platforms, drilling vessels and FPSO (Floating Production Storage and Offloading) vessels.

Real-time simulators for marine systems

Numerical simulators have become important when dealing with marine systems and operations. Complex scenarios are faced including models of the environment, the vessel and mooring lines (Smogeli *et al.*, 2005). Real-time simulators can be used for the training of personnel for ship operations and handling in realistic but controlled environments. They can also be used for failure detection and validation of new control system designs. Marine simulators are beneficial for both the design engineers and the operators. Figure 1.2 presents an illustration of a marine simulator.

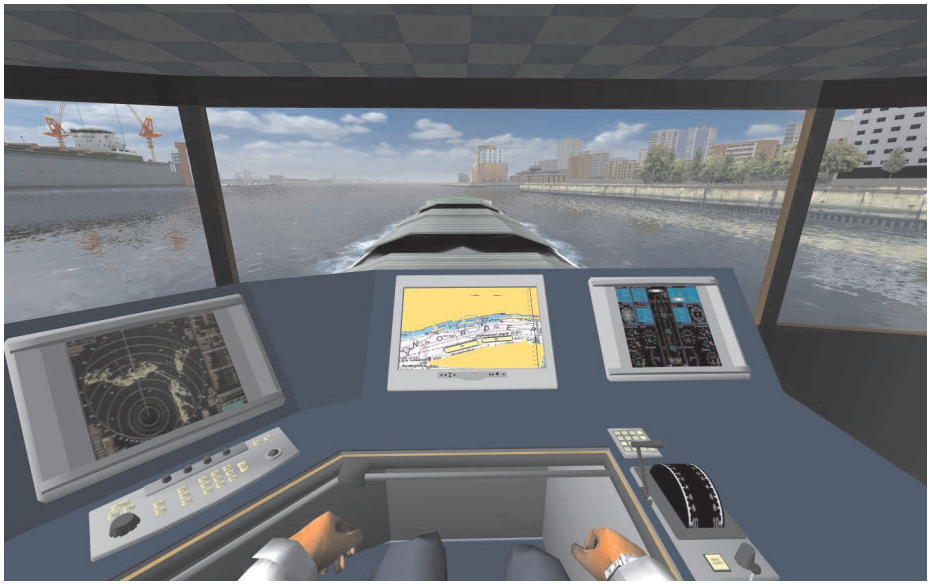

Figure 1.2: Example of vessel simulator. Courtesy of Lighthouse Interactive, www.lighthouse-interactive.com.

Offshore wave power plants

Energy demand is growing worldwide, and it is necessary to seek environmentally sound sources to obtain energy. Wave power is a renewable energy source with an estimated harvesting potential of 2000 TWh/yr (Thorpe, 1999).

As a response to the emerging oil crises in the 1970s research on wave energy began. Several commercial and governmental research projects were initiated and the technology was considerably advanced. Despite this, it resulted in few commercial plants which were economically sound enough to deliver supplies of electricity from wave energy (Trinnaman and Clarke, 2004).

By technology transfer from the offshore oil and gas industry during the mid-1990s and up to today the technology has matured. Today several commercial plants exist and promising projects are in the start phase (Trinnaman and Clarke, 2004). An example of a wave power plant developed based on technology from the offshore industry is the wave energy converter Pelamis by Ocean Power Delivery Ltd, which is pictured in Figure 1.3. The device is slack-moored and allows the segments to weave with respect to each other when incoming waves are present. This actuates hydraulic cylinders which are built into the joints, and pumps oil to drive a hydraulic generator.

Figure 1.3: Example of wave energy plant; the Pelamis wave energy converter developed by Ocean Power Delivery. Courtesy of Ocean Power Delivery, www.oceanpd.com.

1.2 Background Material

The radiation forces and moments appear as a consequence of the change in the momentum of the fluid and the waves generated due to the motion of the body in the fluid (Faltinsen, 1990). In the frequency domain these forces and moments are linearly related to the accelerations and the velocities of the body. The term proportional to the accelerations is called added mass and the term proportional to the velocities is called damping. Both the added mass and the damping parameters are dependent on the frequency of excitation.

The simplest approach to model this effect is to neglect the frequency dependence, and approximate the added mass and damping with constant matrices. This gives a set of 6×6 coupled 2nd order ordinary differential equations. This type of simplification is valid for steady state harmonic motion.

The first connection to transient time domain models was made by Cummins (1962), who considered the behavior of the fluid and the structure in the time domain. He obtained a description of the radiation forces including a convolution integral from body velocity to force. The second-order linear differential equations with constant coefficients could be replaced by integro-differential equations. Time domain simulations of body motions in waves could now be carried out by recalculating the convolution integral for every time step. Takagi *et al.* (1984) gave a comparison between the equations of motion containing convolution integrals and the simpler second-order linear differential equations with constant coefficients. It was concluded that the former representation gave a richer representation of the radiation forces. Similar discussions are found in (Oortmerssen, 1976). The convolution representation proposed by Cummins has been common in different marine applications e.g. time domain simulations of vessel motions in waves (Bishop *et al.*, 1973; Bishop and Price, 1979; Bailey *et al.*, 1997, 2000; Ballard, 2002; Tahar and Kim, 2003) and wave energy converters (Eidsmoen, 1996).

In the work of Ogilvie (1964) an extension to the understanding of Cummins' work was done. Here the connection between the frequency dependent added mass and damping parameters and the time domain convolution representation was presented. As a result of this, expressions were obtained for the radiation forces' impulse response and frequency response.

As control systems become more common in marine applications, there is a need for models which are in accordance with the common formulations within this field. The common formulations used in control design are state-space models in the time domain. The convolution representation proposed by Cummins can be approximated with a numerically more efficient state-

space model. There are two approaches for the identification of the radiation forces' state-space model, either by the use of time domain identification of the impulse response or by the use of frequency domain identification of the frequency response.

The first attempt in this direction was done by Tick (1959) in the frequency domain. He modeled the frequency dependent added mass and damping parameters by polynomial filters. Further, Schmiechen (1973) proposed to use rational function filters in the frequency domain for the approximation of the radiation forces. He was the first to model the radiation forces as state-space models in the time domain. These models were used for the problem of collision of ships, where the frequency excitations are broad-banded. While Schmiechen was concerned with the identification of marine vessels, Jeffreys modeled wave-energy converters by using state-space methods (Jeffreys, 1980, 1984). A least squares fit in the frequency domain was used to approximate the transfer function representing the radiation forces. It was concluded that the transfer function representation introduced fewer errors than the numerical calculation of the convolution kernel and subsequent integration of the resulting model. Several others followed in this direction and did work on the identification of radiation forces in different marine applications; ship maneuvering in waves (McCreight, 1986), moored vessel (Jiang *et al.*, 1987; Jiang and Schelin, 1990; Jordán and Beltrán-Aguedo, 2004; Jordán, 2006), crane ships (Schelin *et al.*, 1993), investigation of stability, bifurcation and chaos of two-point mooring systems (Chung and Bernitsas, 1997), ship rolling (Holappa and Falzarano, 1999), wave energy (Damaren, 2000, 2001).

McCabe *et al.* (2005) proposed to use invfreqs, implemented in MATLAB in order to find a transfer function approximation from the frequency response of the radiation forces. This is a least-squares based method to identify the best model from the given data. Others have followed this approach (Lande, 2006).

Kaasen and Mo (2004) fitted the real part of the transfer function to the frequency dependent damping parameters. An iterative least squares fitting was used to fit the damping transfer function. The overall transfer function was found by a relation between the residues and the poles of the damping transfer function and the radiation force transfer function.

Instead of approximation from the frequency response, time domain approximation can be done based on the information from the impulse response of the radiation forces. Yu and Maeda (1991) approximated the impulse response of the radiation forces by a combination of trigonometric and exponential functions in the time domain. The radiation forces were to be included in a model for a wave power system. Further in Yu (1992) and Yu *et al.* (1993, 1994) a matrix exponential function was used to approximate

the impulse response of the radiation forces. Yu and Falnes (1995) used impulse response curve fitting in order to find the parameters in a state-space model of the radiation force for a vertical cylinder in heave. This was done by minimizing the error between the original impulse response and the state-space matrices at chosen time instants. The state-space matrices were chosen to be in observer companion form in order to reduce the parameters to be decided. It was mentioned here that this type of representation could be of use not only for wave energy converters, but also for vessels and other dynamic systems in ocean engineering.

Another approach for the identification of state-space representations from the impulse response was proposed by Duclos *et al.* (2001). In Duclos *et al.* (2001); Babarit *et al.* (2004); Babarit and Clément (2006), Prony's method, due to de Prony (1795), was used to model the radiation forces in a model for latching control of a wave energy device. The impulse response of the radiation forces were approximated by a sum of exponential functions found by Prony's method. By differentiating this representation, and including it in the overall model, the equations of motion could be represented in state-space form.

Kristiansen and Egeland (2003) extended the approximation of the impulse response of the radiation forces by state-space models to marine vessels. A minimal state-space realization was obtained from the radiation forces impulse response by use of Markov parameters. This routine (imp2ss) is a built-in function in MATLAB and relies on singular value decomposition (SVD) of the Markov parameters from the impulse response. This realization procedure was proposed by Kung (1978). Further, this method has been used and suggested used in different marine models, among others, DP vessels, marine systems simulators, wave energy plants and hydroelastic marine structures (Hjulstad *et al.*, 2004; Hjulstad, 2004; Skaare, 2004; Fossen and Smogeli, 2004; Kristiansen *et al.*, 2005; Smogeli *et al.*, 2005; Fossen, 2005; Bjarte-Larsson *et al.*, 2006; Taghipour *et al.*, 2007).

The stability properties of the radiation forces have also been investigated. Jeffreys (1984) showed that the radiation forces are bounded-input bounded-output (BIBO) stable. He also showed that the relative degree of the transfer functions representing the radiation forces should be one. Further, Damaren (2000) showed that the radiation forces are passive and suggests the model structure based on this. This point is also made by Kristiansen *et al.* (2005). Jordán and Beltrán-Aguedo (2004) investigated properties of the frequency response based on the added mass and damping matrices and made suggestions on the model structure based on this.

1.3 Contributions of this Thesis

The following are considered to be the main contributions of the thesis:

- Presentation and discussion of already existing approaches for modeling of radiation forces from different marine fields, i.e. wave energy community and the offshore vessel community. In the beginning these communities worked more separately, however in recent years more interaction has been common.

- Investigation of the radiation forces from a control theoretical approach, where stability and passivity properties have been analyzed. These stability and passivity results are given by the properties of the frequency dependent added mass and damping parameters. Based on information from the same data sets, appropriate model structures have been suggested for state-space representation in the time domain and transfer function representation in the frequency domain of the radiation forces.

- One of the approaches for modeling the radiation forces includes model reduction. For model reduction, balanced truncation methods have been used, which are well suited for systems of moderate size. A review of existing balanced truncation methods is given, where the focus is on passivity preserving methods. A new scheme for positive real truncation is proposed, together with conditions which have to be fulfilled in order to get positive real truncated systems. These are used in order to obtain an algorithm for positive real frequency weighted truncation.

- Numerical studies of different ways of obtaining the radiation forces. Here three approaches are investigated: SISO identification of each mode; MIMO identification of the overall system; SISO identification of each mode followed by MIMO order reduction of the overall model. The identification can be done either in the time domain or in the frequency domain. Existing identification algorithms are used in order to compare the two approaches for the different modeling approaches. The proposed modeling approaches are compared in terms of estimated model order, accuracy of fit, use of available information, ease of use and generation of positive real systems.

1.4 Publications

The following is a complete list of the publications written during the work contained in this thesis. This includes accepted papers.

Journal Paper

- K. Unneland, P. Van Dooren and O. Egeland, New Schemes for Positive Real Truncation, in *Modeling, Identification and Control (MIC)*, 2007, Vol. 28, No. 3, pp. 53-66.

Conference Papers

- K. Unneland, T. Perez and O. Egeland, MIMO and SISO Identification of Radiation Force Terms for Models of Marine Structures in Waves, in *Proceedings of the IFAC Conference on Control Applications in Marine Systems 2007*, Bol, Croatia, September 2007.

- G. Fanizza and K. Unneland, Low order radiation forces by analytic interpolation with degree constraints, in *Proceedings of the 46th IEEE Conference on Decision and Control*, New Orleans, USA, December 2007. *Accepted*

- K. Unneland, P. Van Dooren and O. Egeland, A Novel Scheme for Positive Real Balanced Truncation, in *Proceedings of the 26th American Control Conference*, New York City, USA, July 2007.

- K. Unneland, T.I. Fossen, O. Egeland and P. Van Dooren, Low order potential damping models for surface vessels, in *Proceedings of the 7th IFAC Conference on Manoeuvering and Control of Marine Craft*, Lisbon, Portugal, September 2006.

- K. Unneland and O. Egeland, Positive real modeling of ships for dynamic positioning, in *Proceedings of the 17th International Symposium on Mathematical Theory of Networks and Systems*, Kyoto, Japan, July 2006.

- K. Unneland, E. Kristiansen and O. Egeland, Comparative study of algorithms obtaining reduced order state-space form of radiation forces, in *Proceedings of the OCEANS'05*, Washington D.C., USA, September 2005.

Posters

- G. Fanizza and K. Unneland, Low order radiation forces by analytic interpolation with degree contstraints, at the *European Research Network System Identification Workshop 2007*, Venice, Italy, October 2007.

- K. Unneland, O. Egeland and P. Van Dooren, Model Reduction in Marine Applications, at the *Interuniversity Attraction Pole V/22 Day on Dynamical Systems and Control: Computation, Identification and Modeling*, Court St. Etienne, Belgium, May 2006.

- K. Unneland, O. Egeland and P. Van Dooren, Positive Realness and Balanced Truncation, at the *2006 Conference of the Dutch-Flemish Numerical Analysis Communities*, Zeist, The Netherlands, October 2006.

1.5 Organization of Thesis

This thesis is organized as follows:

Chapter 2: Modeling of Marine Structures in Waves. The equations of motion with force and moment superpositioning are revisited together with a definition of reference frames. The radiation forces and moments are a part of these equations, and they consist of the added mass and damping forces. Different approaches for modeling of the radiation forces are investigated, giving representations both in the time and in the frequency domains. Further, these representations are related, giving expressions for the impulse response and frequency response of the radiation forces based on the added mass and damping parameters obtained from numerical software. Finally, a relation between the frequency dependent added mass and damping coefficients is reviewed.

Chapter 3: Properties of Radiation Force Models. The stability properties of the radiation forces are investigated. Based on the properties of the added mass and damping matrices, stability and passivity of the radiation forces can be shown. Since expressions for the impulse response and frequency response of the radiation forces exist, state-space models in the time domain, and transfer functions in the frequency domain, can be used to represent these forces. The structures of the state-space and transfer function models of the radiation forces are investigated based on the available information.

Chapter 4: Identification Methods. Both the impulse response and the frequency response of the radiation forces are given, hence both time domain and frequency domain methods can be used to identify the state-space or transfer function representations of the forces. In this chapter a short overview over existing techniques in the time and frequency domains will be given, intended for use in later chapters.

Chapter 5: Model Reduction. The identified models might be of high order and hence it is of interest to use model reduction techniques to obtain low order efficient models. A review of existing balanced truncation methods will be given. A new algorithm which will keep the positive real properties in the reduction process will be given. Further, it is investigated which properties the reduction algorithms need to satisfy in order to give reduced order positive real systems. Finally, this result is used to develop positive real frequency weighted truncation, to illustrate the use of this generalization.

Chapter 6: Case Studies. The radiation forces for two different vessel models will be identified using different approaches both in the time and in the frequency domains: SISO identification of every mode; MIMO identification of all modes; SISO identification of every mode with model reduction of the overall MIMO system. A discussion on the different approaches follows.

Chapter 7: Final Remarks. This chapter presents the overall conclusions to this thesis and presents some suggestions for further research.

Chapter 2

Modeling of Marine Structures in Waves

2.1 Introduction

Floating bodies (i.e. vessels, offshore platforms, wave energy converters) operate under different speed regimes and environmental conditions. This feature is reflected in the hydrodynamical modeling. Traditionally, vessel dynamics have been separated in maneuvering and seakeeping (Fossen, 2005). In maneuvering it is common to assume absence of wave excitation, e.g. vessel motion in sheltered waters or in a harbor. The model is developed under a low-frequency assumption, such that the radiation forces can be represented by hydrodynamic derivatives. Seakeeping deals with all types of wave excitation of vessels with constant speed and heading, including zero speed which will be investigated in this thesis. In these models the radiation forces are dependent on the frequency of the excitation, and it is not sufficient to represent them by hydrodynamic derivatives.

In this chapter different approaches to the modeling of radiation forces will be investigated. First, in Section 2.2 the different reference frames in use will be presented together with the equations of motion intended for use. The equations of motion include the radiation forces and moments, and in Section 2.3 a frequency dependent representation valid for harmonic motion will be reviewed. The radiation forces consist of added mass forces and damping forces. Further, in Section 2.4 a time domain representation valid for all types of low-amplitude motion will be presented. In Section 2.5 the frequency domain representation will be related to the time domain representation. Finally, in Section 2.6 a relationship will be reviewed between the added mass and the damping coefficients in the radiation forces model.

2.2 Reference Frames and Equations of Motion

The equations of motion for a seagoing vessel are in general based on the Newton-Euler equations of motion for rigid bodies and kinematic transformations (Fossen, 2002). Numerical software can be used to obtain the added mass and damping matrices and other parameters used as a basis for the equations of motion for a vessel. The coordinate frames used in numerical hydrodynamics do not correspond to the coordinate frames used in the equations of motion for control, observers and simulators for vessels (Fossen and Smogeli, 2004).

Three orthogonal reference frames are used to describe the motions of the vessel in 6-DOF,

- Body-fixed frame (b-frame)
- North-East-Down frame (n-frame)
- Hydrodynamic frame (h-frame)

The equations of motion used for control and simulation of vessels can be expressed as a combination of n-frame and b-frame coordinates (Fossen, 2002).

- Body-fixed frame (b-frame; $o_b, \vec{x}_b, \vec{y}_b, \vec{z}_b$)
  The frame is assumed fixed to the vessel hull. The origin o_b is determined by letting the axes of this frame coincide with the principal axes of inertia, with $\vec{x}_b,\ \vec{y}_b,\ \vec{z}_b$ pointing respectively towards the bow, starboard and down.
- North-East-Down frame (n-frame; $o_n, \vec{x}_n, \vec{y}_n, \vec{z}_n$) The frame is fixed relative to the Earth's surface. The origin o_n is located on the mean water free-surface, with $\vec{x}_n,\ \vec{y}_n,\ \vec{z}_n$ pointing respectively towards North, East and down from the Earth tangent plane.

The generalized position vector is defined in the n-frame as a combination of the North-, East-, Down-positions, $[n, e, d]^T$, and the Euler angles in roll, pitch and yaw, $[\phi, \theta, \psi]^T$:

$$\boldsymbol{\eta} = [n, e, d, \phi, \theta, \psi]^T \tag{2.1}$$

The generalized velocity is defined in the b-frame. It is a combination of the linear velocities surge, sway and heave in o_b, and the angular velocities roll, pitch and yaw of the moving vessel in the b-frame with respect to the n-frame:

$$\boldsymbol{\nu} = [u, v, w, p, q, r]^T \tag{2.2}$$

The position vector $\boldsymbol{\eta}$ is related to the velocity vector $\boldsymbol{\nu}$ through the velocity transformation $\boldsymbol{J}(\boldsymbol{\Theta})$ defined in (Fossen, 2002):

$$\dot{\boldsymbol{\eta}} = \boldsymbol{J}(\boldsymbol{\Theta})\boldsymbol{\nu} \tag{2.3}$$

The equations of motion in numerical hydrodynamics are usually expressed in the h-frame. In this formulation of the equations of motion, the generalized position vector $\boldsymbol{\xi}$ is defined in the h-frame. In this thesis the h-frame will be defined as in the hydrodynamic software intended for use, i.e. WAMIT (www.wamit.com, 2006) and VERES (Fathi, 2004):

- *Hydrodynamic frame (h-frame; $o_h, \vec{x}_h, \vec{y}_h, \vec{z}_h$)* For a vessel operating at zero forward speed the h-frame is fixed to the Earth. The positive axes $\vec{x}_h$, $\vec{y}_h$ and $\vec{z}_h$ are pointing forward, port and upwards, whereas the horizontal plane spanned by $\vec{x}_h$ and $\vec{y}_h$ correspond to the still water plane and the plane spanned by $\vec{x}_h$ and $\vec{z}_h$ correspond to the center-plane of the vessel. The origin o_h is placed such that the $\vec{z}_h$ axis is placed on the same axis as the center of gravity (CG).

Here $\boldsymbol{\xi}$ represents the position and angles of the body

$$\boldsymbol{\xi} = [\xi_1, \xi_2, \xi_3, \xi_4, \xi_5, \xi_6]^T \tag{2.4}$$

where ξ_i represents the displacements in ξ_1-surge, ξ_2-sway, ξ_3-heave, ξ_4-roll, ξ_5-pitch and ξ_6-yaw. Note that other definitions of the h-frame exists (Perez, 2005; Perez and Fossen, 2007).

The models investigated and applied in this thesis will be developed in the h-frame. The vessel models will be valid for vessels operating at zero forward speed. In order to use these models in control design and synthesis they can be transformed into the $n-$ and $b-$frame formulations. A good overview over the necessary transformations is given in Perez and Fossen (2007), in addition to general linearity assumptions that the equations in this thesis are based on.

The equations of motion for a seagoing vessel are based on the Newton-Euler equations of motion for rigid bodies. Here, these are formulated in the h-frame

$$\boldsymbol{M}_{RB}\ddot{\boldsymbol{\xi}}(t) = \boldsymbol{\tau}_R + \boldsymbol{\tau}_H + \boldsymbol{\tau}_{visc} + \boldsymbol{\tau}_{ext} + \boldsymbol{\tau}_A \tag{2.5}$$

Here $\boldsymbol{M}_{RB} \in \mathbb{R}^{6\times 6}$ is the rigid-body system inertia matrix, $\boldsymbol{\tau}_R \in \mathbb{R}^6$ represents the radiation forces and moments, $\boldsymbol{\tau}_H \in \mathbb{R}^6$ represents the hydrostatic forces and moments, $\boldsymbol{\tau}_A \in \mathbb{R}^6$ represents the actuator forces and moments, $\boldsymbol{\tau}_{ext} \in \mathbb{R}^6$ represents the external forces and moments and $\boldsymbol{\tau}_{visc} \in \mathbb{R}^6$ represents the viscous forces and moments. A more precise description of the

forces is given below. In the following the forces and moments will just be referred to as the forces, i.e. the radiation forces and moments will just be written as radiation forces.

Hydrostatic forces

The hydrostatic forces are restoring forces due to gravity and buoyancy. By assuming that the restoring forces are linear, it is a good approximation to express them as proportional to the displacement $\boldsymbol{\xi}(t)$ of the vessel (Perez, 2005).

$$\boldsymbol{\tau}_H(t) = -\boldsymbol{C}_h \boldsymbol{\xi}(t) \tag{2.6}$$

where $\boldsymbol{C}_h \in \mathbb{R}^{6\times 6}$ is the matrix of restoring forces. For vessels with port-starboard and fore-aft symmetry where small angles are assumed, $\boldsymbol{C}_h$ can usually be written as $\boldsymbol{C}_h = \text{diag}\,[0, 0, C_{h33}, C_{h44}, C_{h55}, 0]$.

Viscous forces

The viscous forces are nonlinear damping forces appearing due to nonlinear non-conservative phenomena, and kinetic energy of the hull is transferred to heat due to viscous effects (skin friction, flow separation and eddy making). These forces depend on the relative velocities between the hull and the fluid (Perez, 2005).

Actuator forces

For vessels, the actuator forces $\boldsymbol{\tau}_A$ can be due to propellers or thrusters. In other applications, such as wave energy plants, the actuator forces can be generated by other devices.

External forces

The external forces $\boldsymbol{\tau}_{ext}$ can be composed of

- Time varying forces due to waves
- Time varying forces due to wind
- Restoring forces from mooring systems.

Radiation forces

These forces appear as a consequence of the change in the momentum of the fluid and the waves generated due to the motion of the hull. These forces are linearly related to the accelerations and velocities of the vessel. The focus in this thesis will be on the modeling of the radiation forces, and in the following sections the focus will be on different approaches for modeling the radiation forces.

2.3 Frequency Dependent Radiation Forces

The vessel body is considered to be a rigid body, and the irrotational flow of an inviscid and incompressible fluid is assumed. Potential theory can be used to describe the interactions between the fluid and the floating vessel (Newman, 1977). The fluid flow around the vessel is completely defined by a velocity potential. From this potential the velocity and the pressure in the fluid can be obtained and the forces acting on the body can be calculated. The radiation forces are due to forced harmonic motions in the absence of incident waves.

Due to assumption of linearity, it is common to solve the equations for the radiation forces based on potential theory in the frequency domain. Assume that the motion occurs at one single frequency. Then the position, velocity and accelerations of the vessel can be described by

$$\boldsymbol{\xi}(t) = \mathrm{Re}\{\hat{\boldsymbol{\xi}} e^{j\omega t}\} \tag{2.7}$$

$$\dot{\boldsymbol{\xi}}(t) = \mathrm{Re}\{j\omega \hat{\boldsymbol{\xi}} e^{j\omega t}\} \tag{2.8}$$

$$\ddot{\boldsymbol{\xi}}(t) = \mathrm{Re}\{-\omega^2 \hat{\boldsymbol{\xi}} e^{j\omega t}\} \tag{2.9}$$

Here $\hat{\boldsymbol{\xi}}$ is the amplitude of the vessel oscillations. For an inviscid and incompressible fluid where the fluid is irrotational, the fluid velocity can be expressed as the gradient of a velocity potential. Due to the forced oscillations of the vessel, this potential can be expressed as (Vugts, 1970)

$$\Phi_R(\boldsymbol{r}, \omega, t) = \mathrm{Re}\{\hat{\boldsymbol{\varphi}}^T(\boldsymbol{r}, \omega) \hat{\boldsymbol{\xi}} e^{j\omega t}\} \tag{2.10}$$

Here $\hat{\boldsymbol{\varphi}}(r, \omega)$ is the complex radiation potential due to the forced harmonic oscillations of the vessel in each of its six degrees of freedom. The complex radiation potential is dependent on the frequency ω, the position vector of a point on the vessel hull surface $\boldsymbol{r}$ and has unit amplitudes. Certain boundary conditions must be fulfilled by the radiation potential Φ_R. These are described in e.g. Ogilvie (1964) and Newman (1977).

From the linearized Bernoulli equation the hydrodynamic pressure on the surface of the vessel follows from

$$p = -\rho \frac{\partial \Phi_R}{\partial t}(\boldsymbol{r}, \omega, t) \tag{2.11}$$

$$= -\rho \, \mathrm{Re}\{j\omega \hat{\boldsymbol{\varphi}}^T(\boldsymbol{r}, \omega) \hat{\boldsymbol{\xi}} e^{j\omega t}\} \tag{2.12}$$

where ρ is the water density. The oscillating hydrodynamic forces are (Kristiansen *et al.*, 2005):

$$\boldsymbol{\tau}_R(t) = \rho \int_S \int \boldsymbol{f} \frac{\Phi_R}{\partial t}(\boldsymbol{r}, \omega, t) \, dS \tag{2.13}$$

$$= \rho \int_S \int \boldsymbol{f} \, \mathrm{Re}\{j\omega \hat{\boldsymbol{\varphi}}^T(\boldsymbol{r}, \omega) \hat{\boldsymbol{\xi}} e^{j\omega t}\} \, dS \tag{2.14}$$

Here, $\boldsymbol{f}$ is defined as,

$$\boldsymbol{f} = \begin{bmatrix} \boldsymbol{n} \\ \boldsymbol{r} \times \boldsymbol{n} \end{bmatrix} \tag{2.15}$$

where $\boldsymbol{n}$ is the unit vector normal to the wet surface, S, pointing out to the fluid, and $\boldsymbol{r}$ is the position vector of a point on the hull surface. Let now $\hat{\boldsymbol{\varphi}}(\boldsymbol{r}, \omega)$ be split into its real and imaginary parts, $\hat{\boldsymbol{\varphi}}(\boldsymbol{r}, \omega) = \boldsymbol{\varphi}_{re}(\boldsymbol{r}, \omega) + j\boldsymbol{\varphi}_{im}(\boldsymbol{r}, \omega)$:

$$\boldsymbol{\tau}_R(t) = \rho \int_S \int \boldsymbol{f} \, \mathrm{Re}\{j\omega \left(\boldsymbol{\varphi}_{re}^T(\boldsymbol{r}, \omega) + j\boldsymbol{\varphi}_{im}^T(\boldsymbol{r}, \omega)\right) \hat{\boldsymbol{\xi}} e^{j\omega t}\} \, dS \tag{2.16}$$

$$= \frac{\rho}{\omega} \int_S \int \boldsymbol{f} \boldsymbol{\varphi}_{im}^T(\boldsymbol{r}, \omega) \, dS \, \mathrm{Re}\{-\omega^2 \hat{\boldsymbol{\xi}} e^{j\omega t}\} + \rho \int_S \int \boldsymbol{f} \boldsymbol{\varphi}_{re}^T(\boldsymbol{r}, \omega) \, dS \, \mathrm{Re}\{j\omega \hat{\boldsymbol{\xi}} e^{j\omega t}\} \tag{2.17}$$

$$= -\left[-\frac{\rho}{\omega} \int_S \int \boldsymbol{f} \boldsymbol{\varphi}_{im}^T(\boldsymbol{r}, \omega) \, dS\right] \ddot{\boldsymbol{\xi}}(t) - \left[-\rho \int_S \int \boldsymbol{f} \boldsymbol{\varphi}_{re}^T(\boldsymbol{r}, \omega) \, dS\right] \dot{\boldsymbol{\xi}}(t) \tag{2.18}$$

$$= -\boldsymbol{A}(\omega) \ddot{\boldsymbol{\xi}}(t) - \boldsymbol{B}(\omega) \dot{\boldsymbol{\xi}}(t) \tag{2.19}$$

The frequency dependent matrices $\boldsymbol{A}(\omega) \in \mathbb{R}^{6\times6} \times \mathbb{R}^+$ and $\boldsymbol{B}(\omega) \in \mathbb{R}^{6\times6} \times \mathbb{R}^+$ can now be found from

$$\boldsymbol{A}(\omega) = \left[-\frac{\rho}{\omega} \int_S \int \boldsymbol{f} \boldsymbol{\varphi}_{im}^T(\boldsymbol{r}, \omega) \, dS\right] \tag{2.20}$$

$$\boldsymbol{B}(\omega) = \left[-\rho \int_S \int \boldsymbol{f} \boldsymbol{\varphi}_{re}^T(\boldsymbol{r}, \omega) \, dS\right] \tag{2.21}$$

The frequency dependent matrices $\boldsymbol{A}(\omega)$ and $\boldsymbol{B}(\omega)$ will vary depending on the vessel form and frequency of oscillation. If there is no current the matrices are symmetrical, (Faltinsen, 1990):

$$\boldsymbol{A}(\omega) = \boldsymbol{A}(\omega)^T, \quad \boldsymbol{B}(\omega) = \boldsymbol{B}(\omega)^T \tag{2.22}$$

The hydrodynamic coefficients in sway $A_{22}(\omega)$ and $B_{22}(\omega)$ for a S-175 tanker are plotted in Figure 2.1. The matrix $\boldsymbol{A}(\omega)$ contains added mass coefficients and the matrix $\boldsymbol{B}(\omega)$ contains damping coefficients. For a moving vessel, energy is supplied to the fluid through generated waves. This is represented by the damping forces, and in the frequency domain these forces are proportional to the velocities of the vessel. When the vessel is accelerating it gets added mass due to the inertia of the fluid surrounding the hull. In the frequency domain this is represented by the added mass forces, and the forces are proportional to the vessel accelerations. The damping matrix $\boldsymbol{B}(\omega)$ is associated with energy dissipation by the radiated waves, hence (Lewandowski, 2004):

$$\det(\boldsymbol{B}(\omega)) \geq 0, \ \forall \ \omega \tag{2.23}$$

From this one can see that the damping elements on the diagonal have to be positive semidefinite

$$B_{ii}(\omega) \geq 0, \ \forall \ \omega \tag{2.24}$$

The off-diagonal terms $B_{ij}(\omega)$ can be both positive and negative, as long as the whole matrix is positive semidefinite. A similar result does not apply for the added mass matrix $\boldsymbol{A}(\omega)$, except at $\omega = \infty$ where the added mass matrix, $\boldsymbol{M}_A = \boldsymbol{M}_A^T = \boldsymbol{A}(\infty)$, is positive definite (Fossen, 2002):

$$\det(\boldsymbol{A}(\infty)) > 0 \tag{2.25}$$

hence,

$$A_{ii}(\infty) > 0 \tag{2.26}$$

The equations of motion obtained for the radiation forces (2.19) are presented here in the frequency domain only. In classical vessel motion theory, the simplest way to approximate the radiation forces has been to approximate the frequency dependent added mass and damping in (2.19) by constant matrices

$$\boldsymbol{\tau}_R(t) = -\boldsymbol{A}(\omega_k)\ddot{\boldsymbol{\xi}}(t) - \boldsymbol{B}(\omega_k)\dot{\boldsymbol{\xi}}(t) \tag{2.27}$$

where ω_k is a fixed frequency. This approximation represents a description in the frequency domain of an oscillating motion at the frequency of motion ω_k. However, this type of model does not describe the vessel dynamics accurately enough when looking at transient responses (Holappa and Falzarano, 1999).

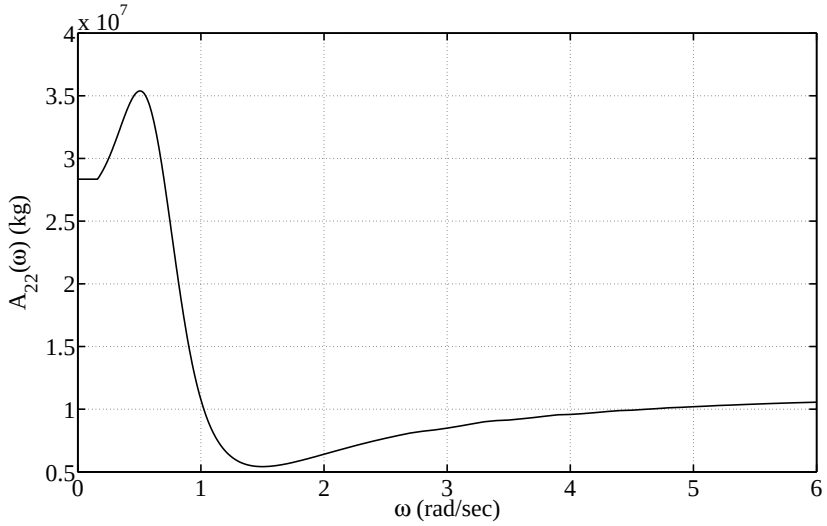

(a) Frequency dependent added mass $A_{22}(\omega)$ in sway.

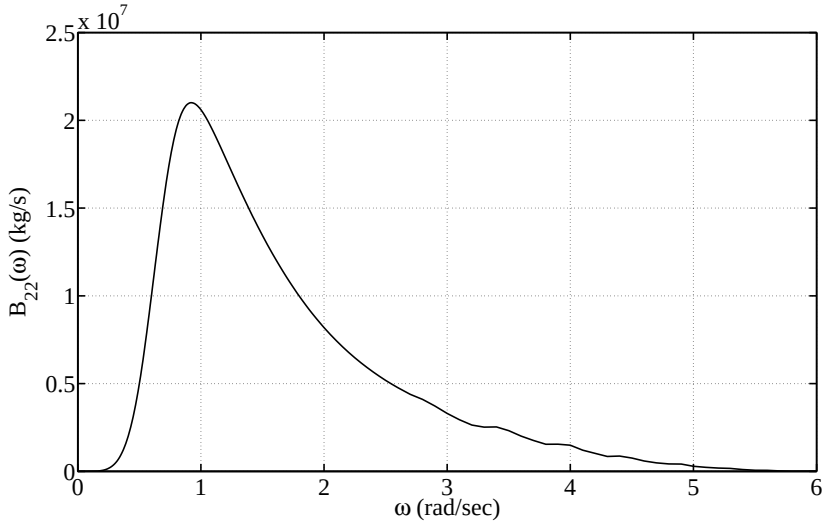

(b) Frequency dependent damping $B_{22}(\omega)$ in sway.

Figure 2.1: Hydrodynamic radiation coefficients in surge for a S-175 tanker.

In the next section it will be shown how to obtain time domain equations which are valid for all types of motion at zero speed, and then this solution is connected to the frequency dependent added mass and damping matrices.

2.4 Radiation Forces in the Time Domain

Let the ship motion in the time domain be given by $\boldsymbol{\xi}(t)$. If the vessel is given an impulsive displacement, the surrounding water will start to move and remain moving after the impulse. This gives the vessel a response lasting much longer than the impulse. The radiated waves from the vessel implies a time dependence of the fluid motion. This memory effect can be captured in the description of a time domain radiation potential, $\boldsymbol{\Phi}_R(\boldsymbol{r}, t)$, by using a formula presented by Cummins (1962). A convolution integral is used to describe how the fluid motion at a given time is dependent on the previous history of motion

$$\Phi_R(\boldsymbol{r}, t) = \boldsymbol{\psi}^T(\boldsymbol{r})\dot{\boldsymbol{\xi}}(t) + \int_0^t \boldsymbol{\chi}^T(\boldsymbol{r}, t-\tau)\dot{\boldsymbol{\xi}}(\tau)d\tau \tag{2.28}$$

A review on how this equation is obtained is given in Oortmerssen (1976). Here $\boldsymbol{r}$ is the position vector of a point on the hull surface. The potential $\boldsymbol{\psi}(\boldsymbol{r}) \in \mathbb{R}^6$ represents the instantaneous response of the fluid due to the vessel motion, whereas $\boldsymbol{\chi}(\boldsymbol{r}, t) \in \mathbb{R}^6 \times \mathbb{R}^+$ describes motion of the fluid after an impulsive movement of the vessel; a fluid memory effect. The total velocity potential (2.28) now adequately describes the fluid motions due to arbitrary vessel motions. This makes the following equations valid for all types of motions, not only harmonic motion. Following the same approach as in the previous section, given the velocity potential, the pressure on the vessel hull can be found from the linearized Bernoulli equation

$$p = -\rho\frac{\partial \Phi_R}{\partial t}(\boldsymbol{r}, t) \tag{2.29}$$

where p represents the hydrodynamical pressure and ρ the water density. Substituting the partial derivative of the radiation potential from (2.28) in (2.29) gives

$$p = -\rho\left(\boldsymbol{\psi}(\boldsymbol{r})^T\ddot{\boldsymbol{\xi}}(t) + \int_0^t \frac{\partial \boldsymbol{\chi}^T(\boldsymbol{r}, t-\tau)}{\partial t}\dot{\boldsymbol{\xi}}(\tau)d\tau\right) \tag{2.30}$$

Here $\boldsymbol{f}$ is defined as in (2.15). Integration of the pressure over the wet hull surface, S, gives the forces acting on the body due to the the radiation forces (Kristiansen *et al.*, 2005)

$$\boldsymbol{\tau}_R(t) = \rho\int_S\int \boldsymbol{f}\frac{\partial \Phi_R(\boldsymbol{r}, t)}{\partial t}\, dS \tag{2.31}$$

The integral (2.31) can be solved for different types of body geometries. Inserting from (2.30) gives

$$\boldsymbol{\tau}_R(t) = \rho \int_S\int \boldsymbol{f}\boldsymbol{\psi}(\boldsymbol{r})^T \ddot{\boldsymbol{\xi}}(t) dS + \rho \int_S\int \boldsymbol{f} \int_0^t \frac{\partial \boldsymbol{\chi}^T(\boldsymbol{r}, t-\tau)}{\partial t} \dot{\boldsymbol{\xi}}(\tau) d\tau dS \quad (2.32)$$

$$= -\left[-\rho \int_S\int \boldsymbol{f}\boldsymbol{\psi}(\boldsymbol{r})^T dS\right] \ddot{\boldsymbol{\xi}}(t) - \int_0^t \left[-\rho \int_S\int \boldsymbol{f} \frac{\partial \boldsymbol{\chi}^T(\boldsymbol{r}, t-\tau)}{\partial t} dS\right] \dot{\boldsymbol{\xi}}(t)\ d\tau \quad (2.33)$$

$$= -\boldsymbol{M}_A \ddot{\boldsymbol{\xi}}(t) - \int_0^t \boldsymbol{k}(t-\tau)\dot{\boldsymbol{\xi}}(\tau)\ d\tau \quad (2.34)$$

This result is due to Cummins (1962), and $\boldsymbol{M}_A$ and $\boldsymbol{k}(t-\tau)$ can now be found from

$$\boldsymbol{M}_A = \left[-\rho \int_S\int \boldsymbol{f}\boldsymbol{\psi}^T(\boldsymbol{r})\ dS\right] \quad (2.35)$$

$$\boldsymbol{k}(t-\tau) = \left[-\rho \int_S\int \boldsymbol{f} \frac{\partial \boldsymbol{\chi}^T(\boldsymbol{r}, t-\tau)}{\partial t}\ dS\right] \quad (2.36)$$

where $\boldsymbol{M}_A = \boldsymbol{M}_A^T \in \mathbb{R}^{6\times 6}$ and the impulse response function $\boldsymbol{k}(t) = \boldsymbol{k}^T(t) \in \mathbb{R}^{6\times 6} \times \mathbb{R}^+$ is real and causal.

2.5 Relating Frequency and Time Domain Solutions

Ogilvie (1964) showed how the time domain solution is related to the frequency dependent added mass and damping matrices in (2.20) and (2.21). The time domain equations (2.34) describe all types of motion, including harmonic motions. Let the vessel perform simple harmonic motion with frequency ω, $\boldsymbol{\xi}(t) = \mathrm{Re}\{\hat{\boldsymbol{\xi}} e^{j\omega t}\}$, then (2.34) can be written as

$$\boldsymbol{\tau}_R(t) = -\boldsymbol{M}_A \ddot{\boldsymbol{\xi}}(t) - \int_0^t \boldsymbol{k}(t-\tau)\dot{\boldsymbol{\xi}}(\tau)\ d\tau \quad (2.37)$$

$$= -\boldsymbol{M}_A \ddot{\boldsymbol{\xi}}(t) - \int_0^t \boldsymbol{k}(\tau)\dot{\boldsymbol{\xi}}(t-\tau)\ d\tau \quad (2.38)$$

$$= -\boldsymbol{M}_A\ \mathrm{Re}\{-\omega^2 \hat{\boldsymbol{\xi}} e^{j\omega t}\} - \int_0^t \boldsymbol{k}(\tau)\ \mathrm{Re}\{j\omega \hat{\boldsymbol{\xi}} e^{j\omega t} e^{-j\omega\tau}\}\ d\tau \quad (2.39)$$

$$= -\boldsymbol{M}_A \ \mathrm{Re}\{-\omega^2\hat{\boldsymbol{\xi}}(\cos\omega t + j\sin\omega t)\}$$
$$-\int_0^t \boldsymbol{k}(\tau)\mathrm{Re}\{j\omega\hat{\boldsymbol{\xi}}(\cos\omega t + j\sin\omega t)(\cos\omega\tau - j\sin\omega\tau)\}\ d\tau \quad (2.40)$$
$$= \omega^2\cos\omega t\boldsymbol{M}_A\hat{\boldsymbol{\xi}} - \omega\cos\omega t\int_0^t \boldsymbol{k}(\tau)\hat{\boldsymbol{\xi}}\sin\omega\tau\ d\tau$$
$$+ \omega\sin\omega t\int_0^t \boldsymbol{k}(\tau)\hat{\boldsymbol{\xi}}\cos\omega\tau\ d\tau \quad (2.41)$$

This expression can be related to (2.19)

$$\boldsymbol{\tau}_R(t) = -\boldsymbol{A}(\omega)\ddot{\boldsymbol{\xi}}(t) - \boldsymbol{B}(\omega)\dot{\boldsymbol{\xi}}(t) \quad (2.42)$$
$$= -\boldsymbol{A}(\omega)\ \mathrm{Re}\{-\omega^2\hat{\boldsymbol{\xi}}e^{j\omega t}\} - \boldsymbol{B}(\omega)\ \mathrm{Re}\{j\omega\hat{\boldsymbol{\xi}}e^{j\omega t}\} \quad (2.43)$$
$$= -\boldsymbol{A}(\omega)\ \mathrm{Re}\{-\omega^2\hat{\boldsymbol{\xi}}(\cos\omega t + j\sin\omega t)\}$$
$$- \quad \boldsymbol{B}(\omega)\ \mathrm{Re}\{j\omega\hat{\boldsymbol{\xi}}(\cos\omega t + j\sin\omega t)\} \quad (2.44)$$
$$= \omega^2\cos\omega t\ \boldsymbol{A}(\omega)\hat{\boldsymbol{\xi}} + \omega\sin\omega t\ \boldsymbol{B}(\omega)\hat{\boldsymbol{\xi}} \quad (2.45)$$

Comparing the parts depending on $\cos\omega t$ and $\sin\omega t$ in (2.41) and (2.45), the following relations follow

$$\boldsymbol{A}(\omega) = \boldsymbol{M}_A - \frac{1}{\omega}\int_0^t \boldsymbol{k}(\tau)\sin\omega\tau\ d\tau \quad (2.46)$$
$$\boldsymbol{B}(\omega) = \int_0^t \boldsymbol{k}(\tau)\cos\omega\tau\ d\tau \quad (2.47)$$

By using the Riemann-Lebesgue lemma (B.1)-(B.2), one gets the following values for $\boldsymbol{B}(\infty)$ and $\boldsymbol{A}(\infty)$ (Ogilvie, 1964)

$$\boldsymbol{B}(\infty) = \lim_{\omega\to\infty}\boldsymbol{B}(\omega) = \lim_{\omega\to\infty}\int_0^t \boldsymbol{k}(\tau)\cos\omega\tau\ d\tau = 0 \quad (2.48)$$

$$\omega(\boldsymbol{A}(\infty) - \boldsymbol{M}_A) = \lim_{\omega\to\infty}\omega(\boldsymbol{A}(\omega) - \boldsymbol{M}_A) = \lim_{\omega\to\infty} -\int_0^t \boldsymbol{k}(\tau)\sin\omega\tau\ d\tau = 0 \quad (2.49)$$

The latter implies that $(\boldsymbol{A}(\infty) - \boldsymbol{M}_A)$ goes to zero faster than ω tends to ∞, and in addition

$$\boldsymbol{M}_A = \boldsymbol{A}(\infty) \Rightarrow \boldsymbol{M}_A = \boldsymbol{M}_A^T \quad (2.50)$$

From now, let $\boldsymbol{k}(\tau)$ be written as $\boldsymbol{k}(t)$. The Fourier transform (B.3) of the kernel $\boldsymbol{k}(t)$ is

$$\mathfrak{F}\{\boldsymbol{k}(t)\} = \boldsymbol{K}(j\omega) = \int_0^t e^{-j\omega t}\boldsymbol{k}(t)\ dt \quad (2.51)$$
$$= \int_0^t \boldsymbol{k}(t)(cos\omega t - j\sin\omega t)\ dt. \quad (2.52)$$

Let $\boldsymbol{K}(j\omega)$ be split in its real and imaginary parts, $\boldsymbol{K}(j\omega) = \boldsymbol{K}_{re}(j\omega) + j\boldsymbol{K}_{im}(j\omega)$ and compare (2.52) with (2.46) and (2.47)

$$\boldsymbol{K}_{re}(j\omega) = \int_0^t \boldsymbol{k}(t)\cos\omega t\ dt = \boldsymbol{B}(\omega) \tag{2.53}$$

$$\boldsymbol{K}_{im}(j\omega) = -\int_0^t \boldsymbol{k}(t)\sin\omega t\ dt = \omega(\boldsymbol{A}(\omega) - \boldsymbol{M}_A) \tag{2.54}$$

$$\boldsymbol{K}(j\omega) = \boldsymbol{B}(\omega) + j\omega(\boldsymbol{A}(\omega) - \boldsymbol{M}_A) \tag{2.55}$$

We know from (2.22) that $\boldsymbol{A}(\omega) = \boldsymbol{A}^T(\omega)$ and $\boldsymbol{B}(\omega) = \boldsymbol{B}^T(\omega)$, hence

$$K_{ij}(j\omega) = K_{ji}(j\omega),\ i = (1,\ldots,6),\ j = (1,\ldots,6) \tag{2.56}$$

or

$$\boldsymbol{K}(j\omega) = \begin{bmatrix} K_{11}(j\omega) & K_{21}(j\omega) & K_{31}(j\omega) & K_{41}(j\omega) & K_{51}(j\omega) & K_{61}(j\omega) \\ K_{21}(j\omega) & K_{22}(j\omega) & K_{32}(j\omega) & K_{42}(j\omega) & K_{52}(j\omega) & K_{62}(j\omega) \\ K_{31}(j\omega) & K_{32}(j\omega) & K_{33}(j\omega) & K_{43}(j\omega) & K_{53}(j\omega) & K_{63}(j\omega) \\ K_{41}(j\omega) & K_{42}(j\omega) & K_{43}(j\omega) & K_{44}(j\omega) & K_{54}(j\omega) & K_{64}(j\omega) \\ K_{51}(j\omega) & K_{52}(j\omega) & K_{53}(j\omega) & K_{54}(j\omega) & K_{55}(j\omega) & K_{65}(j\omega) \\ K_{61}(j\omega) & K_{62}(j\omega) & K_{63}(j\omega) & K_{64}(j\omega) & K_{65}(j\omega) & K_{66}(j\omega) \end{bmatrix} \tag{2.57}$$

The magnitude, $|K_{ij}(j\omega)|$, and the phase, $\angle K_{ij}(j\omega)$, of $K_{ij}(j\omega)$ can now be expressed as

$$|K_{ij}(j\omega)| = \sqrt{(B_{ij}(\omega))^2 + (\omega(A_{ij}(\omega) - M_{Aij}))^2} \tag{2.58}$$

$$\angle K_{ij}(j\omega) = \arctan\left(\frac{\omega(A_{ij}(\omega) - M_{Aij})}{B_{ij}(\omega)}\right) \tag{2.59}$$

In Figure 2.2 the Bode plot of $K_{22}(j\omega)$ in sway for the S-175 tanker is shown, and in Figure 2.3 the damping term $B_{22}(\omega)$ and the added mass term $\omega(A_{22}(\omega) - M_{A22}))$ is plotted. As we can see from the plots, when the phase is zero, it is the damping term $B_{22}(\omega)$ which dominates the dynamics, while when the phase is $+/-90$ (deg) it is the added mass term $\omega(A_{22}(\omega) - M_{A22})$ which dominates the dynamics. In Figure 2.4 it is illustrated how the phase of $K_{ij}(j\omega)$ varies depending on the values of $B_{ij}(\omega)$ and $\omega(A_{ij}(\omega) - M_{Aij})$.

The impulse response $\boldsymbol{k}(t)$ can now be found from the added mass matrix $\boldsymbol{A}(\omega)$ or the damping matrix $\boldsymbol{B}(\omega)$ either by inverse Fourier cosine transform (B.6) or inverse Fourier sine transform (B.8)

$$\boldsymbol{k}(t) = \mathfrak{F}_c^{-1}[\boldsymbol{K}_{re}(j\omega)] = \frac{2}{\pi}\int_0^\infty \boldsymbol{B}(\omega)\cos\omega t\ d\omega \tag{2.60}$$

$$\boldsymbol{k}(t) = \mathfrak{F}_s^{-1}[\boldsymbol{K}_{im}(j\omega)] = -\frac{2}{\pi}\int_0^\infty \omega(\boldsymbol{A}(\omega) - \boldsymbol{M}_A)\sin\omega t\ d\omega \tag{2.61}$$

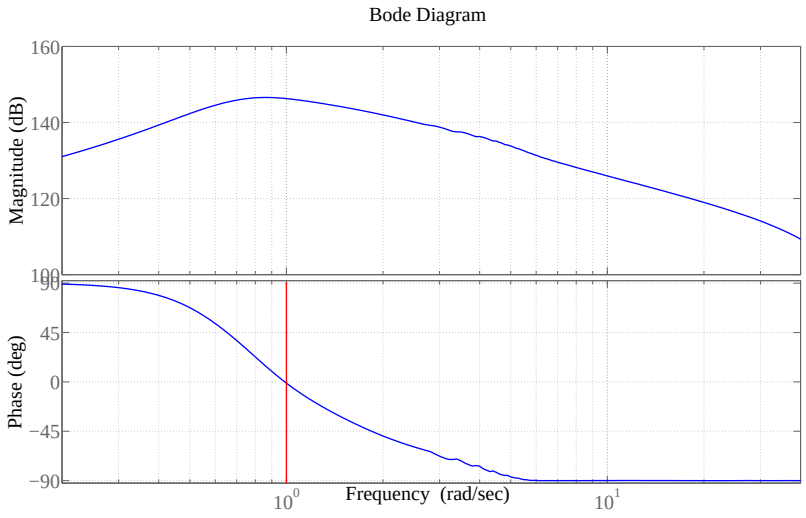

Figure 2.2: Bode plot of the radiation transfer function $K_{22}(j\omega)$ for the S-175 tanker.

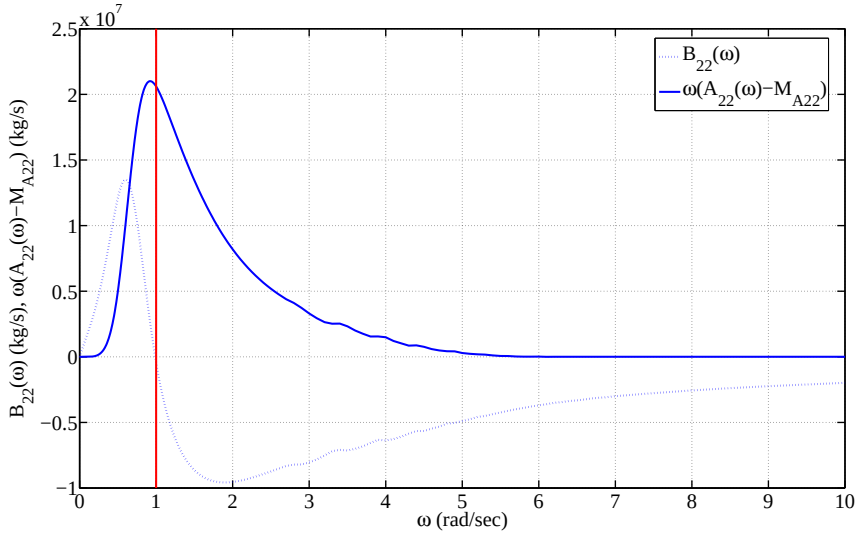

Figure 2.3: Radiation parameters $B_{22}(\omega)$ and $\omega(A_{22}(\omega) - M_{A22})$ for the S-175 tanker as a function of the frequency ω.

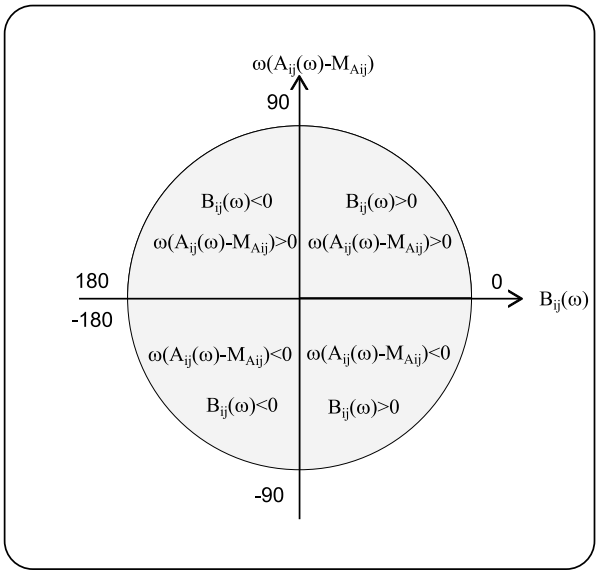

Figure 2.4: The phase of the frequency response $K_{ij}(j\omega)$ depending on the values of $B_{ij}(\omega)$ and $\omega(A_{ij}(\omega) - M_{Aij})$.

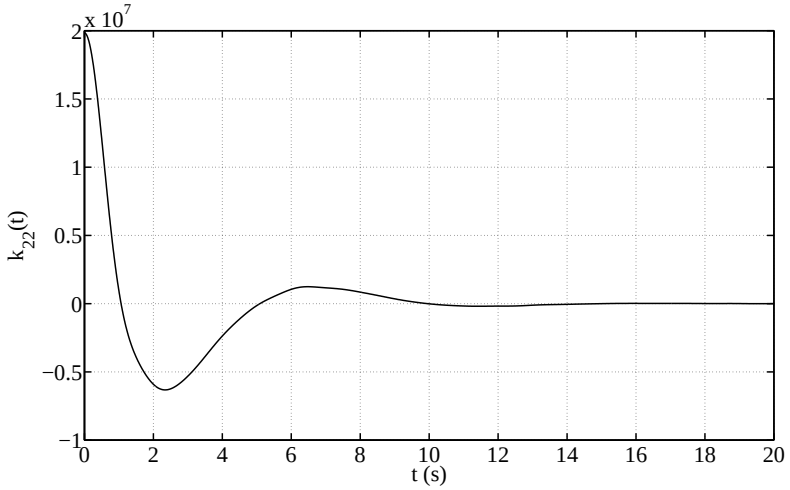

Figure 2.5: Radiation impulse response function $k_{22}(t)$ (kg/s^2) in sway for the S-175 tanker.

The first integral tends to converge fastest since $\boldsymbol{B}(\omega)$ tends to zero faster than $\omega(\boldsymbol{A}(\omega) - \boldsymbol{M}_A)$, and it is common to use this equation for finding the impulse response of the system. An overview of different methods to compute the retardation function $\boldsymbol{k}(t)$ is given in Ballard (2002). The impulse response function obtained from the damping matrix $\boldsymbol{B}(\omega)$ in Figure 2.1 is plotted in Figure 2.5.

2.6 Relating Damping and Added Mass

It can be shown that the real and imaginary parts of the Fourier transform of $\boldsymbol{k}(t)$ are related since the function is causal. This is a well-known result in probability, statistics and system theory (Bendat and Piersol, 2000), but for the radiation forces it was first mentioned by Kotik and Mangulis (1962). These authors showed that the real and imaginary parts of the frequency response of the radiation forces are related through the Hilbert transform (B.9). For the frequency response in (2.55) this gives

$$\boldsymbol{K}_{im}(j\omega) = -\mathcal{H}\{\boldsymbol{K}_{re}(j\omega)\} = -\frac{1}{\pi}\int_{-\infty}^{\infty} \frac{\boldsymbol{K}_{re}(ju)}{\omega - u}\, du \tag{2.62}$$

This equals

$$\omega\left(\boldsymbol{A}(\omega) - \boldsymbol{M}_A\right) = -\frac{1}{\pi}\int_{-\infty}^{\infty} \frac{\boldsymbol{B}(u)}{\omega - u}\, du \tag{2.63}$$

Further, the real part can be found from the inverse Hilbert transform (B.10) of the imaginary part,

$$\boldsymbol{K}_{re}(j\omega) = -\mathcal{H}^{-1}\{\boldsymbol{K}_{im}(j\omega)\} = \frac{1}{\pi}\int_{-\infty}^{\infty} \frac{\boldsymbol{K}_{im}(ju)}{\omega - u}\, du \tag{2.64}$$

This equals

$$\boldsymbol{B}(\omega) = \frac{1}{\pi}\int_{-\infty}^{\infty} \frac{u(\boldsymbol{A}(u) - \boldsymbol{M}_A)}{\omega - u}\, du \tag{2.65}$$

Given the matrices $\boldsymbol{A}(\omega)$ and $\boldsymbol{B}(\omega)$, a way to determine whether $\boldsymbol{K}(j\omega)$ represents a physically realizable causal system is to check if $\boldsymbol{K}_{re}(j\omega) = \boldsymbol{B}(\omega)$ is the Hilbert transform of $-\boldsymbol{K}_{im}(j\omega) = -\omega(\boldsymbol{A}(\omega) - \boldsymbol{M}_A)$. If only one of the matrices $\boldsymbol{A}(\omega)$ or $\boldsymbol{B}(\omega)$ is available $\boldsymbol{K}_{re}(j\omega)$ or $\boldsymbol{K}_{im}(j\omega)$ can still be found through (2.63) and (2.65).

2.7 Concluding Remarks

The radiation forces consist of added mass forces and damping forces. Frequency dependent added mass and damping matrices can be obtained by

using hydrodynamic software. In this chapter a review has been given of how these matrices relate to the frequency response and impulse response of the radiation forces.

Time domain simulation of the radiation forces can be done by convoluting the impulse response of the radiation forces with the vessel velocity. The equations of motion describing the radiation forces by use of convolution terms are not consistent with the common formulations in control engineering. The common formulations in control engineering are state-space models in the time domain or transfer functions in the frequency domain. Hence, the formulations of the impulse response and frequency response of the radiation forces will be used in order to identify radiation force models. In the next chapters radiation force models will be expressed in state-space form or as transfer functions.

Chapter 3

Properties of Radiation Force Models

3.1 Introduction

When the models of radiation forces are to be included in marine applications, it is important that they reflect the dynamical properties of the system. It is also important to develop models which are in accordance with the common formulations in a field, e.g. for control purposes. The common formulations used in control design are state-space representations in the time domain or transfer function representations in the frequency domain. The convolution representation in the time domain of the radiation forces from Chapter 2 can be approximated by state-space representations. Further, the frequency response representations of the radiation forces from Chapter 2 can be approximated by rational transfer functions in the frequency domain. In this chapter the focus will be on what properties and structure these models should have, based on knowledge about the frequency dependent added mass and damping coefficients from hydrodynamic software.

In Section 3.2 properties like stability and passivity of the given model are investigated. It will be shown that the convolution part of the radiation forces represents a stable system. Subsequently, it will be shown that the radiation forces are passive, and that the overall vessel-water system is passive. In Section 3.3 the structure of the state-space models and transfer functions used for approximation of the radiation forces will be investigated. Further, in Section 3.4 an alternative representation of the radiation forces will be investigated. This representation introduces a convolution integral containing the acceleration of the vessel instead of the velocity.

3.2 Stability Properties

In this section properties like stability and passivity from control theory will be investigated. These properties are useful in numerical simulations and control synthesis and design.

The time-domain equations for the floating body can be written

$$\boldsymbol{M}_{RB}\ddot{\boldsymbol{\xi}}(t) + \boldsymbol{C}_h\boldsymbol{\xi}(t) = \boldsymbol{\tau}_R + \boldsymbol{\tau}_{visc} + \boldsymbol{\tau}_{ext} + \boldsymbol{\tau}_A \tag{3.1}$$

where

$$\boldsymbol{\tau}_R(t) = -\boldsymbol{M}_A\ddot{\boldsymbol{\xi}}(t) - \int_0^t \boldsymbol{k}(t-\tau)\dot{\boldsymbol{\xi}}(\tau)d\tau \tag{3.2}$$

Let the radiation forces be partitioned accordingly

$$\boldsymbol{\tau}_R(t) = -\boldsymbol{\tau}_{R1}(t) - \boldsymbol{\tau}_{R2}(t) \tag{3.3}$$

$$\boldsymbol{\tau}_{R1}(t) = \boldsymbol{M}_A\ddot{\boldsymbol{\xi}}(t) \tag{3.4}$$

$$\boldsymbol{\tau}_{R2}(t) = \int_0^t \boldsymbol{k}(t-\tau)\dot{\boldsymbol{\xi}}(\tau)d\tau \tag{3.5}$$

Further it is known that a system is bounded-input bounded-output (BIBO) stable if for every bounded input the system gives a bounded output (see Theorem B.1). The following proposition can be stated

Proposition 3.1 *The linear SISO systems represented by the impulse responses $k_{ij}(t)$ in (3.5) are BIBO stable.*

Proof. As time goes to infinity, the Riemann-Lebesgue lemma (B.2) can be used to find the final value of the impulse response $\boldsymbol{k}(t)$. By the use of (B.2) and (2.60) it can be seen that the impulse response tends towards zero as time goes to infinity

$$\lim_{t\to\infty} \boldsymbol{k}(t) = \lim_{t\to\infty} \frac{2}{\pi}\int_0^\infty \boldsymbol{B}(\omega)\cos\omega t \; d\omega = \boldsymbol{0} \tag{3.6}$$

hence,

$$\lim_{t\to\infty} k_{ij}(t) = 0, \;\forall\; i = (1,\ldots,6), \;\; j = (1,\ldots,6) \tag{3.7}$$

Since $k_{ij}(t)$ is absolutely integrable

$$\int_0^\infty |k_{ij}(t)| < \infty, \;\forall\; i = (1,\ldots,6), \;\; j = (1,\ldots,6) \tag{3.8}$$

it can be concluded that the SISO systems represented by the impulse responses $k_{ij}(t)$ are BIBO stable. ■

Related to BIBO stability is $\mathcal{L}_p$ input-output stability. The following proposition can be stated,

Proposition 3.2 *The linear SISO systems represented by the impulse responses $k_{ij}(t)$ in (3.5) are $\mathcal{L}_p$ input-output stable for $1 \leq p \leq \infty$.*

Proof. For SISO systems, the $\mathcal{L}_1$ and the $\mathcal{L}_\infty$ norms of the convolution operator $\mathcal{S} : u \mapsto y = \mathcal{S}(u) = h * u$ are the same and equal to $\int_0^\infty |h(t)|\, dt$ (Antoulas, 2005). By use of (3.8) and Proposition B.1 it can be concluded that the SISO systems represented by the impulse responses $k_{ij}(t)$ are $\mathcal{L}_p$ input-output stable for $1 \leq p \leq \infty$. ■

Passivity theory is useful in the design and analysis of control systems (Lozano *et al.*, 2000; Egeland and Gravdahl, 2002). It is important that the mathematical model reflects this property to avoid nonphysical behavior when it is used in simulations. Passivity characterizes useful properties of the system which can be used in the modeling process. In Damaren (2000) and Kristiansen *et al.* (2005) it is pointed out that the radiation forces are passive because of the use of energy functions in the time domain. Here it is proposed to show the same result in the frequency domain by using the properties of the added mass matrix $\boldsymbol{A}(\omega)$ and the damping matrix $\boldsymbol{B}(\omega)$.

The Laplace transform (B.15) of the radiation forces is

$$
\begin{aligned}
-\boldsymbol{\tau}_R(s) &= \mathcal{L}\left\{-\boldsymbol{\tau}_R(t)\right\} && (3.9)\\
&= \int_0^\infty \left(\boldsymbol{M}_A \ddot{\boldsymbol{\xi}}(t) + \int_0^t \boldsymbol{k}(t-\tau)\dot{\boldsymbol{\xi}}(\tau) d\tau \right) e^{-st} dt && (3.10)\\
&= (\boldsymbol{M}_A s + \boldsymbol{K}(s))\dot{\boldsymbol{\xi}}(s) && (3.11)\\
&= \bar{\boldsymbol{H}}(s)\dot{\boldsymbol{\xi}}(s) && (3.12)
\end{aligned}
$$

Where $\bar{\boldsymbol{H}}(s)$ is a 6×6 MIMO system describing the motion in each mode. From (Egeland, 1993) we know that a MIMO system is passive if it satisfies

$$
\lambda_{min}\left[\boldsymbol{H}(j\omega) + \boldsymbol{H}^T(-j\omega)\right] \geq 0, \quad \forall\ \omega \tag{3.13}
$$

where λ_{min} is the smallest eigenvalue of the matrix $\boldsymbol{H}(j\omega) + \boldsymbol{H}^T(-j\omega)$. The frequency response of $\boldsymbol{H}(j\omega)$ is $\boldsymbol{H}(s)$ along the $j\omega$ axis.

Proposition 3.3 *The mapping from $\dot{\boldsymbol{\xi}} \mapsto -\boldsymbol{\tau}_R$ in (3.12) is passive.*

Proof. Using the expression for $\boldsymbol{K}(j\omega)$ from (2.55) gives

$$
\begin{aligned}
\bar{\boldsymbol{H}}(j\omega) &= \boldsymbol{M}_A j\omega + \boldsymbol{K}(j\omega) && (3.14)\\
&= \boldsymbol{B}(\omega) + j\omega\boldsymbol{A}(\omega) && (3.15)
\end{aligned}
$$

Using the properties from (2.22) and (2.23) gives

$$\bar{\boldsymbol{H}}(j\omega) + \bar{\boldsymbol{H}}^T(-j\omega) \tag{3.16}$$
$$= \boldsymbol{B}(\omega) + j\omega\boldsymbol{A}(\omega) + \boldsymbol{B}^T(\omega) - j\omega\boldsymbol{A}^T(\omega) \tag{3.17}$$
$$= 2\boldsymbol{B}(\omega) \tag{3.18}$$
$$\Longrightarrow \lambda_{min}\left[\bar{\boldsymbol{H}}(j\omega) + \bar{\boldsymbol{H}}^T(-j\omega)\right] \geq 0 \tag{3.19}$$

and it can be concluded that the mapping $\dot{\boldsymbol{\xi}} \mapsto -\boldsymbol{\tau}_R$ is passive. ■
According to (B.13), the passivity of the mapping $\dot{\boldsymbol{\xi}} \mapsto -\boldsymbol{\tau}_R$ implies that there exists a matrix $E_1 \geq 0$ such that

$$\int_0^T -\dot{\boldsymbol{\xi}}^T(t)\boldsymbol{\tau}_R(t)\, dt \geq -E_1. \tag{3.20}$$

This result also implies that the elements on the diagonal of $\bar{\boldsymbol{H}}(s)$ satisfies

$$\bar{\boldsymbol{H}}(s) \geq 0 \Rightarrow \bar{H}_{ii}(s) \geq 0,\ i = (1, \ldots, 6) \tag{3.21}$$

The same arguments as above can be used for $\boldsymbol{K}(j\omega)$.

Proposition 3.4 *The mapping from $\dot{\boldsymbol{\xi}} \mapsto \boldsymbol{\tau}_{R2}$ in (3.5) is passive.*

Proof. Using the expression for $\boldsymbol{K}(j\omega)$ from (2.55) and the properties from (2.22) and (2.23) gives

$$\boldsymbol{K}(j\omega) + \boldsymbol{K}^T(-j\omega) \tag{3.22}$$
$$= \boldsymbol{B}(\omega) + j\omega(\boldsymbol{A}(\omega) - \boldsymbol{M}_A) + \boldsymbol{B}^T(\omega) - j\omega(\boldsymbol{A}^T(\omega) - \boldsymbol{M}_A^T) \tag{3.23}$$
$$= 2\boldsymbol{B}(\omega) \tag{3.24}$$
$$\Longrightarrow \lambda_{min}\left[\boldsymbol{K}(j\omega) + \boldsymbol{K}^T(-j\omega)\right] \geq 0 \tag{3.25}$$

and it can be concluded that the mapping $\dot{\boldsymbol{\xi}} \mapsto \boldsymbol{\tau}_{R2}$ is passive. ■
According to (B.13), the passivity of the mapping $\dot{\boldsymbol{\xi}} \mapsto \boldsymbol{\tau}_{R2}$ there exists a matrix $E_2 \geq 0$ such that

$$\int_0^T \dot{\boldsymbol{\xi}}^T(t)\boldsymbol{\tau}_{R2}(t)\, dt \geq -E_2 \tag{3.26}$$

Also, the elements on the diagonal of $\boldsymbol{K}(s)$ satisfies

$$\boldsymbol{K}(s) \geq 0 \Rightarrow K_{ii}(s) \geq 0,\ i = (1, \ldots, 6) \tag{3.27}$$

In Figure 3.1 the Nyquist plot of the frequency response $K_{22}(j\omega)$ is shown for the S-175 tanker. The plot indicates that the system should be described by a positive real function.

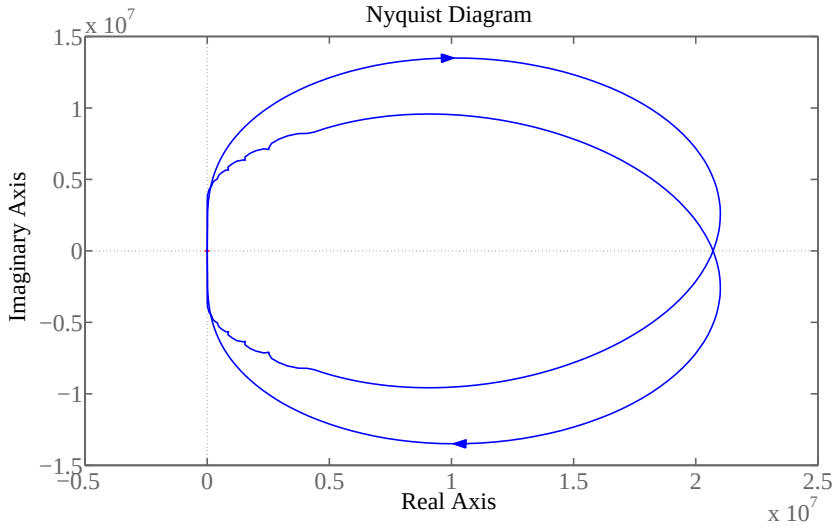

Figure 3.1: Nyquist plot of the radiation transfer function $K_{22}(j\omega)$ for the S-175 tanker.

Further, the passivity of the vessel model will be investigated in the same style as in Sørensen (1993) and Kristiansen *et al.* (2005). Combining (3.1) and (3.2) gives the following equations of motion

$$\boldsymbol{M}\ddot{\boldsymbol{\xi}}(t) + \int_0^t \boldsymbol{k}(t-\tau)\dot{\boldsymbol{\xi}}(\tau)d\tau + \boldsymbol{C}_h\boldsymbol{\xi}(t) = \boldsymbol{\tau}_{visc}(t) + \boldsymbol{\tau}_{ext}(t) + \boldsymbol{\tau}_A(t), \quad (3.28)$$

where $\boldsymbol{M} = \boldsymbol{M}_{RB} + \boldsymbol{M}_A$. For marine structures, where the system inertia and added mass matrix is positive definite,

$$\boldsymbol{M} > 0 \quad (3.29)$$

and the matrix of restoring forces is positive semidefinite,

$$\boldsymbol{C}_h \geq 0 \quad (3.30)$$

the following proposition is valid.

Proposition 3.5 *The vessel-water system in (3.28) with input* $\boldsymbol{\tau} = \boldsymbol{\tau}_{visc} + \boldsymbol{\tau}_A + \boldsymbol{\tau}_{ext}$ *and output* $\dot{\boldsymbol{\xi}}$ *is passive.*

Proof. The total energy in the system consists of kinetic and potential energy,

$$V = \text{total energy} = \text{kinetic energy} + \text{potential energy} \quad (3.31)$$

Choose the energy function

$$V(t) = \frac{1}{2}\dot{\boldsymbol{\xi}}^T(t)\boldsymbol{M}\dot{\boldsymbol{\xi}}(t) + \frac{1}{2}\boldsymbol{\xi}^T(t)\boldsymbol{C}_h\boldsymbol{\xi}(t) \geq 0 \tag{3.32}$$

The time derivative of the energy function is

$$\begin{aligned}
\dot{V}(t) &= \dot{\boldsymbol{\xi}}^T(t)\boldsymbol{M}\ddot{\boldsymbol{\xi}}(t) + \dot{\boldsymbol{\xi}}^T(t)\boldsymbol{C}_h\boldsymbol{\xi}(t) && (3.33)\\
&= \dot{\boldsymbol{\xi}}^T(t)\left(\boldsymbol{\tau}(t) - \int_0^t \boldsymbol{k}(t-\tau)\dot{\boldsymbol{\xi}}(\tau)d\tau\right) && (3.34)\\
&= \dot{\boldsymbol{\xi}}^T(t)\boldsymbol{\tau}(t) - \dot{\boldsymbol{\xi}}^T(t)\boldsymbol{\tau}_{R2}(t) && (3.35)
\end{aligned}$$

Taking (3.26) into consideration, and by use of (B.14) from Lozano *et al.* (2000) it follows that the mapping $\boldsymbol{\tau}(t) \mapsto \dot{\boldsymbol{\xi}}(t)$ is passive. ■

3.3 Model Without Convolution Term

The time domain equations for the floating body are now,

$$\boldsymbol{M}\ddot{\boldsymbol{\xi}}(t) + \int_0^t \boldsymbol{k}(t-\tau)\dot{\boldsymbol{\xi}}(\tau)d\tau + \boldsymbol{C}_h\xi(t) = \boldsymbol{\tau}_{visc}(t) + \boldsymbol{\tau}_{ext}(t) + \boldsymbol{\tau}_A(t). \tag{3.36}$$

The formulation of the equations of motion for a floating body based on the use of convolution terms is not in agreement with the common formulations used in control engineering. A state-space representation of the impulse response kernel $\boldsymbol{k}(t)$ is more efficient than a calculation based on the use of convolution integrals. Let the convolution part of the equations of motion in (3.36) be written as

$$\boldsymbol{\tau}_{R2}(t) = \int_0^t \boldsymbol{k}(t-\tau)\dot{\boldsymbol{\xi}}(\tau)d\tau \tag{3.37}$$

It is known from the control literature (Chen, 1999; Kailath, 1980) that this type of system can also be presented in the time domain in state-space form by assuming that $\boldsymbol{k}(t)$ is realizable:

$$\begin{aligned}
\dot{\boldsymbol{x}}(t) &= \boldsymbol{A}\boldsymbol{x}(t) + \boldsymbol{B}\dot{\boldsymbol{\xi}}(t) && (3.38)\\
\boldsymbol{\tau}_{R2}(t) &= \boldsymbol{C}\boldsymbol{x}(t) + \boldsymbol{D}\dot{\boldsymbol{\xi}}(t) && (3.39)
\end{aligned}$$

Since $\boldsymbol{A}(\infty) = \boldsymbol{M}_A$ is taken out from the frequency response of the radiation forces and represented in (3.4), there is no direct throughput from $\dot{\boldsymbol{\xi}}(t)$ to $\boldsymbol{\tau}_{R2}(t)$, hence $\boldsymbol{D} = 0$

$$\begin{aligned}
\dot{\boldsymbol{x}}(t) &= \boldsymbol{A}\boldsymbol{x}(t) + \boldsymbol{B}\dot{\boldsymbol{\xi}}(t) && (3.40)\\
\boldsymbol{\tau}_{R2}(t) &= \boldsymbol{C}\boldsymbol{x}(t) && (3.41)
\end{aligned}$$

By use of Theorem B.2 and Proposition 3.2 it can be concluded that $\boldsymbol{A}$ in the realization in (3.40)-(3.41) should be Hurwitz. The associated transfer function is

$$\boldsymbol{K}(s) = \boldsymbol{C}(sI - \boldsymbol{A})^{-1}\boldsymbol{B} \tag{3.42}$$

where the rational transfer functions $K_{ij}(s)$ can be written

$$K_{ij}(s) = \frac{N_{ij}(s)}{D_{ij}(s)} = \frac{b_{n-1}s^{n-1} + \cdots + b_1 s + b_0}{s^n + a_{n-1}s^{n-1} + \cdots + a_1 s + a_0} \tag{3.43}$$

The relative degree (see Definition B.2) of the transfer functions will be at least 1 since $D = 0$.

The passivity or positive realness of $K(s)$ implies that the approximated transfer functions on the diagonal of K_{ii} are positive real. From Egeland and Gravdahl (2002) it is known that the relative degree of a positive real SISO system can be $+/-1$ or 0. Due to (3.43) it can be stated that these will be of relative degree 1. In the following it will be investigated if this is consistent with information given by the frequency data given from hydrodynamical software. The properties of the off-diagonal transfer functions will also be investigated. Some of these results are presented in Jeffreys (1984) and Jordán and Beltrán-Aguedo (2004).

Frequency response at $\boldsymbol{\omega = 0}$

The value of $\boldsymbol{K}(j\omega)$ as ω tends to zero is

$$\lim_{\omega \to 0} \boldsymbol{K}(j\omega) = \lim_{\omega \to 0} \left(\boldsymbol{B}(\omega) + j\omega(\boldsymbol{A}(\omega) - \boldsymbol{M}_A)\right) = \boldsymbol{B}(0) \tag{3.44}$$

For a vessel with zero speed the frequency dependent matrix $B(\omega)$ is zero at zero frequency (Faltinsen, 1990),

$$\lim_{\omega \to 0} \boldsymbol{K}(j\omega) = \boldsymbol{B}(0) = \boldsymbol{0} \tag{3.45}$$

hence

$$\lim_{\omega \to 0} K_{ij}(j\omega) = 0, \ \forall \ i = (1, \ldots, 6), \ j = (1, \ldots, 6) \tag{3.46}$$

Take the same limit for the transfer function in (3.43)

$$\lim_{\omega \to 0} K_{ij}(j\omega) = \lim_{\omega \to 0} \frac{b_{n-1}(j\omega)^{n-1} + \cdots + b_1(j\omega) + b_0}{(j\omega)^n + a_{n-1}(j\omega)^{n-1} + \cdots + a_1(j\omega) + a_0} = \frac{b_0}{a_0} \tag{3.47}$$

In order for this to be in accordance with (3.46) b_0 must be equal to 0 in the transfer functions. Then the transfer functions $K_{ij}(s)$ can be written

$$K_{ij}(s) = \frac{b_{n-1}s^{n-1} + \cdots + b_1 s}{s^n + a_{n-1}s^{n-1} + \cdots + a_1 s + a_0} \tag{3.48}$$

Frequency response at $\omega = \infty$

From (2.48) and (2.49) it can be seen that

$$\lim_{\omega\to\infty} \boldsymbol{K}(j\omega) = \lim_{\omega\to\infty} (\boldsymbol{B}(\omega) + j\omega(\boldsymbol{A}(\omega) - \boldsymbol{M}_A)) = \boldsymbol{0} \tag{3.49}$$

hence

$$\lim_{\omega\to\infty} K_{ij}(j\omega) = 0,\ \forall\ i = (1,\ldots,6),\ j = (1,\ldots,6) \tag{3.50}$$

Let us now take the same limit for the transfer function in (3.48)

$$\lim_{\omega\to\infty} K_{ij}(j\omega) = \frac{b_{n-1}(j\omega)^{n-1} + \cdots + b_1(j\omega)}{(j\omega)^n + a_{n-1}(j\omega)^{n-1} + \cdots + a_1(j\omega) + a_0} = 0 \tag{3.51}$$

This is in accordance with (3.50).

Initial value of impulse response

$\boldsymbol{B}(\omega)$ converges to zero for an ω_1 far less than ∞. Hence we can split the integral in (2.60) in two parts,

$$\boldsymbol{k}(t) = \frac{2}{\pi}\int_0^{\omega_1} \boldsymbol{B}(\omega)\cos(\omega t)\ d\omega + \frac{2}{\pi}\int_{\omega_1}^{\infty} \boldsymbol{B}(\omega)\cos(\omega t)\ d\omega, \tag{3.52}$$

where the latter part is zero. The following expression for $\boldsymbol{k}(t)$ at time zero follows

$$\boldsymbol{k}(t{=}0) = \frac{2}{\pi}\int_0^{\omega_1} \boldsymbol{B}(\omega)\ d\omega \tag{3.53}$$

It is known from (2.23) that $\det(\boldsymbol{B}(\omega)) \geq 0,\ \forall\ \omega$, then $\boldsymbol{k}(0) \in \mathbb{R}^{6\times 6}$ satisfies

$$\det(\boldsymbol{k}(0)) \geq 0 \tag{3.54}$$

Since $\boldsymbol{B}(\omega)$ is positive semidefinite the following holds

$$k_{ii}(0) \geq 0,\ \forall\ i = (1,\ldots,6) \tag{3.55}$$

while the off-diagonal terms $k_{ij}(0)\ \forall\ i = (1,\ldots,6), j = (1,\ldots,6), i \neq j$, can be both zero, positive and negative. Assume now that all the terms in $k_{ij}(t)$ are nonzero, and use the initial-value theorem (B.18) on (3.48)

$$\lim_{t\to 0^+} k_{ij}(t) = \lim_{s\to\infty} sK_{ij}(s) = \lim_{s\to\infty} \frac{s(b_{n-1}s^{n-1} + \cdots + b_1 s)}{s^n + a_{n-1}s^{n-1} + \cdots + a_1 s + a_0} = b_{n-1} \tag{3.56}$$

Writing this in matrix form gives

$$\lim_{t\to 0^+} \boldsymbol{k}(t) = \lim_{s\to\infty} s\boldsymbol{K}(s) = \begin{bmatrix} b_{11_{n-1}} & \dots & b_{16_{n-1}} \\ \vdots & \ddots & \vdots \\ b_{61_{n-1}} & \dots & b_{66_{n-1}} \end{bmatrix} \tag{3.57}$$

where $b_{ij_{n-1}}$ represents the b_{n-1} parameters of each transfer function $K_{ij}(s)$ in the matrix $\boldsymbol{K}(s)$. The degree n of each transfer function can vary, depending on the accuracy needed to approximate the given data. Given the nonzero initial value $\boldsymbol{k}(0)$ in (3.54), the parameters $b_{ij_{n-1}}$ should satisfy

$$\begin{bmatrix} b_{11_{n-1}} & \dots & b_{16_{n-1}} \\ \vdots & \ddots & \vdots \\ b_{61_{n-1}} & \dots & b_{66_{n-1}} \end{bmatrix} = \boldsymbol{k}(0) \tag{3.58}$$

From this it can be concluded that in the modes where $k_{ij}(0) \neq 0$ the transfer function should be of relative degree 1.

Example 3.1 *Given a transfer function*

$$K_{ij}(s) = \frac{b_1 s}{s^2 + 2s + 4}, \tag{3.59}$$

where b_1 is given the values $[1, 1.5, 2, 2.5]$ will have the impulse responses given in Figure 3.2. This example illustrates how the initial value of the impulse response of a transfer function of relative degree 1 varies with the choice of b_{n-1}, which in this example is b_1.

Final value of impulse response

Use of the final-value theorem (B.17) on (3.48) gives

$$\lim_{t\to\infty} k_{ij}(t) = \lim_{s\to 0} sK_{ij}(s) = \lim_{s\to 0} \frac{s(b_{n-1}s^{n-1} + \dots + b_1 s)}{s^n + a_{n-1}s^{n-1} + \dots + a_1 s + a_0} = 0 \tag{3.60}$$

This is in accordance with the result in (3.7).

The transfer functions representing the hydrodynamic actions can now be written

$$K_{ij}(s) = \frac{b_{n-1}s^{n-1} + \dots + b_1 s}{s^n + a_{n-1}s^{n-1} + \dots + a_1 s + a_0} \tag{3.61}$$

This formulation is in accordance with the values of the frequency responses at $\omega = 0$ and $\omega = \infty$ in addition to the initial values and final values of the impulse responses of the system.

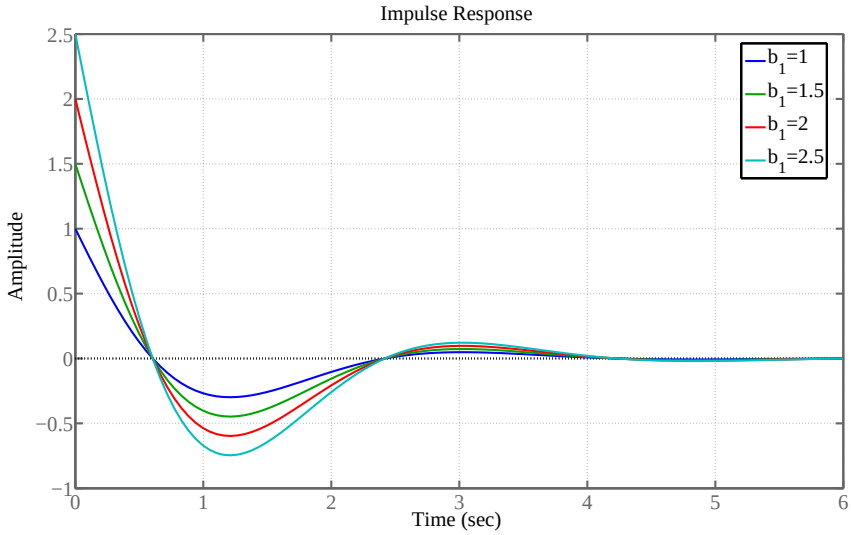

Figure 3.2: Initial value of impulse response depending on value of b_1 in (3.59)

Now, the convolution term in the equations of motion can be approximated by a state-space model in the time domain

$$\begin{aligned} \boldsymbol{M}\ddot{\boldsymbol{\xi}}(t) + \boldsymbol{\tau}_{R2}(t) + \boldsymbol{C}_h\boldsymbol{\xi}(t) &= \boldsymbol{\tau}_{visc} + \boldsymbol{\tau}_{ext}(t) + \boldsymbol{\tau}_A(t) && (3.62)\\ \dot{\boldsymbol{x}}(t) &= \boldsymbol{A}\boldsymbol{x}(t) + \boldsymbol{B}\dot{\boldsymbol{\xi}}(t) && (3.63)\\ \boldsymbol{\tau}_{R2}(t) &= \boldsymbol{C}\boldsymbol{x}(t) && (3.64) \end{aligned}$$

where $\boldsymbol{\tau}_{R2}$ represents the hydrodynamic actions caused by added mass and damping. By defining the state vector

$$\boldsymbol{z}(t) = \begin{bmatrix} \dot{\boldsymbol{\xi}}(t) \\ \boldsymbol{\xi}(t) \\ \boldsymbol{x}(t) \end{bmatrix} \tag{3.65}$$

this can be written on state-space form as

$$\begin{bmatrix} \ddot{\boldsymbol{\xi}}(t) \\ \dot{\boldsymbol{\xi}}(t) \\ \dot{\boldsymbol{x}}(t) \end{bmatrix} = \begin{bmatrix} -\boldsymbol{M}^{-1}\boldsymbol{C}_h & \boldsymbol{0} & -\boldsymbol{M}^{-1}\boldsymbol{C} \\ \boldsymbol{I} & \boldsymbol{0} & \boldsymbol{0} \\ \boldsymbol{B} & \boldsymbol{0} & \boldsymbol{A} \end{bmatrix} \begin{bmatrix} \dot{\boldsymbol{\xi}}(t) \\ \boldsymbol{\xi}(t) \\ \boldsymbol{x}(t) \end{bmatrix} + \begin{bmatrix} \boldsymbol{I} \\ \boldsymbol{0} \\ \boldsymbol{0} \end{bmatrix} (\boldsymbol{\tau}_{visc}+\boldsymbol{\tau}_A+\boldsymbol{\tau}_{ext}) \tag{3.66}$$

This vessel model is illustrated in Figure 3.3. It gives the following representation in the Laplace domain

$$\boldsymbol{M}\ddot{\boldsymbol{\xi}}(s) + \boldsymbol{K}(s)\dot{\boldsymbol{\xi}}(s) + \boldsymbol{C}_h\boldsymbol{\xi}(s) = \boldsymbol{\tau}_{visc}(s) + \boldsymbol{\tau}_{ext}(s) + \boldsymbol{\tau}_A(s) \tag{3.67}$$

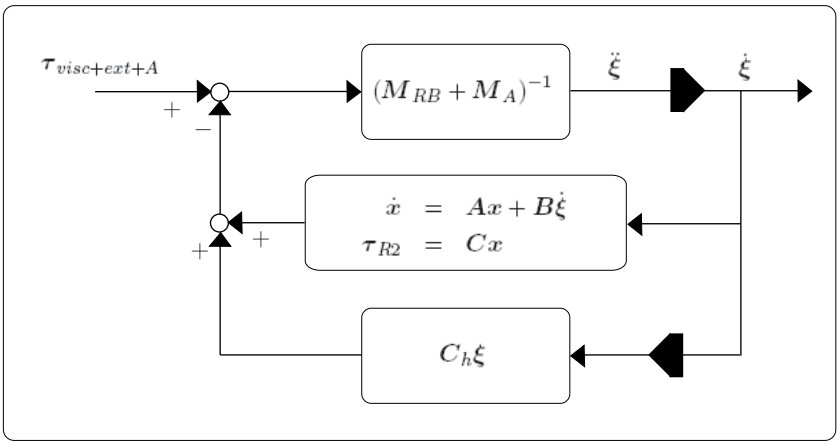

Figure 3.3: The vessel model

Exploiting symmetry properties

The 6-DOF equations of motion give 36 impulse response functions. Since the matrices $\boldsymbol{A}(\omega)$ and $\boldsymbol{B}(\omega)$ are symmetric, this simplifies the identification of the overall system. Different body symmetries simplify the realization. Examples of some of the body symmetries are given below (Fossen, 2002).

1. xz-plane of symmetry (port/starboard symmetry)

$$\boldsymbol{K}(j\omega) = \boldsymbol{K}^T(j\omega) = \begin{bmatrix} K_{11} & 0 & K_{13} & 0 & K_{15} & 0 \\ 0 & K_{22} & 0 & K_{24} & 0 & K_{26} \\ K_{13} & 0 & K_{33} & 0 & K_{35} & 0 \\ 0 & K_{24} & 0 & K_{44} & 0 & K_{46} \\ K_{15} & 0 & K_{35} & 0 & K_{55} & 0 \\ 0 & K_{26} & 0 & K_{46} & 0 & K_{66} \end{bmatrix} \tag{3.68}$$

2. xy-plane of symmetry (bottom/top symmetry)

$$\boldsymbol{K}(j\omega) = \boldsymbol{K}^T(j\omega) = \begin{bmatrix} K_{11} & K_{12} & 0 & 0 & 0 & K_{16} \\ K_{21} & K_{22} & 0 & 0 & 0 & K_{26} \\ 0 & 0 & K_{33} & K_{34} & K_{35} & 0 \\ 0 & 0 & K_{34} & K_{44} & K_{45} & 0 \\ 0 & 0 & K_{35} & K_{45} & K_{55} & 0 \\ K_{16} & K_{26} & 0 & 0 & 0 & K_{66} \end{bmatrix} \tag{3.69}$$

3. yz-plane of symmetry (fore/aft symmetry)

$$\boldsymbol{K}(j\omega) = \boldsymbol{K}^T(j\omega) = \begin{bmatrix} K_{11} & 0 & 0 & 0 & K_{15} & K_{16} \\ 0 & K_{22} & K_{23} & K_{24} & 0 & 0 \\ 0 & K_{23} & K_{33} & K_{34} & 0 & 0 \\ 0 & K_{24} & K_{34} & K_{44} & 0 & 0 \\ K_{15} & 0 & 0 & 0 & K_{55} & K_{56} \\ K_{16} & 0 & 0 & 0 & K_{65} & K_{66} \end{bmatrix} \tag{3.70}$$

4. xz-and yz-planes of symmetry (port/starboard and fore/aft symmetries)

$$\boldsymbol{K}(j\omega) = \boldsymbol{K}^T(j\omega) = \begin{bmatrix} K_{11} & 0 & 0 & 0 & K_{15} & 0 \\ 0 & K_{22} & 0 & K_{24} & 0 & 0 \\ 0 & 0 & K_{33} & 0 & 0 & 0 \\ 0 & K_{24} & 0 & K_{44} & 0 & 0 \\ K_{15} & 0 & 0 & 0 & K_{55} & 0 \\ 0 & 0 & 0 & 0 & 0 & K_{66} \end{bmatrix} \tag{3.71}$$

5. xz-,yz-and xy-planes of symmetry (port/starboard, fore/aft and bottom/top symmetries)

$$\boldsymbol{K}(j\omega) = \boldsymbol{K}^T(j\omega) = \text{diag}\left[K_{11}, K_{22}, K_{33}, K_{44}, K_{55}, K_{66}\right] \tag{3.72}$$

Hence, the symmetry properties of a marine structure are important information. This can be used in the identification process to reduce the number of systems which need to be identified.

Based on what we have found in Section 3.2 and this Section, the following identification criteria can be put up,

- The overall 6×6 transfer function matrix $\boldsymbol{K}(s)$ should be positive real.
- The transfer functions $K_{ij}(s)\ \forall\ i = (1, \ldots, 6),\ j = (1, \ldots, 6)$ should be strictly proper of relative degree 1 and stable.

- The transfer functions $K_{ii}(s)\ \forall\ i = (1, \ldots, 6)$ should be positive real.
- Symmetry properties can be utilized to reduce the number of transfer functions that need to be identified, since $K_{ij}(s) = K_{ji}(s)$ and some elements might be 0 due to body symmetry.

3.4 Alternative Convolution Representation

An alternative convolution representation of the radiation forces was proposed by Wehausen (1971) and Falnes (2002)

$$\boldsymbol{\tau}_R(t) = -\boldsymbol{M}_A\ddot{\boldsymbol{\xi}}(t) - \int_0^t \boldsymbol{l}(t-\tau)\ddot{\boldsymbol{\xi}}(\tau)\ d\tau \tag{3.73}$$

$$\boldsymbol{\tau}_{R1}(t) = \boldsymbol{M}_A\ddot{\boldsymbol{\xi}}(t) \tag{3.74}$$

$$\boldsymbol{\tau}_{R2}(t) = \int_0^t \boldsymbol{l}(t-\tau)\ddot{\boldsymbol{\xi}}(\tau)\ d\tau \tag{3.75}$$

where the kernel of the convolution can be found from (Falnes, 2002)

$$\boldsymbol{l}(t) = \frac{2}{\pi}\int_0^\infty (\boldsymbol{A}(\omega) - \boldsymbol{M}_A)\cos(\omega t)\ d\omega \tag{3.76}$$

$$= \frac{2}{\pi}\int_0^\infty \frac{\boldsymbol{B}(\omega)}{\omega}\sin(\omega t) d\omega \tag{3.77}$$

The frequency response can be written as

$$\boldsymbol{L}(j\omega) = (\boldsymbol{A}(\omega) - \boldsymbol{M}_A) + \frac{\boldsymbol{B}(\omega)}{j\omega} \tag{3.78}$$

$$= (\boldsymbol{A}(\omega) - \boldsymbol{M}_A) - j\frac{\boldsymbol{B}(\omega)}{\omega} \tag{3.79}$$

In Falnes (2002) it is assumed that $\boldsymbol{B}(\omega)$ tends sufficiently fast to zero at $\omega \to 0$ to make $\boldsymbol{L}(j\omega)$ non-singular at $\omega = 0$. The magnitude, $|L_{ij}(j\omega)|$, and the phase, $\angle L_{ij}(j\omega)$, of $L_{ij}(j\omega)$ are

$$|L_{ij}(j\omega)| = \sqrt{(A_{ij}(\omega) - M_{Aij})^2 + \left(-\frac{B_{ij}(\omega)}{\omega}\right)^2} \tag{3.80}$$

$$\angle L_{ij}(j\omega) = \arctan\left(\frac{-B_{ij}(\omega)}{\omega(A_{ij}(\omega) - M_{Aij})}\right) \tag{3.81}$$

Let the Laplace transform (B.15) of the radiation forces be written as

$$\begin{aligned} -\boldsymbol{\tau}_R(s) &= \mathcal{L}\{-\boldsymbol{\tau}_R(t)\} && (3.82)\\ &= \int_0^\infty \left(\boldsymbol{M}_A \ddot{\xi}(t) + \int_0^t \boldsymbol{l}(t-\tau)\ddot{\boldsymbol{\xi}}(\tau)\ d\tau \right) e^{-st} dt && (3.83)\\ &= (\boldsymbol{M}_A + \boldsymbol{L}(s))\ddot{\boldsymbol{\xi}}(s) && (3.84)\\ &= \hat{\boldsymbol{H}}(s)\ddot{\boldsymbol{\xi}}(s) && (3.85) \end{aligned}$$

Using the expression for $\boldsymbol{L}(j\omega)$ from (3.79) gives

$$\begin{aligned} \hat{\boldsymbol{H}}(j\omega) &= \boldsymbol{M}_A + \boldsymbol{L}(j\omega) && (3.86)\\ &= \boldsymbol{A}(\omega) - j\frac{\boldsymbol{B}(\omega)}{\omega} && (3.87) \end{aligned}$$

The two representations (3.12) and (3.85) for the radiation forces in the Laplace domain exist

$$\begin{aligned} -\boldsymbol{\tau}_R(s) &= \bar{\boldsymbol{H}}(s)\dot{\boldsymbol{\xi}}(s) && (3.88)\\ &= \hat{\boldsymbol{H}}(s)\ddot{\boldsymbol{\xi}}(s) && (3.89) \end{aligned}$$

where the transfer function $\hat{\boldsymbol{H}}(s)$ can be split into

$$\begin{aligned} \hat{\boldsymbol{H}}(s) &= \hat{\boldsymbol{H}}(\infty) + \hat{\boldsymbol{H}}_{sp}(s) && (3.90)\\ \hat{\boldsymbol{H}}(\infty) &= \boldsymbol{M}_A && (3.91)\\ \hat{\boldsymbol{H}}_{sp}(s) &= \boldsymbol{L}(s) && (3.92) \end{aligned}$$

where *sp* stands for strictly proper. Further the radiation forces can be written out as

$$\begin{aligned} -\boldsymbol{\tau}_R(s) &= (\boldsymbol{M}_A s + \boldsymbol{K}(s))\dot{\boldsymbol{\xi}}(s) && (3.93)\\ &= (\boldsymbol{M}_A + \boldsymbol{L}(s))\ddot{\boldsymbol{\xi}}(s) && (3.94)\\ &= (\boldsymbol{M}_A s + s\boldsymbol{L}(s))\dot{\boldsymbol{\xi}}(s) && (3.95) \end{aligned}$$

hence

$$\begin{aligned} \boldsymbol{M}_A s + s\boldsymbol{L}(s) &= \boldsymbol{M}_A s + \boldsymbol{K}(s) && (3.96)\\ &\Downarrow && (3.97)\\ \boldsymbol{L}(s) &= \frac{1}{s}\boldsymbol{K}(s) && (3.98) \end{aligned}$$

Taking the inverse Laplace transform (B.19) gives the following relation between the two convolution representations

$$\boldsymbol{l}(t) = \int_0^t \boldsymbol{k}(\tau)\ d\tau \qquad (3.99)$$

Using (3.61) together with (3.98) gives the following expressions for the transfer function $L_{ij}(s)$,

$$L_{ij}(s) = \frac{b_{n-1}s^{n-2} + \cdots + b_2 s + b_1}{s^n + a_{n-1}s^{n-1} + \cdots + a_1 s + a_0} \tag{3.100}$$

It was shown in Section 3.2 that the mapping from $\dot{\boldsymbol{\xi}} \rightarrow -\boldsymbol{\tau}_R$ is passive. The same general conclusion cannot be done for the mapping from $\ddot{\boldsymbol{\xi}} \rightarrow -\boldsymbol{\tau}_R$. Since we have strictly proper transfer functions of relative degree 2, the mapping $\ddot{\boldsymbol{\xi}} \rightarrow -\boldsymbol{\tau}_R$ does not have the same positive real property as the mapping $\dot{\boldsymbol{\xi}} \rightarrow -\boldsymbol{\tau}_R$.

As for the transfer functions $K_{ij}(s)$ the relative degree of the transfer function $L_{ij}(s)$ can be confirmed by comparing it with the values of the frequency responses at $\omega = 0$ and $\omega = \infty$ together with the initial and final values of the impulse responses.

Frequency response at $\boldsymbol{\omega = 0}$

The value of $\boldsymbol{L}(j\omega)$ as ω tends to zero is

$$\lim_{\omega \to 0} \boldsymbol{L}(j\omega) = \lim_{\omega \to 0}((\boldsymbol{A}(\omega) - \boldsymbol{M}_A) - j\frac{\boldsymbol{B}(\omega)}{\omega}) = (\boldsymbol{A}(0) - \boldsymbol{M}_A) \tag{3.101}$$

hence

$$\lim_{\omega \to 0} L_{ij}(j\omega) = (A_{ij}(0) - M_{Aij}),\ \forall\ i = (1, \ldots, 6),\ j = (1, \ldots, 6) \tag{3.102}$$

Let us now take the limit of the transfer function in (3.100):

$$\lim_{\omega \to 0} L_{ij}(j\omega) = \lim_{\omega \to 0} \frac{b_{n-1}(j\omega)^{n-2} + \cdots + b_2(j\omega) + b_1}{(j\omega)^n + a_{n-1}(j\omega)^{n-1} + \cdots + a_1(j\omega) + a_0} = \frac{b_1}{a_0} \tag{3.103}$$

In order for this to be in accordance with (3.102)

$$(A_{ij}(0) - M_{Aij}) = \frac{b_1}{a_0} \tag{3.104}$$

Frequency response at $\boldsymbol{\omega = \infty}$

The value of the frequency response at $\omega = \infty$ is

$$\lim_{\omega \to \infty} \boldsymbol{L}(j\omega) = \lim_{\omega \to \infty}((\boldsymbol{A}(\omega) - \boldsymbol{M}_A) - j\frac{\boldsymbol{B}(\omega)}{\omega}) = \boldsymbol{0} \tag{3.105}$$

hence

$$\lim_{\omega \to \infty} L_{ij}(j\omega) = 0,\ \forall\ i = (1, \ldots, 6),\ j = (1, \ldots, 6) \tag{3.106}$$

Let us now take the same limit for the transfer function in (3.100)

$$\lim_{\omega\to\infty} L_{ij}(j\omega) = \lim_{\omega\to\infty} L_{ij}(j\omega) = \frac{b_{n-1}(j\omega)^{n-2} + \cdots + b_2(j\omega) + b_1}{(j\omega)^n + a_{n-1}(j\omega)^{n-1} + \cdots + a_1(j\omega) + a_0} = 0 \tag{3.107}$$

This is in accordance with the result in (3.106).

Initial value of impulse response

Use of the initial value theorem on (3.100) gives

$$\lim_{t\to 0^+} l_{ij}(t) = \lim_{s\to\infty} sL_{ij}(s) = \lim_{s\to\infty} \frac{s(b_{n-1}s^{n-2} + \cdots + b_1)}{s^n + a_{n-1}s^{n-1} + \cdots + a_1 s + a_0} = 0 \tag{3.108}$$

Final value of impulse response

As time goes to infinity, the Riemann-Lebesgue lemma can be used to find the final value of the impulse response $l(t)$. By comparing (B.1) and (3.77), one can see that the impulse response tends to zero as times goes to infinity

$$\lim_{t\to\infty} \boldsymbol{l}(t) = \lim_{t\to\infty} \frac{2}{\pi} \int_0^\infty \frac{\boldsymbol{B}(\omega)}{\omega} \sin(\omega t)\, d\omega = \mathbf{0} \tag{3.109}$$

hence

$$\lim_{t\to\infty} l_{ij}(t) = 0,\ \forall\ i = (1,\ldots,6),\ j = (1,\ldots,6) \tag{3.110}$$

Use of the final-value theorem (B.17) on (3.100) gives

$$\lim_{t\to\infty} l(t) = \lim_{s\to 0} sL_{ij}(s) = \lim_{s\to 0} \frac{s(b_{n-1}s^{n-2} + \cdots + b_1)}{s^n + a_{n-1}s^{n-1} + \cdots + a_1 s + a_0} = 0 \tag{3.111}$$

This is in accordance with the result in (3.109). The transfer functions representing the hydrodynamic actions can now be written

$$L_{ij}(s) = \frac{b_{n-1}s^{n-2} + \cdots + b_1}{s^n + a_{n-1}s^{n-1} + \cdots + a_1 s + a_0} \tag{3.112}$$

As for the convolution from velocity to force BIBO stability can be shown and the following proposition can be stated,

Proposition 3.6 *The linear SISO systems represented by the impulse responses $l_{ij}(t)$ in (3.75) are BIBO stable.*

Proof. Since $l_{ij}(t)$ is absolutely integrable

$$\int_0^\infty |l_{ij}(t)| < \infty, \ \forall \ i = (1, \ldots, 6), \ j = (1, \ldots, 6) \tag{3.113}$$

it can be concluded that the SISO systems represented by the impulse responses $l_{ij}(t)$ are BIBO stable (see Theorem B.1). ■
Further, in the same manner as for the convolution from velocity to force $\mathcal{L}_p$ input-output stability can be shown.

Proposition 3.7 *The linear SISO systems represented by the impulse responses $l_{ij}(t)$ in (3.75) are $\mathcal{L}_p$ input-output stable for $1 \leq p \leq \infty$.*

Proof. For SISO systems, the $\mathcal{L}_1$ and the $\mathcal{L}_\infty$ norms of the convolution operator $\mathcal{S} : u \mapsto y = \mathcal{S}(u) = h * u$ are the same and equal to $\int_0^\infty |h(t)| \, dt$ (Antoulas, 2005). By use of (3.113) and Proposition B.1 it can be concluded that the SISO systems represented by the impulse responses $l_{ij}(t)$ are $\mathcal{L}_p$ input-output stable for $1 \leq p \leq \infty$. ■

When the SISO systems $L_{ij}(s)$ are represented by transfer functions of relative degree two, the overall state-space system representing the hydrodynamic actions can be written

$$\dot{\boldsymbol{x}}(t) = \boldsymbol{A}\boldsymbol{x}(t) + \boldsymbol{B}\ddot{\boldsymbol{\xi}}(t) \tag{3.114}$$

$$\boldsymbol{\tau}_{R2}(t) = \boldsymbol{C}\boldsymbol{x}(t) \tag{3.115}$$

or in the Laplace domain as

$$\boldsymbol{\tau}_{R2}(s) = \boldsymbol{L}(s)\ddot{\boldsymbol{\xi}}(s) \tag{3.116}$$

$$\boldsymbol{L}(s) = \boldsymbol{C}(sI - \boldsymbol{A})^{-1}\boldsymbol{B} \tag{3.117}$$

By use of Theorem B.2 and Proposition 3.7 it can be concluded that $\boldsymbol{A}$ in (3.117) should be Hurwitz. Now, the convolution term in the equations of motion can be replaced by the state-space model in the time domain

$$\boldsymbol{M}\ddot{\xi}(t) + \boldsymbol{\tau}_{R2}(t) + \boldsymbol{C}_h\boldsymbol{\xi}(t) = \boldsymbol{\tau}_{visc} + \boldsymbol{\tau}_{ext} + \boldsymbol{\tau}_A \tag{3.118}$$

$$\dot{\boldsymbol{x}}(t) = \boldsymbol{A}\boldsymbol{x}(t) + \boldsymbol{B}\ddot{\boldsymbol{\xi}}(t) \tag{3.119}$$

$$\boldsymbol{\tau}_{R2}(t) = \boldsymbol{C}\boldsymbol{x}(t) \tag{3.120}$$

taking (3.84) into consideration, this can also be written as

$$\boldsymbol{M}_{RB}\ddot{\boldsymbol{\xi}}(t) + \boldsymbol{\tau}_R(t) + \boldsymbol{C}_h\boldsymbol{\xi}(t) = \boldsymbol{\tau}_{visc} + \boldsymbol{\tau}_{ext} + \boldsymbol{\tau}_A \tag{3.121}$$

$$\dot{\boldsymbol{x}}(t) = \boldsymbol{A}\boldsymbol{x}(t) + \boldsymbol{B}\ddot{\boldsymbol{\xi}}(t) \tag{3.122}$$

$$\boldsymbol{\tau}_R(t) = \boldsymbol{C}\boldsymbol{x}(t) + \boldsymbol{M}_A\ddot{\boldsymbol{\xi}}(t) \tag{3.123}$$

This gives the following representation in the Laplace domain

$$(\boldsymbol{M} + \boldsymbol{L}(s))\ddot{\boldsymbol{\xi}}(s) + \boldsymbol{C}_h\boldsymbol{\xi}(s) = \boldsymbol{\tau}_{visc}(s) + \boldsymbol{\tau}_{ext}(s) + \boldsymbol{\tau}_A(s) \tag{3.124}$$

Figure 3.4 shows the vessel model with the acceleration convolution. Having

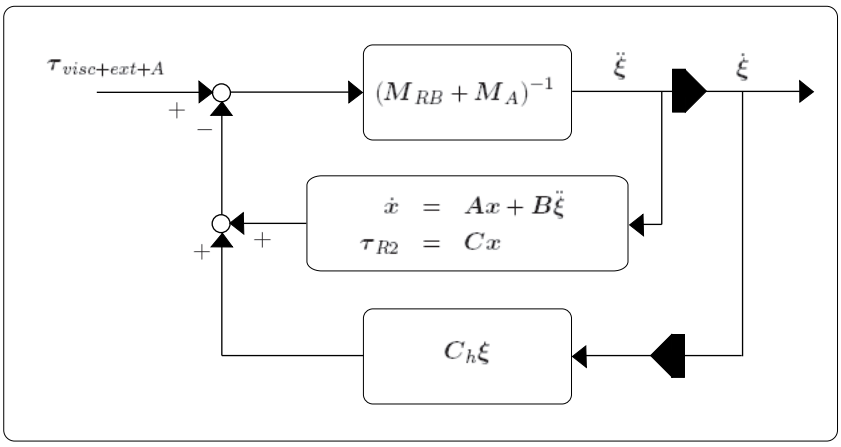

Figure 3.4: The vessel model with acceleration convolution

the defined state vector as in (3.65), one can see that the system in (3.118)-(3.120) cannot be represented by a state-space system as compared to the system in (3.62)-(3.64). Hence it is preferable to use the velocity convolution compared to the acceleration convolution. Also the positive real property of the velocity convolution gives a lot of information in the identification process. Furthermore, positive realness of $\boldsymbol{K}(s)$ ensures the passivity of the mapping from $\boldsymbol{\tau}_{visc} + \boldsymbol{\tau}_A + \boldsymbol{\tau}_{ext} \rightarrow \dot{\boldsymbol{\xi}}$ because of the properties satisfied by the matrices $\boldsymbol{M}$ and $\boldsymbol{C}_h$ (see (3.29) and (3.30)).

3.5 Concluding Remarks

In this chapter the stability properties of the radiation forces have been investigated. It has been shown that the convolution part of the radiation forces, as approximated by a state-space model, represents a stable system. Further it has been shown that the radiation forces are passive. The inclusion of passive radiation forces in the overall vessel model will give a passive system from force input, $\boldsymbol{\tau}_{visc} + \boldsymbol{\tau}_{ext} + \boldsymbol{\tau}_A$, to the velocity output, $\dot{\boldsymbol{\xi}}$.

Further it has been shown that the convolution representation can be approximated by a state-space representation. The structure of this type

of model has been developed based on knowledge about the frequency dependent added mass and damping, and the design criteria for the radiation forces model have been discussed.

An alternative convolution representation for the radiation forces has also been investigated. This convolution contains the vessel acceleration instead of the velocity. The convolution containing velocity is passive, while the one containing acceleration is not. Also the convolution containing velocity is more appropriate for numerical simulations than the one containing acceleration. Hence, it is concluded to use the velocity convolution, and replace this with a state-space representation.

The next chapter will give an overview of different identification methods to approximate the radiation forces.

Chapter 4

Identification Methods

4.1 Introduction

The frequency dependent added mass matrix $\boldsymbol{A}(\omega)$ and damping $\boldsymbol{B}(\omega)$ are given by the numerical hydrodynamic software. As seen in the previous chapters, the frequency response of the radiation forces is given by

$$\boldsymbol{K}(j\omega) = \boldsymbol{B}(\omega) + j\omega(\boldsymbol{A}(\omega) - \boldsymbol{M}_A) \tag{4.1}$$

and the impulse response can be found from (2.60)

$$\boldsymbol{k}(t) = \frac{2}{\pi}\int_0^\infty \boldsymbol{B}(\omega)\cos\omega t \; d\omega \tag{4.2}$$

Given the frequency domain description in (4.1) or the time domain description in (4.2) it is preferable to represent radiation forces as a state-space model like in (3.63)-(3.64). This can be done either by time domain identification or by frequency domain identification as illustrated in Figure 4.1.

In this chapter, methods intended for use in the identification of the radiation forces will be reviewed. Section 4.2 reviews a scheme for identification from the impulse response. This is based on Markov parameter estimation, and was first proposed by Kung (1978).

The frequency response is a nonparametric representation of the relationship between the inputs and outputs as a function of frequency. The convolution kernel can be used in simulations, while for the frequency response a parametric model has to be created. Two different frequency domain identification methods are reviewed in Section 4.3: a least squares and a prediction-error minimization approach.

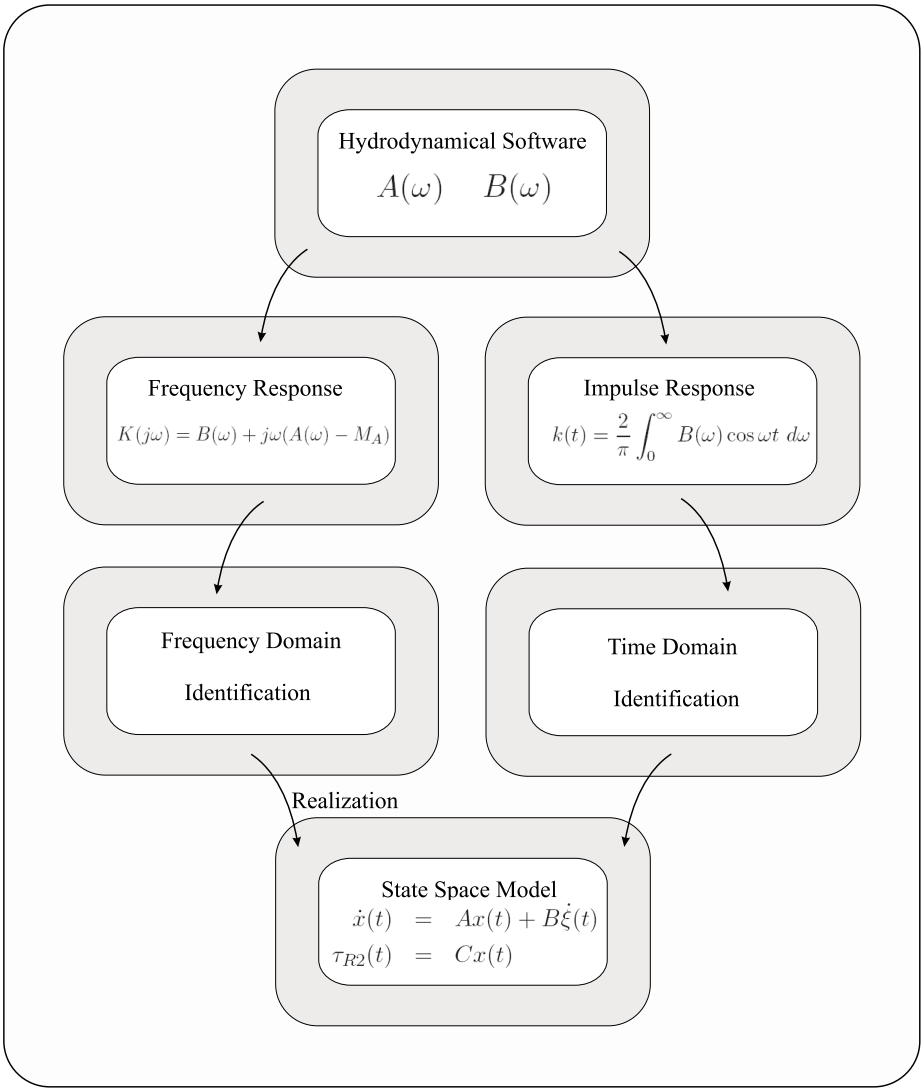

Figure 4.1: Identification of the convolution term

4.2 Time Domain Identification

Given the impulse response $\boldsymbol{k}(t)$, we now want to find a state-space realization $(\boldsymbol{A}, \boldsymbol{B}, \boldsymbol{C}, \boldsymbol{D})$ of the hydrodynamic actions. Kristiansen *et al.* (2005) proposed to represent the state-space system of the radiation forces by the use of Markov parameter estimation. This approach will be further explored

in this section.

The overview here follows Antoulas (2005). Given a SISO transfer function $H(s)$ it can be written as

$$H(s) = \boldsymbol{C}(sI - \boldsymbol{A})^{-1}\boldsymbol{B} + \boldsymbol{D} = \frac{N(s)}{D(s)} + \boldsymbol{D} \tag{4.3}$$

$H(s)$ is then expanded in a Taylor series

$$\begin{aligned} H(s) &= \boldsymbol{D} + \frac{1}{s}\boldsymbol{CB} + \frac{1}{s^2}\boldsymbol{CAB} + \cdots + \frac{1}{s^k}\boldsymbol{CA}^{k-1}\boldsymbol{B} + \cdots & (4.4)\\ &= h_0 + h_1\frac{1}{s} + h_2\frac{1}{s^2} + \cdots + h_{k-1}\frac{1}{s^k} + \cdots & (4.5) \end{aligned}$$

The parameters h_i are called the Markov parameters of the system,

$$\mathcal{M} = (h_0, h_1, h_2, \ldots, h_{k-1}, \ldots) \tag{4.6}$$

The Markov parameters can also be found from the impulse response of the SISO system,

$$\begin{aligned} y(t) &= \int_0^\infty h(t-\tau)u(\tau)\ d\tau & (4.7)\\ &= h_0 u(t) + \int_0^\infty h_a(t-\tau)u(\tau)\ d\tau & (4.8) \end{aligned}$$

By assuming that $h_a(t)$ is an analytic function, $h_a(t)$ can be determined by the coefficients of its Taylor series expansion around $t = 0^+$

$$h_a(t) = h_1 + \frac{t}{1!}h_2 + \cdots + \frac{t^{k-2}}{(k-2)!}h_{k-1} + \cdots \tag{4.9}$$

The Markov parameters of the radiation forces can be computed from the integral

$$k_{ij}(t) = \frac{2}{\pi}\int_0^t B_{ij}(\omega)\cos(\omega t)\ d\omega \tag{4.10}$$

Hence, given a large set of Markov parameters of an unknown transfer function $K_{ij}(s)$ we want to find a minimal realization $(\boldsymbol{A}, \boldsymbol{B}, \boldsymbol{C}, \boldsymbol{D})$ whose transfer function $K_{ij}(s) = \boldsymbol{C}(sI - \boldsymbol{A})^{-1}\boldsymbol{B} + \boldsymbol{D}$, where the impulse response $k_{ij}(t)$ satisfies

$$k_{ij}(t) = \boldsymbol{C}e^{\boldsymbol{A}t}\boldsymbol{B} + \delta(t)\boldsymbol{D}, \quad t \geq 0 \tag{4.11}$$

The Hankel singular value decomposition (SVD) method proposed by Kung (1978) will be used. This method is implemented in the Robust Control

Toolbox in MATLAB as imp2ss. The realization of the model is done in discrete time, before a continuous time model is obtained via the inverse Tustin transformation. Having the impulse response vector taken at the intervals t_k

$$k_{ij}(t_k) \tag{4.12}$$

the Markov parameters can be obtained

$$\begin{aligned} \mathcal{M} &= (k_{ij}(0), k_{ij}(t_1), k_{ij}(t_2), k_{ij}(t_3), \ldots, k_{ij}(t_{2n+1})) && (4.13)\\ &= (k_0, k_1, k_2, \ldots, k_{2n}, k_{2n+1}) && (4.14) \end{aligned}$$

where t_s is the sampling time

$$t_s = t_2 - t_1 \tag{4.15}$$

The input to the function imp2ss are the Markov parameters in (4.14) and the continuous time matrices $(\boldsymbol{A}, \boldsymbol{B}, \boldsymbol{C}, \boldsymbol{D})$ are returned. The algorithm is written out sequentially below.

---

1. From the Markov parameters form the Hankel matrix

$$\mathcal{H}_{n+1} = \begin{bmatrix} k_1 & k_2 & \cdots & k_n \\ k_2 & k_3 & \cdots & k_{n+1} \\ \vdots & \vdots & \ddots & \vdots \\ k_{n+1} & k_{n+2} & \cdots & k_{2n+1} \end{bmatrix} \tag{4.16}$$

2. Take the singular value decomposition of the Hankel matrix

$$\mathcal{H}_{n+1} = \boldsymbol{U}\boldsymbol{\Sigma}\boldsymbol{V}^T \tag{4.17}$$

   here $\boldsymbol{\Sigma} = \text{diag}(\sigma_1 \geq \sigma_2 \geq \ldots \geq \sigma_k \geq 0, \ldots, 0)$ where k gives the McMilan degree of the system.

3. Form the matrices

$$\begin{aligned} \bar{\boldsymbol{U}} &= \boldsymbol{U}\boldsymbol{\Sigma}^{1/2} && (4.18)\\ \bar{\boldsymbol{V}} &= \boldsymbol{\Sigma}^{1/2}\boldsymbol{V}^T && (4.19) \end{aligned}$$

   where $\boldsymbol{\Sigma}^{1/2} = \text{diag}(\sigma_1^{1/2}, \sigma_2^{1/2}, \ldots, \sigma_k^{1/2}, 0, \ldots, 0)$. Further, let

$$\begin{aligned} \boldsymbol{U}_1^{\dagger} &= \bar{\boldsymbol{U}}(1:n, 1:k) && (4.20)\\ \boldsymbol{U}_2 &= \bar{\boldsymbol{U}}(2:n+1, 1:k) && (4.21)\\ \boldsymbol{U}^1 &= \bar{\boldsymbol{U}}(1, 1:k) && (4.22)\\ \boldsymbol{V}^1 &= \bar{\boldsymbol{V}}(1:k, 1) && (4.23) \end{aligned}$$

4. Compute the discrete-time system matrices in the transfer function $H_d(z) = \boldsymbol{C}_d(z\boldsymbol{I} - \boldsymbol{A}_d)\boldsymbol{B}_d + \boldsymbol{D}_d$

$$\begin{aligned} \boldsymbol{A}_d &= \boldsymbol{U}_1^{\dagger}\boldsymbol{U}_2 && (4.24)\\ \boldsymbol{B}_d &= \boldsymbol{V}^1 && (4.25)\\ \boldsymbol{C}_d &= \boldsymbol{U}^1 && (4.26)\\ \boldsymbol{D}_d &= k_0 && (4.27) \end{aligned}$$

5. The continuous-time state-space matrices can now be obtained through the bilinear Tustin transformation $H_d(z)|_{z=\frac{\frac{2}{t_s}+s}{\frac{2}{t_s}-s}} \rightarrow H(s)$

$$\begin{aligned} \boldsymbol{A} &= \frac{2}{t_s}(\boldsymbol{A}_d + \boldsymbol{I})^{-1}(\boldsymbol{A}_d - \boldsymbol{I}) && (4.28)\\ \boldsymbol{B} &= \frac{2}{\sqrt{t_s}}(\boldsymbol{A}_d + \boldsymbol{I})^{-1}\boldsymbol{B}_d && (4.29)\\ \boldsymbol{C} &= \frac{2}{\sqrt{t_s}}\boldsymbol{C}_d(\boldsymbol{A}_d + \boldsymbol{I})^{-1} && (4.30)\\ \boldsymbol{D} &= \boldsymbol{D}_d - \boldsymbol{C}_d(\boldsymbol{A}_d + \boldsymbol{I})^{-1}\boldsymbol{B}_d && (4.31) \end{aligned}$$

The continuous time state-space matrices are obtained through the bilinear Tustin transformation. A discrete-time system is stable if the poles of its transfer function are inside the unit circle in the complex z-plane. The bilinear Tustin approximation ensures that stable state-space systems designed in the discrete-time domain are converted to stable continuous time state-space systems. The algorithm does not ensure a positive real realization. Because of the conversion from discrete-time to continuous-time the $\boldsymbol{D}$ matrix in the realization is nonzero. This type of realization can be used both for SISO and MIMO identification.

4.3 Frequency Domain Identification

This section will investigate the identification of state-space models based on the frequency response of the system. The problem can be formulated as follows: given the n frequencies and frequency response pairs $(\omega_k, \bar{\boldsymbol{K}}(j\omega_k))$ measured at the frequencies $\omega_k,\ k = 1, \ldots, n$ find the system transfer function $\boldsymbol{K}(s)$.

For the different SISO modes the complex frequency response obtained at different frequencies can be written as

$$\bar{\boldsymbol{Z}}^N = \{\bar{K}_{ij}(j\omega_1), \ldots, \bar{K}_{ij}(j\omega_N)\} \quad (4.32)$$

From this a physically parameterized continuous time transfer function can be obtained

$$K_{ij}(s) = \frac{N_{ij}(s)}{D_{ij}(s)} = \frac{b_n s^n + b_{n-1}s^{n-1} + \cdots + b_1 s}{s^n + a_{n-1}s^{n-1} + a_1 s + a_0} \tag{4.33}$$

by use of least squares curve fitting. Replacing s by $j\omega$, the latter equation can be expressed as a function of frequency

$$K_{ij}(j\omega) = \frac{N_{ij}(j\omega)}{D_{ij}(j\omega)} = \frac{b_n j\omega^n + b_{n-1}j\omega^{n-1} + \cdots + b_1 j\omega}{j\omega^n + a_{n-1}j\omega^{n-1} + a_1 j\omega + a_0} \tag{4.34}$$

The transfer function $K_{ij}(s)$ can be found by use of the invfreqs function in the MATLAB Signal Processing Toolbox. The algorithm is based on a least squares approach (Levi, 1959)

$$\min_{b,a} \sum_{k=1}^{N} W(j\omega_k)|\bar{K}_{ij}(j\omega_k)D_{ij}(j\omega_k) - N_{ij}(j\omega_k)|^2 \tag{4.35}$$

in order to fit the best model to the given data. W is a weighting function over the different frequencies. This identification scheme ensures stable systems, but positive realness of the identified system is not ensured. As implemented in invfreqs the scheme only supports SISO identification.

Another approach is to use prediction-error minimization identification, a function called pem is provided in the System Identification Toolbox in MATLAB. This function supports both time and frequency domain identification. Local optimization algorithms are used in prediction error minimization methods. Given the original data set, a parameterized continuous time model can be obtained for each mode

$$\dot{\boldsymbol{x}}_{ij}(t) = \boldsymbol{A}_{ij}(\boldsymbol{\theta})\boldsymbol{x}_{ij}(t) + \boldsymbol{B}_{ij}(\boldsymbol{\theta})\dot{\xi}_i(t) \tag{4.36}$$

$$y_j(t,\boldsymbol{\theta}) = \boldsymbol{C}_{ij}(\boldsymbol{\theta})\boldsymbol{x}_{ij}(t) \tag{4.37}$$

Here $\tau_{R2j}(t)$ is approximated by $y_j(t,\boldsymbol{\theta})$. This corresponds to the following frequency response

$$K_{ij}(j\omega,\boldsymbol{\theta}) = \boldsymbol{C}_{ij}(\boldsymbol{\theta})(j\omega\boldsymbol{I} - \boldsymbol{A}_{ij}(\boldsymbol{\theta}))^{-1}\boldsymbol{B}_{ij}(\boldsymbol{\theta}) \tag{4.38}$$

In the time domain, the prediction error associated with a certain choice of parameters, $\boldsymbol{\theta}_*$ can be expressed as

$$\varepsilon(t,\boldsymbol{\theta}_*) = y(t) - y(t,\boldsymbol{\theta}_*) \tag{4.39}$$

The optimal choice of the parameters in $\boldsymbol{\theta}$ can be done in different ways. Given the time domain data set of the system

$$\boldsymbol{Z}^N = [y_1, u_1, y_2, u_2, \ldots, y_N, u_N] \tag{4.40}$$

choose a cost function (this is just an example of a possible choice, a lot of different criteria can be used)

$$V_N(\boldsymbol{\theta}, \boldsymbol{Z}^N) = \frac{1}{N}\sum_{t=1}^{N}\frac{1}{2}\varepsilon(t,\boldsymbol{\theta})^2 \tag{4.41}$$

pick the best model

$$\hat{\boldsymbol{\theta}}_N = \arg\min_{\boldsymbol{\theta}\in\boldsymbol{\Theta}} V_N(\boldsymbol{\theta}, \boldsymbol{Z}^N) \tag{4.42}$$

A similar expression can be found for the frequency domain approach. A thorough overview over the different approaches in the time and frequency domain is given in Ljung (1999). When frequency domain data are given, the algorithm is initialized by the use of subspace approximation before an iterative optimization search is done in order to find the best model fit. The scheme ensures stable systems, but positive realness is not ensured. The scheme supports both SISO and MIMO identification.

4.4 Concluding Remarks

A review of time and frequency identification methods has been given in this chapter. One method is intended for identification of state-space models from the impulse response of the radiation forces. This method is based on Markov parameter estimation. Two frequency domain approaches have also been investigated. One is based on a least squares curve fitting and the other is based on prediction error minimization.

Both the time domain and frequency domain identification schemes presented here do not ensure positive realness of the overall model. It is out of the scope of this thesis to deal with this subject. Relevant references are among others Damaren *et al.* (1996) and Coelho *et al.* (2004).

In Chapter 6 the different methods presented in this chapter will be used in order to obtain state-space models of radiation forces for inclusion in the vessel models. The different identification schemes will be compared for this use.

Chapter 5

Model Reduction

5.1 Introduction

In simulation and control there is a need for efficient and compact mathematical models. Model reduction is a tool for reducing the size of high order mathematical models, where the focus is on approximating the most important dynamical features of the original model. Model order reduction is used in a wide variety of applications and different fields, such as very large-scale integration (VLSI) chip design, simulation of micro-electro-mechanical systems (MEMS), image processing, financial models, weather and air quality prediction and control design and synthesis.

This chapter gives an overview of already existing model reduction methods. First the focus is on order reduction by balanced truncation, which is well suited and efficient for systems of moderate size (say, of an order of a few thousands). Recent results have shown that this type of algorithms also is promising for higher order systems, as more efficient algorithms are being developed (Benner *et al.*, 2005).

Positive real systems describe a class of systems which cannot generate energy internally; they can store and dissipate energy, but they cannot produce energy. For such systems, it is important that any approximate model reflects this property in order to avoid nonphysical behavior when used in numerical simulations. This is a useful property, which we would like to preserve in the model reduction process, and there are balanced truncation methods that indeed preserve the positive realness of a system during the reduction process. In this chapter a new algorithm in this class is presented, which is computationally efficient.

An introduction to the most common balancing schemes is given in Section 5.2, Lyapunov balancing and stochastic balancing. Based on these al-

gorithms a novel algorithm, which constructs positive real reduced order systems, is proposed. A numerical example is given, where the different schemes are compared in terms of computational efficiency and accuracy. In Section 5.3 properties are stated which are required in order to yield positive real reduced order systems. Then this result is used to develop a method for positive real frequency weighted truncation.

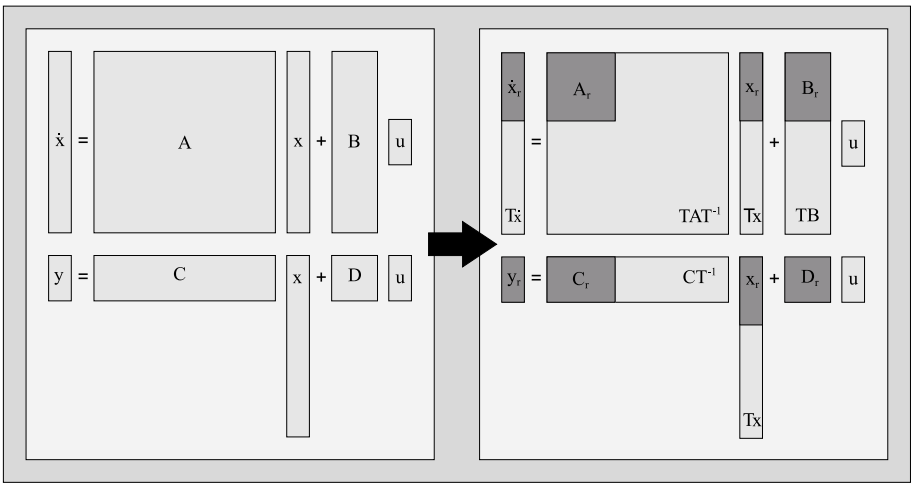

Figure 5.1: Order reduction by projection

5.2 Balanced Truncation

For an nth order minimal linear time invariant (LTI) system in state-space form

$$\dot{\boldsymbol{x}}(t) = \boldsymbol{A}\boldsymbol{x}(t) + \boldsymbol{B}\boldsymbol{u}(t) \tag{5.1}$$
$$\boldsymbol{y}(t) = \boldsymbol{C}\boldsymbol{x}(t) + \boldsymbol{D}\boldsymbol{u}(t) \tag{5.2}$$

where $\boldsymbol{A} \in \mathbb{R}^{n\times n}$, $\boldsymbol{B} \in \mathbb{R}^{n\times m}$, $\boldsymbol{C} \in \mathbb{R}^{p\times n}$ and $\boldsymbol{D} \in \mathbb{R}^{p\times m}$, the associated transfer function is given by

$$\boldsymbol{G}(s) = \boldsymbol{C}(s\boldsymbol{I}_n - \boldsymbol{A})^{-1}\boldsymbol{B} + \boldsymbol{D} \tag{5.3}$$

Model reduction deals with finding a reduced order system, with order $r \leq n$, which captures the main features of the original system, i.e. its dynamics,

system stability, system passivity and possibly some structural properties. The reduced model of order $r \leq n$ is written as

$$\dot{\boldsymbol{x}}_r(t) = \boldsymbol{A}_r \boldsymbol{x}_r(t) + \boldsymbol{B}_r \boldsymbol{u}(t) \tag{5.4}$$
$$\boldsymbol{y}(t) = \boldsymbol{C}_r \boldsymbol{x}_r(t) + \boldsymbol{D}_r \boldsymbol{u}(t) \tag{5.5}$$

where $\boldsymbol{A}_r \in \mathbb{R}^{r\times r}$, $\boldsymbol{B}_r \in \mathbb{R}^{r\times m}$, $\boldsymbol{C}_r \in \mathbb{R}^{p\times r}$ and $\boldsymbol{D}_r \in \mathbb{R}^{p\times m}$, and its associated transfer function is given by

$$\boldsymbol{G}_r(s) = \boldsymbol{C}_r(s\boldsymbol{I}_r - \boldsymbol{A}_r)^{-1}\boldsymbol{B}_r + \boldsymbol{D}_r \tag{5.6}$$

Many different coordinate systems can be used to describe the dynamical system in (5.1). Let $\boldsymbol{T} \in \mathbb{R}^{n\times n}$ be a nonsingular matrix, and let the system undergo a state-space transformation

$$\bar{\boldsymbol{x}}(t) = \boldsymbol{T}\boldsymbol{x}(t) \tag{5.7}$$
$$\dot{\bar{\boldsymbol{x}}}(t) = \boldsymbol{T}\boldsymbol{A}\boldsymbol{T}^{-1}\bar{\boldsymbol{x}}(t) + \boldsymbol{T}\boldsymbol{B}\boldsymbol{u}(t) \tag{5.8}$$
$$\boldsymbol{y}(t) = \boldsymbol{C}\boldsymbol{T}^{-1}\boldsymbol{x}(t) + \boldsymbol{D}\boldsymbol{u}(t) \tag{5.9}$$

The transformed system (5.8)-(5.9) has the same dynamics for any nonsingular matrix $\boldsymbol{T}$. Model reduction can now be done by choosing $\boldsymbol{T}$, in terms of some physical measure, and discard the parts of the transformed state $\bar{\boldsymbol{x}}(t)$ which are less important in terms of that measure. Partitioning the matrices $\boldsymbol{T}\boldsymbol{A}\boldsymbol{T}^{-1}$, $\boldsymbol{T}\boldsymbol{B}$, $\boldsymbol{C}\boldsymbol{T}^{-1}$ accordingly

$$\boldsymbol{T}\boldsymbol{A}\boldsymbol{T}^{-1} = \begin{bmatrix} \bar{\boldsymbol{A}}_{11} & \bar{\boldsymbol{A}}_{12} \\ \bar{\boldsymbol{A}}_{21} & \bar{\boldsymbol{A}}_{22} \end{bmatrix} \tag{5.10}$$
$$\boldsymbol{T}\boldsymbol{B} = \begin{bmatrix} \bar{\boldsymbol{B}}_1 \\ \bar{\boldsymbol{B}}_2 \end{bmatrix} \tag{5.11}$$
$$\boldsymbol{C}\boldsymbol{T}^{-1} = \begin{bmatrix} \bar{\boldsymbol{C}}_1 & \bar{\boldsymbol{C}}_2 \end{bmatrix} \tag{5.12}$$

the reduced order system can thus be written as

$$\boldsymbol{A}_r = \bar{\boldsymbol{A}}_{11},\ \boldsymbol{B}_r = \bar{\boldsymbol{B}}_1,\ \boldsymbol{C}_r = \bar{\boldsymbol{C}}_1,\ \boldsymbol{D}_r = \boldsymbol{D} \tag{5.13}$$

This is illustrated in Figure 5.1. This procedure for reducing systems is called projection-based model order reduction (PBMOR). Different classes of PBMOR are obtained depending on which properties the PBMOR keeps (e.g. stability or passivity) or on how $\boldsymbol{T}$ is chosen.

One important class of the PBMOR methods is balanced truncation, where the coordinate transformation $\boldsymbol{T}$ in (5.7)-(5.9) is chosen such that

two given positive definite matrices (say, $\boldsymbol{M}$ and $\boldsymbol{N}$) are transformed via $\bar{\boldsymbol{M}} := \boldsymbol{T}\boldsymbol{M}\boldsymbol{T}^T$, $\bar{\boldsymbol{N}} := \boldsymbol{T}^{-T}\boldsymbol{N}(\boldsymbol{T}^{-1})$ to become equal and diagonal:

$$\bar{\boldsymbol{M}} = \bar{\boldsymbol{N}} = \boldsymbol{\Sigma} \tag{5.14}$$

The resulting transformed system is then in a so-called balanced coordinate system based on $\boldsymbol{M}$ and $\boldsymbol{N}$. For instance, in order to obtain asymptotically stable systems one chooses $\boldsymbol{M}$ and $\boldsymbol{N}$ as the solution of a Lyapunov equation; for positive real systems one chooses them as a solution of the positive real lemma. The matrices $\boldsymbol{M}$ and $\boldsymbol{N}$ are then clearly related to the properties of the system (i.e. the Lyapunov equations, the positive real equations) and will lead to different types of balancing and hence also to different types of reduced order models. The idea of balanced systems was introduced by Mullis and Roberts (1976) in digital filters, and later introduced to the system and control community by Moore (1981). A comprehensive survey of balanced truncation methods is given in Gugercin and Antoulas (2004).

5.2.1 Lyapunov Balancing

Lyapunov balanced truncation was introduced to the control community by Moore (1981). It is based on the solution of two Lyapunov equations, defining the controllability gramian $\boldsymbol{P}$, and the observability gramian $\boldsymbol{Q}$:

$$\boldsymbol{A}\boldsymbol{P} + \boldsymbol{P}\boldsymbol{A}^T + \boldsymbol{B}\boldsymbol{B}^T = \boldsymbol{0} \tag{5.15}$$

$$\boldsymbol{A}^T\boldsymbol{Q} + \boldsymbol{Q}\boldsymbol{A} + \boldsymbol{C}^T\boldsymbol{C} = \boldsymbol{0} \tag{5.16}$$

Notice that the gramians are positive definite if the system is minimal. The idea behind Lyapunov balancing is to transform the mathematical model to a coordinate system where the states that are difficult to control are also hard to observe. The reduced model is obtained by discarding the states which have this property. In Table 5.1 an algorithm for finding the transformations $\boldsymbol{T}$ and $\boldsymbol{T}^{-1}$ satisfying (5.7)-(5.9) is recalled. Lyapunov balanced truncation then amounts to using the positive definite controllability and observability gramians $(\boldsymbol{P}, \boldsymbol{Q})$ for the matrices $(\boldsymbol{M}, \boldsymbol{N})$.

The physical interpretation of the Lyapunov balancing can be related to the L_2-norm of the input and the output of the system. The controllability and observability gramians $\boldsymbol{P}$ and $\boldsymbol{Q}$ are related to the energy demanded to control and observe the system (Glover, 1984). The controllability gramian $\boldsymbol{P}$ is connected to the solution of the minimum L_2-norm problem

$$\min_{\boldsymbol{u}\in L_2(-\infty,0)} \left\{ \int_{-\infty}^{0} \boldsymbol{u}(t)^T\boldsymbol{u}(t)\, dt \text{ s.t. } \boldsymbol{x}(0) = \boldsymbol{x}_0 \right\} = \boldsymbol{x}_0^T\boldsymbol{P}^{-1}\boldsymbol{x}_0 \tag{5.17}$$

Table 5.1: Balanced Truncation Algorithm

1. Choose a pair of positive definite matrices $(\boldsymbol{M}, \boldsymbol{N})$
2. Compute the Cholesky factorizations of $\boldsymbol{M}$ and $\boldsymbol{N}$
   $\boldsymbol{M} = \boldsymbol{L}_M \boldsymbol{L}_M^T, \quad \boldsymbol{N} = \boldsymbol{L}_N \boldsymbol{L}_N^T$
3. Compute the SVD of $\boldsymbol{L}_M^T \boldsymbol{L}_N$
   $\boldsymbol{L}_M^T \boldsymbol{L}_N = \boldsymbol{U} \boldsymbol{\Sigma} \boldsymbol{V}^T$
4. Construct the balancing transformations
   $\boldsymbol{T} = \boldsymbol{\Sigma}^{1/2} \boldsymbol{U}^T \boldsymbol{L}_M^{-1}, \ \boldsymbol{T}^{-1} = \boldsymbol{L}_N^{-T} \boldsymbol{V} \boldsymbol{\Sigma}^{1/2}$
5. Construct the balanced realization
   $\bar{\boldsymbol{A}} = \boldsymbol{T} \boldsymbol{A} \boldsymbol{T}^{-1}$, $\bar{\boldsymbol{B}} = \boldsymbol{T} \boldsymbol{B}$, $\bar{\boldsymbol{C}} = \boldsymbol{C} \boldsymbol{T}^{-1}$,
   yielding $\boldsymbol{T} \boldsymbol{M} \boldsymbol{T}^T = \boldsymbol{T}^{-T} \boldsymbol{N} \boldsymbol{T}^{-1} = \boldsymbol{\Sigma}$
6. Truncate $\bar{\boldsymbol{A}}, \bar{\boldsymbol{B}}, \bar{\boldsymbol{C}}$ to form the reduced order system
   $\boldsymbol{A}_r, \boldsymbol{B}_r, \boldsymbol{C}_r$

In this setting the size of the eigenvalues of $\boldsymbol{P}$ describes (in the L_2-norm) how much input energy is needed to control the associated state eigenvector. The observability gramian $\boldsymbol{Q}$ is related to the L_2-norm of the output. If the system is released at $\boldsymbol{x}(0) = \boldsymbol{x}_0$ with $\boldsymbol{u}(t) = 0, \forall t \geq 0$, the following equality holds

$$\int_0^\infty \boldsymbol{y}(t)^T \boldsymbol{y}(t) \ dt = \boldsymbol{x}_0^T \boldsymbol{Q} \boldsymbol{x}_0 \tag{5.18}$$

In this setting, the size of the eigenvalues of $\boldsymbol{Q}$ describes (in the L_2-norm) how much output energy is produced when the associated state eigenvector is in free evolution.

The balanced system is based on the positive definite matrices $(\boldsymbol{P}, \boldsymbol{Q})$

$$\bar{\boldsymbol{A}} = \boldsymbol{T} \boldsymbol{A} \boldsymbol{T}^{-1}, \ \bar{\boldsymbol{B}} = \boldsymbol{T} \boldsymbol{B}, \ \bar{\boldsymbol{C}} = \boldsymbol{C} \boldsymbol{T}^{-1} \tag{5.19}$$

where

$$\boldsymbol{T} \boldsymbol{P} \boldsymbol{T}^T = \boldsymbol{T}^{-T} \boldsymbol{Q} \boldsymbol{T}^{-1} = \boldsymbol{\Sigma} \tag{5.20}$$

are now in a coordinate system where the observability and controllability gramians are equal and diagonal. Here $\boldsymbol{\Sigma}$ represents the singular values of the system

$$\boldsymbol{\Sigma} = \text{diag}(\sigma_1 \geq \sigma_2 \geq \ldots \geq \sigma_n) \tag{5.21}$$

Since the system is in a balanced coordinate system, the singular values give a measure of which states are difficult to control and observe, and can therefore be discarded without affecting the input-output behavior too much. Hence, looking at the singular values of a system provides a good way to measure which states to keep and which ones to discard.

An attractive part of the Lyapunov balancing is that there is a well defined error bound between the original and reduced order system (Glover, 1984)

$$||\boldsymbol{G}(s) - \boldsymbol{G}_r(s)||_\infty \leq \sum_{k=r+1}^{n} \sigma_k \tag{5.22}$$

where n is the order of the original system and r is the order of the reduced order system.

When applied to an asymptotically stable system, Lyapunov balancing preserves the stability of the system, but a property like passivity might not be preserved. We will call a state transformation $\boldsymbol{T}$ which guarantees that the reduced order system is stable as well, a stable state-space transformation.

Definition 5.1 *Let $\boldsymbol{G}(s)$ in (5.3) be a stable minimal realization, then $\boldsymbol{T} \in \mathbb{R}^{n\times n}$ is called a stable state transformation if all the truncated systems*

$$\boldsymbol{G}_r(s) = \boldsymbol{C}_r(s\boldsymbol{I} - \boldsymbol{A}_r)^{-1}\boldsymbol{B}_r + \boldsymbol{D}_r,\ r = (1, \ldots, n-1) \tag{5.23}$$

obtained from the transformed system (5.7)-(5.9) are stable.

5.2.2 Stochastic Balancing

Stochastic balancing was first proposed by Desai and Pal (1984) where it was used to balance stochastic systems; Harshavardhana *et al.* (1984) then showed that it preserves the positive realness of the original system. In Green (1988) it it shown how this can be applied to LTI systems. The idea behind stochastic balancing leads to three different model order reduction algorithms, as will be shown in this section.

Let $\boldsymbol{\Phi}$ be the power spectrum of the positive real minimal degree transfer function $\boldsymbol{Z}(s) = \boldsymbol{H}(s\boldsymbol{I}_n - \boldsymbol{F})^{-1}\boldsymbol{G} + \boldsymbol{J}$. Then we have the following relation (Obinata and Anderson, 2001)

$$\boldsymbol{\Phi} = \boldsymbol{Z}(s) + \boldsymbol{Z}^T(-s) = \boldsymbol{V}(s)\boldsymbol{V}^T(-s) = \boldsymbol{W}^T(-s)\boldsymbol{W}(s) \tag{5.24}$$

Here $\boldsymbol{Z}(s)$ denotes the phase system, $\boldsymbol{V}(s)$ the left spectral factor of $\boldsymbol{Z}(s)$, and $\boldsymbol{W}(s)$ the right spectral factor of $\boldsymbol{Z}(s)$. The system $\boldsymbol{Z}(s) = (\boldsymbol{F}, \boldsymbol{G}, \boldsymbol{H}, \boldsymbol{J})$,

which is positive real (PR), satisfies the positive real lemma equations

$$\boldsymbol{F}\boldsymbol{R} + \boldsymbol{R}\boldsymbol{F}^T = -\boldsymbol{G}_l\boldsymbol{G}_l^T \tag{5.25}$$

$$\boldsymbol{R}\boldsymbol{H}^T - \boldsymbol{G} = -\boldsymbol{G}_l\boldsymbol{J}_l^T \tag{5.26}$$

$$-\boldsymbol{J} - \boldsymbol{J}^T = -\boldsymbol{J}_l\boldsymbol{J}_l^T \tag{5.27}$$

Here $\boldsymbol{R} = \boldsymbol{R}^T > \boldsymbol{0}$, $\boldsymbol{G}_l$ and $\boldsymbol{J}_l$ can be solved from these equations. A dual pair of positive real equations can be obtained by pre- and post-multiplying (5.25) by $\boldsymbol{R}^{-1}$, and pre-multiplying (5.26) by $\boldsymbol{R}^{-1}$. By defining;

$$\boldsymbol{O} := \boldsymbol{R}^{-1} \tag{5.28}$$

$$\boldsymbol{H}_r := -\boldsymbol{L}^T\boldsymbol{G}_l^T\boldsymbol{R}^{-1} \tag{5.29}$$

$$\boldsymbol{J}_r := \boldsymbol{L}^T\boldsymbol{J}_l^T \tag{5.30}$$

where $\boldsymbol{L}$ is an arbitrary orthogonal matrix (i.e. $\boldsymbol{L}\boldsymbol{L}^T = \boldsymbol{I}$), the dual positive real (DPR) equations are obtained, given by

$$\boldsymbol{F}^T\boldsymbol{O} + \boldsymbol{O}\boldsymbol{F} = -\boldsymbol{H}_r^T\boldsymbol{H}_r \tag{5.31}$$

$$\boldsymbol{O}\boldsymbol{G} - \boldsymbol{H}^T = -\boldsymbol{H}_r^T\boldsymbol{J}_r \tag{5.32}$$

$$-\boldsymbol{J} - \boldsymbol{J}^T = -\boldsymbol{J}_r^T\boldsymbol{J}_r \tag{5.33}$$

Here $\boldsymbol{O} = \boldsymbol{O}^T > \boldsymbol{0}$, $\boldsymbol{H}_r$ and $\boldsymbol{J}_r$ can be solved from these equations, which shows that the dual system $\boldsymbol{Z}^T(-s) = \boldsymbol{G}^T(s\boldsymbol{I} - \boldsymbol{F}^T)^{-1}\boldsymbol{H}^T + \boldsymbol{J}^T$ of $\boldsymbol{Z}(s)$ is positive real.

The solutions $\boldsymbol{R}$ and $\boldsymbol{O}$ of (5.25)-(5.27) and (5.31)-(5.33) form convex sets (Willems, 1971)

$$\boldsymbol{0} < \boldsymbol{R}_{min} \leq \boldsymbol{R} \leq \boldsymbol{R}_{max} \tag{5.34}$$

$$\boldsymbol{0} < \boldsymbol{O}_{min} \leq \boldsymbol{O} \leq \boldsymbol{O}_{max} \tag{5.35}$$

Given the solution $\boldsymbol{R}$ to the PR equations, then $\boldsymbol{O} = \boldsymbol{R}^{-1}$ is a solution to the DPR equations, hence $\boldsymbol{R}_{min} = \boldsymbol{O}_{max}^{-1}$ and $\boldsymbol{O}_{min} = \boldsymbol{R}_{max}^{-1}$.

Let $(\boldsymbol{R}, \boldsymbol{G}_l, \boldsymbol{J}_l)$ be the solution to the PR equations (5.25)-(5.27), then the left spectral factor associated with $(\boldsymbol{R}, \boldsymbol{H}_l, \boldsymbol{J}_l)$ is

$$\boldsymbol{V}(s) = \boldsymbol{H}(s\boldsymbol{I} - \boldsymbol{F})^{-1}\boldsymbol{G}_l + \boldsymbol{J}_l \tag{5.36}$$

Let $(\boldsymbol{O}, \boldsymbol{H}_r, \boldsymbol{J}_r)$ be the solution to the DPR equations in (5.31)-(5.33), then the right spectral factor associated with $(\boldsymbol{O}, \boldsymbol{H}_r, \boldsymbol{J}_r)$ is

$$\boldsymbol{W}(s) = \boldsymbol{H}_r(s\boldsymbol{I} - \boldsymbol{F})^{-1}\boldsymbol{G} + \boldsymbol{J}_r \tag{5.37}$$

A function $\boldsymbol{F}_c$ can now be defined using $\boldsymbol{F}$, $\boldsymbol{G}_l$ and $\boldsymbol{H}_r$ from (5.25) and (5.31) such that (Obinata and Anderson, 2001)

$$\begin{bmatrix} \boldsymbol{Z}(s) & \boldsymbol{V}(s) \\ \boldsymbol{W}(s) & \boldsymbol{F}_c(s) \end{bmatrix} = \begin{bmatrix} \boldsymbol{H} \\ \boldsymbol{H}_r \end{bmatrix} (s\boldsymbol{I} - \boldsymbol{F})^{-1} \begin{bmatrix} \boldsymbol{G} & \boldsymbol{G}_l \end{bmatrix} + \begin{bmatrix} \boldsymbol{J} & \boldsymbol{J}_l \\ \boldsymbol{J}_h & 0 \end{bmatrix} \tag{5.38}$$

By doing balanced truncation on $\boldsymbol{F}_c(s) = \boldsymbol{H}_r(s\boldsymbol{I} - \boldsymbol{F})^{-1}\boldsymbol{G}_l$ based on its controllability gramian and observability gramian,

$$\boldsymbol{F}\boldsymbol{P} + \boldsymbol{P}\boldsymbol{F}^T + \boldsymbol{G}_l\boldsymbol{G}_l^T = \boldsymbol{0} \tag{5.39}$$

$$\boldsymbol{F}^T\boldsymbol{Q} + \boldsymbol{Q}\boldsymbol{F} + \boldsymbol{H}_r^T\boldsymbol{H}_r = \boldsymbol{0} \tag{5.40}$$

induced truncations of the realizations $\boldsymbol{Z}(s)$, $\boldsymbol{V}(s)$ and $\boldsymbol{W}(s)$ are simultaneously obtained. Depending on whether one chooses the system $\boldsymbol{G}(s)$, which is to be reduced, equal to $\boldsymbol{Z}(s)$, $\boldsymbol{V}(s)$ or $\boldsymbol{W}(s)$ one ends up with three different order reduction algorithms; Riccati balancing (phase system balancing), left spectral factor balancing and right spectral factor balancing.

Riccati balancing (phase system balancing)

By choosing the phase system equal to the system transfer function, $\boldsymbol{Z}(s) = \boldsymbol{G}(s)$, one obtains Riccati balancing, also called phase system balancing. It is now assumed that $\boldsymbol{G}(s) = (\boldsymbol{A}, \boldsymbol{B}, \boldsymbol{C}, \boldsymbol{D})$ is a minimal positive real transfer function, hence the system will satisfy the PR equations (5.25)-(5.27) and the DPR equations (5.31)-(5.33).

In Riccati balancing the minimal solution $(\boldsymbol{R}_{min}, \boldsymbol{O}_{min})$ to (5.25)-(5.27) and (5.31)-(5.33) is used. These can be obtained by rewriting (5.25)-(5.27) and (5.31)-(5.33) as a dual pair of Riccati equations, and then solve for $\boldsymbol{R} > \boldsymbol{0}$ and $\boldsymbol{O} > \boldsymbol{0}$;

$$\boldsymbol{F}\boldsymbol{R} + \boldsymbol{R}\boldsymbol{F}^T + (\boldsymbol{R}\boldsymbol{H}^T - \boldsymbol{G})(\boldsymbol{J} + \boldsymbol{J}^T)^{-1}(\boldsymbol{H}\boldsymbol{R} - \boldsymbol{G}^T) = \boldsymbol{0} \tag{5.41}$$

$$\boldsymbol{F}^T\boldsymbol{O} + \boldsymbol{O}\boldsymbol{F} + (\boldsymbol{O}\boldsymbol{G} - \boldsymbol{H}^T)(\boldsymbol{J} + \boldsymbol{J}^T)^{-1}(\boldsymbol{G}^T\boldsymbol{O} - \boldsymbol{H}) = \boldsymbol{0} \tag{5.42}$$

When $\boldsymbol{Z}(s) = \boldsymbol{G}(s)$ this gives

$$\boldsymbol{A}\boldsymbol{R} + \boldsymbol{R}\boldsymbol{A}^T + (\boldsymbol{R}\boldsymbol{C}^T - \boldsymbol{B})(\boldsymbol{D} + \boldsymbol{D}^T)^{-1}(\boldsymbol{C}\boldsymbol{R} - \boldsymbol{B}^T) = \boldsymbol{0} \tag{5.43}$$

$$\boldsymbol{A}^T\boldsymbol{O} + \boldsymbol{O}\boldsymbol{A} + (\boldsymbol{O}\boldsymbol{B} - \boldsymbol{C}^T)(\boldsymbol{D} + \boldsymbol{D}^T)^{-1}(\boldsymbol{B}^T\boldsymbol{O} - \boldsymbol{C}) = \boldsymbol{0} \tag{5.44}$$

By performing Riccati balancing the system is transformed to a basis where

$$\boldsymbol{R} = \boldsymbol{O} = \boldsymbol{\Sigma} \tag{5.45}$$

Since these are the minimal solutions to (5.25)-(5.27) and (5.31)-(5.33) (Antoulas, 2005)

$$\boldsymbol{R}_{min} = \boldsymbol{O}_{min} = \boldsymbol{\Sigma} \tag{5.46}$$

In Green (1988) it is shown that since the minimal solutions $\boldsymbol{R}_{min}$ and $\boldsymbol{O}_{min}$ are balanced, $\boldsymbol{O}_{min}^{-1} = \boldsymbol{R}_{max} \geq \boldsymbol{R}_{min}$ the σ_i in (5.46) are all less than or equal to 1, hence for Riccati balancing

$$\boldsymbol{\Sigma} \leq \boldsymbol{I} \tag{5.47}$$

When applied to positive real systems, this property is preserved in the reduction process. We will refer to such a state transformation $\boldsymbol{T}$ given by the balancing of $(\boldsymbol{R}, \boldsymbol{O})$ as a positive real state transformation:

Definition 5.2 *Let $\boldsymbol{G}(s)$ in (5.3) be a positive real minimal realization, then $\boldsymbol{T} \in \mathbb{R}^{n \times n}$ is called a positive real state transformation if all the truncated systems*

$$\boldsymbol{G}_r(s) = \boldsymbol{C}_r(s\boldsymbol{I} - \boldsymbol{A}_r)^{-1}\boldsymbol{B}_r + \boldsymbol{D}_r, \;\; r = (1, \ldots, n-1) \tag{5.48}$$

obtained from the transformed system (5.7)-(5.9) are positive real.

As with the Lyapunov balancing this also has a physical interpretation. Another way of checking if a system is passive, is in terms of Lyapunov theory and the use of storage functions (Willems, 1971). In these terms a system is said to be passive if there exists a storage function, $V(\boldsymbol{x}(t)) > 0$, such that the following inequality holds

$$V(\boldsymbol{x}(t)) \leq V(\boldsymbol{x}(0)) + \int_0^t s(\boldsymbol{u}(t), \boldsymbol{y}(t)) \; dt \tag{5.49}$$

Here $s(\boldsymbol{u}(t), \boldsymbol{y}(t))$ is called the supply function, and describes the rate at which power is supplied to the system. Two quantities can be defined from the notion of a storage function (Willems, 1971): the required supply, V_r, and the available storage, V_a. The required supply, V_r, is defined as

$$0 \leq V_r(\boldsymbol{x}_0) = \inf_{\boldsymbol{u}(t)|\boldsymbol{x}(0)=\boldsymbol{x}_0} \left[\int_{-\infty}^0 s(\boldsymbol{u}(t), \boldsymbol{y}(t)) \; dt \right] \tag{5.50}$$

and it is the minimum amount of energy required in order to control the system to state $\boldsymbol{x}_0$ at time 0. The solution of (5.41) is related to the required supply (Phillips *et al.*, 2003)

$$\boldsymbol{x}_0^T \boldsymbol{R}^{-1} \boldsymbol{x}_0 = V_r(\boldsymbol{x}_0) \tag{5.51}$$

In this setting, the size of the eigenvalues of $\boldsymbol{R}$ describes how much energy is needed to control the associated state eigenvector. Small eigenvalues of $\boldsymbol{R}$ imply that a large amount of energy is needed to reach the associated mode. $\boldsymbol{R}$ can be regarded as an input energy gramian; we will refer to $\boldsymbol{R}$ as the required supply gramian.

The available storage is defined as

$$0 \leq V_a(\boldsymbol{x}_0) = \sup_{\boldsymbol{x}(0)=\boldsymbol{x}_0} -\left[\int_0^\infty s(\boldsymbol{u}(t), \boldsymbol{y}(t))\ dt\right] \tag{5.52}$$

and is the maximum amount of energy which can be extracted from the system in free evolution (Lozano *et al.*, 2000). The solution of (5.42) is related to the available storage (Phillips *et al.*, 2003)

$$\boldsymbol{x}_0^T \boldsymbol{O} \boldsymbol{x}_0 = V_a(\boldsymbol{x}_0) \tag{5.53}$$

Here, the size of the eigenvalues of $\boldsymbol{O}$ describes how much energy can be extracted from the system in free evolution. Small eigenvalues of $\boldsymbol{O}$ imply that a small amount of energy can be extracted from the associated mode. $\boldsymbol{O}$ can be interpreted as an output energy gramian; we will refer to $\boldsymbol{O}$ as the available storage gramian.

By doing Riccati balancing, the system is balanced in terms of its required supply and available storage. States which are associated with a small amount of available storage and large amounts of required supply will be discarded. This balancing scheme is commonly used to reduce positive real systems, and will preserve this property in the reduction process.

Left spectral factor balancing

Having the relation (5.24):

$$\boldsymbol{Z}(s) + \boldsymbol{Z}^T(-s) = \boldsymbol{V}(s)\boldsymbol{V}^T(-s) \tag{5.54}$$

the left spectral factor $\boldsymbol{V}(s)$ can be found from the solution, $(\boldsymbol{R}, \boldsymbol{G}_l, \boldsymbol{J}_l)$, to the PR equations (5.25)-(5.27)

$$\boldsymbol{V}(s) = \boldsymbol{H}(s\boldsymbol{I} - \boldsymbol{F})^{-1}\boldsymbol{G}_l + \boldsymbol{J}_l \tag{5.55}$$

Let the left spectral factor be the transfer function to be reduced, $\boldsymbol{V}(s) = \boldsymbol{G}(s)$:

$$\boldsymbol{V}(s) = \boldsymbol{H}(s\boldsymbol{I} - \boldsymbol{F})^{-1}\boldsymbol{G}_l + \boldsymbol{J}_l = \boldsymbol{C}(s\boldsymbol{I} - \boldsymbol{A})^{-1}\boldsymbol{B} + \boldsymbol{D} = \boldsymbol{G}(s) \tag{5.56}$$

Then there exists a positive real function $\boldsymbol{Z}(s)$

$$\boldsymbol{Z}(s) = \boldsymbol{H}(s\boldsymbol{I} - \boldsymbol{F})^{-1}\boldsymbol{G} + \boldsymbol{J} = \boldsymbol{C}(s\boldsymbol{I} - \boldsymbol{A})^{-1}\boldsymbol{G} + \boldsymbol{J} \tag{5.57}$$

which is connected to $\boldsymbol{V}(s)$ through the PR equations in (5.25)-(5.27). They can now be written as

$$\boldsymbol{A}\boldsymbol{R} + \boldsymbol{R}\boldsymbol{A}^T = -\boldsymbol{B}\boldsymbol{B}^T \tag{5.58}$$

$$\boldsymbol{R}\boldsymbol{C}^T - \boldsymbol{G} = -\boldsymbol{B}\boldsymbol{D}^T \tag{5.59}$$

$$-\boldsymbol{J} - \boldsymbol{J}^T = -\boldsymbol{D}\boldsymbol{D}^T \tag{5.60}$$

The controllability gramian $\boldsymbol{R}$ of the left spectral factor can be solved from (5.58), hence it is the same as the required supply gramian, $\boldsymbol{R}$, of the positive real function $\boldsymbol{Z}(s)$. By first solving for $\boldsymbol{R}$ in (5.58), $\boldsymbol{G}$ in (5.59) can be solved for

$$\boldsymbol{G} = \boldsymbol{R}\boldsymbol{C}^T + \boldsymbol{B}\boldsymbol{D}^T \tag{5.61}$$

The dual positive real equations for $\boldsymbol{Z}(s)$ in (5.57) are now

$$\boldsymbol{A}^T\boldsymbol{O} + \boldsymbol{O}\boldsymbol{A} = -\boldsymbol{H}_r^T\boldsymbol{H}_r \tag{5.62}$$

$$\boldsymbol{O}\boldsymbol{G} - \boldsymbol{C}^T = -\boldsymbol{H}_r^T\boldsymbol{J}_r \tag{5.63}$$

$$-\boldsymbol{J} - \boldsymbol{J}^T = -\boldsymbol{J}_r\boldsymbol{J}_r^T \tag{5.64}$$

Let this be rewritten as a Riccati equation, where $\boldsymbol{J} + \boldsymbol{J}^T$ has been substituted for $\boldsymbol{D}\boldsymbol{D}^T$ in (5.60)

$$\boldsymbol{A}^T\boldsymbol{O} + \boldsymbol{O}\boldsymbol{A} + (\boldsymbol{O}\boldsymbol{G} - \boldsymbol{C}^T)(\boldsymbol{D}\boldsymbol{D}^T)^{-1}(\boldsymbol{G}^T\boldsymbol{O} - \boldsymbol{C}) = \boldsymbol{0} \tag{5.65}$$

By balancing $\boldsymbol{G}(s)$ based on the solution matrices $(\boldsymbol{R}, \boldsymbol{O})$, left spectral balancing can be obtained. Given $\boldsymbol{G}(s)$, the equations which need to be solved are (5.58), (5.61) and (5.65).

Right spectral factor balancing

As for the left spectral factor, when the relation (5.24) is given

$$\boldsymbol{Z}(s) + \boldsymbol{Z}^T(-s) = \boldsymbol{W}^T(-s)\boldsymbol{W}(s) \tag{5.66}$$

the right spectral factor $\boldsymbol{W}(s)$ can be found from the solution $(\boldsymbol{O}, \boldsymbol{H}_r, \boldsymbol{J}_r)$ to the DPR equations (5.31)-(5.33)

$$\boldsymbol{W}(s) = \boldsymbol{H}_r(s\boldsymbol{I} - \boldsymbol{F})^{-1}\boldsymbol{G} + \boldsymbol{J}_r \tag{5.67}$$

Let the right spectral factor be set equal to the transfer function of the system $\boldsymbol{W}(s) = \boldsymbol{G}(s)$

$$\boldsymbol{W}(s) = \boldsymbol{H}_r(s\boldsymbol{I} - \boldsymbol{F})^{-1}\boldsymbol{G} + \boldsymbol{J}_r = \boldsymbol{C}(s\boldsymbol{I} - \boldsymbol{A})^{-1}\boldsymbol{B} + \boldsymbol{D} = \boldsymbol{G}(s) \tag{5.68}$$

Table 5.2: Overview over the different balancing schemes.

$\Phi(s) = V(s)V^T(-s) = Z(s) + Z^T(-s) = W^T(-s)W(s)$		
Left Spectral Factor $V(s) = H(sI-F)^{-1}G_l + J_l$	Phase System $Z(s) = H(sI-F)^{-1}G + J$	Right Spectral Factor $W(s) = H_r(sI-F)^{-1}G + J_r$
$V(s) = C(sI-A)^{-1}G_l + J_l$	$G(s) = (A, B, C, D)$ given $Z(s) = G(s)$ $Z(s) = C(sI-A)^{-1}B + D$	$W(s) = H_r(sI-A)^{-1}B + J_r$
Lyapunov Balancing:	-solve for (P, Q)	-balance (P, Q)
	Controllability gramian, P: $AP + PA^T + BB^T = 0$ $\times$ Observability gramian, Q: $A^TQ + QA + C^TC = 0$	
Riccati Balancing:	-solve for (R, O)	-balance (R, O)
Contr. gramian, R: $\Leftarrow$ $AR + RA^T + G_lG_l^T = 0$	$\Rightarrow$Req. supply gramian, R: $AR + RA^T = -G_lG_l^T$ $RC^T - B = -G_lJ_l^T$ $-D - D^T = -J_lJ_l^T$ $\Updownarrow$ $AR + RA^T + (RC^T - B)(D + D^T)^{-1}(CR - B^T) = 0$ $\times$	
	Av. storage gramian, O:$\Leftarrow$ $A^TO + OA = -H_r^TH_r$ $OB - C^T = -H_r^TJ_r$ $-D - D^T = -J_r^TJ_r$ $\Updownarrow$ $A^TO + OA + (OB - C^T)(D + D^T)^{-1}(B^TO - C) = 0$	$\Rightarrow$Obs. gramian, O: $A^TO + OA + H_r^TH_r = 0$
Mixed Gramian Balancing:	-solve for (P, O) or (R, Q)	-balance (P, O) or (R, Q)
	Controllability gramian, P: $AP + PA^T + BB^T = 0$ $\times$ Av. storage gramian, O:$\Leftarrow$ $A^TO + OA + (OB - C^T)(D + D^T)^{-1}(B^TO - C) = 0$	$\Rightarrow$Obs. gramian, O: $A^TO + OA + H_r^TH_r = 0$
Contr. gramian, R:$\Leftarrow$ $AR + RA^T + G_lG_l^T = 0$	or $\Rightarrow$Req. supply gramian, R: $AR + RA^T + (RC^T - B)(D + D^T)^{-1}(CR - B^T) = 0$ $\times$ Observability gramian, Q: $A^TQ + QA + C^TC = 0$	

(Continued on next page)

$\Phi(s) = V(s)V^T(-s) = Z(s) + Z^T(-s) = W^T(-s)W(s)$		
Left Spectral Factor $V(s)=H(sI-F)^{-1}G_l+J_l$	Phase System $Z(s) = H(sI-F)^{-1}G + J$	Right Spectral Factor $W(s)=H_r(sI-F)^{-1}G+J_r$
$G(s) = (A, B, C, D)$ given $V(s) = G(s)$ $V(s) = C(sI - A)^{-1}B + D$	$Z(s) = C(sI - A)^{-1}G + J$	$W(s) = H_r(sI - A)^{-1}G + J_r$
Left Spectral Factor Bal.:	-solve for (R, G, O)	-balance (R, O)
Contr. gramian, R:$\Leftarrow$ $AR + RA^T + BB^T = 0$	$\Rightarrow$Req. supply gramian, R: $AR + RA^T = -BB^T$ $G = RC^T + BD^T$ $-J-J^T = -DD^T$ $\times$ Av. storage gramian, O:$\Leftarrow$	 $\Rightarrow$Obs. gramian, O
$A^TO+OA+(OG-C^T)(DD^T)^{-1}(G^TO-C)=0$		$A^TO + OA + H_r^T H_r = 0$
  $V(s) = H(sI - A)^{-1}G_l + J_l$	 $Z(s) = H(sI - A)^{-1}B + J$	$G(s) = (A, B, C, D)$ given $W(s) = G(s)$ $W(s) = C(sI - A)^{-1}B + D$
Right Spectral Factor Bal.:	-solve for (O, H, R)	-balance (R, O)
     Contr. gramian, R: $AR + RA^T + G_lG_l^T = 0$	Av. storage gramian, O:$\Rightarrow$ $A^TO + OA = -C^TC$ $H^T = OB + C^TD$ $-J - J^T = -D^TD$ $\times$ Req. supply gramian, R: $AR+RA^T+(RH^T-B)(D^TD)^{-1}(HR-B^T)=0$	$\Leftarrow$ Obs. gramian, O: $A^TO + OA + C^TC = 0$

Now there exists a positive real function $\boldsymbol{Z}(s)$

$$\boldsymbol{Z}(s) = \boldsymbol{H}(s\boldsymbol{I} - \boldsymbol{F})^{-1}\boldsymbol{G} + \boldsymbol{J} = \boldsymbol{H}(s\boldsymbol{I} - \boldsymbol{A})^{-1}\boldsymbol{B} + \boldsymbol{J} \tag{5.69}$$

which is connected to $\boldsymbol{W}(s)$ through the DPR equations in (5.31)-(5.33). The DPR equations can now be written as

$$\boldsymbol{A}^T\boldsymbol{O} + \boldsymbol{O}\boldsymbol{A} = -\boldsymbol{C}\boldsymbol{C}^T \tag{5.70}$$

$$\boldsymbol{O}\boldsymbol{B} - \boldsymbol{H}^T = -\boldsymbol{C}^T\boldsymbol{D} \tag{5.71}$$

$$-\boldsymbol{J} - \boldsymbol{J}^T = -\boldsymbol{D}^T\boldsymbol{D} \tag{5.72}$$

The observability gramian $\boldsymbol{O}$ of the right spectral factor can be solved from (5.70), hence it is the same as the available storage gramian $\boldsymbol{O}$ of the positive real function $\boldsymbol{Z}(s)$. By first solving for $\boldsymbol{O}$ in (5.70), $\boldsymbol{H}$ in (5.71) can be solved for

$$\boldsymbol{H}^T = \boldsymbol{O}\boldsymbol{B} + \boldsymbol{C}^T\boldsymbol{D}. \tag{5.73}$$

The positive real equations for $\boldsymbol{Z}(s)$ given in (5.69) are now

$$\boldsymbol{A}\boldsymbol{R} + \boldsymbol{R}\boldsymbol{A}^T = -\boldsymbol{G}_l\boldsymbol{G}_l^T \tag{5.74}$$

$$\boldsymbol{R}\boldsymbol{H}^T - \boldsymbol{B} = -\boldsymbol{G}_l\boldsymbol{J}_l^T \tag{5.75}$$

$$-\boldsymbol{J} - \boldsymbol{J}^T = -\boldsymbol{J}_l\boldsymbol{J}_l^T \tag{5.76}$$

Let this be rewritten as a Riccati equation where $\boldsymbol{J}+\boldsymbol{J}^T$ has been substituted for $\boldsymbol{D}^T\boldsymbol{D}$ in (5.72)

$$\boldsymbol{A}\boldsymbol{R} + \boldsymbol{R}\boldsymbol{A}^T + (\boldsymbol{R}\boldsymbol{H}^T - \boldsymbol{B})(\boldsymbol{D}^T\boldsymbol{D})^{-1}(\boldsymbol{H}\boldsymbol{R} - \boldsymbol{B}^T) = \boldsymbol{0} \tag{5.77}$$

By balancing $\boldsymbol{G}(s)$ based on the solution matrices $(\boldsymbol{R}, \boldsymbol{O})$, right spectral balancing can be obtained. Given $\boldsymbol{G}(s)$, the equations which need to be solved are (5.70), (5.73) and (5.77). In Table 5.2 an overview over the different balancing schemes induced by balancing $\boldsymbol{F}_c$ in (5.38) is given.

Equality of the balancing schemes

For SISO systems, the reduced order systems generated by the left spectral factor balancing and the right spectral factor balancing will have the same transfer function. The state-space representations of two systems are said to be zero-state equivalent if they have the same transfer matrix (see Theorem B.3) For SISO systems the transfer function $G(s) = G^T(s)$. Hence, for SISO systems, the dual system $G^T(s)$ is zero-state equivalent with the given system $G(s)$. Here, we propose

Proposition 5.1 *For SISO systems, the reduced order systems $G_r(s)$ given by left spectral factor balancing and right spectral factor balancing of the system $G(s)$ are zero-state equivalent.*

Proof. Substitute the system $G(s)$ with the dual system $G^T(s)$ in (5.56):

$$V(s) = G^T(s) = \boldsymbol{B}^T(s\boldsymbol{I} - \boldsymbol{A}^T)\boldsymbol{C}^T + \boldsymbol{D}^T \tag{5.78}$$

Left spectral factor balancing of the dual system $G^T(s)$ gives the following equations

$$\boldsymbol{A}^T\boldsymbol{R} + \boldsymbol{R}\boldsymbol{A} = -\boldsymbol{C}^T\boldsymbol{C} \tag{5.79}$$

$$\boldsymbol{G} = \boldsymbol{R}\boldsymbol{B} + \boldsymbol{C}^T\boldsymbol{D} \tag{5.80}$$

$$-\boldsymbol{J} - \boldsymbol{J}^T = \boldsymbol{D}^T\boldsymbol{D} \tag{5.81}$$

$$\boldsymbol{A}\boldsymbol{O} + \boldsymbol{O}\boldsymbol{A}^T - (\boldsymbol{O}\boldsymbol{G} - \boldsymbol{B}^T)(\boldsymbol{D}^T\boldsymbol{D})^{-1}(\boldsymbol{G}^T\boldsymbol{O} - \boldsymbol{B}^T) = \boldsymbol{0} \tag{5.82}$$

Looking at Table 5.2, one can see that left spectral factor balancing of the dual system $G^T(s)$ is the same as right spectral factor balancing of the system $G(s)$. The same yields for right spectral factor balancing of the dual system $G^T(s)$, which gives the same equations as for left spectral factor balancing of $G(s)$. Due to this duality the reduced order systems $G_r(s)$ given by left spectral factor balancing or right spectral factor balancing of $G(s)$ will be zero-state equivalent. ■

There is no similar physical interpretation to the left and right spectral factor balancing schemes, as for the Lyapunov and Riccati balancing schemes. But in Opdenacker and Jonckheere (1986) it is shown that these schemes give reduced spectral factors such that their phases approximate the phases of the original spectral factors. Hence, left spectral factor balancing and right spectral factor balancing can be interpreted as phase matching reduction algorithms. For positive real SISO systems the phase will be in the interval $[-90°, +90°]$, hence as long as the phase of the original system is well fitted the positive real property will be preserved.

5.2.3 Mixed Gramian Balancing

So far, the only algorithm presented which will guarantee positive real reduced order systems is the Riccati balancing. When Riccati balancing is used, the system is balanced based on the solution of two Riccati equations. Since the balanced system satisfies the PR equations, this gives positive real reduced order systems. However, the solution of two Riccati equations is computationally demanding. In this section a mixed gramian balancing approach is proposed. The idea behind the mixed gramian balancing is to solve one Riccati equation and one Lyapunov equation, which is less computationally demanding. As long as one of the PR equations is satisfied, this also holds for the balanced system, and hence for the reduced order system.

By taking the controllability gramian $\boldsymbol{P}$

$$\boldsymbol{AP} + \boldsymbol{PA}^T + \boldsymbol{BB}^T = \boldsymbol{0} \tag{5.83}$$

and the available storage gramian $\boldsymbol{O}$

$$\boldsymbol{A}^T\boldsymbol{O} + \boldsymbol{OA} + (\boldsymbol{OB} - \boldsymbol{C}^T)(\boldsymbol{D} + \boldsymbol{D}^T)^{-1}(\boldsymbol{B}^T\boldsymbol{O} - \boldsymbol{C}) = \boldsymbol{0} \tag{5.84}$$

and balancing the system $\boldsymbol{G}(s)$ by using $(\boldsymbol{P}, \boldsymbol{O})$, a positive real reduced order system is obtained. A similar result can be obtained if the pair $(\boldsymbol{R}, \boldsymbol{Q})$, consisting of the required supply gramian and the observability gramian, is

balanced:

$$\boldsymbol{A}\boldsymbol{R} + \boldsymbol{R}\boldsymbol{A}^T + (\boldsymbol{R}\boldsymbol{C}^T - \boldsymbol{B})(\boldsymbol{D} + \boldsymbol{D}^T)^{-1}(\boldsymbol{C}\boldsymbol{R} - \boldsymbol{B}^T) = \boldsymbol{0} \tag{5.85}$$

$$\boldsymbol{A}^T\boldsymbol{Q} + \boldsymbol{Q}\boldsymbol{A} + \boldsymbol{C}^T\boldsymbol{C} = \boldsymbol{0} \tag{5.86}$$

Definition 5.3 *The positive real minimal system $\boldsymbol{G}(s)$ is called mixed gramian balanced if*

$$\boldsymbol{P} = \boldsymbol{O} = \boldsymbol{\Sigma} = \mathrm{diag}(\sigma_1 I_{m1}, \ldots, \sigma_q I_{mq}) \tag{5.87}$$

or

$$\boldsymbol{R} = \boldsymbol{Q} = \boldsymbol{\Sigma} = \mathrm{diag}(\sigma_1 I_{m1}, \ldots, \sigma_q I_{mq}) \tag{5.88}$$

where $\sigma_1 > \sigma_2 > \ldots > \sigma_q > 0$ and m_i where $i = (1, \ldots, q)$ are the multiplicities of σ_i and $m_1 + \ldots + m_q = n$.

The following theorem can now be stated.

Theorem 5.1 *Let the positive real and minimal system $\boldsymbol{G}(s)$ have the mixed gramian balanced realization*

$$\boldsymbol{G}(s) = \left[\begin{array}{c|c} \boldsymbol{A} & \boldsymbol{B} \\ \hline \boldsymbol{C} & \boldsymbol{D} \end{array}\right] = \left[\begin{array}{cc|c} \boldsymbol{A}_{11} & \boldsymbol{A}_{12} & \boldsymbol{B}_1 \\ \boldsymbol{A}_{21} & \boldsymbol{A}_{22} & \boldsymbol{B}_2 \\ \hline \boldsymbol{C}_1 & \boldsymbol{C}_2 & \boldsymbol{D} \end{array}\right] \tag{5.89}$$

where

$$\boldsymbol{P} = \boldsymbol{O} = \boldsymbol{\Sigma} = \mathrm{diag}(\boldsymbol{\Sigma}_1, \boldsymbol{\Sigma}_2) \tag{5.90}$$

or

$$\boldsymbol{R} = \boldsymbol{Q} = \boldsymbol{\Sigma} = \mathrm{diag}(\boldsymbol{\Sigma}_1, \boldsymbol{\Sigma}_2) \tag{5.91}$$

with

$$\boldsymbol{\Sigma}_1 = \mathrm{diag}(\sigma_1 I_{m1}, \ldots, \sigma_k I_{mk}) \tag{5.92}$$

$$\boldsymbol{\Sigma}_2 = \mathrm{diag}(\sigma_{k+1} I_{m_{k+1}}, \ldots, \sigma_q I_q) \tag{5.93}$$

Then the reduced order model

$$\boldsymbol{G}_r(s) = \left[\begin{array}{cc} \boldsymbol{A}_{11} & \boldsymbol{B}_1 \\ \boldsymbol{C}_1 & \boldsymbol{D} \end{array}\right] \tag{5.94}$$

obtained by truncation is positive real.

Proof. We give a proof for the pair $(\boldsymbol{P}, \boldsymbol{O})$. Since the system $(\boldsymbol{A}, \boldsymbol{B}, \boldsymbol{C}, \boldsymbol{D})$ is balanced, the two gramians $(\boldsymbol{P}, \boldsymbol{O})$ are equal and diagonal, $\boldsymbol{P} = \boldsymbol{O} = \boldsymbol{\Sigma}$, and satisfy one Lyapunov equation and one Riccati equation

$$\boldsymbol{A}\boldsymbol{\Sigma} + \boldsymbol{\Sigma}\boldsymbol{A}^T + \boldsymbol{B}\boldsymbol{B}^T = \boldsymbol{0} \tag{5.95}$$

$$\boldsymbol{A}^T\boldsymbol{\Sigma} + \boldsymbol{\Sigma}\boldsymbol{A} + (\boldsymbol{\Sigma}\boldsymbol{B} - \boldsymbol{C}^T)(\boldsymbol{D} + \boldsymbol{D}^T)^{-1}(\boldsymbol{B}^T\boldsymbol{\Sigma} - \boldsymbol{C}) = \boldsymbol{0} \tag{5.96}$$

Writing out the second equation in terms of its partitioned matrices gives the following $(1,1)$ block

$$\boldsymbol{A}_{11}^T\boldsymbol{\Sigma}_1 + \boldsymbol{\Sigma}_1\boldsymbol{A}_{11} + (\boldsymbol{\Sigma}_1\boldsymbol{B}_1 - \boldsymbol{C}_1^T)(\boldsymbol{D} + \boldsymbol{D}^T)^{-1}(\boldsymbol{B}_1^T\boldsymbol{\Sigma}_1 - \boldsymbol{C}_1) = \boldsymbol{0} \tag{5.97}$$

Since $\boldsymbol{\Sigma}_1 > \boldsymbol{0}$ the positive realness of the reduced order system $(\boldsymbol{A}_{11}, \boldsymbol{B}_1, \boldsymbol{C}_1, \boldsymbol{D})$ can be concluded. The same can be shown for the pair $(\boldsymbol{R}, \boldsymbol{Q})$. ■

Further it can be shown for SISO systems that the transfer function of the reduced order system $G_r(s) = (\boldsymbol{A}_{11}, \boldsymbol{B}_1, \boldsymbol{C}_1, \boldsymbol{D})$ will be the same if either the gramian pair $(\boldsymbol{P}, \boldsymbol{O})$ or the gramian pair $(\boldsymbol{R}, \boldsymbol{Q})$ is used as a basis for the mixed gramian balanced truncation algorithm.

The dual of the system $G(s)$ is written

$$G^T(-s) = \left[\begin{array}{c|c} \boldsymbol{A}^T & \boldsymbol{C}^T \\ \hline \boldsymbol{B}^T & \boldsymbol{D}^T \end{array}\right] \tag{5.98}$$

Substituting the system $G(s)$ with the dual system $G^T(-s)$ in the equations (5.83)-(5.84) gives the following equations

$$\boldsymbol{A}^T\boldsymbol{P} + \boldsymbol{P}\boldsymbol{A} + \boldsymbol{C}^T\boldsymbol{C} = \boldsymbol{0} \tag{5.99}$$

$$\boldsymbol{A}\boldsymbol{O} + \boldsymbol{O}\boldsymbol{A}^T + (\boldsymbol{O}\boldsymbol{C}^T - \boldsymbol{B})(\boldsymbol{D} + \boldsymbol{D}^T)^{-1}(\boldsymbol{C}\boldsymbol{O} - \boldsymbol{B}^T) = \boldsymbol{0} \tag{5.100}$$

Solving for these equations, where the original system $G(s)$ has been substituted with its dual, $G^T(-s)$, is the same as solving for the required supply gramian (5.85) and the observability gramian (5.86) of the original system $G(s)$.

Subsequently, $G(s)$ is replaced with its dual $G^T(-s)$ in the equations (5.85)-(5.86)

$$\boldsymbol{A}^T\boldsymbol{R} + \boldsymbol{R}\boldsymbol{A} + (\boldsymbol{R}\boldsymbol{B} - \boldsymbol{C}^T)(\boldsymbol{D}^T + \boldsymbol{D})^{-1}(\boldsymbol{B}^T\boldsymbol{R} - \boldsymbol{C}) = \boldsymbol{0} \tag{5.101}$$

$$\boldsymbol{A}\boldsymbol{Q} + \boldsymbol{Q}\boldsymbol{A}^T + \boldsymbol{B}\boldsymbol{B}^T = \boldsymbol{0} \tag{5.102}$$

Solving for these equations is the same as solving for the controllability gramian and the available storage gramian of the original system $G(s)$. Due to this duality, which comes from the duality of the Lyapunov equations and

the Riccati equations, when the systems are reduced, the transfer function $G_r(s) = (\boldsymbol{A}_{11}, \boldsymbol{B}_1, \boldsymbol{C}_1, \boldsymbol{D})$ will be zero-state equivalent. An overview over the different balancing schemes presented so far is given in Table 5.2. The connections the different balancing schemes have to the spectral factor of the system is also shown.

5.2.4 Numerical Example

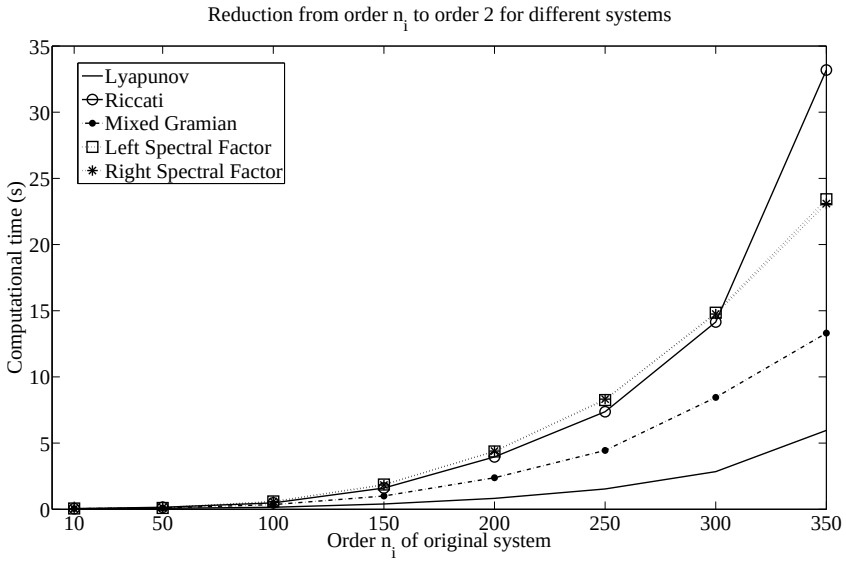

Figure 5.2: Computational time when reducing the original system of order n_i down to order 2 for the different balancing schemes.

In this section the different balancing schemes presented in the preceding section will be compared in terms of computational time and accuracy. A positive real SISO system of order 350 is given and 8 different truncated systems are first constructed, respectively of orders 350, 300, 250, 200, 150, 100, 50 and 10. All these systems are reduced further to a system of order 2 by using the different balancing schemes presented in the Sections 5.2.1-5.2.3. The computations were done on a Dell Latitude D800 Notebook with Intel Centrino processor 2 GHz and 1 GB RAM running MATLAB under Windows XP. The computing times are shown in Figure 5.2. As one can see from this figure, the Lyapunov balancing is the most efficient in terms of time. This is expected since it is faster to solve Lyapunov equations com-

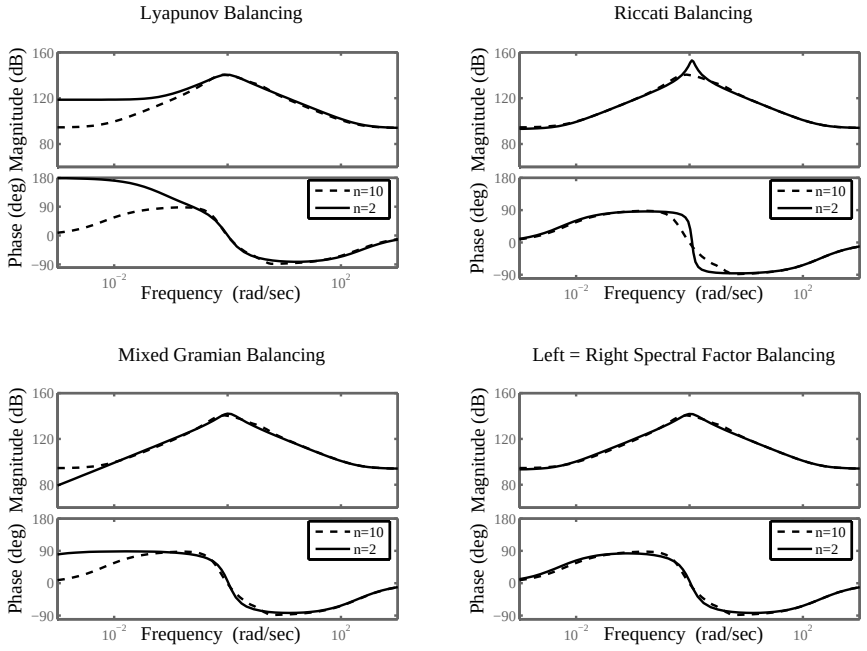

Figure 5.3: Bode plot of the difference between the original system of order $n = 10$ and reduced order system of order $n = 2$ using the different balancing schemes.

pared to Riccati equations, since the solution of Riccati equations involves matrix inversions. The mixed gramian balancing lies between the Riccati and Lyapunov balancing in computational time, this is expected since one Lyapunov equation and one Riccati equation is solved. In this example the left and right spectral factor balancing schemes use approximately the same time as the Riccati balancing. The left and right spectral factor balancing schemes are expected to use more time than the mixed gramian balancing. Even though these algorithms also balance the solution of one Lyapunov and one Riccati equation, more equations are to be solved than for the mixed gramian balancing scheme. The errors between the system of order $n = 10$ and the reduced order system of $n = 2$ are given in Table 5.3. The Bode plots of the original system and the different reduced order systems are shown in Figure 5.3. The Lyapunov balancing has the best error-performance, but looking at the Bode plot one can see that the reduced order system is not passive since the phase of the reduced order system exceeds 90 deg. The

Table 5.3: $||\cdot||_\infty$-error between original and reduced order system of order $n = 10$ and $n = 2$.

Balancing scheme:	$\|\|G(s) - G_r(s)\|\|_\infty$
Lyapunov	$9.08 \cdot 10^5$
Riccati	$3.53 \cdot 10^7$
Mixed gramian	$2.71 \cdot 10^6$
Left/Right spectral factor	$2.42 \cdot 10^6$

reduced order system using left/right spectral factor balancing is passive, even though this might not be the case, and has the best error performance for this system. The only algorithms which guarantee positive real reduced order systems are Riccati and mixed gramian balancing. In this example, the mixed gramian balancing can compete with the Riccati balancing both in terms of computational time and reduction error.

5.3 Extending Balanced Truncation

Stable systems can be characterized by the solution of a Lyapunov equation and positive real systems can be characterized by the solution of the positive real lemma. In this section we show that as long as one of the gramians in the balanced truncation scheme satisfies one of these equations the reduced order system generated will be stable or positive real.

5.3.1 Stable Projection

A stable system is characterized by Theorem B.4. Let $\boldsymbol{Y} = \boldsymbol{Y}^T > \boldsymbol{0}$ be an arbitrary positive real matrix, and $\boldsymbol{P} = \boldsymbol{P}^T > \boldsymbol{0}$ be the solution to (B.22). By substituting $(\boldsymbol{M}, \boldsymbol{N})$ by the pair $(\boldsymbol{P}, \boldsymbol{Y})$ in the balanced truncation algorithm in Table 5.1, it can be shown that the reduced order system will be stable.

Theorem 5.2 *Let the stable and minimal system $\boldsymbol{G}(s)$ have the balanced realization*

$$\boldsymbol{G}(s) = \left[\begin{array}{c|c} \boldsymbol{A} & \boldsymbol{B} \\ \hline \boldsymbol{C} & \boldsymbol{D} \end{array}\right] = \left[\begin{array}{cc|c} \boldsymbol{A}_{11} & \boldsymbol{A}_{12} & \boldsymbol{B}_1 \\ \boldsymbol{A}_{21} & \boldsymbol{A}_{22} & \boldsymbol{B}_2 \\ \hline \boldsymbol{C}_1 & \boldsymbol{C}_2 & \boldsymbol{D} \end{array}\right] \tag{5.103}$$

with $\boldsymbol{P} = \boldsymbol{Y} = \boldsymbol{\Sigma} = \mathrm{diag}(\boldsymbol{\Sigma}_1, \boldsymbol{\Sigma}_2)$*, where the pair* $(\boldsymbol{P}, \boldsymbol{Y})$ *comes from*

$$\text{arbitrary } \boldsymbol{Y} = \boldsymbol{Y}^T > \boldsymbol{0} \tag{5.104}$$

$$\boldsymbol{A}\boldsymbol{P} + \boldsymbol{P}\boldsymbol{A}^T + \boldsymbol{Q} = \boldsymbol{0} \tag{5.105}$$

$$\boldsymbol{P} = \boldsymbol{P}^T > \boldsymbol{0} \tag{5.106}$$

$$\boldsymbol{Q} = \boldsymbol{Q}^T > \boldsymbol{0} \tag{5.107}$$

Then the associated state transformation $\boldsymbol{T}$ *will be a stable state transformation and the reduced order model obtained by truncation is stable.*

Proof. Since $(\boldsymbol{A}, \boldsymbol{B}, \boldsymbol{C}, \boldsymbol{D})$ is balanced, the two gramians $(\boldsymbol{P}, \boldsymbol{Y})$ are equal and diagonal $\boldsymbol{P} = \boldsymbol{Y} = \boldsymbol{\Sigma}$, and satisfy the following equations

$$\boldsymbol{P} = \boldsymbol{Y} = \boldsymbol{\Sigma} = \begin{bmatrix} \boldsymbol{\Sigma}_1 & \boldsymbol{0} \\ \boldsymbol{0} & \boldsymbol{\Sigma}_2 \end{bmatrix} > \boldsymbol{0} \tag{5.108}$$

$$\boldsymbol{A}\boldsymbol{\Sigma} + \boldsymbol{\Sigma}\boldsymbol{A}^T + \boldsymbol{Q} = \boldsymbol{0} \tag{5.109}$$

Writing out the latter equation in terms of its partitioned blocks gives

$$\begin{bmatrix} \boldsymbol{A}_{11}\boldsymbol{\Sigma}_1 + \boldsymbol{\Sigma}_1\boldsymbol{A}_{11}^T + \boldsymbol{Q}_{11} & \boldsymbol{A}_{12}\boldsymbol{\Sigma}_2 + \boldsymbol{\Sigma}_1\boldsymbol{A}_{21}^T + \boldsymbol{Q}_{12} \\ \boldsymbol{A}_{21}\boldsymbol{\Sigma}_1 + \boldsymbol{\Sigma}_1\boldsymbol{A}_{11}^T + \boldsymbol{Q}_{21} & \boldsymbol{A}_{22}\boldsymbol{\Sigma}_2 + \boldsymbol{\Sigma}_2\boldsymbol{A}_{22}^T + \boldsymbol{Q}_{22} \end{bmatrix} = \boldsymbol{0} \tag{5.110}$$

For the truncated system $(\boldsymbol{A}_{11}, \boldsymbol{B}_1, \boldsymbol{C}_1, \boldsymbol{D})$ it follows that

$$\boldsymbol{\Sigma}_1 = \boldsymbol{\Sigma}_1^T > \boldsymbol{0} \tag{5.111}$$

$$\boldsymbol{Q}_{11} = \boldsymbol{Q}_{11}^T > \boldsymbol{0} \tag{5.112}$$

$$\boldsymbol{A}_{11}\boldsymbol{\Sigma}_1 + \boldsymbol{\Sigma}_1\boldsymbol{A}_{11}^T + \boldsymbol{Q}_{11} = \boldsymbol{0} \tag{5.113}$$

and stability of $\boldsymbol{G}_r(s)$ can be concluded. ■
In the next section this result will be extended to positive real systems, and used as a tool for finding new types of algorithms.

5.3.2 Positive Real Projection

In this section we extend the results of Section 5.2.3. As long as one of the gramians in the balanced truncation algorithm satisfies the PR or DPR equations this will give positive real state transformations. Hence, only one of the gramians in the balanced truncation algorithm must satisfy the positive real lemma.

The positive real system $\boldsymbol{G}(s) = (\boldsymbol{A}, \boldsymbol{B}, \boldsymbol{C}, \boldsymbol{D})$ will satisfy the positive real equations

$$\boldsymbol{A}\boldsymbol{R} + \boldsymbol{R}\boldsymbol{A}^T = -\boldsymbol{B}_l\boldsymbol{B}_l^T \tag{5.114}$$

$$\boldsymbol{R}\boldsymbol{C}^T - \boldsymbol{B} = -\boldsymbol{B}_l\boldsymbol{D}_l^T \tag{5.115}$$

$$-\boldsymbol{D} - \boldsymbol{D}^T = -\boldsymbol{D}_l\boldsymbol{D}_l^T \tag{5.116}$$

where $\boldsymbol{R} = \boldsymbol{R}^T > \boldsymbol{0}$, $\boldsymbol{B}_l$ and $\boldsymbol{D}_l$ are to be solved for. These equations can be rewritten as a linear matrix inequality (LMI)

$$\begin{bmatrix} \boldsymbol{A}\boldsymbol{R} + \boldsymbol{R}\boldsymbol{A}^T & \boldsymbol{R}\boldsymbol{C}^T - \boldsymbol{B} \\ \boldsymbol{C}\boldsymbol{R} - \boldsymbol{B}^T & -\boldsymbol{D} - \boldsymbol{D}^T \end{bmatrix} = -\begin{bmatrix} \boldsymbol{B}_l \\ \boldsymbol{D}_l \end{bmatrix} \begin{bmatrix} \boldsymbol{B}_l^T & \boldsymbol{D}_l^T \end{bmatrix} \leq \boldsymbol{0} \tag{5.117}$$

where $\boldsymbol{R}$ is to be solved for. Having $\boldsymbol{R}$ and balancing this with an arbitrary positive real symmetric matrix $\boldsymbol{Y}$, $\boldsymbol{R} = \boldsymbol{Y} = \boldsymbol{\Sigma}$ will give a positive real state transformation $\boldsymbol{T}$. Associated with the positive real system $\boldsymbol{G}(s)$ is also a pair of dual positive real equations

$$\boldsymbol{A}^T\boldsymbol{O} + \boldsymbol{O}\boldsymbol{A} = -\boldsymbol{C}_r^T\boldsymbol{C}_r \tag{5.118}$$

$$\boldsymbol{O}\boldsymbol{B} - \boldsymbol{C}^T = -\boldsymbol{C}_r^T\boldsymbol{D}_r \tag{5.119}$$

$$-\boldsymbol{D} - \boldsymbol{D}^T = -\boldsymbol{D}_r^T\boldsymbol{D}_r \tag{5.120}$$

where $\boldsymbol{O} = \boldsymbol{O}^T > \boldsymbol{0}$, $\boldsymbol{C}_r$ and $\boldsymbol{D}_r$ are to be solved for. The LMI representation of these equations is

$$\begin{bmatrix} \boldsymbol{A}^T\boldsymbol{O} + \boldsymbol{O}\boldsymbol{A} & \boldsymbol{O}\boldsymbol{B} - \boldsymbol{C}^T \\ \boldsymbol{B}^T\boldsymbol{O} - \boldsymbol{C} & -\boldsymbol{D} - \boldsymbol{D}^T \end{bmatrix} = -\begin{bmatrix} \boldsymbol{C}_r^T \\ \boldsymbol{D}_r^T \end{bmatrix} \begin{bmatrix} \boldsymbol{C}_r & \boldsymbol{D}_r \end{bmatrix} \leq \boldsymbol{0} \tag{5.121}$$

Balancing $\boldsymbol{O}$ with an arbitrary symmetric positive real matrix $\boldsymbol{Y}$ will also give positive real state transformation $\boldsymbol{T}$.

Theorem 5.3 *Let the positive real and minimal system $\boldsymbol{G}(s)$ have the balanced realization*

$$\boldsymbol{G}(s) = \left[\begin{array}{c|c} \boldsymbol{A} & \boldsymbol{B} \\ \hline \boldsymbol{C} & \boldsymbol{D} \end{array}\right] = \left[\begin{array}{cc|c} \boldsymbol{A}_{11} & \boldsymbol{A}_{12} & \boldsymbol{B}_1 \\ \boldsymbol{A}_{21} & \boldsymbol{A}_{22} & \boldsymbol{B}_2 \\ \hline \boldsymbol{C}_1 & \boldsymbol{C}_2 & \boldsymbol{D} \end{array}\right] \tag{5.122}$$

where

$$\boldsymbol{R} = \boldsymbol{Y} = \boldsymbol{\Sigma} \tag{5.123}$$

$$\text{arbitrary } \boldsymbol{Y} = \boldsymbol{Y}^T > \boldsymbol{0} \tag{5.124}$$

$$\begin{bmatrix} \boldsymbol{A}\boldsymbol{R} + \boldsymbol{R}\boldsymbol{A}^T & \boldsymbol{R}\boldsymbol{C}^T - \boldsymbol{B} \\ \boldsymbol{C}\boldsymbol{R} - \boldsymbol{B}^T & -\boldsymbol{D} - \boldsymbol{D}^T \end{bmatrix} \leq \boldsymbol{0} \tag{5.125}$$

$$\boldsymbol{R} = \boldsymbol{R}^T > \boldsymbol{0} \tag{5.126}$$

or

$$\boldsymbol{O} = \boldsymbol{Y} = \boldsymbol{\Sigma} \tag{5.127}$$

$$\text{arbitrary } \boldsymbol{Y} = \boldsymbol{Y}^T > \boldsymbol{0} \tag{5.128}$$

$$\begin{bmatrix} \boldsymbol{A}^T\boldsymbol{O} + \boldsymbol{O}\boldsymbol{A} & \boldsymbol{O}\boldsymbol{B} - \boldsymbol{C}^T \\ \boldsymbol{B}^T\boldsymbol{O} - \boldsymbol{C} & -\boldsymbol{D} - \boldsymbol{D}^T \end{bmatrix} \leq \boldsymbol{0} \tag{5.129}$$

$$\boldsymbol{O} = \boldsymbol{O}^T > \boldsymbol{0} \tag{5.130}$$

Then the reduced order model

$$\boldsymbol{G}_r(s) = \begin{bmatrix} \boldsymbol{A}_{11} & \boldsymbol{B}_1 \\ \boldsymbol{C}_1 & \boldsymbol{D} \end{bmatrix} \tag{5.131}$$

obtained by truncation is positive real.

Proof. Since $(\boldsymbol{A}, \boldsymbol{B}, \boldsymbol{C}, \boldsymbol{D})$ are balanced, the two gramians $(\boldsymbol{R}, \boldsymbol{Y})$ are equal $\boldsymbol{R} = \boldsymbol{Y} = \boldsymbol{\Sigma}$, and satisfy the following equations

$$\boldsymbol{\Sigma} = \boldsymbol{\Sigma}^T = \begin{bmatrix} \boldsymbol{\Sigma}_1 & \boldsymbol{0} \\ \boldsymbol{0} & \boldsymbol{\Sigma}_2 \end{bmatrix} > \boldsymbol{0} \tag{5.132}$$

$$\begin{bmatrix} \boldsymbol{A}\boldsymbol{\Sigma} + \boldsymbol{\Sigma}\boldsymbol{A}^T & \boldsymbol{\Sigma}\boldsymbol{C}^T - \boldsymbol{B} \\ \boldsymbol{C}\boldsymbol{\Sigma} - \boldsymbol{B}^T & -\boldsymbol{D} - \boldsymbol{D}^T \end{bmatrix} \leq \boldsymbol{0} \tag{5.133}$$

Writing out the last equation in terms of its partitioned blocks gives

$$\begin{bmatrix} \boldsymbol{A}_{11}\boldsymbol{\Sigma}_1 + \boldsymbol{\Sigma}_1\boldsymbol{A}_{11}^T & \boldsymbol{A}_{12}\boldsymbol{\Sigma}_2 + \boldsymbol{\Sigma}_1\boldsymbol{A}_{21}^T & \boldsymbol{\Sigma}_1\boldsymbol{C}_1^T - \boldsymbol{B}_1 \\ \boldsymbol{A}_{21}\boldsymbol{\Sigma}_1 + \boldsymbol{\Sigma}_2\boldsymbol{A}_{12}^T & \boldsymbol{A}_{22}\boldsymbol{\Sigma}_2 + \boldsymbol{\Sigma}_2\boldsymbol{A}_{22}^T & \boldsymbol{\Sigma}_2\boldsymbol{C}_2^T - \boldsymbol{B}_2 \\ \boldsymbol{C}_1\boldsymbol{\Sigma}_1 - \boldsymbol{B}_1^T & \boldsymbol{C}_2\boldsymbol{\Sigma}_2 - \boldsymbol{B}_2^T & -\boldsymbol{D} - \boldsymbol{D}^T \end{bmatrix} \leq \boldsymbol{0} \tag{5.134}$$

For the system $(\boldsymbol{A}_{11}, \boldsymbol{B}_1, \boldsymbol{C}_1, \boldsymbol{D})$

$$\boldsymbol{\Sigma}_1 = \boldsymbol{\Sigma}_1^T > \boldsymbol{0} \tag{5.135}$$

$$\begin{bmatrix} \boldsymbol{A}_{11}\boldsymbol{\Sigma}_1 + \boldsymbol{\Sigma}_1\boldsymbol{A}_{11}^T & \boldsymbol{\Sigma}_1\boldsymbol{C}_1^T - \boldsymbol{B}_1 \\ \boldsymbol{C}_1\boldsymbol{\Sigma}_1 - \boldsymbol{B}_1^T & -\boldsymbol{D} - \boldsymbol{D}^T \end{bmatrix} \leq \boldsymbol{0} \tag{5.136}$$

and positive realness of $\boldsymbol{G}_r(s)$ can be concluded. The same can be shown for the pair $(\boldsymbol{O}, \boldsymbol{Y})$. ■

By knowing these properties, it is now possible to develop new positive real balanced truncation methods. In the next section this will be illustrated by using these properties to develop an algorithm for positive real frequency weighted truncation.

5.3.3 Frequency Weighted Truncation

In this section the focus will be on SISO systems. The balancing methods in Section (5.2.1)-(5.2.3) approximate the system $G(s)$ over all frequencies. For some systems it might be of interest to do an approximation only in a certain range of frequencies. This is called frequency weighted truncation. This can be done by weighting the error system by an input weight $W_i(s)$ or/and an output weight $W_o(s)$,

$$||W_o(s)(G(s) - G_r(s))W_i(s)||_\infty \tag{5.137}$$

such that the weighted error is small. Most methods for frequency weighted reduction have focused on keeping the stability properties of the system, good overviews of different methods are given in Obinata and Anderson (2001) and Antoulas (2005). In this section we will extend the frequency weighting to positive real input weighted balancing and positive real output weighted balancing.

Let the positive real minimal system $G(s)$ be written as

$$G(s) = \left[\begin{array}{cc} \boldsymbol{A} & \boldsymbol{B} \\ \boldsymbol{C} & \boldsymbol{D} \end{array}\right] \tag{5.138}$$

and let the input weight be denoted by $W_i(s)$, where

$$W_i(s) = \left[\begin{array}{cc} \boldsymbol{A}_i & \boldsymbol{B}_i \\ \boldsymbol{C}_i & \boldsymbol{D}_i \end{array}\right] \tag{5.139}$$

The augmented system can now be written as

$$\bar{G}(s) = G(s)W_i(s) = \left[\begin{array}{cc} \bar{\boldsymbol{A}}_i & \bar{\boldsymbol{B}}_i \\ \bar{\boldsymbol{C}}_i & \bar{\boldsymbol{D}}_i \end{array}\right] = \left[\begin{array}{cc|c} \boldsymbol{A} & \boldsymbol{B}\boldsymbol{C}_i & \boldsymbol{B}\boldsymbol{D}_i \\ \boldsymbol{0} & \boldsymbol{A}_i & \boldsymbol{B}_i \\ \hline \boldsymbol{C} & \boldsymbol{D}\boldsymbol{C}_i & \boldsymbol{D}_i\boldsymbol{D} \end{array}\right] \tag{5.140}$$

This gives the following weighted error system

$$||(G(s) - G_r(s))W_i(s)||_\infty \tag{5.141}$$

Assuming that $W_i(s)$ is chosen such that the overall system $\bar{G}(s)$ is stable, the controllability gramian for the overall system can be solved for

$$\bar{\boldsymbol{A}}_i\bar{\boldsymbol{P}} + \bar{\boldsymbol{P}}\bar{\boldsymbol{A}}_i^T + \bar{\boldsymbol{B}}_i\bar{\boldsymbol{B}}_i^T = \boldsymbol{0} \tag{5.142}$$

where $\bar{\boldsymbol{P}} = \bar{\boldsymbol{P}}^T > \boldsymbol{0}$ and

$$\bar{\boldsymbol{P}} = \left[\begin{array}{cc} \boldsymbol{P} & \bar{\boldsymbol{P}}_{12} \\ \bar{\boldsymbol{P}}_{21} & \bar{\boldsymbol{P}}_{22} \end{array}\right] \tag{5.143}$$

Expanding (5.142) gives the following (1,1) block

$$\boldsymbol{A}\boldsymbol{P} + \boldsymbol{P}\boldsymbol{A}^T + \boldsymbol{B}\boldsymbol{D}_i\boldsymbol{D}_i^T\boldsymbol{B}^T = \boldsymbol{0} \tag{5.144}$$

where $\boldsymbol{P} = \boldsymbol{P}^T > \boldsymbol{0}$. Further, the available storage gramian is solved for the unweighted system (5.138)

$$\boldsymbol{A}^T\boldsymbol{O} + \boldsymbol{O}\boldsymbol{A} + (\boldsymbol{O}\boldsymbol{B} - \boldsymbol{C}^T)(\boldsymbol{D} + \boldsymbol{D}^T)^{-1}(\boldsymbol{B}^T\boldsymbol{O} - \boldsymbol{C}) = \boldsymbol{0} \tag{5.145}$$

By combining $(\boldsymbol{P}, \boldsymbol{O})$ from (5.144) and (5.145), input weighted positive real reduced order systems can be obtained. Assuming that $(\boldsymbol{P}, \boldsymbol{O})$ are balanced, $\boldsymbol{P} = \boldsymbol{O} = \boldsymbol{\Sigma}$, we obtain the following equations,

$$\boldsymbol{\Sigma} = \boldsymbol{\Sigma}^T = \begin{bmatrix} \boldsymbol{\Sigma}_1 & \boldsymbol{0} \\ \boldsymbol{0} & \boldsymbol{\Sigma}_2 \end{bmatrix} > \boldsymbol{0} \tag{5.146}$$

$$\boldsymbol{A}\boldsymbol{\Sigma} + \boldsymbol{\Sigma}\boldsymbol{A}^T + \boldsymbol{B}\boldsymbol{D}_i\boldsymbol{D}_i^T\boldsymbol{B}^T = \boldsymbol{0} \tag{5.147}$$

$$\boldsymbol{A}^T\boldsymbol{\Sigma} + \boldsymbol{\Sigma}\boldsymbol{A} + (\boldsymbol{\Sigma}\boldsymbol{B} - \boldsymbol{C}^T)(\boldsymbol{D} + \boldsymbol{D}^T)^{-1}(\boldsymbol{B}^T\boldsymbol{\Sigma} - \boldsymbol{C}) = \boldsymbol{0} \tag{5.148}$$

Writing down the $(1,1)$ blocks of the two latter equations gives

$$\boldsymbol{A}_{11}\boldsymbol{\Sigma}_1 + \boldsymbol{\Sigma}_1\boldsymbol{A}_{11}^T + \boldsymbol{B}_1\boldsymbol{D}_i\boldsymbol{D}_i^T\boldsymbol{B}_1^T = \boldsymbol{0} \tag{5.149}$$

$$\boldsymbol{A}_{11}^T\boldsymbol{\Sigma}_1 + \boldsymbol{\Sigma}_1\boldsymbol{A}_{11} + (\boldsymbol{\Sigma}_1\boldsymbol{B}_1 - \boldsymbol{C}_1^T)(\boldsymbol{D} + \boldsymbol{D}^T)^{-1}(\boldsymbol{B}_1^T\boldsymbol{\Sigma}_1 - \boldsymbol{C}_1) = \boldsymbol{0} \tag{5.150}$$

where one can see that the reduced order system satisfies the Riccati equation and hence it will be positive real. By choosing the input weight $W_i(s)$ properly, the weighted error in (5.141) will be small.

This approach can also be used on output weighted systems. Let the output weight of the system be denoted by $W_o(s)$, where

$$W_o(s) = \begin{bmatrix} \boldsymbol{A}_o & \boldsymbol{B}_o \\ \boldsymbol{C}_o & \boldsymbol{D}_o \end{bmatrix} \tag{5.151}$$

The augmented output weighted system can now be written as

$$\hat{G}(s) = W_o(s)G(s) = \begin{bmatrix} \hat{\boldsymbol{A}}_o & \hat{\boldsymbol{B}}_o \\ \hat{\boldsymbol{C}}_o & \hat{\boldsymbol{D}}_o \end{bmatrix} = \left[\begin{array}{cc|c} \boldsymbol{A} & \boldsymbol{0} & \boldsymbol{B} \\ \boldsymbol{B}_o\boldsymbol{C} & \boldsymbol{A}_o & \boldsymbol{B}_o\boldsymbol{D} \\ \hline \boldsymbol{D}_o\boldsymbol{C} & \boldsymbol{C}_o & \boldsymbol{D}_o\boldsymbol{D} \end{array}\right] \tag{5.152}$$

with the associated weighted error system

$$||W_o(s)(G(s) - G_r(s))||_\infty \tag{5.153}$$

Assuming that $W_o(s)$ is chosen such that the overall system $\hat{G}(s)$ is stable, then the observability gramian for the overall system can be solved for

$$\hat{\boldsymbol{A}}_o^T\hat{\boldsymbol{Q}} + \hat{\boldsymbol{Q}}\hat{\boldsymbol{A}}_o + \hat{\boldsymbol{C}}_o^T\hat{\boldsymbol{C}}_o = \boldsymbol{0} \tag{5.154}$$

where $\hat{\boldsymbol{Q}} = \hat{\boldsymbol{Q}}^T > \boldsymbol{0}$. Let $\hat{\boldsymbol{Q}}$ be written as

$$\hat{\boldsymbol{Q}} = \begin{bmatrix} \boldsymbol{Q} & \hat{\boldsymbol{Q}}_{12} \\ \hat{\boldsymbol{Q}}_{21} & \hat{\boldsymbol{Q}}_{22} \end{bmatrix} \tag{5.155}$$

Expanding (5.154) gives the following $(1,1)$ block

$$\boldsymbol{A}^T\boldsymbol{Q} + \boldsymbol{Q}\boldsymbol{A} + \boldsymbol{C}^T\boldsymbol{D}_o^T\boldsymbol{D}_o\boldsymbol{C} = \boldsymbol{0} \tag{5.156}$$

where $\boldsymbol{Q} = \boldsymbol{Q}^T > \boldsymbol{0}$. Further, the required supply gramian is solved for the unweighted system (5.138)

$$\boldsymbol{A}\boldsymbol{R} + \boldsymbol{R}\boldsymbol{A}^T + (\boldsymbol{R}\boldsymbol{C}^T - \boldsymbol{B})(\boldsymbol{D} + \boldsymbol{D}^T)^{-1}(\boldsymbol{C}\boldsymbol{R} - \boldsymbol{B}^T) = \boldsymbol{0} \tag{5.157}$$

By combining $(\boldsymbol{R}, \boldsymbol{Q})$ from (5.156) and (5.157) output weighted positive real reduced order systems can be obtained. When $(\boldsymbol{R}, \boldsymbol{Q})$ are balanced, $\boldsymbol{R} = \boldsymbol{Q} = \boldsymbol{\Sigma}$, we have the following equations

$$\boldsymbol{\Sigma} = \boldsymbol{\Sigma}^T = \begin{bmatrix} \boldsymbol{\Sigma}_1 & \boldsymbol{0} \\ \boldsymbol{0} & \boldsymbol{\Sigma}_2 \end{bmatrix} > \boldsymbol{0} \tag{5.158}$$

$$\boldsymbol{A}\boldsymbol{\Sigma} + \boldsymbol{\Sigma}\boldsymbol{A}^T + \boldsymbol{C}^T\boldsymbol{D}_o^T\boldsymbol{D}_o\boldsymbol{C} = \boldsymbol{0} \tag{5.159}$$

$$\boldsymbol{A}\boldsymbol{\Sigma} + \boldsymbol{\Sigma}\boldsymbol{A}^T + (\boldsymbol{\Sigma}\boldsymbol{C}^T - \boldsymbol{B})(\boldsymbol{D} + \boldsymbol{D}^T)^{-1}(\boldsymbol{C}\boldsymbol{\Sigma} - \boldsymbol{B}^T) = \boldsymbol{0} \tag{5.160}$$

By writing down the $(1,1)$ blocks of the two latter equations

$$\boldsymbol{A}_{11}\boldsymbol{\Sigma}_1 + \boldsymbol{\Sigma}_1\boldsymbol{A}_{11}^T + \boldsymbol{C}_1^T\boldsymbol{D}_o^T\boldsymbol{D}_o\boldsymbol{C}_1 = \boldsymbol{0} \tag{5.161}$$

$$\boldsymbol{A}_{11}\boldsymbol{\Sigma}_1 + \boldsymbol{\Sigma}_1\boldsymbol{A}_{11}^T + (\boldsymbol{\Sigma}_1\boldsymbol{C}_1^T - \boldsymbol{B}_1)(\boldsymbol{D} + \boldsymbol{D}^T)^{-1}(\boldsymbol{C}_1\boldsymbol{\Sigma}_1 - \boldsymbol{B}_1^T) = \boldsymbol{0} \tag{5.162}$$

one can see that the reduced order system satisfies a Riccati equation, and hence it will be positive real.

5.4 Concluding Remarks

A survey of Lyapunov balancing and stochastic balancing has been given. Based on these algorithms a new approach for obtaining positive real balanced truncation has been suggested, which we called mixed gramian balancing. This approach is a combination of Lyapunov balancing and Riccati

balancing and relies upon balancing the solution of one Lyapunov equation and one Riccati equation. Riccati balancing relies upon the solution of two Riccati equations, while the mixed balancing relies on the solution of one Lyapunov equation and one Riccati equation. This is less computationally demanding.

Further it has been shown that in order to obtain positive real truncated systems, only one of the gramians in the balancing algorithm needs to satisfy either the PR or the DPR equations. This opens the way for new combinations of gramians in order to obtain positive real truncated systems. Here it has been used to obtain positive real frequency weighted truncation. For future research it would be of interest to find error bounds for the proposed algorithms.

There already are model reduction methods in the literature for the H_2 or H_∞ norm which give stable systems (Yan and Lam, 1999). For future work it would be interesting to see if it is possible to extend some of this work to positive real systems that exploit the properties in this chapter.

Chapter 6

Case Studies

6.1 Introduction

The preceding chapters have revealed the structure and stability properties of the radiation forces. In this chapter three different approaches for the identification of the radiation forces are investigated; identification of each mode as a SISO system, identification of each mode as a SISO system followed by MIMO reduction of the overall system and MIMO identification of the overall system. The identification is done both in the time and frequency domain in order to compare the two approaches. The proposed approaches are compared in terms of estimated model order, accuracy of fit, use of available information, ease of use and generation of positive real systems. Two different case studies are done. The radiation forces of a 3-DOF horizontal vessel model are identified from the frequency dependent added mass and damping matrices given by the software WAMIT. Subsequently the radiation forces for a lateral vessel model are identified from data sets from the software VERES. Section 6.2 presents the case study with the 3-DOF vessel model and Section 6.3 considers the case study with the lateral vessel model. Finally Section 6.4 discusses the different approaches.

6.2 3-DOF Vessel Model from WAMIT Data

In this section the radiation forces of a 3-DOF vessel will be identified from the frequency dependent added mass and damping matrices obtained from the software WAMIT. The vessel has port/starboard symmetry. The 6-DOF

equations of motion are written as

$$\begin{aligned} \boldsymbol{M}\ddot{\boldsymbol{\xi}}(t) + \boldsymbol{\tau}_{R2}(t) + \boldsymbol{C}_h\boldsymbol{\xi}(t) &= \boldsymbol{\tau}_{visc}(t) + \boldsymbol{\tau}_{ext}(t) + \boldsymbol{\tau}_A(t) && (6.1)\\ \dot{\boldsymbol{x}}(t) &= \boldsymbol{A}\boldsymbol{x}(t) + \boldsymbol{B}\dot{\boldsymbol{\xi}}(t) && (6.2)\\ \boldsymbol{\tau}_{R2}(t) &= \boldsymbol{C}\boldsymbol{x}(t) && (6.3) \end{aligned}$$

In the Laplace domain this is

$$\boldsymbol{M}\ddot{\boldsymbol{\xi}}(s) + \boldsymbol{K}(s)\dot{\boldsymbol{\xi}}(s) + \boldsymbol{C}_h\boldsymbol{\xi}(s) = \boldsymbol{\tau}_{visc}(s) + \boldsymbol{\tau}_{ext}(s) + \boldsymbol{\tau}_A(s) \tag{6.4}$$

A horizontal vessel model can be described by a 3-DOF model containing the displacements in surge, sway and yaw (Fossen, 2002)

$$\boldsymbol{\xi} = [\xi_1, \xi_2, \xi_6]^T \tag{6.5}$$

We then get the following vessel model

$$\begin{aligned} \boldsymbol{M}\ddot{\boldsymbol{\xi}}(t) + \boldsymbol{\tau}_{R2}(t) &= \boldsymbol{\tau}_{visc}(t) + \boldsymbol{\tau}_{ext}(t) + \boldsymbol{\tau}_A(t) && (6.6)\\ \dot{\boldsymbol{x}}(t) &= \boldsymbol{A}\boldsymbol{x}(t) + \boldsymbol{B}\dot{\boldsymbol{\xi}}(t) && (6.7) \end{aligned}$$

This can be written in the Laplace domain as

$$\boldsymbol{M}\ddot{\boldsymbol{\xi}}(s) + \boldsymbol{K}(s)\dot{\boldsymbol{\xi}}(s) = \boldsymbol{\tau}_{visc}(s) + \boldsymbol{\tau}_{ext}(s) + \boldsymbol{\tau}_A(s) \tag{6.8}$$

where

$$\boldsymbol{M} = \begin{bmatrix} M_{11} & 0 & 0 \\ 0 & M_{22} & M_{23} \\ 0 & M_{32} & M_{33} \end{bmatrix}, \ \boldsymbol{K}(s) = \begin{bmatrix} K_{11}(s) & 0 & 0 \\ 0 & K_{22}(s) & K_{26}(s) \\ 0 & K_{62}(s) & K_{66}(s) \end{bmatrix} \tag{6.9}$$

Here $K_{11}(s)$, $K_{22}(s)$ and $K_{66}(s)$ should be strictly proper with relative degree 1 and positive real, and $K_{26} = K_{62}$ should be stable and of relative degree 1 and the transfer function $K(s)$ should be positive real.

WAMIT is developed at the Massachusetts Institute of Technology (MIT). The software is a radiation/diffraction panel program developed for linear analysis of the interaction of surface waves with offshore structures. WAMIT is used to compute the frequency dependent added mass matrix $\boldsymbol{A}(\omega)$ and the frequency dependent damping matrix $\boldsymbol{B}(\omega)$ for a barge (TEST20 in (www.wamit.com, 2006)). The software can calculate the modes,

$$A_{ij}(\omega) \ \forall \ i = (1, \ldots, 6), \ j = (1, \ldots, 6) \tag{6.10}$$

$$B_{ij}(\omega) \ \forall \ i = (1, \ldots, 6), \ j = (1, \ldots, 6). \tag{6.11}$$

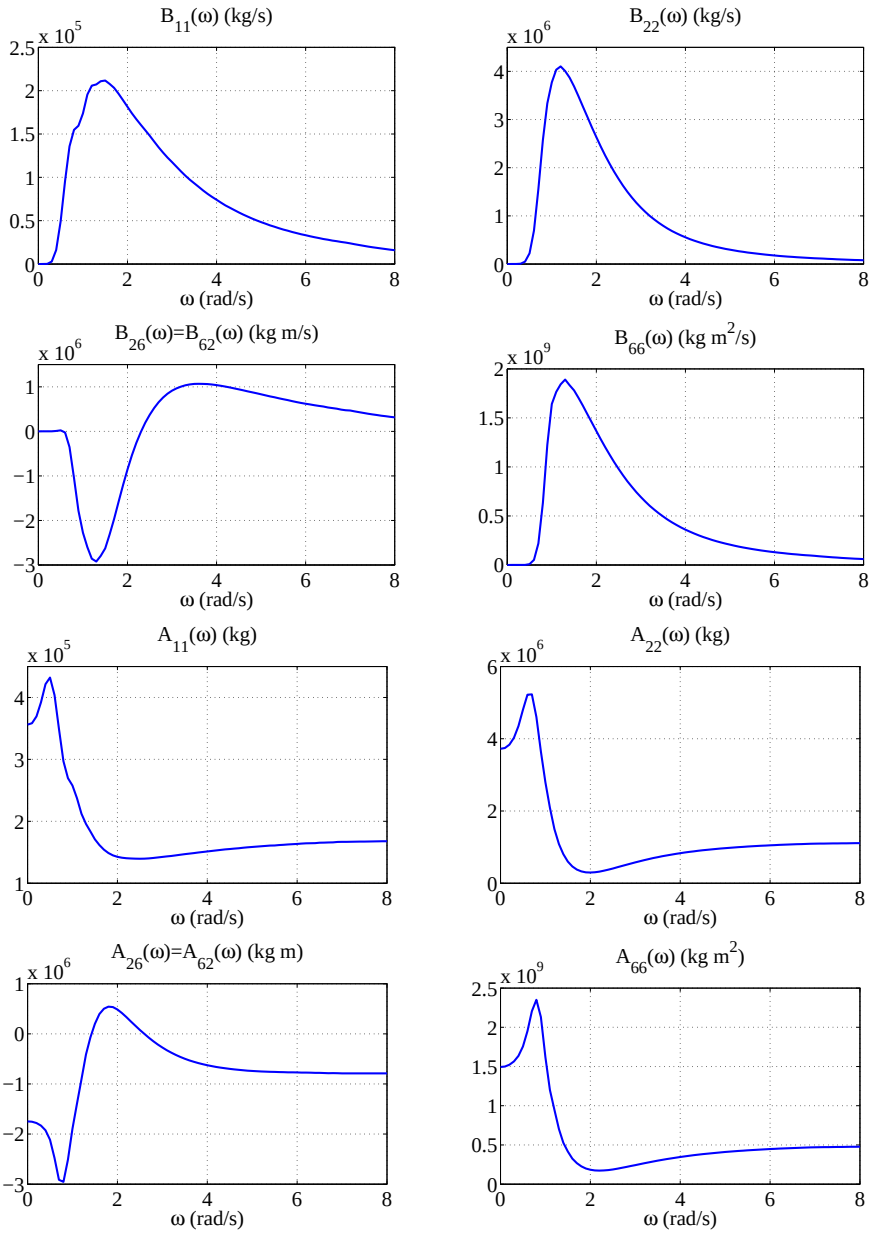

Figure 6.1: Frequency dependent damping parameters $B_{ij}(\omega)$ and frequency dependent added mass parameters $A_{ij}(\omega)$ for the 3-DOF barge model plotted against the frequency ω.

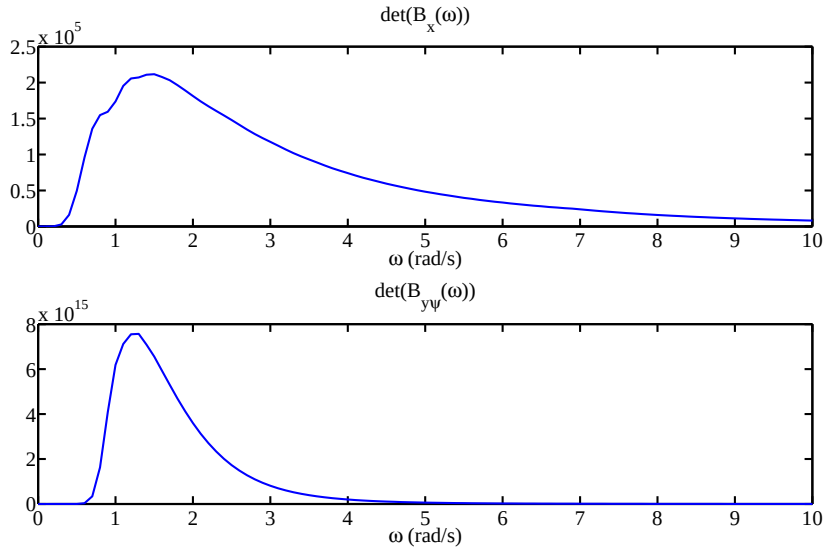

Figure 6.2: The determinants of the matrices $B_x(\omega)$ and $\boldsymbol{B}_{y\psi}(\omega)$ over the frequencies ω.

The frequency dependent added mass matrix $\boldsymbol{A}(\omega)$ and the frequency dependent damping matrix $\boldsymbol{B}(\omega)$ used for the 3-DOF model of the barge are both plotted in Figure 6.1.

First the positive realness of the radiation forces in the system is verified. The 3-DOF system

$$\boldsymbol{K}(s) = \left[\begin{array}{c|cc} K_{11}(s) & 0 & 0 \\ \hline 0 & K_{22}(s) & K_{26}(s) \\ 0 & K_{62}(s) & K_{66}(s) \end{array}\right] \tag{6.12}$$

is positive real if the associated damping matrix is positive real. The system can be decoupled in one system describing the surge dynamics and one system describing the dynamics in sway and yaw,

$$K_x(s) = [K_{11}(s)] \tag{6.13}$$

$$\boldsymbol{K}_{y\psi}(s) = \begin{bmatrix} K_{22}(s) & K_{26}(s) \\ K_{62}(s) & K_{66}(s) \end{bmatrix} \tag{6.14}$$

Hence the system is positive real if

$$\det(B_x(\omega)) = \det([B_{11}(\omega)]) \geq 0, \ \forall \ \omega \tag{6.15}$$

$$\det(\boldsymbol{B}_{y\psi}(\omega)) = \det\left(\begin{bmatrix} B_{22}(\omega) & B_{26}(\omega) \\ B_{62}(\omega) & B_{66}(\omega) \end{bmatrix}\right) \geq 0, \ \forall \ \omega \tag{6.16}$$

The determinant of the matrices $B_x(\omega)$ and $\boldsymbol{B}_{y\psi}(\omega)$ for all frequencies are plotted in Figure 6.2, and it can be concluded that the data set obtained from WAMIT represents a positive real system.

The time domain identification of the system is done from the impulse response of the system. The impulse responses of the system is given by

$$\boldsymbol{k}(t) = \frac{2}{\pi}\int_0^{\Omega} \boldsymbol{B}(\omega)cos(\omega t)\ d\omega = \begin{bmatrix} k_{11}(t) & 0 & 0 \\ 0 & k_{22}(t) & k_{26}(t) \\ 0 & k_{62}(t) & k_{66}(t) \end{bmatrix} \tag{6.17}$$

The upper limit of the integral Ω is set to 20 (rad/s) since the damping matrix $\boldsymbol{B}(\omega)$ has converged to zero for all modes at this frequency (plot of the damping modes are given in Figure 6.1).

The frequency domain identification is done from the frequency response of the radiation forces,

$$\boldsymbol{K}(j\omega) = \boldsymbol{B}(\omega) + j\omega(\boldsymbol{A}(\omega) - \boldsymbol{A}(\infty)) = \begin{bmatrix} K_{11}(j\omega) & 0 & 0 \\ 0 & K_{22}(j\omega) & K_{26}(j\omega) \\ 0 & K_{62}(j\omega) & K_{66}(j\omega) \end{bmatrix} \tag{6.18}$$

The most interesting part is the identification of the system describing the dynamics in surge and sway. This system can be identified by using SISO or MIMO identification, as will be shown. Three different approaches will be used:

- SISO identification of each mode.
- MIMO identification of the overall system.
- SISO identification of each mode followed by MIMO model reduction.

For the approaches the time domain scheme presented in Section 4.2 will be used, before the frequency domain schemes from Section 4.3 will be used. For model reduction the algorithms in Section 5.2.1-5.2.3 will be used.

6.2.1 SISO Identification

The model of the radiation forces for the 3-DOF model are identified by doing SISO identification of each mode individually. By doing SISO identification the order n of each mode can be independently chosen, and the optimal fit in each mode can be chosen. For each mode models of the order of 2, 4 and 6 are obtained by using the different identification methods.

Table 6.1: 10 first singular values of the Hankel matrices in different modes

Modes			
$k_{11}(t)$	$k_{22}(t)$	$k_{26=62}(t)$	$k_{66}(t)$
$(\cdot 10^4)$	$(\cdot 10^5)$	$(\cdot 10^5)$	$(\cdot 10^8)$
116.33	233.83	206.47	112.53
107.02	212.74	174.88	98.26
17.63	33.66	60.28	22.02
10.98	10.38	32.17	7.05
5.68	3.21	8.64	2.20
2.51	2.00	4.37	2.18
2.02	1.05	2.10	0.96
1.93	0.64	1.73	0.79
0.90	0.49	1.53	0.61
0.70	0.42	1.43	0.50

The different identified models are compared in terms of the fit of the impulse response (IR) and the fit of the phase (Ph.) and magnitude (Mag.) in the Bode plot. This has been done by use of the multiple correlation coefficient (squared) (Ljung, 1999)

$$R_y^2 = 1 - \frac{\boldsymbol{e}^T\boldsymbol{e}}{\boldsymbol{y}^T\boldsymbol{y}} \tag{6.19}$$

where $\boldsymbol{e}^T\boldsymbol{e}$ is the sum of squared errors and $\boldsymbol{y}^T\boldsymbol{y}$ is the sum of square of the original data set. The multiple correlation coefficient gives information about the goodness of a fit of a model to the original data set. The reason for using this is to give an indication of how well the identified model fits both the impulse response and the Bode plot. Further the $||\cdot||_\infty$-errors between the original data sets and the identified models are found, $||E(s)||_\infty = \max_\omega |E(j\omega)|$. For the diagonal modes and those modes where the data sets indicate positive realness the identified models are checked for this property. In addition

it is chosen to use structure as a measure, where we know that the time domain (TD) approach does not give the wanted structure, while the frequency domain (FD) approaches will.

The Hankel SVD realization is done in the time domain. The 10 first singular values obtained for the different modes are shown in Table 6.1. From the singular values one can see that most of the dynamics in the different modes can be captured by low order models.

Table 6.2: Error Measures for the SISO Identification

	R_y^2=1 − $\frac{\boldsymbol{e}^T\boldsymbol{e}}{\boldsymbol{y}^T\boldsymbol{y}}$					
	IR	Ph.	Mag.	$\|\|\cdot\|\|_\infty$	PR	Structure
Mode:	K_{11}					
TD:	Hankel SVD					
$n=2$	0.9839	0.9004	0.9750	$4.39 \cdot 10^4$	×	-
$n=4$	0.9853	0.8995	0.9754	$3.01 \cdot 10^4$	×	-
$n=6$	0.9873	0.8989	0.9754	$2.55 \cdot 10^4$	×	-
FD 1:	pem					
$n=2$	0.9852	0.9862	0.9894	$3.38 \cdot 10^4$	×	×
$n=4$	0.9883	0.9874	0.9906	$1.05 \cdot 10^4$	×	×
$n=6$	0.9929	0.9889	0.9907	$3.96 \cdot 10^3$	×	×
FD 2:	invfreqs					
$n=2$	0.9567	0.9684	0.9798	$4.47 \cdot 10^4$	×	×
$n=4$	0.9916	0.9996	0.9996	$1.03 \cdot 10^4$	×	×
$n=6$	0.9869	0.9995	0.9999	$3.85 \cdot 10^3$	×	×
Mode:	K_{22}					
TD:	Hankel SVD					
$n=2$	0.9889	0.8772	0.9870	$7.29 \cdot 10^5$	-	-
$n=4$	0.9985	0.9112	0.9891	$3.18 \cdot 10^5$	×	-
$n=6$	0.9991	0.9123	0.9891	$2.89 \cdot 10^5$	×	-
FD 1:	pem					
$n=2$	0.9835	0.9875	0.9883	$7.78 \cdot 10^5$	×	×
$n=4$	0.9981	0.9916	0.9895	$3.13 \cdot 10^5$	×	×
$n=6$	0.9997	0.9918	0.9886	$7.67 \cdot 10^4$	×	×
FD 2:	invfreqs					
$n=2$	0.9557	0.9869	0.9725	$9.08 \cdot 10^5$	×	×
$n=4$	0.9941	0.9970	0.9991	$1.47 \cdot 10^5$	×	×
$n=6$	0.9978	0.9992	0.9994	$9.48 \cdot 10^4$	×	×

Continued on next page

	R_y^2=1 − $\frac{\boldsymbol{e}^T\boldsymbol{e}}{\boldsymbol{y}^T\boldsymbol{y}}$					
	IR	Ph.	Mag.	$\|\|\cdot\|\|_\infty$	PR	Structure
Mode:	$K_{26} = K_{62}$					
TD:	Hankel SVD					
$n = 2$	0.5029	0.9824	0.8642	$1.07 \cdot 10^6$	NPR	-
$n = 4$	0.9500	0.9920	0.9802	$1.93 \cdot 10^5$	NPR	-
$n = 6$	0.9924	0.9917	0.9823	$2.42 \cdot 10^5$	NPR	-
FD 1:	pem					
$n = 2$	0.3399	0.9329	0.6853	$1.70 \cdot 10^6$	NPR	×
$n = 4$	0.9598	0.9920	0.9869	$2.53 \cdot 10^5$	NPR	×
$n = 6$	0.9362	0.9918	0.9806	$4.51 \cdot 10^5$	NPR	×
FD 2:	invfreqs					
$n = 2$	0.4439	0.9547	0.8578	$1.35 \cdot 10^6$	NPR	×
$n = 4$	0.9818	0.9983	0.9925	$3.25 \cdot 10^5$	NPR	×
$n = 6$	0.8783	0.9996	0.9982	$2.14 \cdot 10^5$	NPR	×
Mode:	K_{66}					
TD:	Hankel SVD					
$n = 2$	0.9847	0.8620	0.9812	$4.83 \cdot 10^8$	-	-
$n = 4$	0.9947	0.9057	0.9873	$1.79 \cdot 10^8$	×	-
$n = 6$	0.9968	0.9065	0.9872	$1.53 \cdot 10^8$	×	-
FD 1:	pem					
$n = 2$	0.9735	0.9874	0.9807	$4.96 \cdot 10^8$	×	×
$n = 4$	0.9934	0.9890	0.9913	$4.77 \cdot 10^7$	×	×
$n = 6$	0.9959	0.9900	0.9907	$3.33 \cdot 10^7$	×	×
FD 2:	invfreqs					
$n = 2$	0.9063	0.9628	0.9524	$5.90 \cdot 10^8$	×	×
$n = 4$	0.9950	0.9988	0.9996	$4.21 \cdot 10^7$	×	×
$n = 6$	0.9955	0.9991	0.9997	$3.48 \cdot 10^7$	×	×

In Table 6.2 the different error measures for the identified models are listed. The table shows that the diagonal modes are well fitted already at an order of 2, while the off-diagonal modes need to be fitted with an order of 4 before the most important dynamics are captured. For most of the positive real modes all the obtained models were positive real. Also the combination of all the 4^{th} or 6^{th} order models into MIMO systems representing the dynamics in sway and yaw, $\boldsymbol{K}_{y\psi}(s)$, were positive real. The impulse responses and Bode plots of the original data sets and the identified models are shown in the Figures 6.3-6.10. In general, the impulse responses are well fitted by both the time and frequency domain algorithms, while in the frequency response in the Bode plots are better approximated by the FD algorithms than the TD approach.

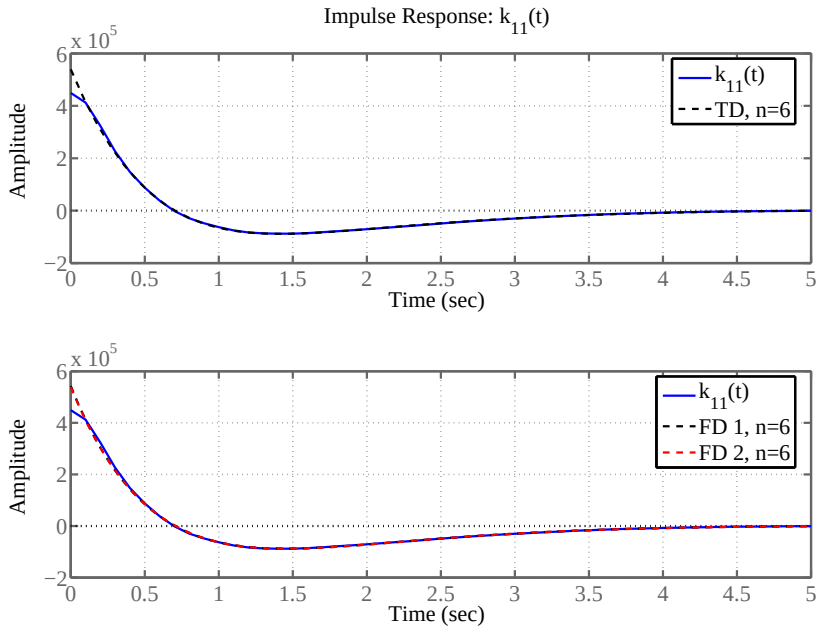

(a) Impulse response.

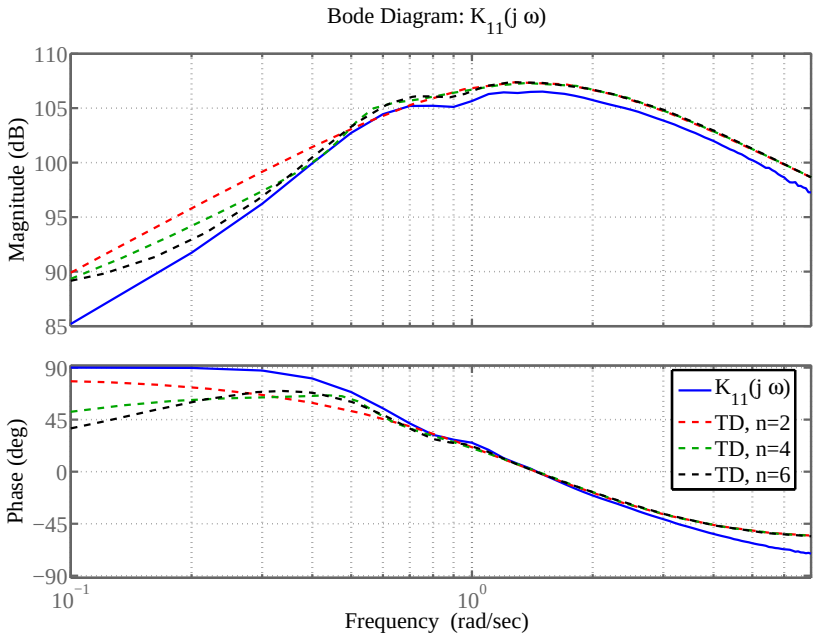

(b) Method: Hankel SVD.

Figure 6.3: Plot of $k_{11}(t)$ and $K_{11}(j\omega)$ versus identified models.

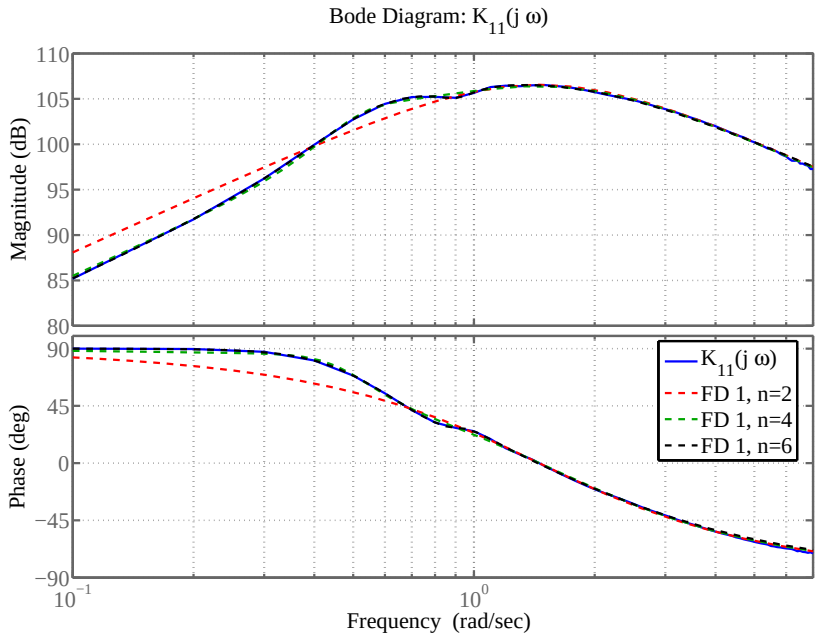

(a) Method: pem.

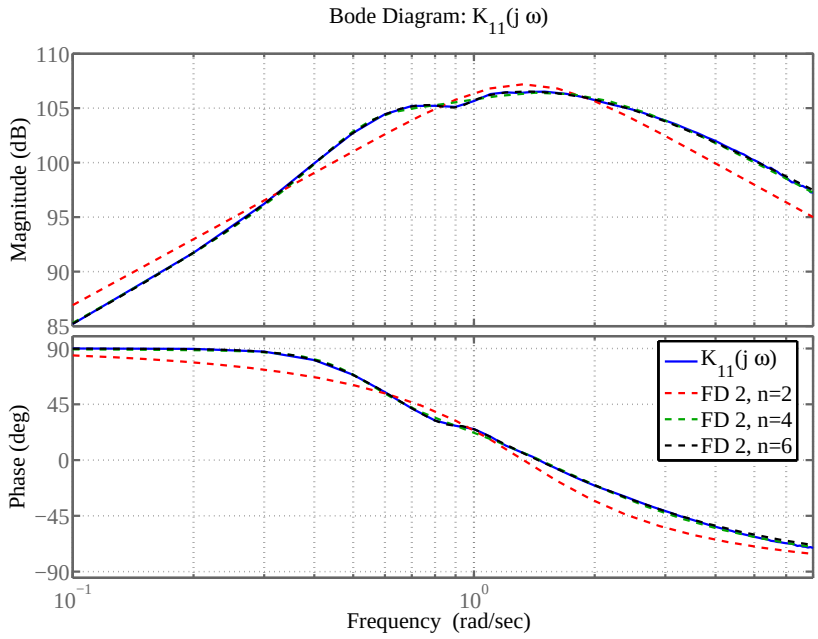

(b) Method: invfreqs.

Figure 6.4: Bode plot of $K_{11}(j\omega)$ and identified models of different orders.

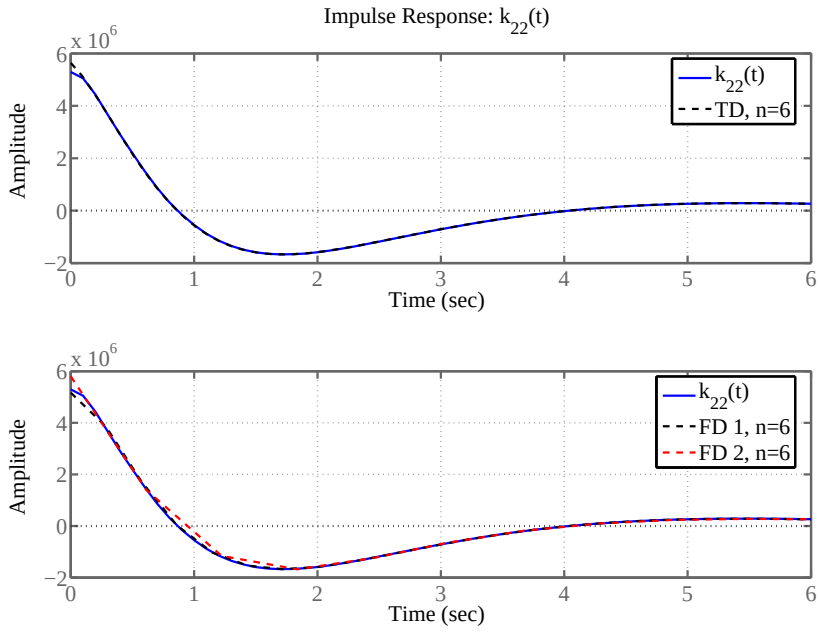

(a) Impulse response.

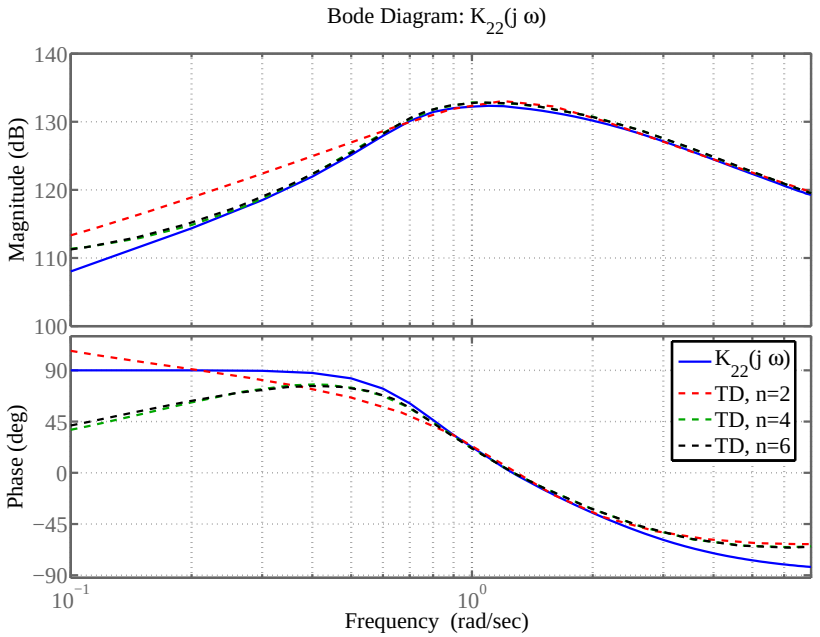

(b) Method: Hankel SVD.

Figure 6.5: Plot of $k_{22}(t)$ and $K_{22}(j\omega)$ versus identified models.

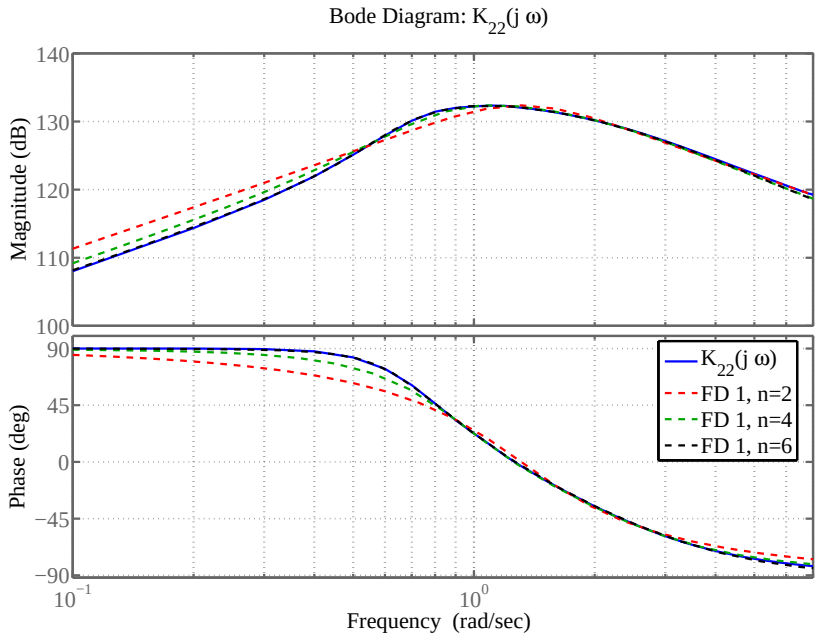

(a) Method: pem.

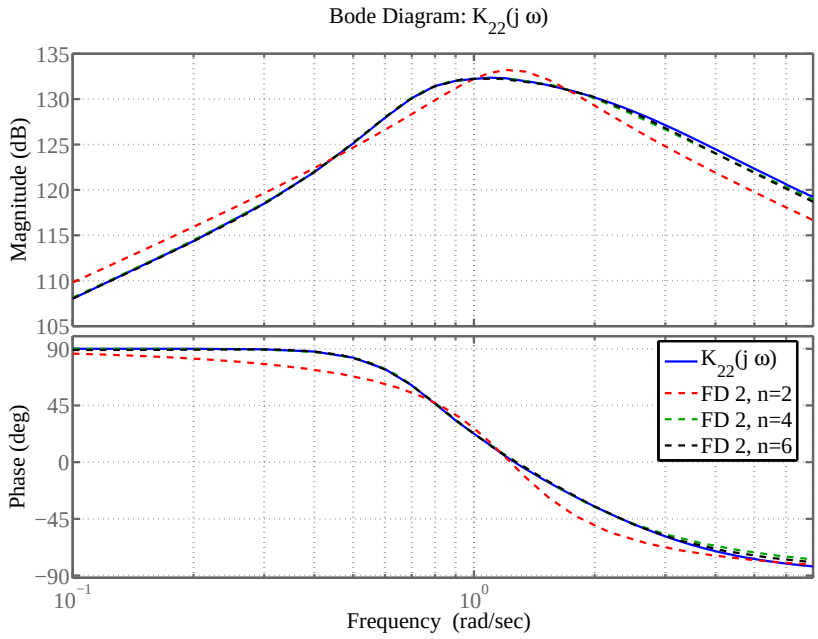

(b) Method: invfreqs.

Figure 6.6: Bode plot of $K_{22}(j\omega)$ and identified models of different orders.

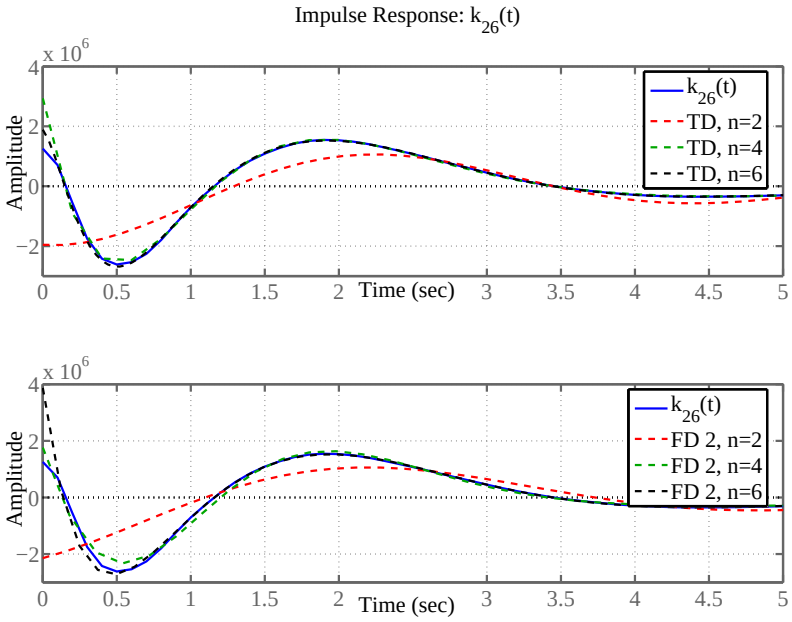

(a) Impulse response.

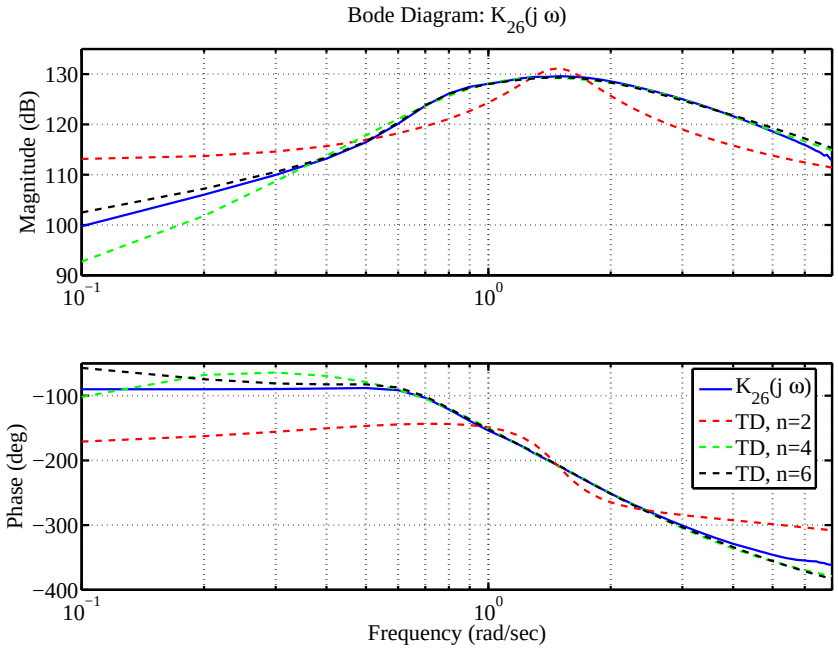

(b) Method: Hankel SVD.

Figure 6.7: Plot of $k_{26}(t)$ and $K_{26}(j\omega)$ versus identified models.

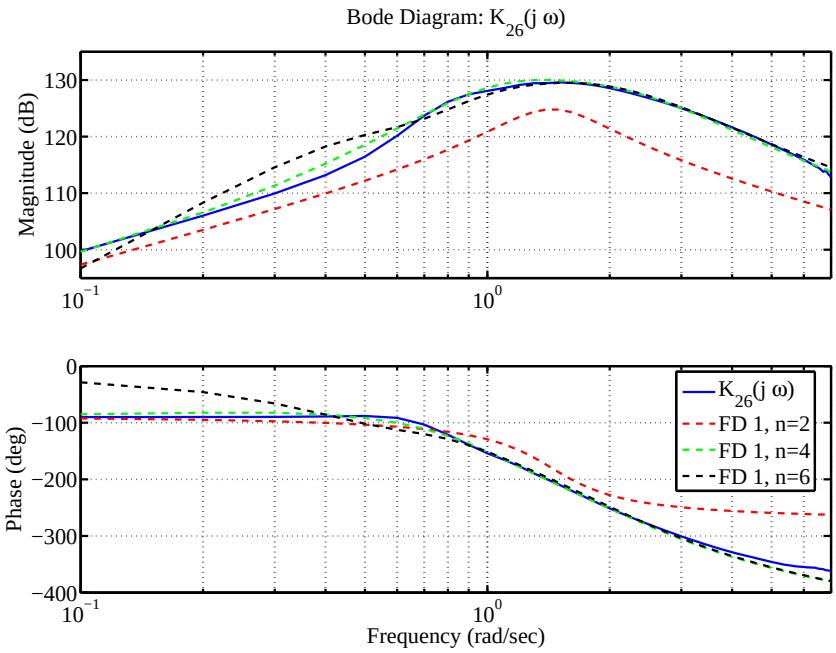

(a) Method: pem.

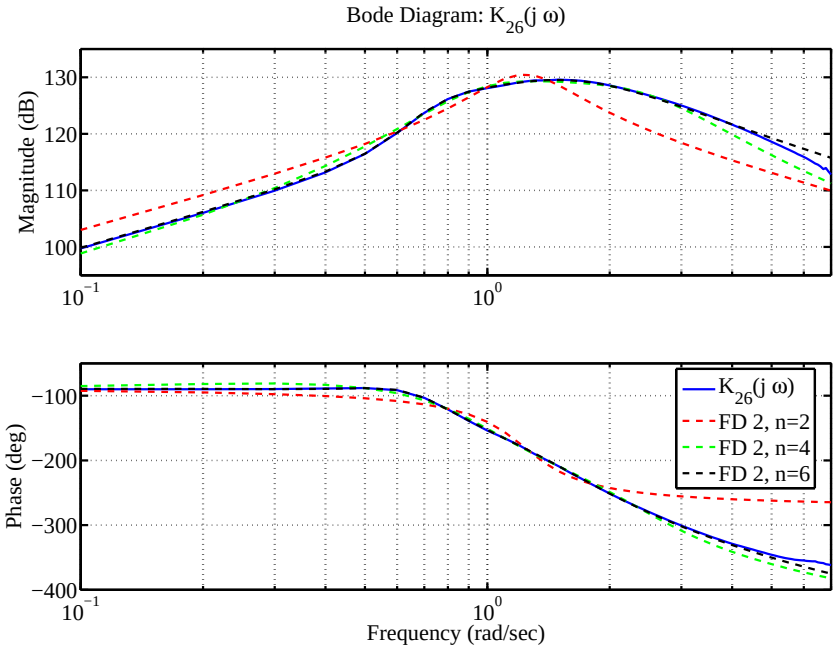

(b) Method: invfreqs.

Figure 6.8: Bode plot of $K_{26}(j\omega)$ and identified models of different orders.

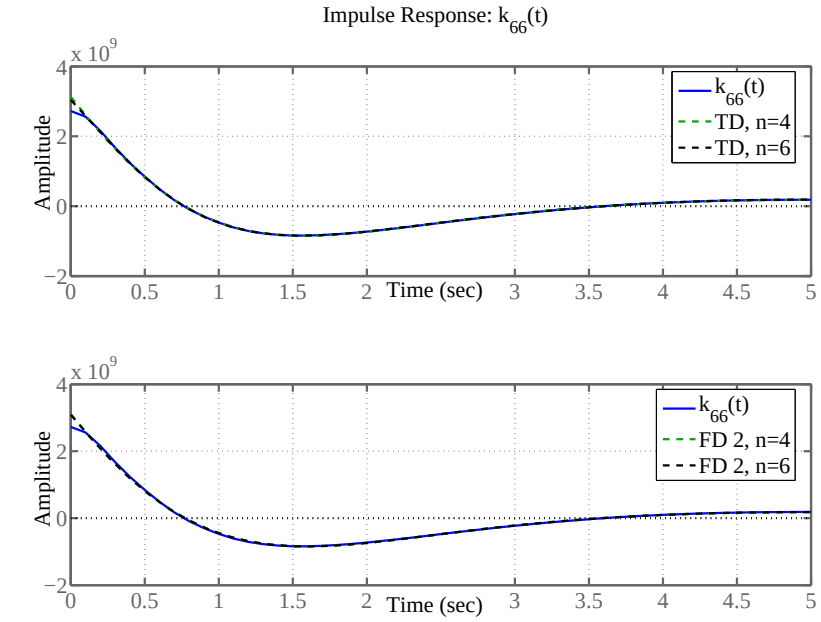

(a) Impulse response.

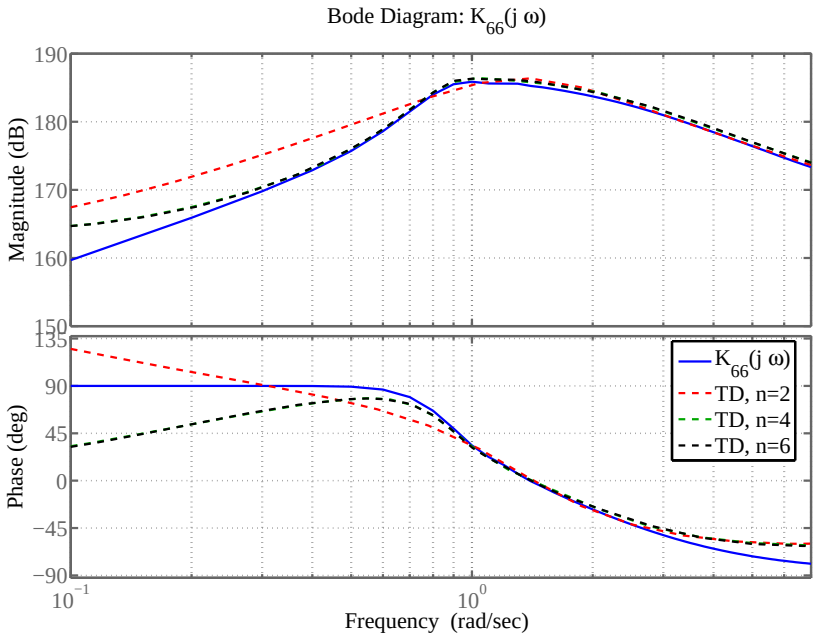

(b) Method: Hankel SVD.

Figure 6.9: Plot of $k_{66}(t)$ and $K_{66}(j\omega)$ versus identified models.

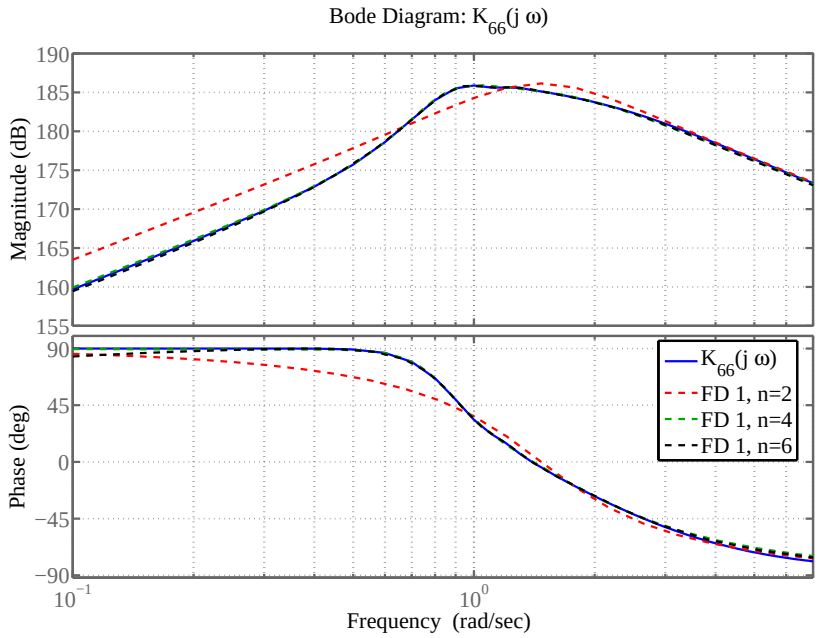

(a) Method: pem.

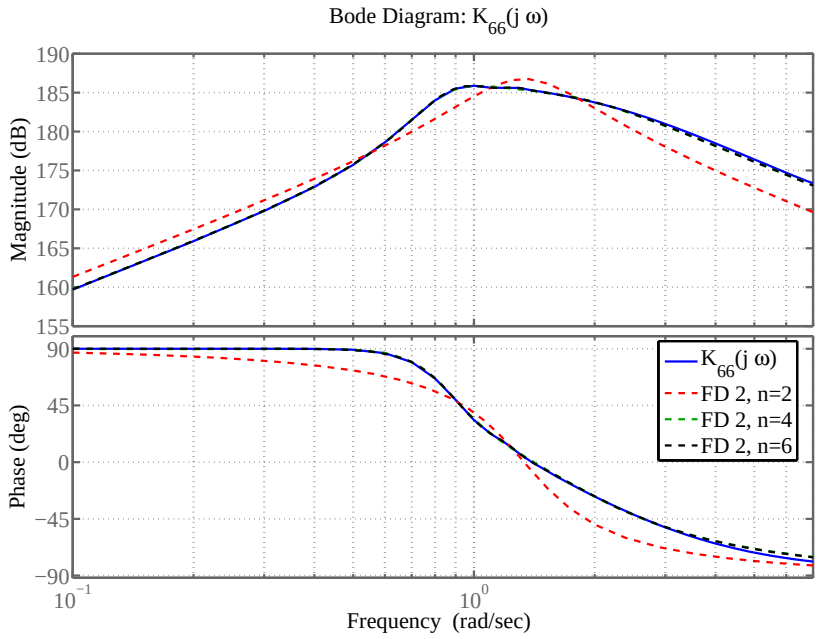

(b) Method: invfreqs.

Figure 6.10: Bode plot of $K_{66}(j\omega)$ and identified models of different orders.

6.2.2 MIMO Identification

The MIMO identification of the system $\boldsymbol{K}_{y\psi}$ from (6.14) is addressed in this section. As a first attempt the overall systems were identified by the use of the Hankel SVD and pem algorithms. The results are shown in Table 6.3. Since there are great differences in the values of the modes K_{22} and K_{66} we get different identified models for the modes K_{26} and K_{62}. Because of the large differences in values of the different modes, the symmetry of the system is not kept. Further, the large differences between the values in the different modes makes it difficult with this approach, even with proper scaling of the different data sets, to identify the system accurate. Systems of high order are needed in order to capture the dynamics of the system. One can also see that the fit of the mode K_{62} is not satisfactory. The orders of the obtained MIMO systems $\boldsymbol{K}_{y\psi}$ were 12, 16 and 24.

As a further approach, a system structure,

$$\boldsymbol{K}_{y\psi} = \begin{bmatrix} K_{22} & K_{26} \\ 0 & K_{66} \end{bmatrix}, \tag{6.20}$$

was used. Then the dynamics of the system K_{26} were used for the K_{62} system, giving the following system,

$$\boldsymbol{K}_{y\psi} = \begin{bmatrix} K_{22} & K_{26} \\ K_{26} & K_{66} \end{bmatrix}. \tag{6.21}$$

Using this approach all the modes have the same denominator, and the overall system $\boldsymbol{K}_{y\psi}$ consist of two multi-input single-output (MISO) systems describing the dynamics in surge and sway. The results of the identification are shown in Table 6.4. This approach gives more compact and accurate models than the direct MIMO identification. This can be seen by comparing the results in Table 6.3 and Table 6.4. The latter approach gives the same dynamics in the modes K_{26} and K_{62}, and the symmetry property of the system is kept. This is a property which can be useful later when designing control systems or observers for the system.

The orders of the overall MIMO systems $\boldsymbol{K}_{y\psi}$ generated were 8, 12 and 16. Compared to the SISO identification this approach gives more compact models with good accuracy. For both approaches all models for the diagonal modes were positive real, as shown in Table 6.3 and Table 6.4. Also the overall MIMO systems were checked and confirmed positive real.

Table 6.3: Different Error Measures for the MIMO Identification

	R_y^2=1 − $\frac{\boldsymbol{e}^T\boldsymbol{e}}{\boldsymbol{y}^T\boldsymbol{y}}$					
	IR	Ph.	Mag.	$\|\|\cdot\|\|_\infty$	PR	Structure
Mode:		K_{22}				
MIMO TD:		Hankel SVD				
$n = 12$	0.9886	0.9107	0.9894	$4.48 \cdot 10^5$	×	-
$n = 16$	0.9874	0.9125	0.9888	$6.02 \cdot 10^5$	×	-
$n = 24$	0.9889	0.9137	0.9889	$5.87 \cdot 10^5$	×	-
MIMO FD:		pem				
$n = 12$	0.9997	0.9919	0.9895	$1.16 \cdot 10^5$	×	×
$n = 16$	0.9970	0.9911	0.9914	$1.57 \cdot 10^5$	×	×
$n = 24$	0.9982	0.9913	0.9903	$7.01 \cdot 10^4$	×	×
Mode:		K_{26}				
MIMO TD:		Hankel SVD				
$n = 12$	0.9426	0.9940	0.9790	$1.90 \cdot 10^5$	NPR	-
$n = 16$	0.9862	0.9927	0.9830	$2.64 \cdot 10^5$	NPR	-
$n = 24$	0.9967	0.9917	0.9786	$2.30 \cdot 10^5$	NPR	-
MIMO FD:		pem				
$n = 12$	0.8439	0.9928	0.9671	$2.10 \cdot 10^5$	NPR	×
$n = 16$	0.9000	0.9942	0.9808	$5.42 \cdot 10^5$	NPR	×
$n = 24$	0.9323	0.9952	0.9745	$7.50 \cdot 10^5$	NPR	×
Mode:		K_{62}				
MIMO TD:		Hankel SVD				
$n = 12$	0.5463	0.9931	0.9055	$7.34 \cdot 10^5$	NPR	-
$n = 16$	0.5569	0.9915	0.8181	$1.93 \cdot 10^6$	NPR	-
$n = 24$	0.8766	0.9878	0.9513	$7.63 \cdot 10^5$	NPR	-
MIMO FD:		pem				
$n = 12$	0.3391	0.9964	0.5720	$3.47 \cdot 10^6$	NPR	×
$n = 16$	0.5746	0.9338	0.8112	$2.07 \cdot 10^6$	NPR	×
$n = 24$	0.9067	0.9869	0.9491	$2.13 \cdot 10^6$	NPR	×
Mode:		K_{66}				
MIMO TD:		Hankel SVD				
$n = 12$	0.9983	0.9089	0.9873	$1.50 \cdot 10^8$	×	-
$n = 16$	0.9990	0.9100	0.9874	$1.50 \cdot 10^8$	×	-
$n = 24$	0.9998	0.9102	0.9874	$1.51 \cdot 10^8$	×	-
MIMO FD:		pem				
$n = 12$	0.9998	0.9916	0.9900	$1.84 \cdot 10^7$	×	×
$n = 16$	0.9980	0.9913	0.9911	$4.05 \cdot 10^7$	×	×
$n = 24$	0.9999	0.9916	0.9905	$1.25 \cdot 10^7$	×	×

In Figures 6.11-6.13 the impulse response of the original data sets are plotted against the impulse response of the obtained models, and the frequency response of the original data sets are plotted against the frequency response of the obtained models. As for the SISO identification, both the algorithms used give models which fit the impulse responses well. While for the frequency responses, one can see from the Bode plots that the frequency domain algorithm gives a better fit.

Table 6.4: Different Error Measures for the MIMO Identification

	R_y^2=$1-\frac{\boldsymbol{e}^T\boldsymbol{e}}{\boldsymbol{y}^T\boldsymbol{y}}$					
	IR	Ph.	Mag.	$\|\|\cdot\|\|_\infty$	PR	Structure
Mode:		K_{22}				
MIMO TD:		Hankel SVD				
$n=8$	0.9984	0.9137	0.9887	$4.86\cdot10^5$	×	-
$n=12$	0.9947	0.9146	0.9898	$4.51\cdot10^5$	×	-
$n=16$	0.9987	0.9109	0.9890	$3.40\cdot10^5$	×	-
MIMO FD:		pem				
$n=8$	0.9976	0.9915	0.9890	$4.07\cdot10^5$	×	×
$n=12$	0.9856	0.9886	0.9923	$2.73\cdot10^5$	×	×
$n=16$	0.9973	0.9911	0.9900	$2.76\cdot10^5$	×	×
Mode:		$K_{26}=K_{62}$				
MIMO TD:		Hankel SVD				
$n=8$	0.9522	0.9918	0.9804	$2.30\cdot10^5$	NPR	-
$n=12$	0.9507	0.9913	0.9806	$2.76\cdot10^5$	NPR	-
$n=16$	0.9453	0.9938	0.9794	$1.91\cdot10^5$	NPR	-
MIMO FD:		pem				
$n=8$	0.9498	0.9931	0.9823	$4.95\cdot10^5$	NPR	×
$n=12$	0.9697	0.9943	0.9863	$4.35\cdot10^5$	NPR	×
$n=16$	0.9513	0.9956	0.9878	$3.06\cdot10^5$	NPR	×
Mode:		K_{66}				
MIMO TD:		Hankel SVD				
$n=8$	0.9048	0.8963	0.9583	$9.08\cdot10^8$	×	-
$n=12$	0.9935	0.9073	0.9877	$2.08\cdot10^8$	×	-
$n=16$	0.9954	0.9070	0.9874	$1.68\cdot10^8$	×	-
MIMO FD:		pem				
$n=8$	0.9151	0.9749	0.9686	$6.45\cdot10^8$	×	×
$n=12$	0.9903	0.9887	0.9911	$1.50\cdot10^8$	×	×
$n=16$	0.9981	0.9913	0.9897	$7.23\cdot10^7$	×	×

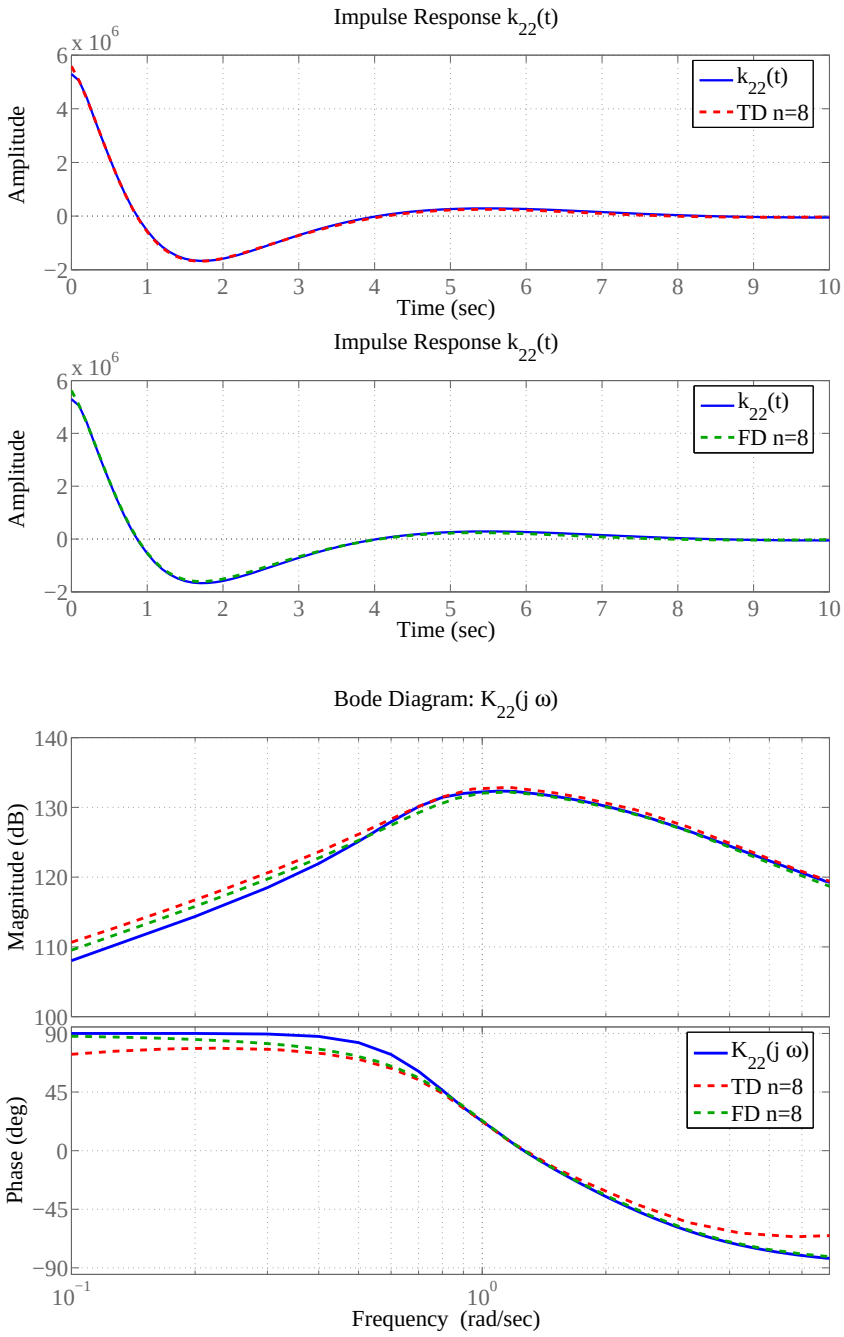

Figure 6.11: Impulse response of $k_{22}(t)$ and identified models, and Bode plot of $K_{22}(j\omega)$ and identified models.

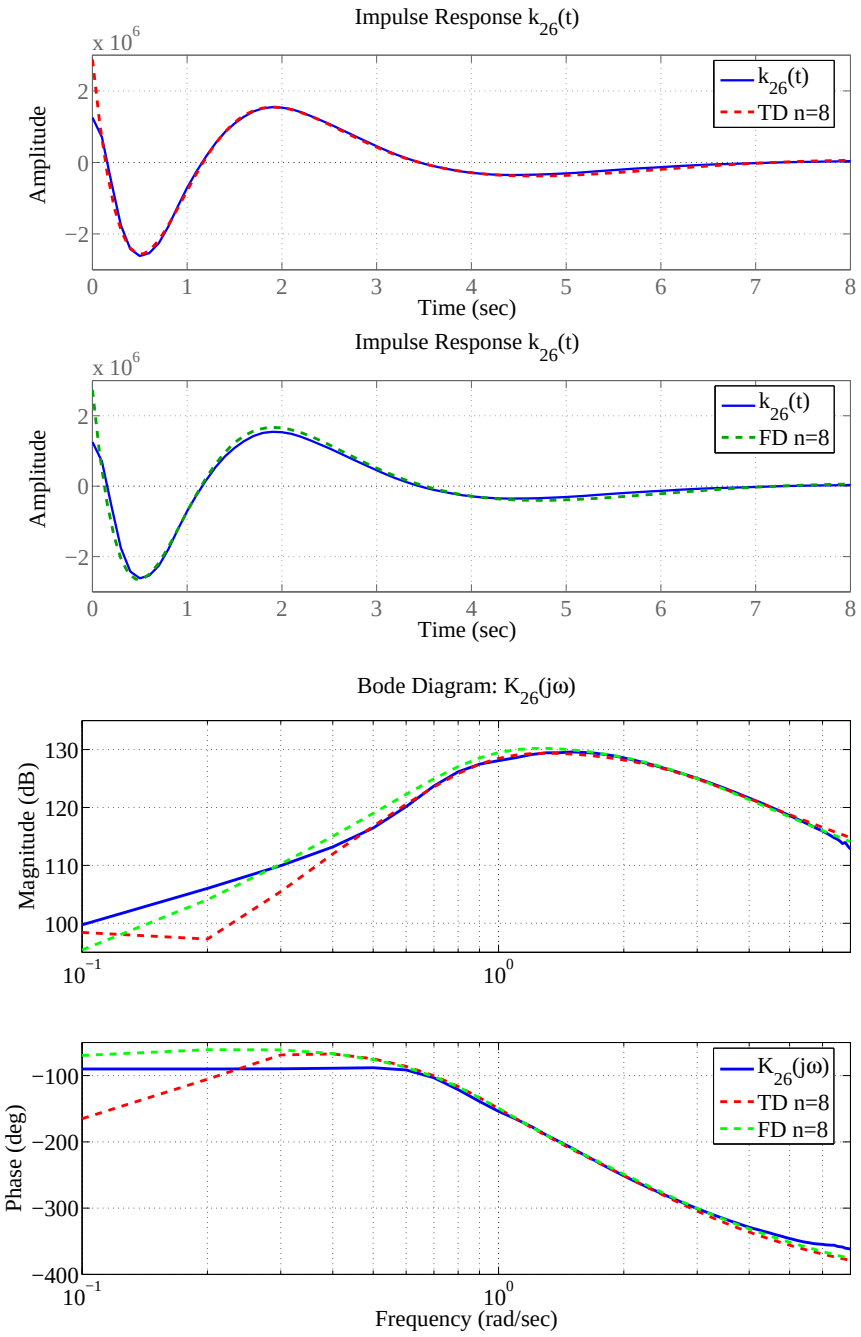

Figure 6.12: Impulse response of $k_{26}(t)$ and identified models, and Bode plot of $K_{26}(j\omega)$ and identified models.

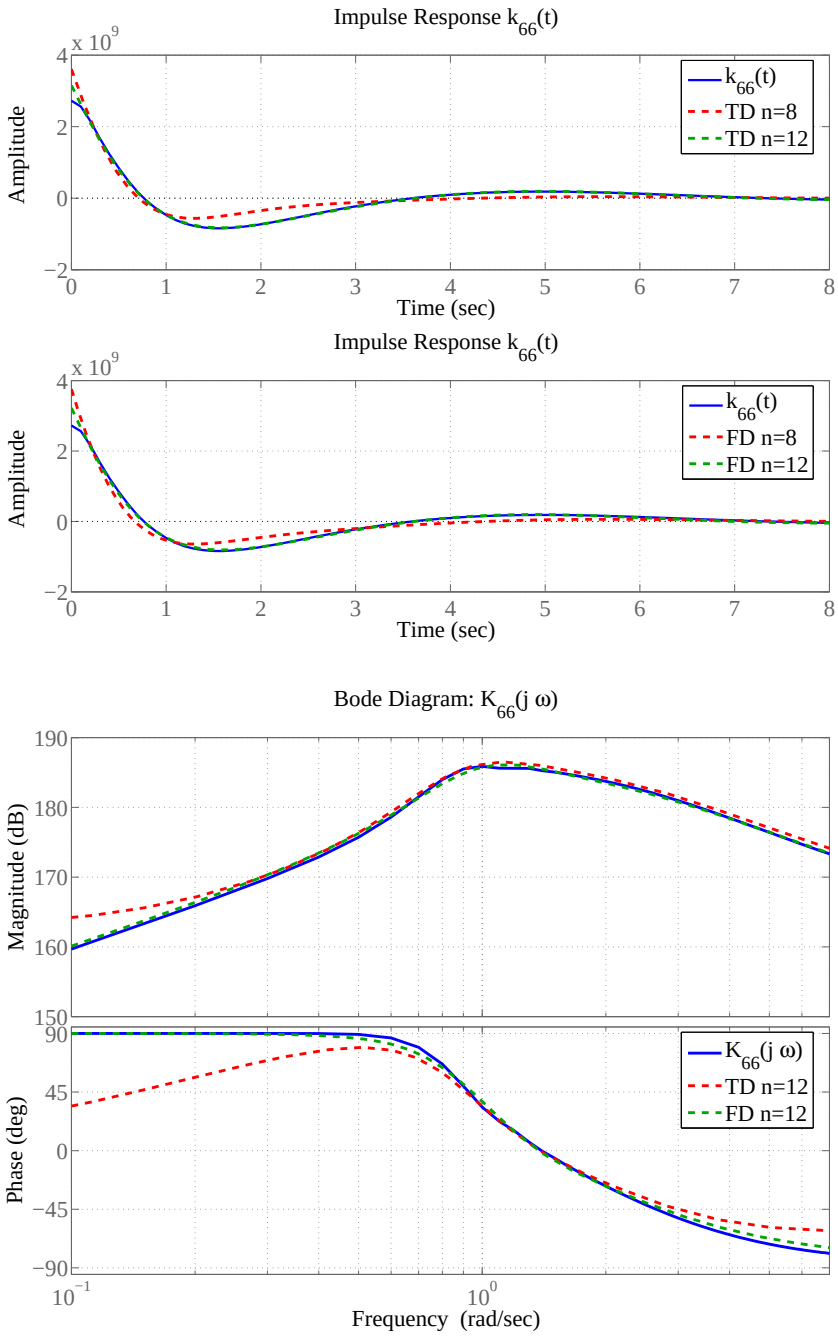

Figure 6.13: Impulse response of $k_{66}(t)$ and identified models, and Bode plot of $K_{66}(j\omega)$ and identified models.

6.2.3 SISO Identification with Reduction

SISO identification of each mode is done in this section, before the overall MIMO system $\boldsymbol{K}_{y\psi}$ is reduced. In this section we have used models obtained by use of the Hankel SVD algorithm. Accurate models of different order were obtained for the different modes, before they were put together as a MIMO system of order 30. Further the reduction algorithms from Chapter 5 were used, and models of orders 10, 12 and 16 were obtained for $\boldsymbol{K}_{y\psi}$. The results are shown in Table 6.5.

The Lyapunov balancing gives positive real reduced order systems of orders 12 and 16. But for order 10, the reduced order system is not positive real. All the reduced order systems generated by Riccati and mixed gramian balancing are positive real, as expected. By comparing the resulting systems with the ones obtained by time domain identification in Table (6.4) and Table (6.2) one can see that the resulting reduced order models have good accuracy.

The mixed gramian balancing does not keep the symmetry properties of the system. This is because the gramians in the algorithm are not the dual of each other, hence we get different error measures in the K_{26} and K_{62} modes. For the system of orders 12 and 16 the difference is minor, but for the system of order 10 it is not acceptable. Both the Lyapunov and Riccati balancing keep the symmetry properties of the original system. This also raises the question whether the mixed gramian balancing is suited for MIMO systems, something which should be investigated further. As mentioned earlier, it is also of interest to keep the symmetry property of the system, since this can be a useful property for use in control and observer design. For all the modes the errors are comparable with the Lyapunov and Riccati balancing schemes, but the symmetry is not kept.

In Figures 6.14-6.16 the impulse response of the original data sets is plotted against the impulse response of the obtained reduced order models together with the Bode plot of the original frequency responses against the Bode plot of the obtained reduced order models. From the plot one can see that both the impulse response and Bode plot are well fitted when this approach has been taken. Hence, this approach is attractive for obtaining compact and efficient models of the radiation forces.

For this system the Lyapunov balancing shows good performance for the systems of orders 12 and 16. But since it cannot ensure reduced order positive real systems, which is the case for the system of order 10, Riccati balancing is preferred. For this particular system the Riccati balancing shows good performance looking at the different error measures. The algorithm shows good fit and accuracy also for the system of order 10.

Table 6.5: Different Error Measures for the Reduction

	R_y^2=1 − $\frac{\boldsymbol{e}^T\boldsymbol{e}}{\boldsymbol{y}^T\boldsymbol{y}}$				
	IR	Ph.	Mag.	$\|\|\cdot\|\|_\infty$	PR
Mode:	K_{22}				
Original $n = 30$	0.9991	0.9902	0.9903	$6.90 \cdot 10^4$	×
Lyapunov $n = 16$	0.9991	0.9902	0.9903	$6.95 \cdot 10^4$	×
Lyapunov $n = 12$	0.9981	0.9889	0.9903	$9.28 \cdot 10^4$	×
Lyapunov $n = 10$	0.9895	0.9510	0.9863	$5.02 \cdot 10^5$	-
Riccati $n = 16$	0.9991	0.9902	0.9903	$6.90 \cdot 10^4$	×
Riccati $n = 12$	0.9991	0.9902	0.9903	$6.90 \cdot 10^4$	×
Riccati $n = 10$	0.9988	0.9902	0.9901	$1.96 \cdot 10^5$	×
Mixed $n = 16$	0.9991	0.9902	0.9903	$6.90 \cdot 10^4$	×
Mixed $n = 12$	0.9989	0.9901	0.9901	$1.21 \cdot 10^5$	×
Mixed $n = 10$	0.9870	0.9866	0.9827	$5.88 \cdot 10^5$	×
Mode:	$K_{26} = K_{62}$				
Original $n = 30$	0.9471	0.9905	0.9841	$1.84 \cdot 10^5$	NPR
Lyapunov $n = 16$	0.9475	0.9904	0.9841	$1.85 \cdot 10^5$	NPR
Lyapunov $n = 12$	0.9464	0.9923	0.9839	$1.82 \cdot 10^5$	NPR
Lyapunov $n = 10$	0.9425	0.9926	0.9829	$1.75 \cdot 10^5$	NPR
Riccati $n = 16$	0.9472	0.9905	0.9841	$1.84 \cdot 10^5$	NPR
Riccati $n = 12$	0.9472	0.9905	0.9842	$1.84 \cdot 10^5$	NPR
Riccati $n = 10$	0.9346	0.9923	0.9805	$5.57 \cdot 10^5$	NPR
$\text{Mixed}_{62\approx26}$ $n = 16$	0.9471	0.9905	0.9841	$1.84 \cdot 10^5$	NPR
$\text{Mixed}_{62\approx26}$ $n = 12$	0.9393	0.9932	0.9826	$3.33 \cdot 10^5$	NPR
Mixed_{26} $n = 10$	0.9451	0.9924	0.9834	$2.58 \cdot 10^6$	NPR
Mixed_{62} $n = 10$	0.5104	0.9948	0.7886	$2.58 \cdot 10^6$	NPR
Mode:	K_{66}				
Original $n = 30$	0.9978	0.9895	0.9910	$3.17 \cdot 10^7$	×
Lyapunov $n = 16$	0.9978	0.9895	0.9910	$3.17 \cdot 10^7$	×
Lyapunov $n = 12$	0.9978	0.9895	0.9910	$3.17 \cdot 10^7$	×
Lyapuniv $n = 10$	0.9978	0.9895	0.9910	$3.17 \cdot 10^7$	×
Riccati $n = 16$	0.9978	0.9895	0.9910	$3.15 \cdot 10^7$	×
Riccati $n = 12$	0.9978	0.9895	0.9910	$3.94 \cdot 10^7$	×
Riccati $n = 10$	0.9978	0.9895	0.9909	$4.41 \cdot 10^7$	×
Mixed $n = 16$	0.9978	0.9895	0.9910	$3.17 \cdot 10^7$	×
Mixed $n = 12$	0.9978	0.9895	0.9910	$3.20 \cdot 10^7$	×
Mixed $n = 10$	0.9978	0.9895	0.9910	$3.48 \cdot 10^7$	×

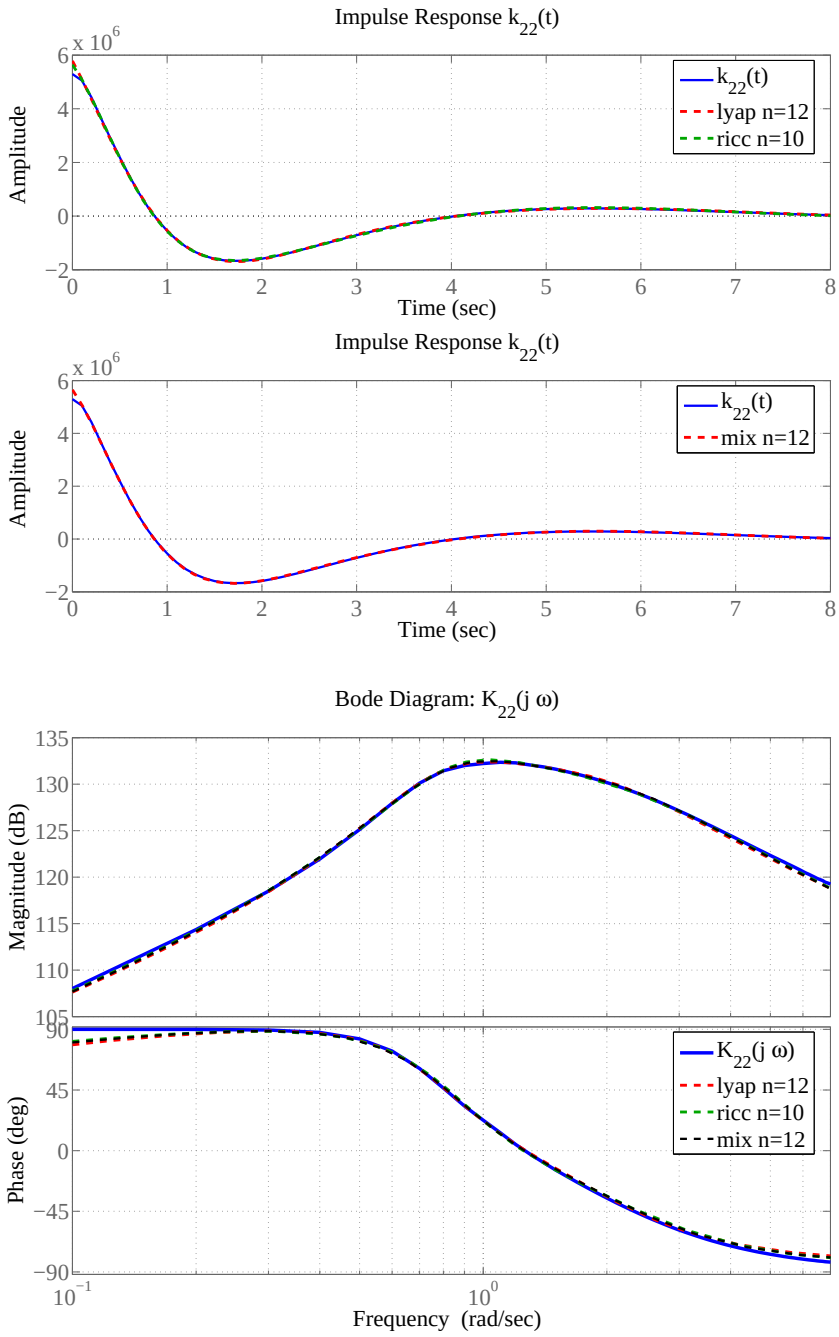

Figure 6.14: Impulse response of $k_{22}(t)$ and reduced order models, and Bode plot of $K_{22}(j\omega)$ and reduced order models.

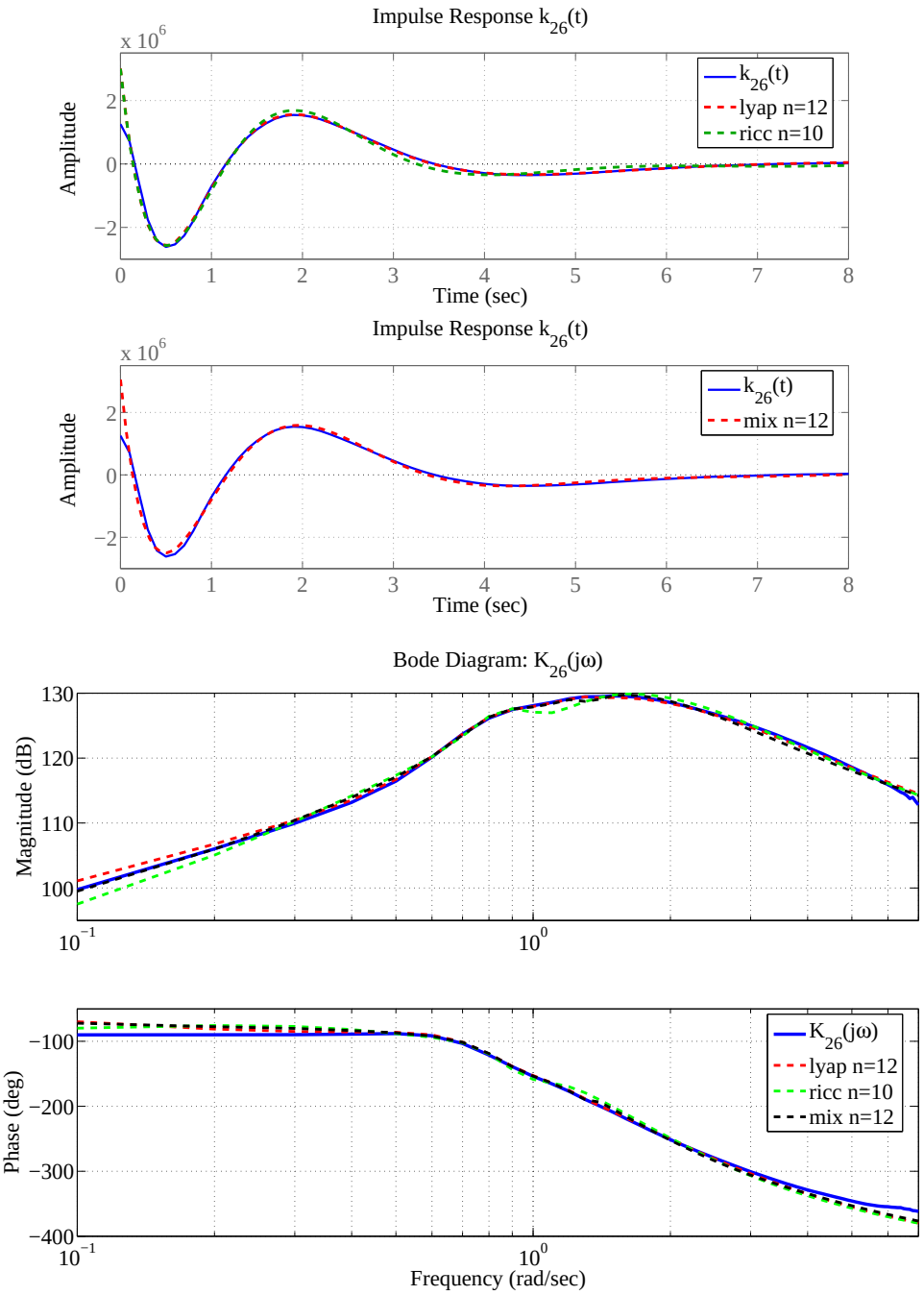

Figure 6.15: Impulse response of $k_{26}(t)$ and reduced order models, and Bode plot of $K_{26}(j\omega)$ and reduced order models.

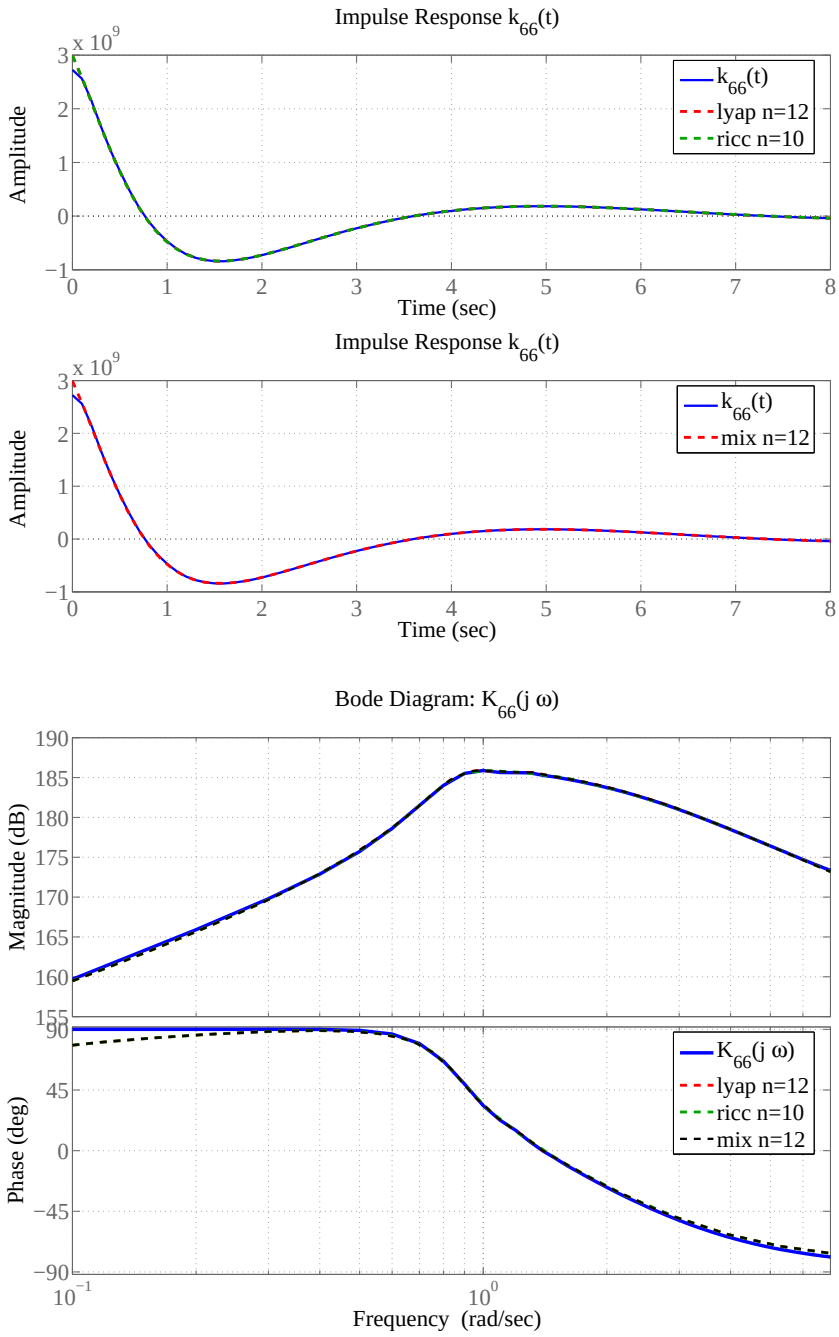

Figure 6.16: Impulse response of $k_{66}(t)$ and reduced order models, and Bode plot of $K_{66}(j\omega)$ and reduced order models.

6.3 Lateral Vessel Model from VERES Data

In this section the radiation forces of a lateral vessel model will be obtained from the frequency dependent added mass matrix $\boldsymbol{A}(\omega)$ and the frequency dependent damping matrix $\boldsymbol{B}(\omega)$ computed by use of VERES. The same approaches will be used as in Section 6.2,

- SISO identification of each mode.
- MIMO identification of the overall system.
- SISO identification of each mode followed by MIMO model reduction.

The identification will be done both in the time and frequency domains with the algorithms presented in Section 4.2-4.3. Further, model reduction will be done with the algorithms presented in the Sections 5.2.1-5.2.3.

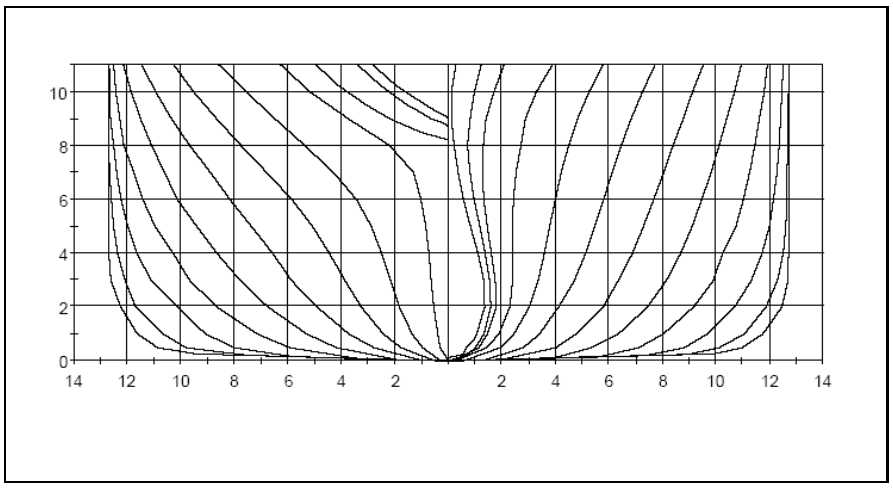

Figure 6.17: The hull form of the $S-175$ tanker

VERES (VEssel RESponse program) is developed at MARINTEK (the Norwegian Marine Technology Research Institute) and offers the ability to calculate ship motions and loads (Fathi, 2004). VERES is used to compute the added mass matrix $\boldsymbol{A}(\omega)$ and damping matrix $\boldsymbol{B}(\omega)$ for a $S-175$ tanker ship (Fathi, 2004). The program can calculate the modes,

$$A_{ij}(\omega) \ \forall \ i = (2, \ldots, 6), \ j = (2, \ldots, 6) \tag{6.22}$$

$$B_{ij}(\omega) \ \forall \ i = (2, \ldots, 6), \ j = (2, \ldots, 6) \tag{6.23}$$

The $S-175$ hull form is given in Figure 6.17. Since VERES does not provide the added mass and damping in surge, a lateral vessel model will be investigated for the $S-175$ tanker. The added mass parameters $A_{ij}(\omega)$ and the damping matrix parameters $B_{ij}(\omega)$ used for the lateral vessel model are plotted in Figure 6.19.

The S-175 tanker has port/starboard symmetry and the 6-DOF equations can be split in one longitudinal system containing the displacements in surge, heave and pitch, and one lateral system containing the displacements in sway, roll and yaw. The position vector of the lateral vessel model can be written as a combination of the displacements in sway, roll and yaw,

$$\boldsymbol{\xi} = [\xi_2, \xi_4, \xi_6]^T \tag{6.24}$$

This gives the following vessel model

$$\begin{aligned} \boldsymbol{M}\ddot{\boldsymbol{\xi}}(t) + \boldsymbol{\tau}_{R2}(t) + \boldsymbol{C}_h\boldsymbol{\xi}(t) &= \boldsymbol{\tau}_{visc}(t) + \boldsymbol{\tau}_{ext}(t) + \boldsymbol{\tau}_A(t) && (6.25)\\ \dot{\boldsymbol{x}}(t) &= \boldsymbol{A}\boldsymbol{x}(t) + \boldsymbol{B}\dot{\boldsymbol{\xi}}(t) && (6.26)\\ \boldsymbol{\tau}_{R2}(t) &= \boldsymbol{C}\boldsymbol{x}(t) && (6.27) \end{aligned}$$

with the following system matrices

$$\boldsymbol{M} = \begin{bmatrix} M_{22} & M_{24} & M_{26} \\ M_{42} & M_{44} & M_{46} \\ M_{62} & M_{64} & M_{66} \end{bmatrix}, \ \boldsymbol{C}_h = \begin{bmatrix} 0 & 0 & 0 \\ 0 & C_{h44} & 0 \\ 0 & 0 & 0 \end{bmatrix} \tag{6.28}$$

In the Laplace domain this can be written

$$\boldsymbol{M}\ddot{\boldsymbol{\xi}}(s) + \boldsymbol{K}_{lat}(s)\dot{\boldsymbol{\xi}}(s) + \boldsymbol{C}_h\boldsymbol{\xi}(s) = \boldsymbol{\tau}_{visc}(s) + \boldsymbol{\tau}_{ext}(s) + \boldsymbol{\tau}_A(s) \tag{6.29}$$

with

$$\boldsymbol{K}_{lat}(s) = \begin{bmatrix} K_{22}(s) & K_{24}(s) & K_{26}(s) \\ K_{42}(s) & K_{44}(s) & K_{46}(s) \\ K_{62}(s) & K_{64}(s) & K_{66}(s) \end{bmatrix} \tag{6.30}$$

First the positive realness of the radiation forces in the system is verified. The lateral vessel system in (6.27) is positive real if the associated damping matrix is positive real. Hence the system is positive real if

$$\det(\boldsymbol{B}(\omega)) = \det\left(\begin{bmatrix} B_{22}(\omega) & B_{24}(\omega) & B_{26}(\omega) \\ B_{42}(\omega) & B_{44}(\omega) & B_{46}(\omega) \\ B_{62}(\omega) & B_{64}(\omega) & B_{66}(\omega) \end{bmatrix} \right) \geq 0, \ \forall\ \omega \tag{6.31}$$

The determinant of the matrix $\boldsymbol{B}(\omega)$ over all frequencies ω is plotted in Figure 6.18, and it can be concluded that the data set obtained from VERES represents a positive real system.

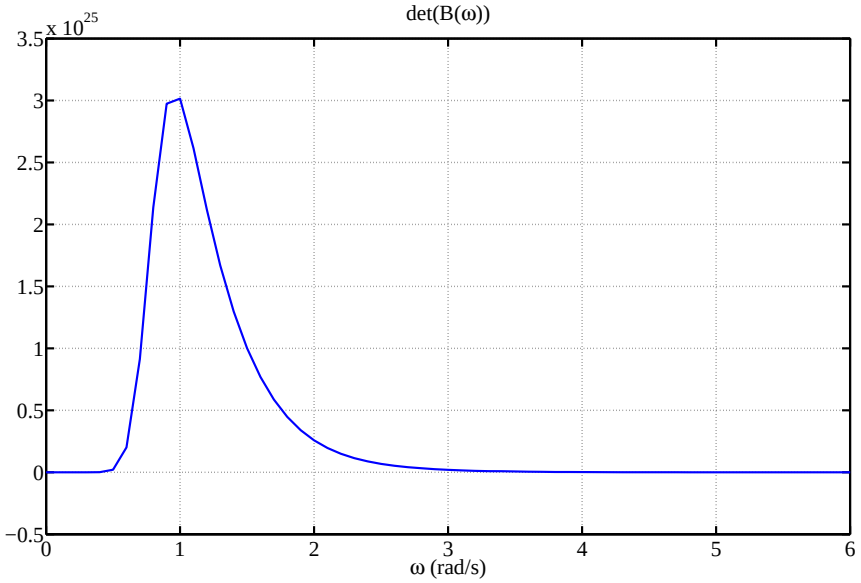

Figure 6.18: The determinant of the positive semidefinite damping matrix $\boldsymbol{B}(\omega)$ for the $S-175$ tanker.

The time domain identification of the system is done from the impulse response of the system. The impulse response of the system is given by,

$$\boldsymbol{k}_{lat}(t) = \frac{2}{\pi}\int_0^{\Omega} \boldsymbol{B}(\omega)\cos(\omega t)\; d\omega = \begin{bmatrix} k_{22}(t) & k_{24}(t) & k_{26}(t) \\ k_{42}(t) & k_{44}(t) & k_{46}(t) \\ k_{62}(t) & k_{64}(t) & k_{66}(t) \end{bmatrix} \tag{6.32}$$

The upper limit of the integral Ω is set to 20 (rad/sec) since the damping matrix $\boldsymbol{B}(\omega)$ has converged to zero for all modes at this frequency (plot of the damping modes are given in Figure 6.19).

The frequency domain identification is done from the frequency response of the radiation forces,

$$\boldsymbol{K}_{lat}(j\omega) = \begin{bmatrix} K_{22}(j\omega) & K_{24}(j\omega) & K_{26}(j\omega) \\ K_{42}(j\omega) & K_{44}(j\omega) & K_{46}(j\omega) \\ K_{62}(j\omega) & K_{64}(j\omega) & K_{66}(j\omega) \end{bmatrix} \tag{6.33}$$

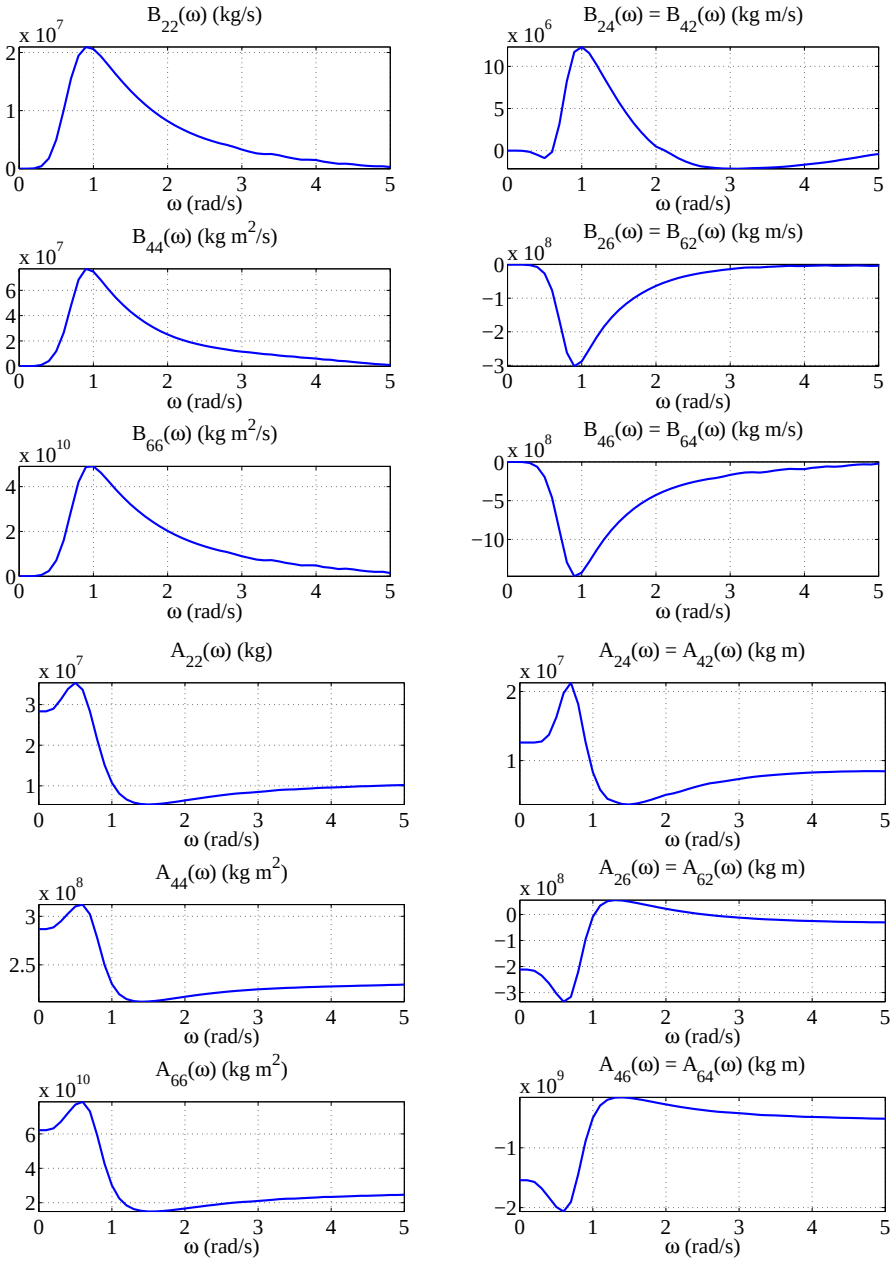

Figure 6.19: The frequency dependent damping parameters $B_{ij}(\omega)$ and the frequency dependent added mass parameters $A_{ij}(\omega)$ plotted versus the frequency ω for the lateral vessel model.

6.3.1 SISO Identification

In this section the 3-DOF lateral vessel model is identified by use of SISO identification of each mode individually. The same error measures are used as in the previous sections.

Table 6.6: Different Error Measures for the Identification

	R_y^2=$1-\frac{\boldsymbol{e}^T\boldsymbol{e}}{\boldsymbol{y}^T\boldsymbol{y}}$					
	IR	Ph.	Mag.	$\|\|\cdot\|\|_\infty$	PR	Structure
Mode:		K_{22}				
SISO TD:		Hankel SVD				
$n=2$	0.9864	0.8216	0.9927	$2.69\cdot10^6$	-	-
$n=4$	0.9995	0.9878	0.9921	$1.51\cdot10^6$	×	-
SISO FD:		invfreqs				
$n=2$	0.9670	0.9823	0.9890	$4.09\cdot10^6$	×	×
$n=4$	0.9774	0.9926	0.9979	$1.56\cdot10^6$	×	×
Mode:		$K_{24}=K_{42}$				
SISO TD:		Hankel SVD				
$n=2$	0.8113	0.7449	0.9377	$3.04\cdot10^6$	NPR	-
$n=4$	0.9784	0.9631	0.9902	$1.27\cdot10^6$	NPR	-
SISO FD:		invfreqs				
$n=2$	0.8118	0.7806	0.9240	$3.44\cdot10^6$	NPR	×
$n=4$	0.9775	0.9351	0.9877	$1.39\cdot10^6$	NPR	×
Mode:		$K_{26}=K_{62}$				
SISO TD:		Hankel SVD				
$n=2$	0.9885	0.9978	0.9923	$3.13\cdot10^7$	NPR	-
$n=4$	0.9999	0.9869	0.9949	$1.47\cdot10^7$	NPR	-
SISO FD:		invfreqs				
$n=2$	0.9719	0.9991	0.9889	$5.43\cdot10^7$	NPR	×
$n=4$	0.9952	0.9997	0.9971	$1.42\cdot10^7$	NPR	×
Mode:		K_{44}				
SISO TD:		Hankel SVD				
$n=2$	0.9874	0.8228	0.9921	$9.98\cdot10^6$	-	-
$n=4$	0.9987	0.9896	0.9930	$5.27\cdot10^6$	×	-
SISO FD:		invfreqs				
$n=2$	0.9588	0.9736	0.9867	$1.51\cdot10^7$	×	×
$n=4$	0.9833	0.9937	0.9911	$1.09\cdot10^7$	×	×

Continued on next page

	R_y^2=1 − $\frac{\boldsymbol{e}^T\boldsymbol{e}}{\boldsymbol{y}^T\boldsymbol{y}}$					
	IR	Ph.	Mag.	$\|\|\cdot\|\|_\infty$	PR	Structure
Mode:		$K_{46} = K_{64}$				
SISO TD:		Hankel SVD				
$n = 2$	0.9897	0.9989	0.9924	$1.78 \cdot 10^8$	NPR	-
$n = 4$	0.9995	0.9862	0.9929	$8.57 \cdot 10^7$	NPR	-
SISO FD:		invfreqs				
$n = 2$	0.9684	0.9984	0.9894	$2.82 \cdot 10^8$	NPR	×
$n = 4$	0.9857	0.9997	0.9978	$7.34 \cdot 10^7$	NPR	×
Mode:		K_{66}				
SISO TD:		Hankel SVD				
$n = 2$	0.9853	0.8119	0.9903	$7.22 \cdot 10^9$	-	-
$n = 4$	0.9993	0.9880	0.9907	$3.63 \cdot 10^9$	×	-
SISO FD:		invfreqs				
$n = 2$	0.9518	0.9670	0.9848	$1.10 \cdot 10^{10}$	×	×
$n = 4$	0.9753	0.9958	0.9983	$3.05 \cdot 10^9$	-	×

For this model, each mode is identified by models of orders 2 and 4. By combining the models for the different modes MIMO systems of orders 24 until 36 can be obtained, depending on the order one chooses in each mode. In this case study the Hankel SVD and the invfreqs algorithms are used to do the identification.

The error measures are listed in Table 6.6. From the table one can see that most of the modes are well fitted already at an order of 2. But the increase to an order of 4 gives better fit and accuracy. For this system both the algorithms fail to give positive real systems in some of the modes, which is something to be aware of when combining the SISO systems into a MIMO model. Looking at the error measures one can see that there is not much difference between the two algorithms.

In Figures 6.20-6.25 the impulse response of the original data set and the impulse responses of the obtained models are plotted together with the Bode plots of the original data sets and the obtained models. In general there is not much difference between the impulse responses of the different models obtained by use of the different algorithms, while the frequency responses are better fitted by use of the frequency domain identification scheme invfreqs. For this model the mode which is most difficult to approximate is $K_{24} = K_{42}$.

Because of the symmetry of the system only 6 modes instead of 9 need to be identified, and the symmetry property is kept.

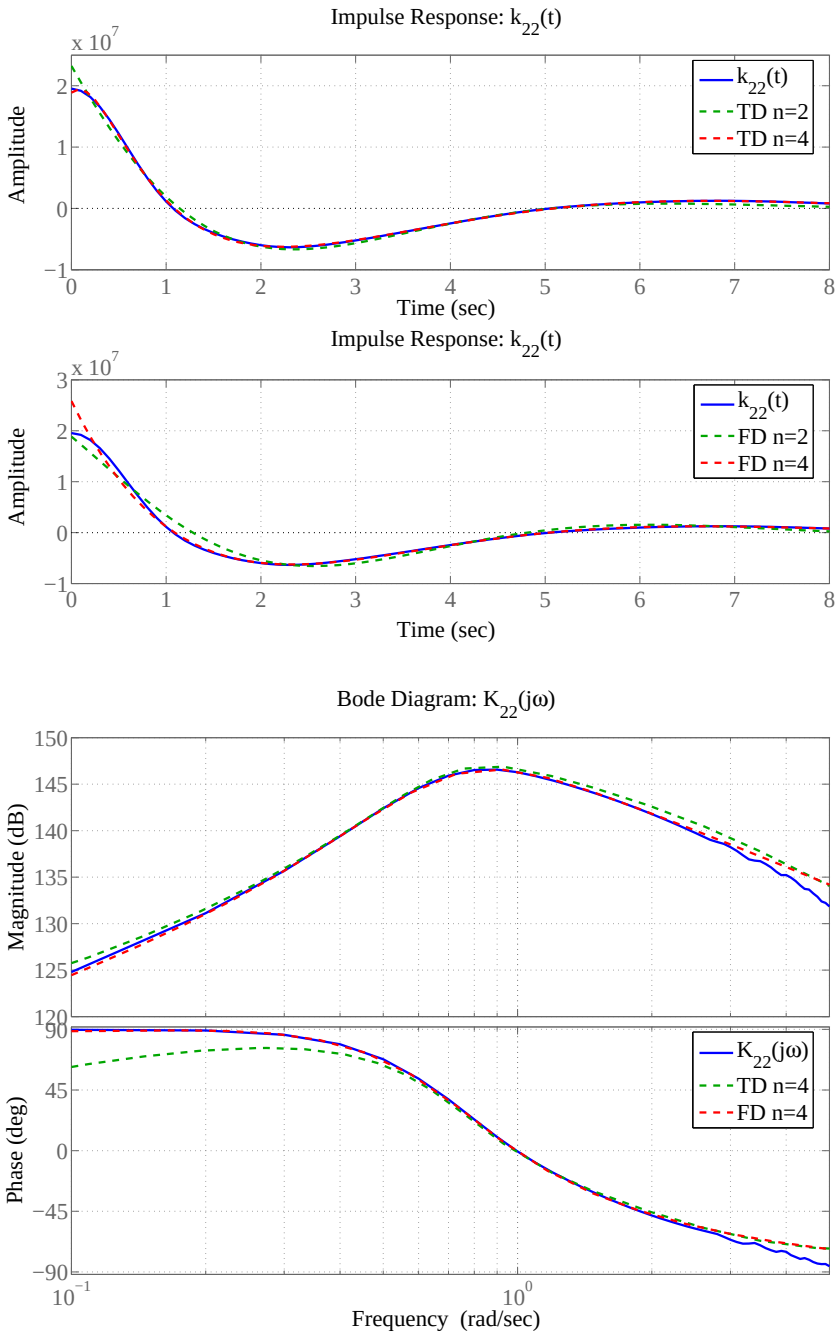

Figure 6.20: Impulse response of $k_{22}(t)$ and identified models, and Bode plot of $K_{22}(j\omega)$ and identified models.

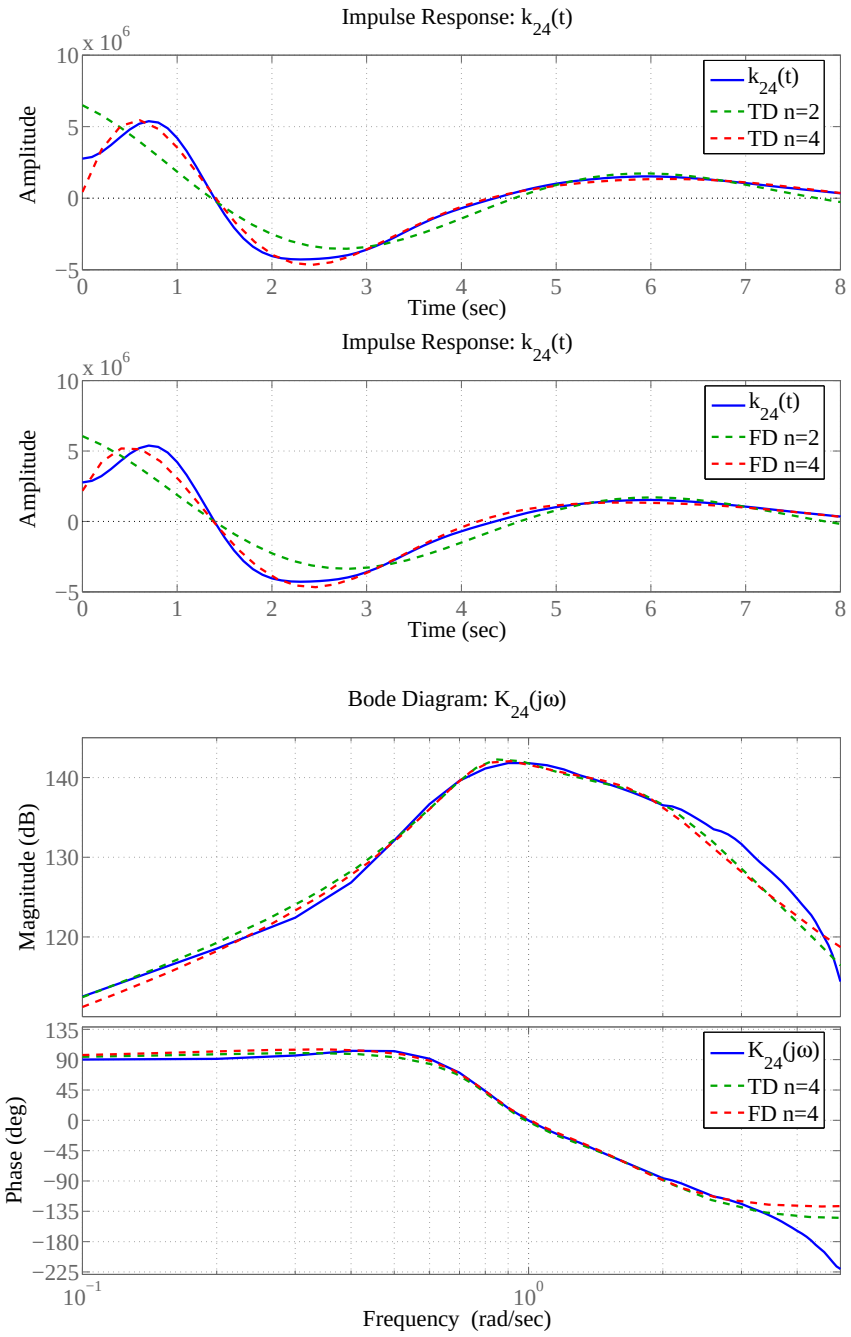

Figure 6.21: Impulse response of $k_{24}(t)$ and identified models, and Bode plot of $K_{24}(j\omega)$ and identified models.

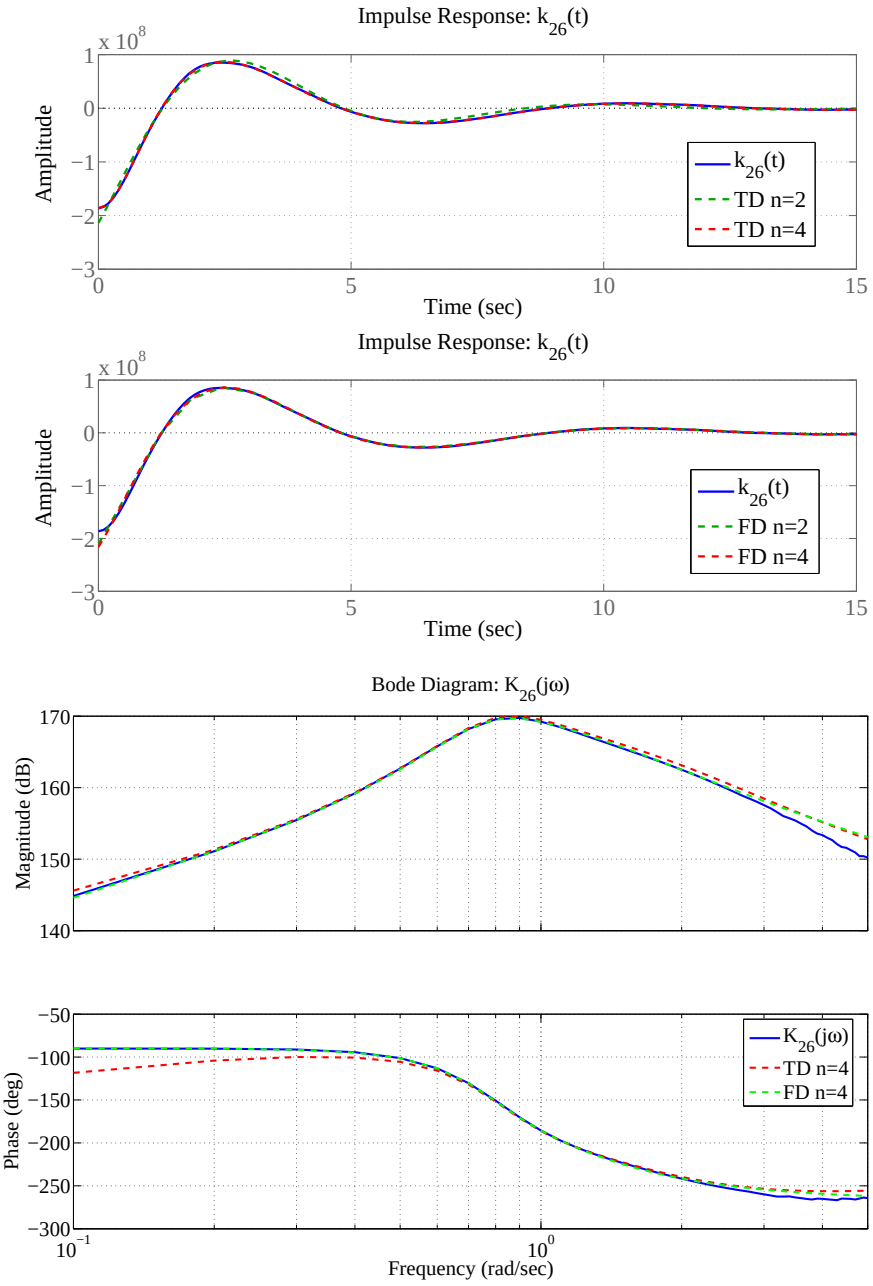

Figure 6.22: Impulse response of $k_{26}(t)$ and identified models, and Bode plot of $K_{26}(j\omega)$ and identified models.

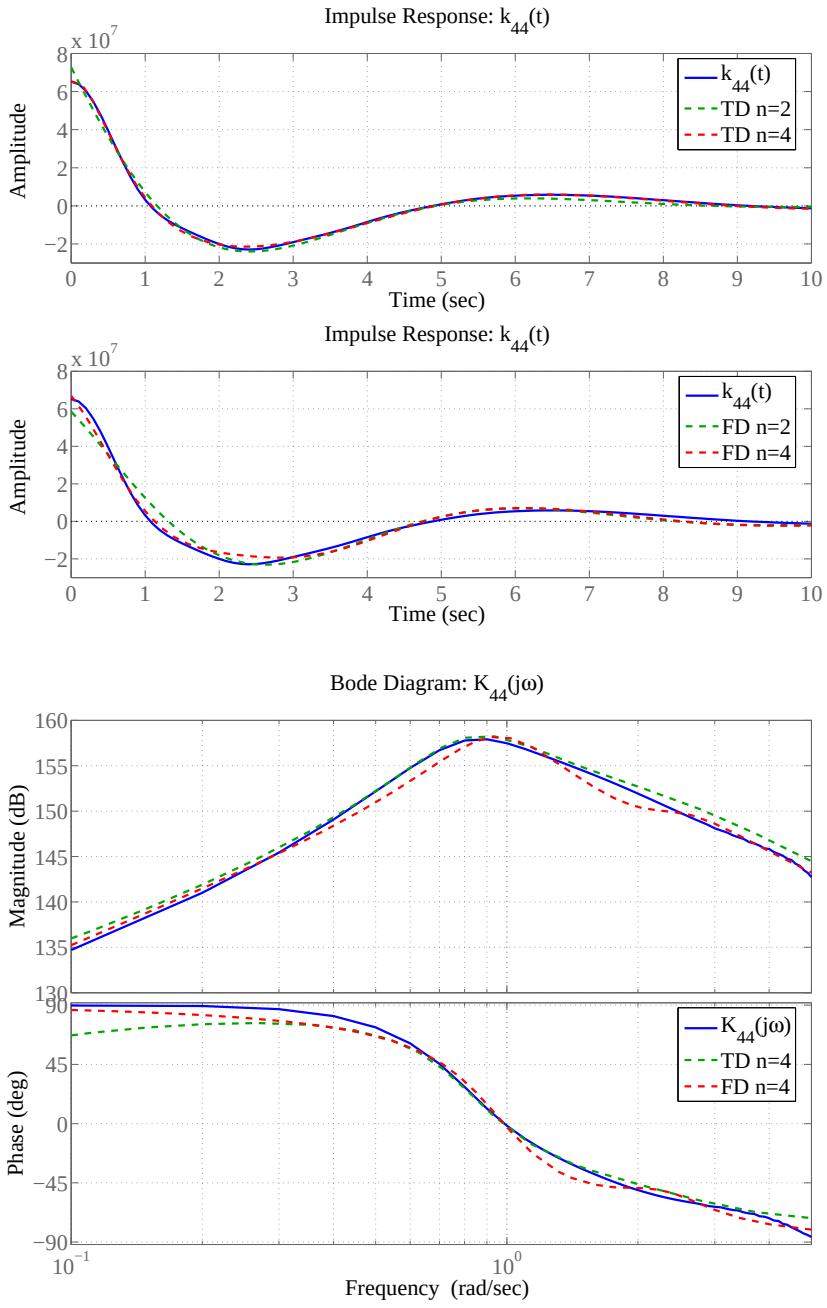

Figure 6.23: Impulse response of $k_{44}(t)$ and identified models, and Bode plot of $K_{44}(j\omega)$ and identified models.

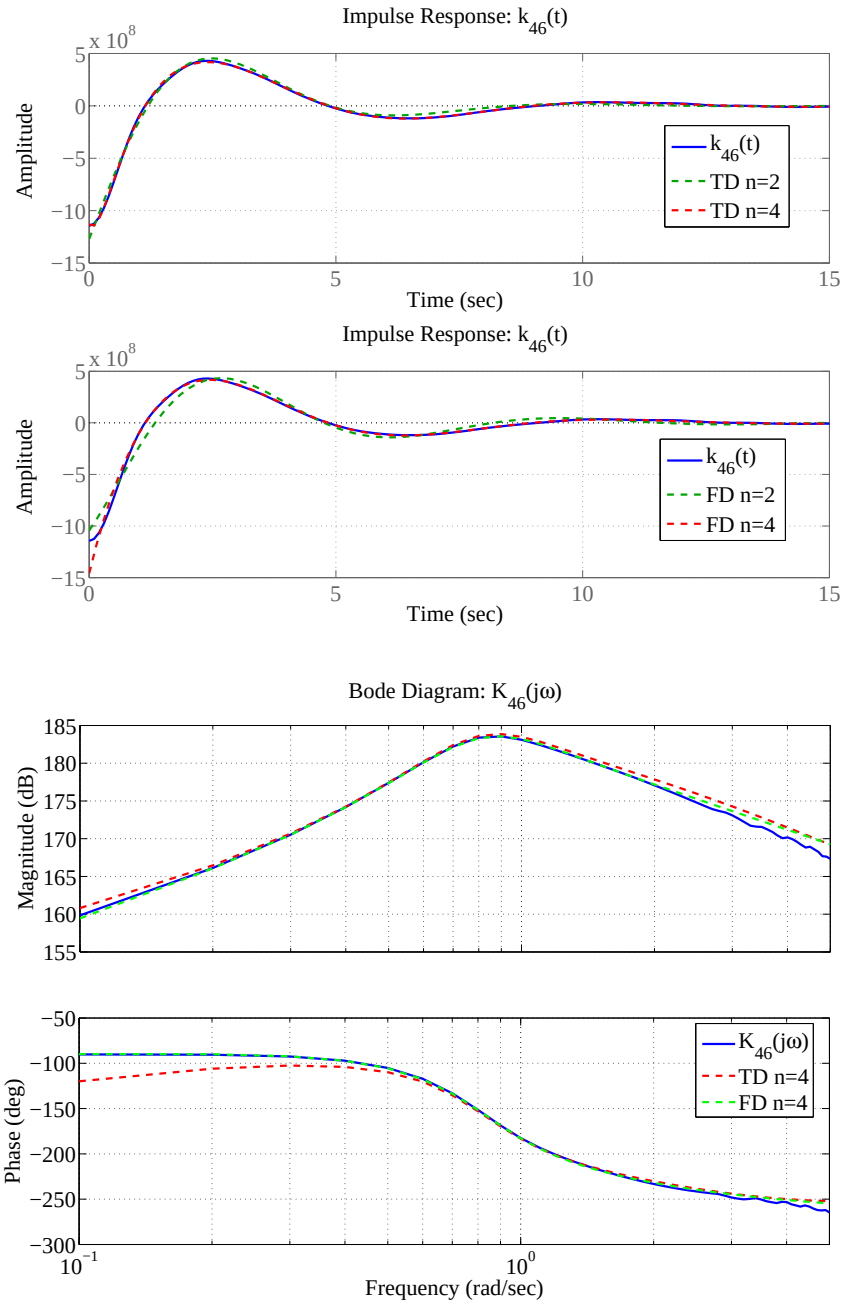

Figure 6.24: Impulse response of $k_{46}(t)$ and identified models, and Bode plot of $K_{46}(j\omega)$ and identified models.

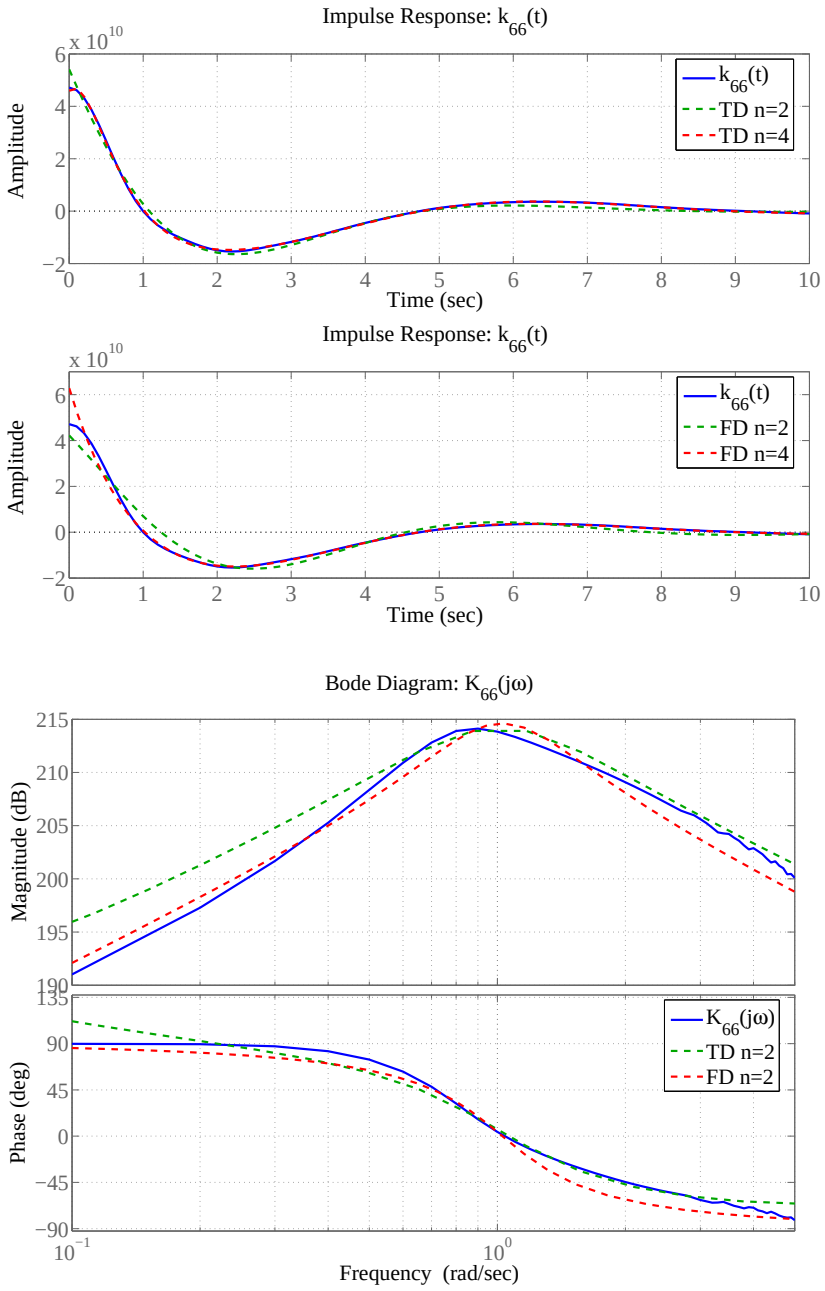

Figure 6.25: Impulse response of $k_{66}(t)$ and identified models, and Bode plot of $K_{66}(j\omega)$ and identified models.

6.3.2 MIMO Identification

This section presents MIMO identification of the overall lateral vessel system. The same approach is followed as in Section 6.2.2. The system structure,

$$\boldsymbol{K}_{lat} = \begin{bmatrix} K_{22} & K_{24} & K_{26} \\ 0 & K_{44} & K_{46} \\ 0 & 0 & K_{66} \end{bmatrix}, \tag{6.34}$$

was used. Then the dynamics for the upper off-diagonal modes were used also for the lower off-diagonal modes,

$$\boldsymbol{K}_{lat} = \begin{bmatrix} K_{22} & K_{24} & K_{26} \\ K_{24} & K_{44} & K_{46} \\ K_{26} & K_{46} & K_{66} \end{bmatrix}. \tag{6.35}$$

For this approach all the systems have the same denominator, and the overall system $\boldsymbol{K}_{lat}$ consists of three MISO systems describing the dynamics in sway, roll and yaw. The symmetry property of the original data set is kept. The error measures for the different modes of the identification are shown in Table 6.7.

For this particular system, the difference in order and accuracy is quite large between the Hankel SVD algorithm and the pem algorithm. In order to get a good fit and generate a positive real system a system of order 36 was necessary with the Hankel SVD algorithm. For the pem algorithm an accurate positive real model was obtained already at an order of 18, and also a system of order 30 was obtained. All the MIMO systems were positive real.

For both approaches the MIMO models are more accurate then the ones obtained by combining the SISO systems into MIMO models. Hence, for this data set, it is a good approach in order to obtain compact, accurate models for the radiation forces.

Figures 6.26-6.31 compare the impulse responses of the original data sets and models together with the comparison of the Bode plots of the original data sets and models. The impulse responses compare well with the models generated both from the Hankel SVD algorithm and the pem algoritm. From the Bode plots one can see that the frequency domain approach gives a better fit to the magnitude and phase than the time domain approach.

Table 6.7: Error Measures for the MIMO Identification

	R_y^2=1 − $\frac{\boldsymbol{e}^T\boldsymbol{e}}{\boldsymbol{y}^T\boldsymbol{y}}$					
	IR	Ph.	Mag.	$\|\|\cdot\|\|_\infty$	PR	Structure
Mode:		K_{22}				
MIMO TD:		Hankel SVD				
$n = 36$	0.9996	0.9882	0.9921	$1.48 \cdot 10^6$	×	-
MIMO FD:		pem				
$n = 18$	0.9909	0.9965	0.9986	$1.43 \cdot 10^6$	×	×
$n = 30$	0.9925	0.9977	0.9991	$9.98 \cdot 10^5$	×	×
Mode:		$K_{24} = K_{42}$				
SISO TD:		Hankel SVD				
$n = 36$	0.9946	0.9798	0.9944	$1.22 \cdot 10^6$	NPR	-
MIMO FD:		pem				
$n = 18$	0.9523	0.8901	0.9690	$2.20 \cdot 10^6$	NPR	×
$n = 30$	0.9819	0.9482	0.9918	$1.19 \cdot 10^6$	NPR	×
Mode:		$K_{26} = K_{62}$				
MIMO TD:		Hankel SVD				
$n = 36$	0.9997	0.9868	0.9945	$1.46 \cdot 10^7$	NPR	-
MIMO FD:		pem				
$n = 18$	0.9961	0.9995	0.9980	$2.14 \cdot 10^7$	NPR	×
$n = 30$	0.9983	0.9999	0.9985	$1.03 \cdot 10^7$	NPR	×
Mode:		K_{44}				
MIMO TD:		Hankel SVD				
$n = 36$	0.9988	0.9896	0.9929	$5.26 \cdot 10^6$	×	-
MIMO FD:		pem				
$n = 18$	0.9916	0.9977	0.9993	$3.22 \cdot 10^6$	×	×
$n = 30$	0.9891	0.9972	0.9996	$3.51 \cdot 10^6$	×	×
Mode:		$K_{46} = K_{64}$				
MIMO TD:		Hankel SVD				
$n = 36$	0.9994	0.9863	0.9927	$8.96 \cdot 10^7$	NPR	-
MIMO FD:		pem				
$n = 18$	0.9943	0.9999	0.9991	$4.86 \cdot 10^7$	NPR	×
$n = 30$	0.9968	0.9999	0.9993	$3.89 \cdot 10^7$	NPR	×
Mode:		K_{66}				
MIMO TD:		Hankel SVD				
$n = 36$	0.9993	0.9880	0.9907	$3.63 \cdot 10^9$	×	-
MIMO FD:		pem				
$n = 18$	0.9888	0.9984	0.9989	$2.25 \cdot 10^9$	×	×
$n = 30$	0.9911	0.9988	0.9993	$1.82 \cdot 10^9$	×	×

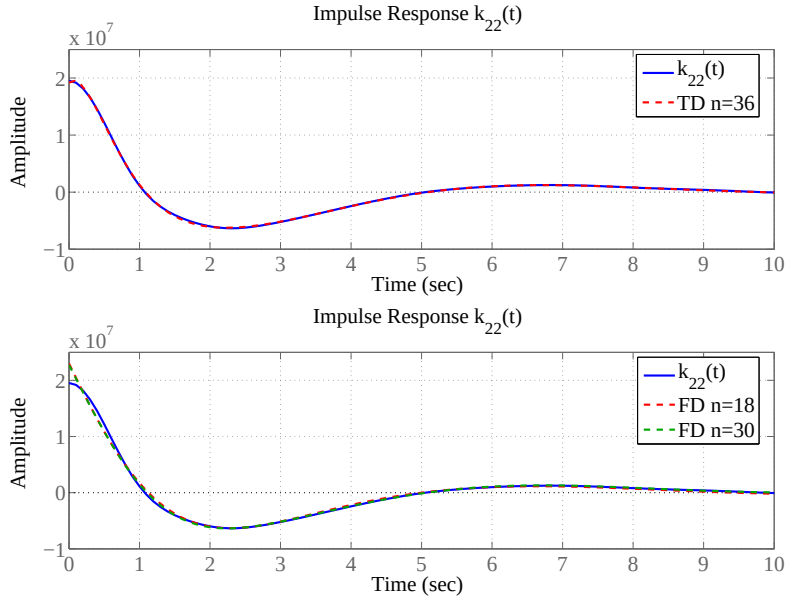

(a) Impulse response.

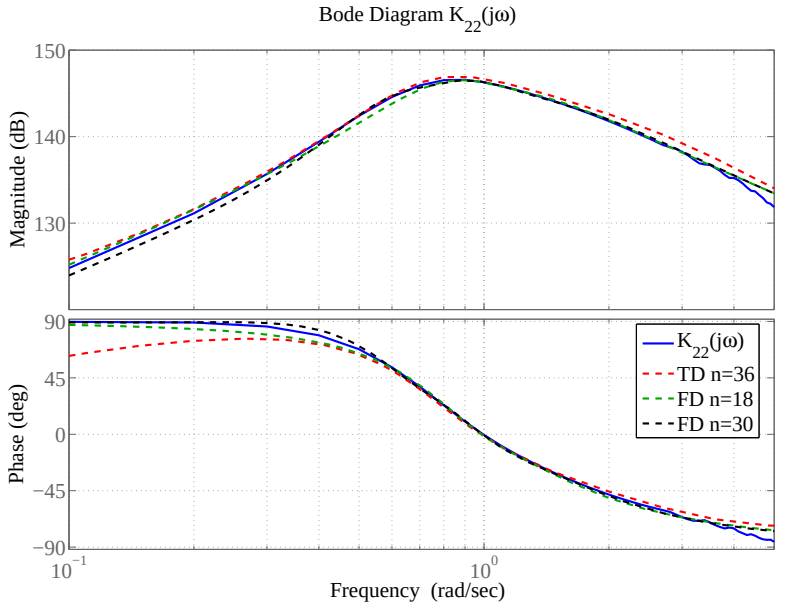

(b) Method: Hankel SVD and pem.

Figure 6.26: Impulse response of $k_{22}(t)$ and identified models, and Bode plot of $K_{22}(j\omega)$ and identified models.

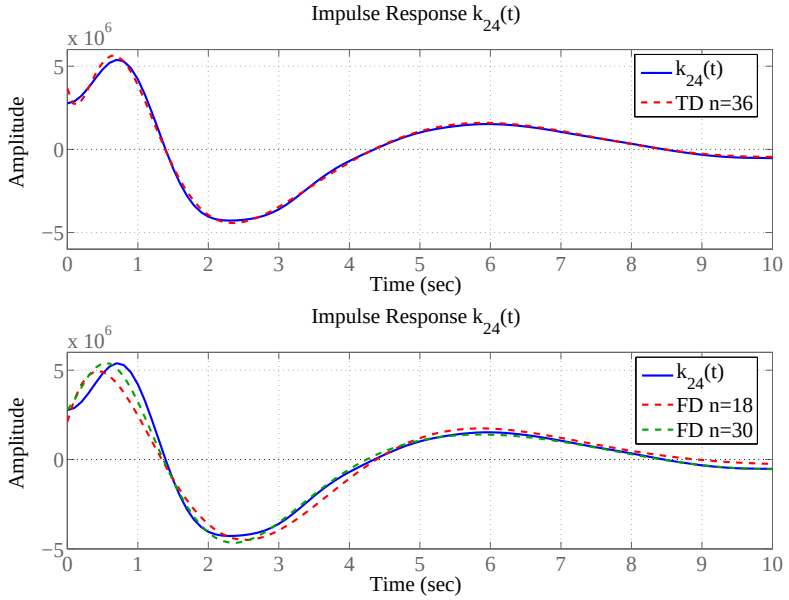

(a) Impulse response.

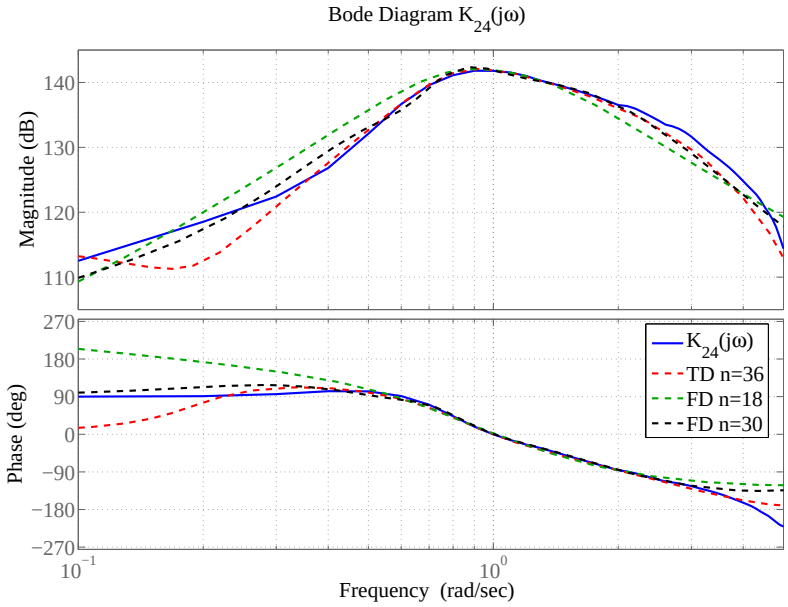

(b) Method: Hankel SVD and pem.

Figure 6.27: Impulse response of $k_{24}(t)$ and identified models, and Bode plot of $K_{24}(j\omega)$ and identified models.

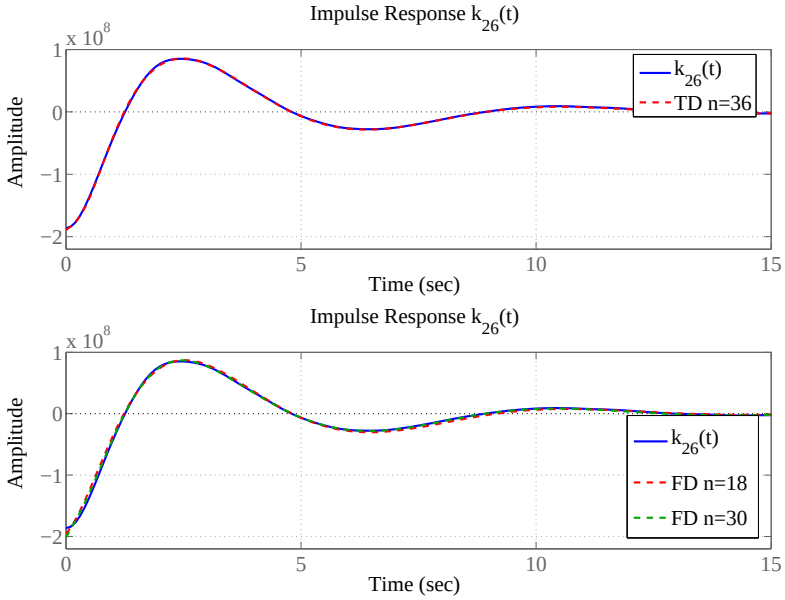

(a) Impulse response.

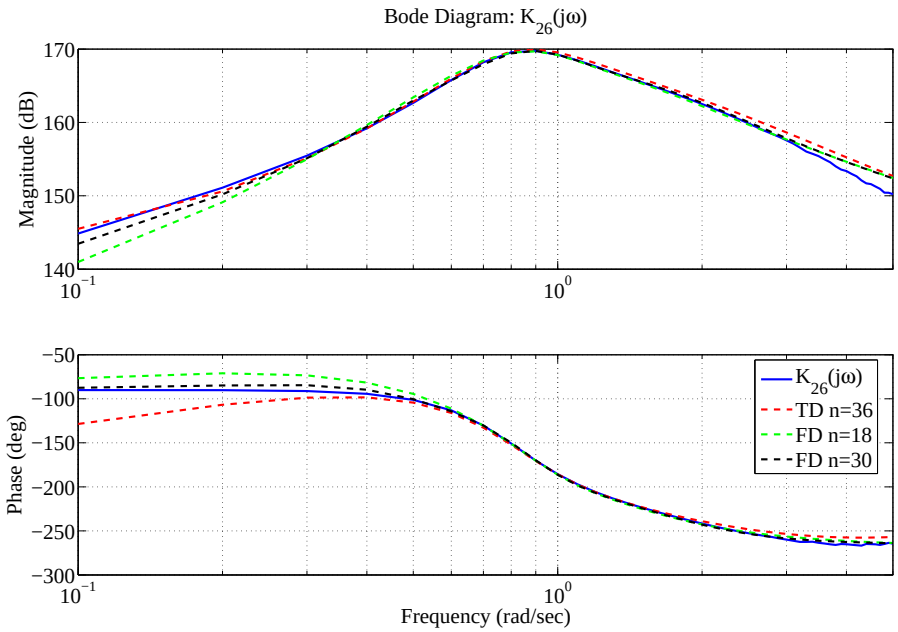

(b) Method: Hankel SVD and pem.

Figure 6.28: Impulse response of $k_{26}(t)$ and identified models, and Bode plot of $K_{26}(j\omega)$ and identified models.

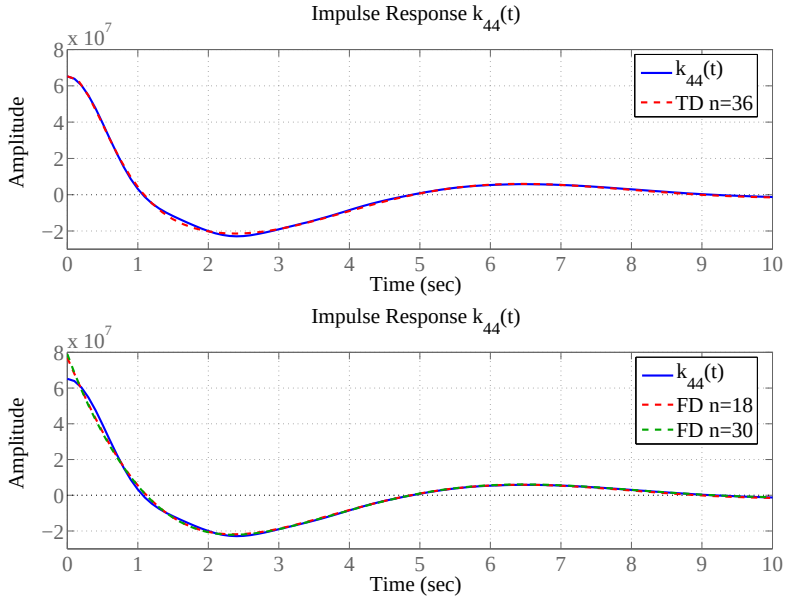

(a) Impulse response.

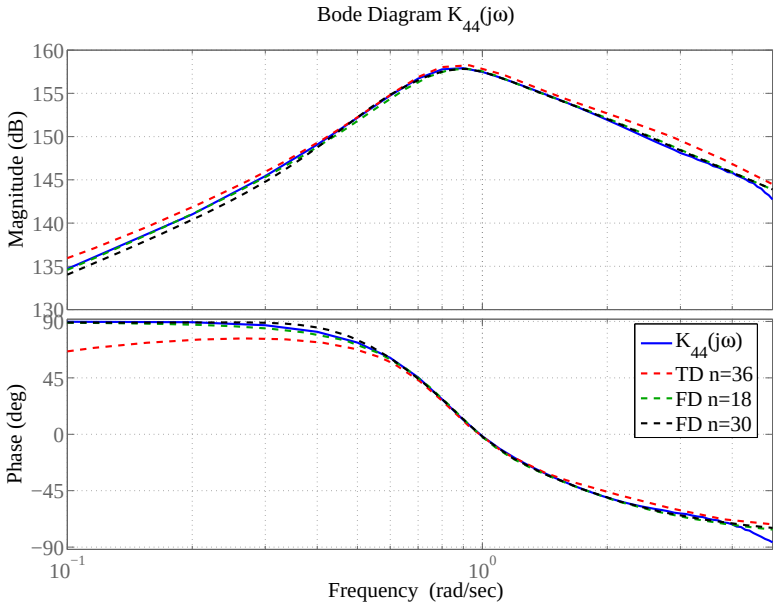

(b) Method: Hankel SVD and pem.

Figure 6.29: Impulse response of $k_{44}(t)$ and identified models, and Bode plot of $K_{44}(j\omega)$ and identified models.

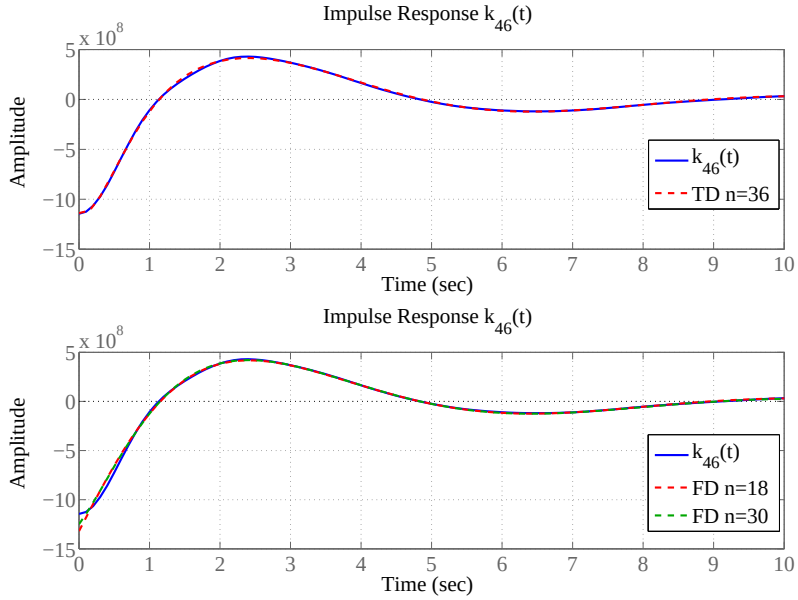

(a) Impulse response.

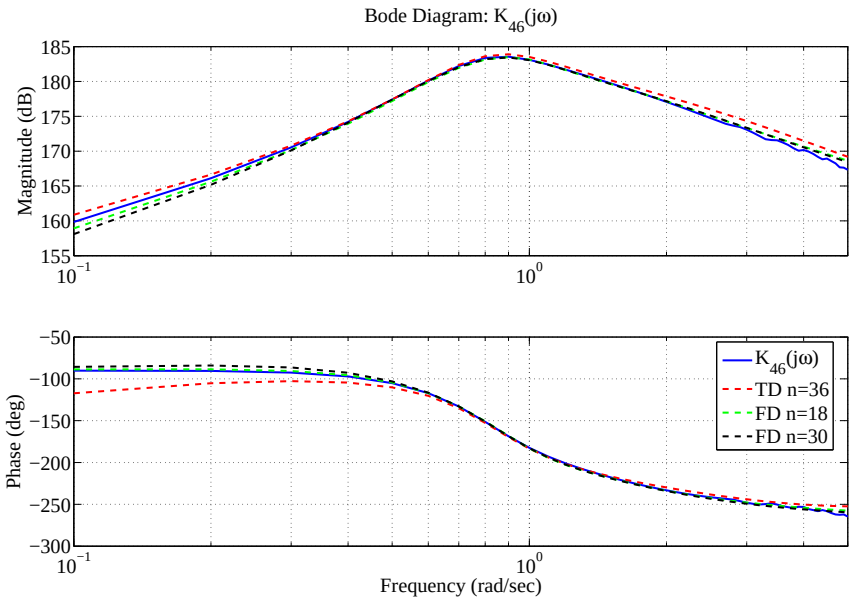

(b) Method: Hankel SVD and pem.

Figure 6.30: Impulse response of $k_{46}(t)$ and identified models, and Bode plot of $K_{46}(j\omega)$ and identified models.

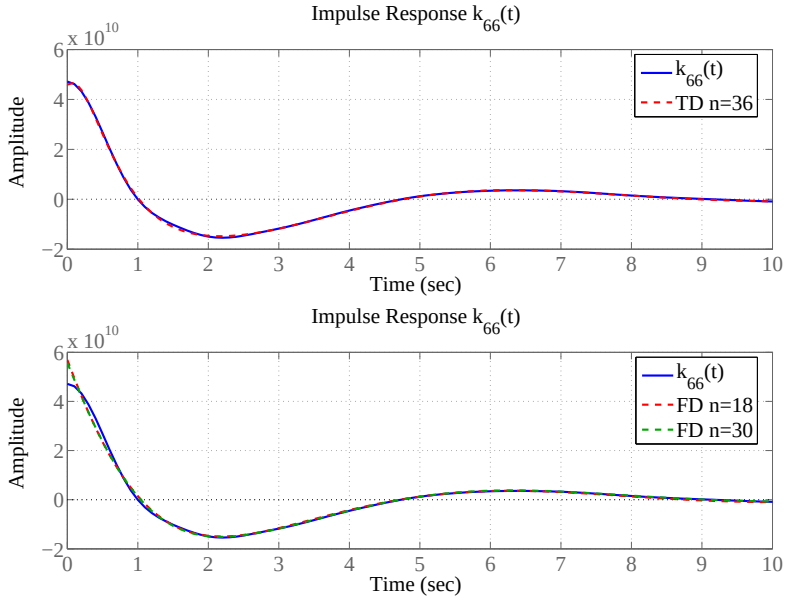

(a) Impulse response.

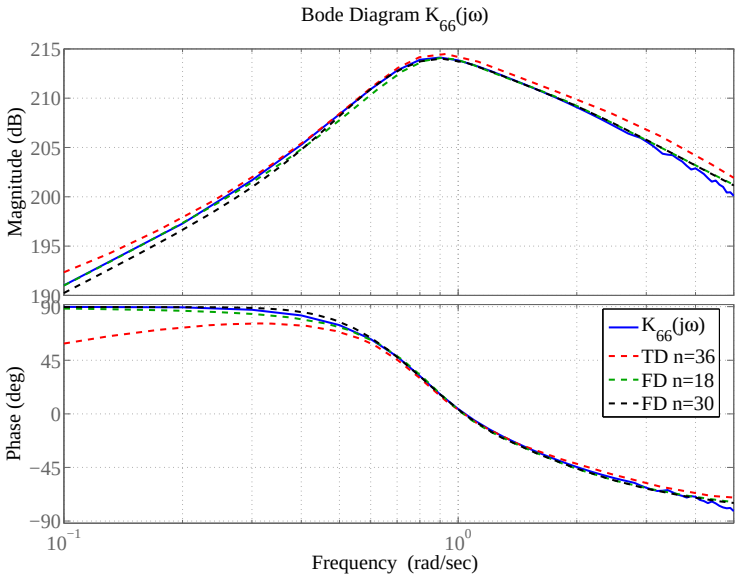

(b) Method: Hankel SVD and pem.

Figure 6.31: Impulse response of $k_{66}(t)$ and identified models and Bode plot of $K_{66}(j\omega)$ and identified models.

6.3.3 SISO Identification with Reduction

In this section SISO identification of each mode is done, followed by a reduction of the overall system $\boldsymbol{K}_{lat}$, by use of the algorithms presented in the Sections 5.2.1-5.2.3. By utilizing the symmetry of the system, only 6 of 9 modes have to be identified when we use SISO identification. The same approach follows as in Section 6.2.3.

Accurate models for the different modes were obtained by use of the Hankel SVD scheme and combined into a MIMO system representing $\boldsymbol{K}_{lat}$. The overall MIMO system was of order 72. Further it was reduced to orders 36, 20 and 16 by the use of Lyapunov, Riccati and mixed gramian balancing. The error measures are given in Table 6.8. The differences between the errors for the MIMO systems of order 36 were so small that only the error measures for the Lyapunov balancing are listed.

The Lyapunov and Riccati balancing keep the symmetry property of the system, while the mixed gramian balancing does not keep this property. For MIMO systems, based on whether the controllability and available storage gramians or the required supply and observability gramians are balanced with each other, the two resulting systems will be the transpose of each other. In this case, the required supply and observability gramians are balanced. If the controllability and available storage gramians were balanced, the obtained error measures would have been the transpose of what we get now, i.e. $K_{26} = K_{62}$ and $K_{62} = K_{26}$. For this case study the differences when using mixed gramian balancing are quite large in some of the modes e.g. the modes K_{24} and K_{42} in the system of order 16. However, in terms of error measures for the different modes the method can compete with the Lyapunov and Riccati balancing schemes. These are the same remarks as mentioned in the first case study.

All the different balancing schemes generated positive real reduced order systems for all the different orders. Further, compact models with good accuracy and fit were obtained. In this case study the Lyapunov balancing was the reduction method giving the systems with best accuracy and fit of the original data sets.

Looking at Tables 6.6-6.8 the different modeling approaches for this case study can be compared. The SISO identification followed by MIMO reduction gives flexibility to choose the best fit of the individual modes in the identification phase, at the same time as compact and accurate models are generated by use of the model reduction. Looking at the different error measures for the various approaches, the approach with identification followed by reduction gives the most compact and accurate models.

Table 6.8: Different Error Measures for the Reduction

	R_y^2=$1-\frac{\boldsymbol{e}^T\boldsymbol{e}}{\boldsymbol{y}^T\boldsymbol{y}}$				
Order	IR	Ph.	Mag.	$\|\|\cdot\|\|_\infty$	PR
Mode:	K_{22}				
Original $n=72$	0.9996	0.9882	0.9921	$1.48\cdot10^6$	×
Lyapunov $n=36$	0.9996	0.9882	0.9921	$1.48\cdot10^6$	×
Lyapunov $n=20$	0.9994	0.9872	0.9921	$1.64\cdot10^6$	×
Riccati $n=20$	0.9996	0.9882	0.9921	$1.48\cdot10^6$	×
Mixed $n=20$	0.9995	0.9881	0.9921	$1.49\cdot10^6$	×
Lyapunov $n=16$	0.9978	0.9901	0.9906	$2.11\cdot10^6$	×
Riccati $n=16$	0.9991	0.9881	0.9918	$1.71\cdot10^6$	×
Mixed $n=16$	0.9993	0.9885	0.9921	$1.63\cdot10^6$	×
Mode:	$K_{24}=K_{42}$				
Original $n=72$	0.9996	0.9971	0.9955	$1.11\cdot10^6$	NPR
Lyapunov $n=36$	0.9996	0.9973	0.9955	$1.12\cdot10^6$	NPR
Lyapunov $n=20$	0.9972	0.9923	0.9970	$1.12\cdot10^6$	NPR
Riccati $n=20$	0.9992	0.9974	0.9950	$1.25\cdot10^6$	NPR
Mixed_{24} $n=20$	0.9992	0.9972	0.9955	$1.02\cdot10^6$	NPR
Mixed_{42} $n=20$	0.9962	0.9976	0.9952	$1.09\cdot10^6$	NPR
Lyapunov $n=16$	0.9911	0.9404	0.9915	$1.65\cdot10^6$	NPR
Riccati $n=16$	0.9982	0.9983	0.9941	$1.71\cdot10^6$	NPR
Mixed_{24} $n=16$	0.9950	0.9944	0.9955	$1.30\cdot10^6$	NPR
Mixed_{42} $n=16$	0.9712	0.9623	0.9875	$2.08\cdot10^6$	NPR
Mode:	$K_{26}=K_{62}$				
Original $n=72$	0.9999	0.9869	0.9952	$1.39\cdot10^7$	NPR
Lyapunov $n=36$	0.9999	0.9869	0.9952	$1.39\cdot10^7$	NPR
Lyapunov $n=20$	0.9999	0.9869	0.9952	$1.37\cdot10^7$	NPR
Riccati $n=20$	0.9997	0.9869	0.9950	$1.51\cdot10^7$	NPR
Mixed_{26} $n=20$	0.9993	0.9867	0.9945	$1.40\cdot10^7$	NPR
Mixed_{62} $n=20$	0.9993	0.9867	0.9945	$1.65\cdot10^7$	NPR
Lyapunov $n=16$	0.9999	0.9869	0.9950	$1.48\cdot10^7$	NPR
Riccati $n=16$	0.9990	0.9869	0.9946	$1.87\cdot10^7$	NPR
Mixed_{26} $n=16$	0.9999	0.9869	0.9952	$1.40\cdot10^7$	NPR
Mixed_{62} $n=16$	0.9935	0.9867	0.9921	$2.49\cdot10^7$	NPR

Continued on next page

	R_y^2=1 − $\frac{\boldsymbol{e}^T\boldsymbol{e}}{\boldsymbol{y}^T\boldsymbol{y}}$				
	IR	Ph.	Mag.	$\|\|\cdot\|\|_\infty$	PR
Mode:	K_{44}				
Original $n = 72$	0.9999	0.9867	0.9926	$5.15 \cdot 10^6$	×
Lyapunov $n = 36$	0.9999	0.9867	0.9926	$5.14 \cdot 10^6$	×
Lyapunov $n = 20$	0.9999	0.9873	0.9926	$5.05 \cdot 10^6$	×
Riccati $n = 20$	0.9998	0.9868	0.9926	$5.16 \cdot 10^6$	×
Mixed $n = 20$	0.9999	0.9866	0.9926	$5.12 \cdot 10^6$	×
Lyapunov $n = 16$	0.9995	0.9870	0.9931	$4.92 \cdot 10^6$	×
Riccati $n = 16$	0.9998	0.9868	0.9925	$5.18 \cdot 10^6$	×
Mixed $n = 16$	0.9991	0.9885	0.9924	$5.19 \cdot 10^6$	×
Mode:	$K_{46} = K_{64}$				
Original $n = 72$	0.9995	0.9862	0.9929	$8.57 \cdot 10^7$	NPR
Lyapunov $n = 36$	0.9995	0.9862	0.9929	$8.57 \cdot 10^7$	NPR
Lyapunov $n = 20$	0.9995	0.9862	0.9929	$8.55 \cdot 10^7$	NPR
Riccati $n = 20$	0.9995	0.9863	0.9929	$8.48 \cdot 10^7$	NPR
Mixed_{46} $n = 20$	0.9995	0.9862	0.9929	$8.55 \cdot 10^7$	NPR
Mixed_{64} $n = 20$	0.9995	0.9862	0.9929	$8.57 \cdot 10^7$	NPR
Lyapunov $n = 16$	0.9995	0.9863	0.9929	$8.50 \cdot 10^7$	NPR
Riccati $n = 16$	0.9996	0.9863	0.9929	$8.55 \cdot 10^7$	NPR
Mixed_{46} $n = 16$	0.9995	0.9862	0.9929	$8.51 \cdot 10^7$	NPR
Mixed_{64} $n = 16$	0.9995	0.9862	0.9929	$8.99 \cdot 10^7$	NPR
Mode:	K_{66}				
Original $n = 72$	0.9993	0.9880	0.9907	$3.62 \cdot 10^9$	×
Lyapunov $n = 36$	0.9993	0.9880	0.9907	$3.63 \cdot 10^9$	×
Lyapunov $n = 20$	0.9993	0.9880	0.9907	$3.63 \cdot 10^9$	×
Riccati $n = 20$	0.9993	0.9880	0.9907	$3.61 \cdot 10^9$	×
Mixed $n = 20$	0.9993	0.9880	0.9907	$3.63 \cdot 10^9$	×
Lyapunov $n = 16$	0.9993	0.9880	0.9907	$3.63 \cdot 10^9$	×
Riccati $n = 16$	0.9993	0.9880	0.9907	$3.64 \cdot 10^9$	×
Mixed $n = 16$	0.9993	0.9880	0.9907	$3.63 \cdot 10^9$	×

In Figures 6.32-6.37 the impulse responses and Bode diagrams of the original data sets and the obtained models are presented. These show good fit and accuracy in most of the modes.

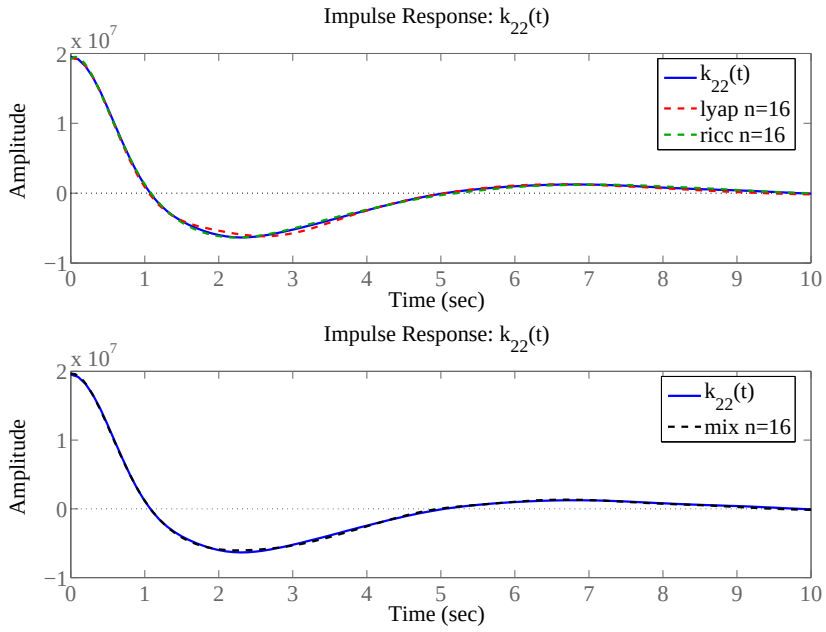

(a) Impulse response.

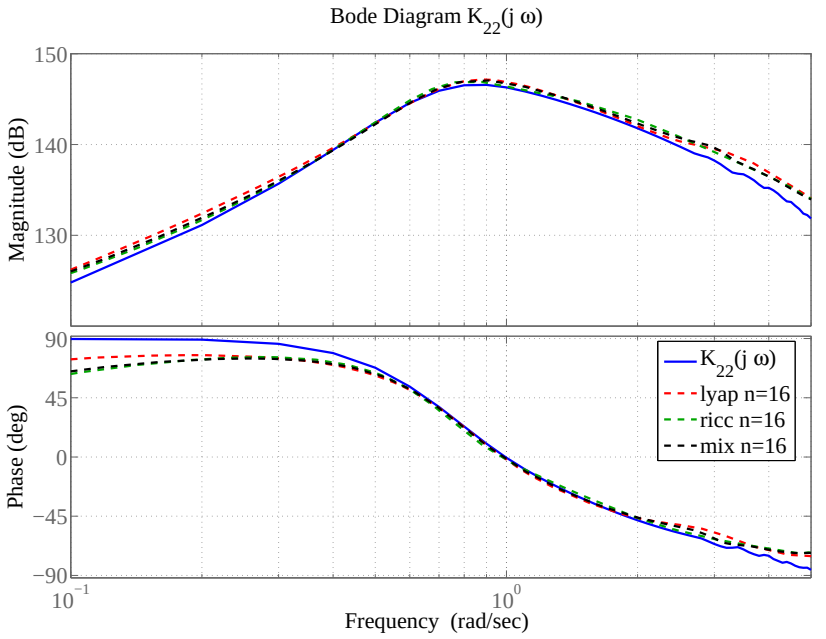

(b) Method: Lyapunov (lyap), Riccati (ricc) and Mixed Gramian (mix) Balancing.

Figure 6.32: Plot of $k_{22}(t)$ and $K_{22}(j\omega)$ versus identified and reduced models.

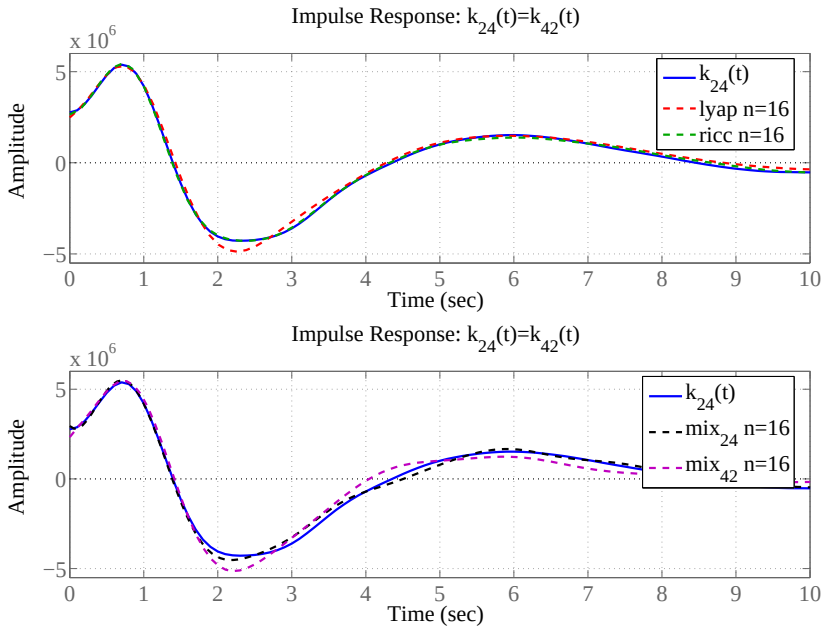

(a) Impulse response.

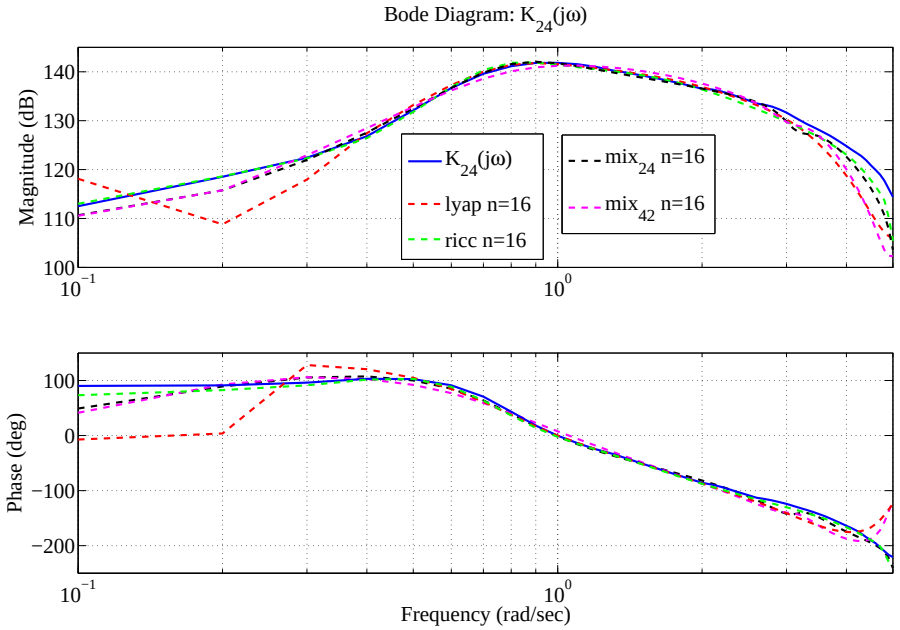

(b) Method: Lyapunov (lyap), Riccati (ricc) and Mixed Gramian (mix) Balancing.

Figure 6.33: Plot of $k_{24}(t)$ and $K_{24}(j\omega)$ versus identified and reduced models.

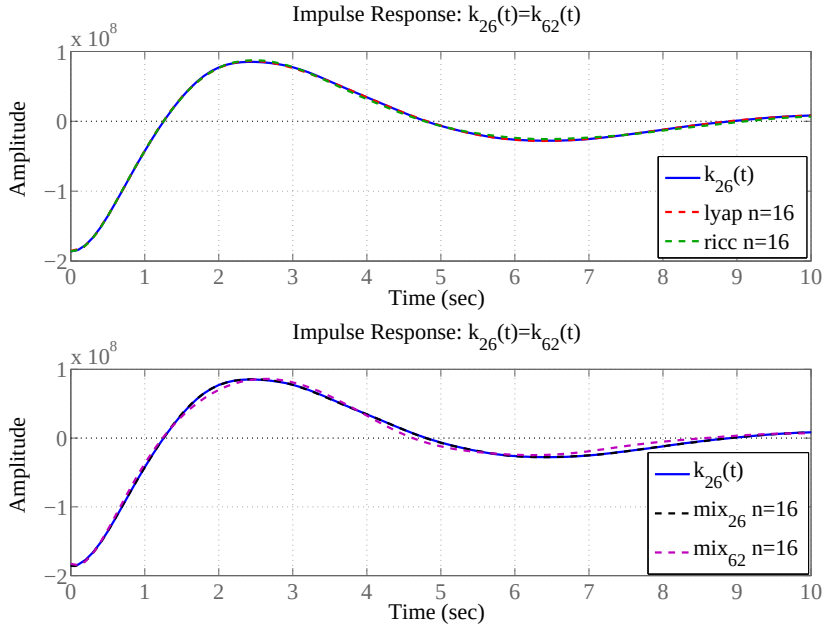

(a) Impulse response.

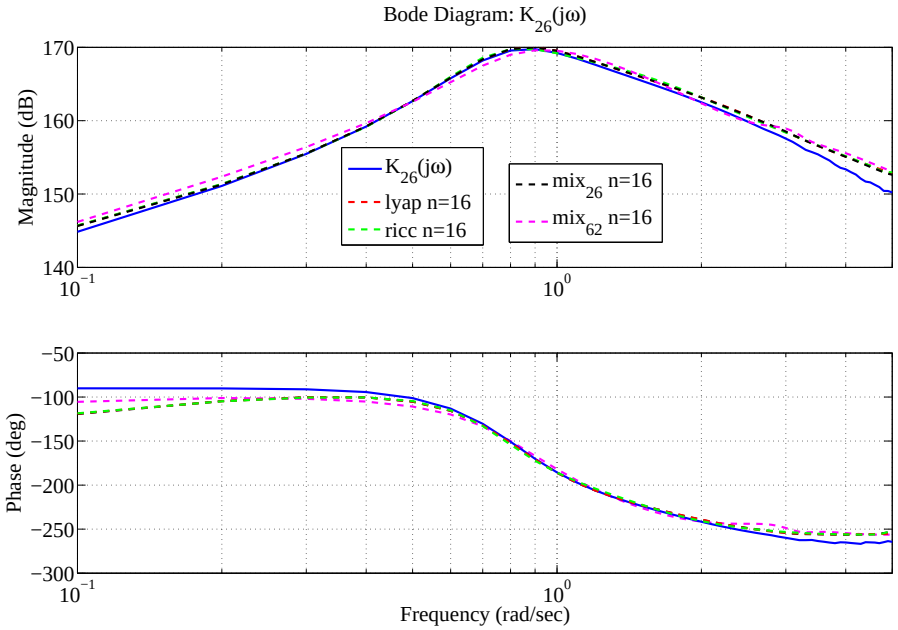

(b) Method: Lyapunov (lyap), Riccati (ricc) and Mixed Gramian (mix) Balancing.

Figure 6.34: Plot of $k_{26}(t)$ and $K_{26}(j\omega)$ versus identified and reduced models.

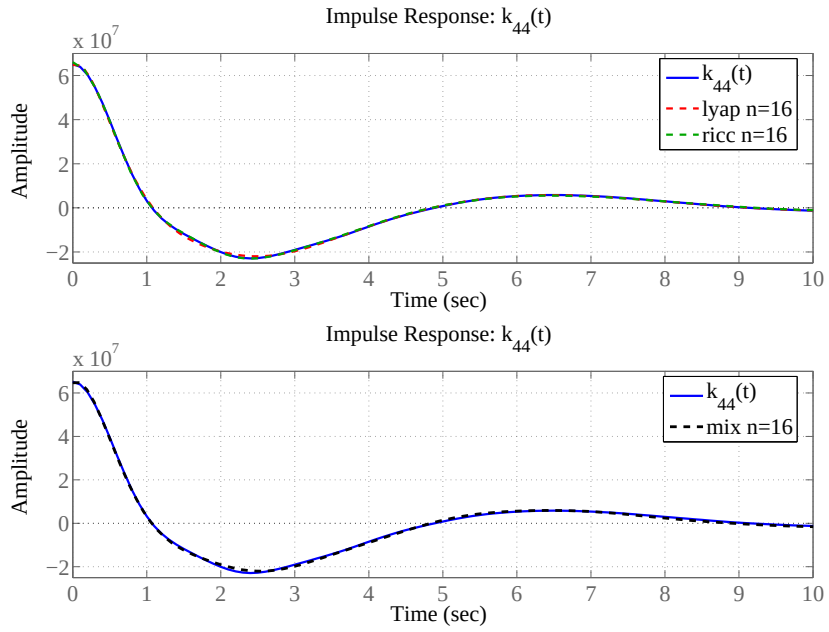

(a) Impulse response.

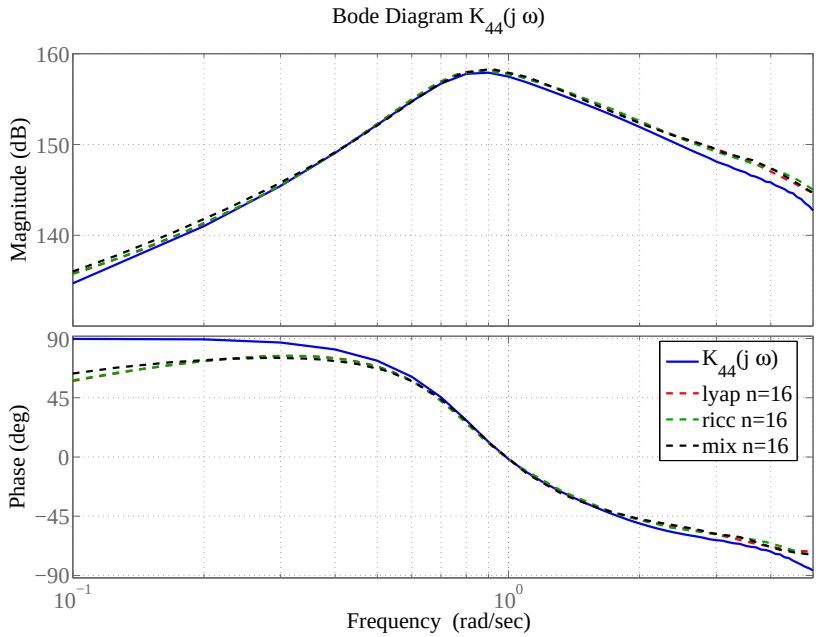

(b) Method: Lyapunov (lyap), Riccati (ricc) and Mixed Gramian (mix) Balancing.

Figure 6.35: Plot of $k_{44}(t)$ and $K_{44}(j\omega)$ versus identified and reduced models.

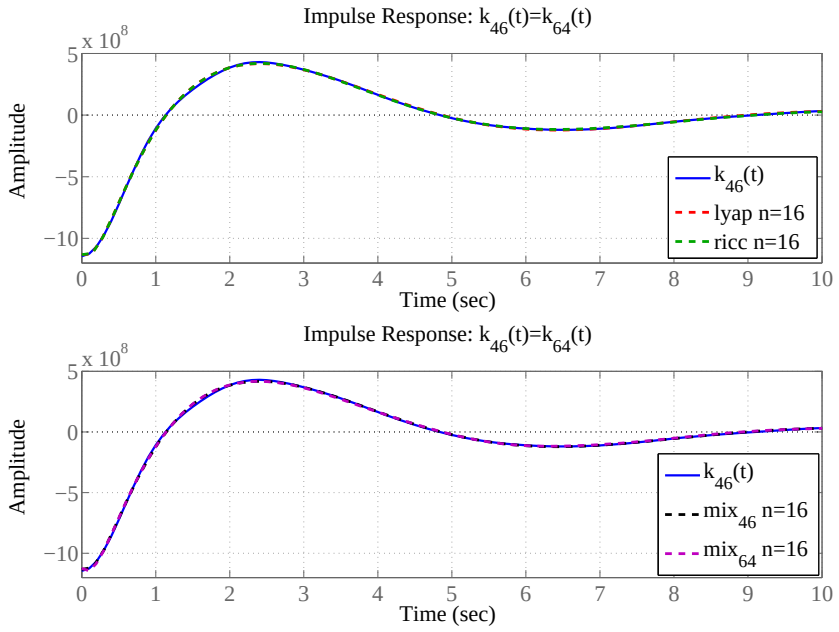

(a) Impulse response.

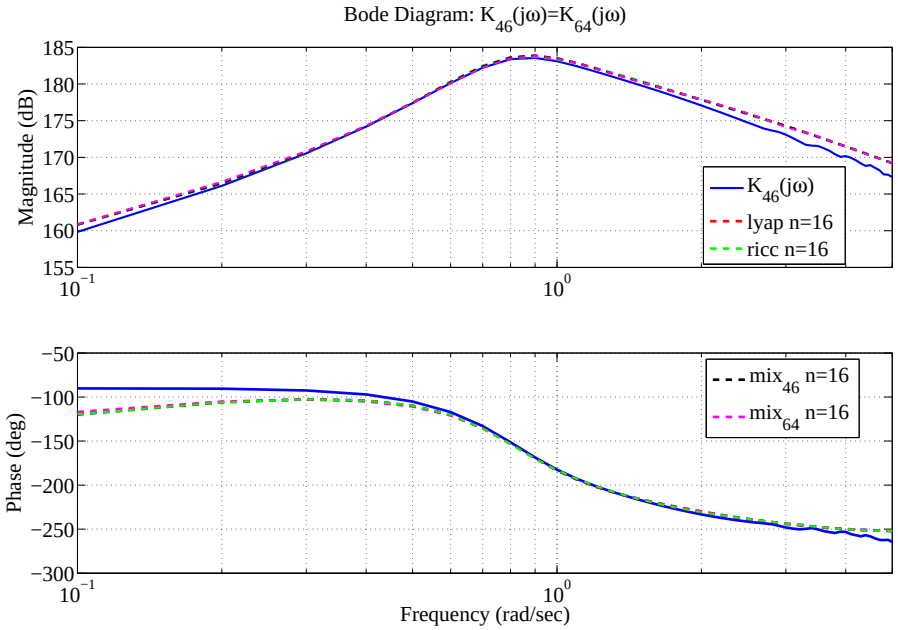

(b) Method: Lyapunov (lyap), Riccati (ricc) and Mixed Gramian (mix) Balancing.

Figure 6.36: Plot of $k_{46}(t)$ and $K_{46}(j\omega)$ versus identified and reduced models.

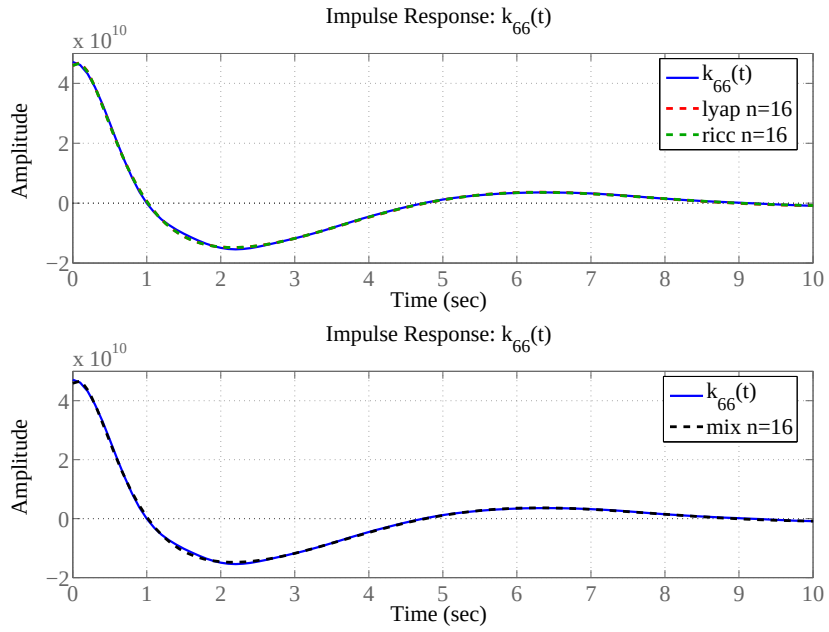

(a) Impulse response.

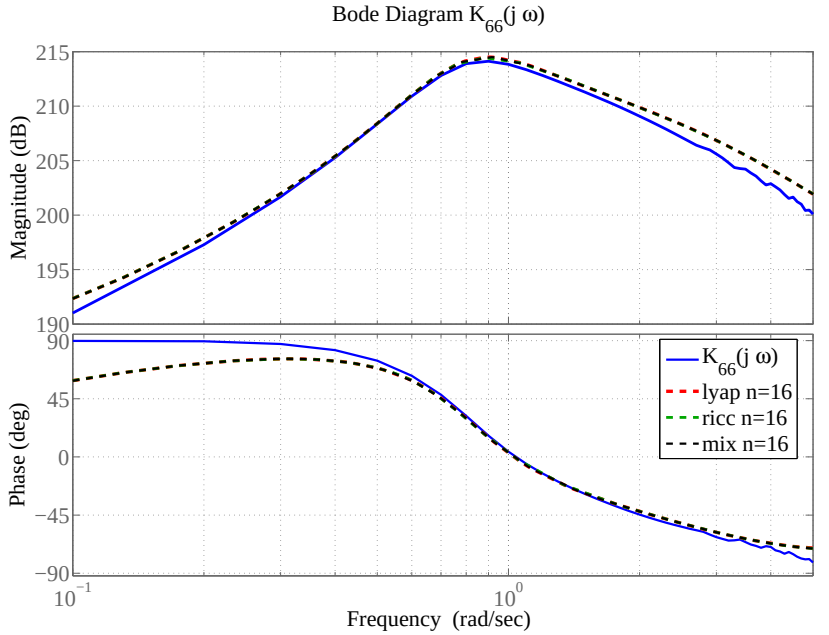

(b) Method: Lyapunov (lyap), Riccati (ricc) and Mixed Gramian (mix) Balancing.

Figure 6.37: Plot of $k_{66}(t)$ and $K_{66}(j\omega)$ versus identified and reduced models.

6.4 Concluding Remarks

Time domain and frequency domain techniques have been applied in this chapter in order to identify the radiation forces. Time domain identification requires the calculation of the impulse responses of the radiation forces before the identification can take place. By using frequency domain techniques the data sets from the hydrodynamic software can be used to express the frequency response, and no further calculations are needed in order for the identification to take place. Hence, less preprocessing of the data sets is needed than for time domain identification.

The case studies showed that both time domain and frequency domain techniques work well for the identification of the radiation forces. The impulse responses were fitted well by both methods, while for the approximation of the magnitude and phase of the system, the frequency domain techniques worked better. For the frequency domain approach the computation of the convolution integral is avoided, and it represents a more direct way of obtaining the models of the radiation forces at the same time as it has very nice performance in terms of accuracy and fit for all the error measures.

Three different approaches were taken for the identification of the radiation forces; SISO identification of every mode; MIMO identification of the overall model; SISO identification of every mode followed by model reduction of the overall MIMO system. All approaches gave models with a good fit to the original data sets, but the latter method proved to be most powerful in terms of obtaining compact and accurate models.

SISO identification with subsequent model reduction gives designers of control systems or simulators flexibility in terms of choosing the order and accuracy of the model. This method also provides the possibility to identify higher order models, used for the verification of controllers that are designed and based on low order models.

Chapter 7

Final Remarks

7.1 Conclusions and Suggestions for Further Work

This thesis has addressed the identification and order reduction of parametric models of radiation forces in marine applications. The motivation behind investigating these forces lies in marine applications where such models are useful for simulator, control and observer design. Examples of such applications include DP systems, marine systems simulators and wave power plants.

The models developed were obtained by use of hydrodynamic software. This is a cheap alternative compared to traditional methods like full-scale experiments, and hence there is a financial motivation for using this approach.

The stability and positive realness of the radiation forces were stated by using the properties revealed in the data sets from the hydrodynamic software. Furthermore, it was shown that the overall vessel model is passive if the radiation forces are modeled positive real. Stability and passivity are dynamical properties which should be reflected in the model of the radiation forces.

By using the frequency dependent added mass and damping matrices from the hydrodynamic software, the radiation forces can either be identified by time domain or frequency domain identification. For time domain identification, a method based on Markov parameter estimation was used and for frequency domain identification two different algorithms were applied; one based on least squares fitting and one prediction error minimization algorithm. All the algorithms used were customized functions implemented in MATLAB.

Two case studies were investigated. The radiation forces for a 3-DOF vessel model were identified where the hydrodynamic data sets were obtained from the software WAMIT. Subsequently, the radiation forces for a

lateral vessel model were identified from data sets obtained form the software VERES. For the case studies three different approaches for use of the identification schemes were investigated: SISO identification of every mode; MIMO identification of the overall system; SISO identification of every mode followed by model reduction of the overall MIMO system.

Time domain identification of the radiation forces requires the computation of the impulse response from either the added mass matrix or from the damping matrix. Frequency domain identification can be used directly on the frequency response of the radiation forces, which is easily obtained from the frequency dependent added mass and damping matrices. Hence the latter represents a more direct way of obtaining the radiation force models. In addition, the frequency domain techniques gave more accurate models than the time domain approach. All the identification algorithms used guaranteed stable models, while positive realness was not ensured. However, the schemes applied generated positive real systems in most of the cases where the data sets indicated this property.

The three different approaches for use of the identification schemes gave accurate models with good fit to the original data sets. However, identification followed by model reduction proved to be the most powerful in terms of obtaining compact and accurate models. SISO identification followed by MIMO reduction gives flexibility in the model generation. This approach makes it possible to develop models with different accuracy, e.g. where a low order model can be used for controller design while a model of higher order and with better accuracy can be used for verification of the controller. It can be concluded that combining identification and model reduction offers flexibility in the choice of model complexity and accuracy.

For the two case studies investigated the vessels had relatively simple dynamics. For future research it would be of interest to apply these methods to systems with more challenging dynamics. The models developed are only valid for vessels at zero speed, and future research could consider the case of forward speed. For a vessel with forward speed the frequency dependent added mass and damping parameters are also dependent on the velocity of the vessel.

In terms of model reduction, an overview of existing balanced truncation methods was given, before a new algorithm keeping the positive realness of the reduced order systems was developed; mixed gramian balancing. This showed nice properties in terms of accuracy and computational time compared to existing methods. The method works well for SISO systems, but for MIMO systems one has to be aware of that the symmetry properties of systems will not be kept, since the gramians are not dual to each other.

It has been shown that in order to obtain positive real truncated systems,

only one of the gramians in the balancing algorithm needs to satisfy either the PR or the DPR equations. This opens the way for new combinations of gramians in order to obtain positive real truncated systems. Here it has been used to obtain positive real frequency weighted truncation. For the existing balanced truncation methods investigated well established error measures are developed. For future research it would be of interest to find error bounds for the proposed algorithms in this thesis. Further, an extension to descriptor systems could be investigated. In the literature there already exist order reduction methods focusing on the approximation error in the H_2- and H_∞-norms which give stable systems. For future work it would be of interest to see if it is possible to extend some of this work to positive real systems exploiting the properties resulting in mixed gramian balancing and positive real frequency weighted truncation.

Bibliography

Antoulas, A.C. (2005). *Approximation of Large-Scale Dynamical Systems*. SIAM.

Babarit, A. and A.H. Clément (2006). Optimal latching control of wave energy device in regular and irregular waves. *Applied Ocean Research* **28**, 77–91.

Babarit, A., G. Duclos and A.H. Clément (2004). Comparison of latching control strategies for heaving wave energy device in random sea. *Applied Ocean Research* **26**, 227–238.

Bailey, P.A., E.J. Ballard, D.A. Hudson and P. Temarel (2000). Time domain analysis of vessels in waves accounting for fluid memory effects. In: *Proceedings of NAV2000*.

Bailey, P.A., W.G. Price and P. Temarel (1997). A unified mathematical model describing the maneuvering of a ship travelling in a seaway. *Trans. RINA* **140**, 131–149.

Ballard, E.J. (2002). Time Domain Simulation of Ship Motions in Waves. PhD dissertation. University of Southampton. The Faculty of Engineering and Applied Science.

Bendat, J.G. and A.G. Piersol (2000). *Random Data, Analysis and Measurement Procedures*. John Wiley & Sons, Inc.

Benner, P., V. Mehrmann and D.C. Sorensen (2005). *Dimension Reduction of Large-Scale Systems*. Springer.

Bishop, R.E.D. and W.G. Price (1979). An investigation into the linear theory of ship response to waves. *Journal of Sound and Vibration* **62**, 353–363.

Bishop, R.E.D., R.K. Burcher and W.G. Price (1973). The uses of functional analysis in ship dynamics. In: *Proceedings of the Royal Society, London*. Vol. A332. pp. 25–35.

Bjarte-Larsson, T., J. Falnes and T. Moan (2006). Comparison of results from time-domain simulations and model tests of a water-pumping wave-power unit. In: *Proceedings of the Sixteenth International Offshore and Polar Engineering Conference*. San Fransisco, California, USA.

Chen, C-T. (1999). *Linear System Theory and Design*. Oxford University Press.

Chung, J-S. and M.M. Bernitsas (1997). Hydrodynamic memory effect on stability, bifurcation, and chaos of two-point mooring systems. *Journal of Ship Research* **41**, 26–44.

Coelho, C.P., J. Phillips and L.M. Silveira (2004). A convex programming approach for generating guaranteed passive approximations to tabulated frequency-data. *IEEE Transactions on Computer-Aided Design of Integrated Circuits and Systems* **23**, 293–301.

Cummins, W. (1962). The impulse response function and ship motions. *Schiffstechnik* **9**, 101–109.

Damaren, C.J. (2000). Time-domain floating body dynamics by rational approximation of the radiation impedance and diffraction mapping. *Ocean Engineering* **27**, 687–705.

Damaren, C.J. (2001). The hydrodynamics of thin floating plates. *Ocean Engineering* **28**, 1145–1170.

Damaren, C.J., H.J. Marquez and H.J. Buckley (1996). Optimal strictly positive real approximations for stable transfer functions. In: *IEE Proceedings-Control Theory and Applications*. Vol. 143. pp. 537–542.

de Prony, Baron G. R. (1795). Essai éxperimental et analytique: sur les lois de la dilatabilité de fluides élastique et sur celles de la force expansive de la vapeur de l'alkool, à différentes températures. *Journal de l'École Polytechnique* **1**, 24–76.

Desai, U.B. and D. Pal (1984). A transformation approach to stochastic model reduction. *IEEE Transactions on Automatic Control* **AC-29**, 1097–1100.

Duclos, G., A.H. Clément and G. Chatry (2001). Absorption of outgoing waves in a numerical wave tank using a self-adaptive boundary condition. *International Journal of Offshore and Polar Engineering* **3**, 168–175.

Egeland, O. (1993). *Servoteknikk*. Tapir Forlag.

Egeland, O. and J. Gravdahl (2002). *Modeling and Simulation for Automatic Control*. Marine Cybernetics.

Eidsmoen, H. (1996). Simulation of a tight-moored amplitude-limited heaving-buoy wave-energy converter with phase control. Technical report. Department of Physics, Norwegian University of Science and Technology.

Falnes, J. (2002). *Ocean waves and oscillating systems : linear interactions including wave-energy extraction*. Cambridge University Press.

Faltinsen, O.M. (1990). *Sea Loads on Ships and Offshore Structures*. Cambridge University Press.

Fathi, D. (2004). *ShipX Vessel Responses (VERES), Ship Motions and Global Loads, User's Manual*. SINTEF.

Fossen, T.I. (2002). *Marine Control Systems: Guidance, Navigation and Control of Ships, Rigs and Underwater Vehicles*. Marine Cybernetics.

Fossen, T.I. (2005). A nonlinear unified state-space model for ship maneuvering and control in a seaway. *International Journal of Bifurcation and Chaos* **15**(9), 2717–2746.

Fossen, T.I. and Ø.N. Smogeli (2004). Nonlinear time-domain strip theory formulation for low-speed manouvering and station-keeping. *Modeling, Identification and Control* **MIC-25**, 201–221.

Glover, K. (1984). All optimal Hankel-norm approximations of linear multivariable systems and their L^∞-error bounds. *International Journal of Control* **39**, 1115–1193.

Green, M. (1988). Balanced Stochastic Realizations. *Linear Algebra and its Applications* **98**, 211–247.

Gugercin, S. and A.C. Antoulas (2004). A survey of model reduction and some new results. *International Journal of Control* **77**, 748–766.

Harshavardhana, P., E.A. Jonckheere and L.M. Silverman (1984). Stochastic balancing and approximation-stability and minimality. *IEEE Transaction on Automatic Control* **29**, 744–746.

Hjulstad, Å. (2004). State-space representation of convolution terms for surface vessels with forward speed. Master's thesis. Department of Engineering Cybernetics, Norwegian University of Science and Technology.

Hjulstad, Å., E. Kristiansen and O. Egeland (2004). State-space representation of frequency-dependent hydrodynamic coefficients. In: *Proceedings of the 6th IFAC Conference on Control Applications in Marine Systems*. Ancona, Italy.

Holappa, K.W. and J.M. Falzarano (1999). Application of extended state space to nonlinear ship rolling. *Ocean Engineering* **26**, 227–240.

Jeffreys, E.R. (1980). *Power from Sea Waves*. Chap. Device Characterization, pp. 413–438. Academic Press.

Jeffreys, E.R. (1984). Simulation of wave power devices. *Applied Ocean Research* **6**, 31–39.

Jiang, T. and T.E. Schelin (1990). Motion prediction of a single point moored tanker subjected to current, wind and waves. *Journal of Offshore Mechanics and Arctic Engineering* **112**, 83–90.

Jiang, T., T.E. Schelin and S.D. Sharma (1987). Maneuvering simulation of a tanker morred in a steady current including hydrodynamic memory effects and stability analysis. In: *Proceedings RINA International Conference on Ship Manoeuvrability*.

Jordán, M.A. (2006). On-line identification and convergence analysis of excitation-force and drag-fore models for moored floating structures. *Ocean Engineering* **33**, 1161–1213.

Jordán, M.A. and R. Beltrán-Aguedo (2004). Optimal identification of potential-radiation hydrodynamics for moored floating structures- a new general approach in state space. *Ocean Engineering* **31**, 1859–1914.

Kaasen, K.E. and K. Mo (2004). Efficient time-domain model for frequency dependent added mass and damping. In: *Proceedings of the 23rd International Conference on Offshore Mechanics and Arctic Engineering*.

Kailath, T. (1980). *Linear Systems*. Prentice Hall.

Kotik, J. and V. Mangulis (1962). On the kramers-kronig relations for ship motions. *Int. Shipbuilding Progress* **9**(97), 361–368.

Kristiansen, E., Å. Hjulstad and O. Egeland (2005). State space representation of raditation forces in time domain vessel models. *Oceanic Engineering* **32**, 2195–2216.

Kristiansen, E. and O. Egeland (2003). Frequency-dependent added mass in models for controller design for wave motion damping. In: *IFAC Conference on Manoeuvering and Control of Marine Crafts*. Girona, Spain.

Kung, S.Y. (1978). A new identification and model reduction algorithm via singular value decomposition. In: *Proc. of the Twelth Asilomar Conf. on Circuits, Systems and Computers*. pp. 705–714.

Lande, Ø. (2006). Application of system identification methods to time-domain models of marine structures based on frequency-domain data. Master's thesis. Department of Marine Technology, Norwegian University of Science and Technology.

Levi, E.C. (1959). Complex-curve fitting. *IRE Transactions on Autiomatic Control* **AC-4**, 37–44.

Lewandowski, E.M. (2004). *The Dynamics of Marine Craft, Maneuvering and Seakeeping*. World Scientific.

Ljung, L. (1999). *System Identification, Theory for the User*. Prentice Hall.

Lozano, R., B. Brogliato, O. Egeland and B. Masche (2000). *Dissipative Systems Analysis and Control, Theory and Applications*. Springer.

McCabe, A.P., A. Bradshaw and M.B. Widden (2005). A time-domain model of a floating body using transforms. In: *Proceedings of the 6th European Wave and Tidal Energy Conference*. Glasgow, Scotland.

McCreight, W.R. (1986). Ship maneuvering in waves. In: *Proceedings Sixteenth Symposium on Naval Hydrodynamics*. pp. 456–469.

Moore, B.C. (1981). Principal component analysis in linear systems: Controllability, observability, and model reduction. *IEEE Transactions on Automatic Control* **23**, 17–32.

Mullis, C.T. and R.A. Roberts (1976). Synthesis of minimum roundoff noise fixed point digital filters. *IEEE Transactions on Circuits and Systems* **CAS-23**, 551–562.

Newman, J.N. (1977). *Marine Hydrodynamics*. The MIT Press, Cambridge, Massachusetts.

Obinata, G. and B.D.O. Anderson (2001). *Model Reduction for Control System Design*. Springer.

Ogilvie, T.F. (1964). Recent progress towards the understanding and prediction of ship motions. In: *The Fifth Symposium on Naval Hydrodynamics*. pp. 3–79.

Oortmerssen, G. Van (1976). The motions of a moored ship in waves. Tehcnical Report Publication No. 510. Netherlands Ship Model Basin, Wageningen, The Netherlands.

Opdenacker, P.C. and E.A. Jonckheere (1986). A state space approach to approximation by phase matching. *Modelling, Identification and Robust Control*.

Perez, T. (2005). *Ship Motion Control, Autopilots with Rudder Roll Stabilisation and Combined Rudder-Fin Stabilisers*. Springer.

Perez, T. and T.I. Fossen (2007). Kinematic models for seakeeping and manoeuvring of marine vessels. *Modeling, Identification and Control* **1**, 1–11.

Phillips, J.R., L. Daniel and L.M. Silveira (2003). Guaranteed passive balancing transformations for model order reduction. *IEEE Transactions on Computer-Aided Design of Integrated Circuits and Systems* **22**, 1027–1041.

Schelin, T.E., T. Jiang and C. Östergaard (1993). Response analysis and operating limits of crane ships. *Journal of Ship Research* **3**, 225–238.

Schmiechen, M. (1973). On state space models and their applications to hydrodynamic systems. Naut report 5002. Department of Naval Architecture, University of Tokyo.

Skaare, B. (2004). Control of Loads Through the Wave Zone in Marine Operations. PhD thesis. Department of Engineering Cybernetics, Norwegian University of Science and Technology.

Skogestad, S. and I. Postlethwaite (1996). *Multivariable Feedback Control, Analysis and Design*. Wiley.

Smogeli, Ø.N., T. Perez, T.I. Fossen and A.J. Sørensen (2005). The marine systems simulator state-space model representation for dynamically positioned surface vessels. In: *International Maritime Association of the Mediterranean IMAM Conference*. Lisbon, Portugal.

Sørensen, A.J. (1993). Modeling and control of ses dynamics in the vertical plane. Doctoral Thesis 12. Norwegian Institute of Technology.

Taghipour, R., T. Peres and T. Moan (2007). Time domain hydroelastic analysis of a flexible marine structure using state-space models. In: *Proceedings of the 26th International Conference on Offshore Mechanics and Arctic Engineering*.

Tahar, A. and M.H. Kim (2003). Hull/mooring/riser coupled dynamics analysis and sensitivity study of tanker-based fpso. *Applied Ocean Research* **25**, 367–382.

Takagi, M., K. Saito and S. Nakamura (1984). Comparisons of simulation methods for motions of a moored body in waves. In: *Proceedings of the International Offshore Mechanics & Arctic Engineering Conference*. pp. 214–224.

Thorpe, T.W. (1999). A brief review of wave energy. Technical report. ETSU Report R-122 for the UK Department of Trade and Industry.

Tick, L.J. (1959). Differential equations with frequency-dependent coefficients. *Journal of Ship Research* **3**, 45–46.

Trinnaman, J. and Clarke, A., Eds.) (2004). *2004 Survey of Energy Resources*. Elsevier.

Vugts, J.H. (1970). *The Hydrodynamic Forces and Ship Motions in Waves*. Uitgeverij Waltman, Delft.

Wehausen, J.V. (1971). The motion of floating bodies. *Annual review of fluid mechanics* **3**, 237–268.

Willems, J.C. (1971). Dissipative dynamical systems, Part I: General Theory. *Arch. Rat. Mech. An.* **45**, 321–351.

www.wamit.com (2006). *WAMIT USER MANUAL*. WAMIT, Inc.

Yan, W-Y and J. Lam (1999). An approximate approach to H^2 optimal model reduction. *IEEE Transaction on Automatic Control* **44**, 1341–1358.

Yu, Z. (1992). Dynamic response of an owc wave power system. In: *Proc. Functional Material and Energy Source Science*. Shanghai, China.

Yu, Z. and H. Maeda (1991). On the modelling of an owc wave power system. *J. Kansai Soc. Naval Architects, Japan* **215**, 123–128.

Yu, Z. and J. Falnes (1995). State-space modelling of a vertical cylinder in heave. *Applied Ocean Research* **17**, 265–275.

Yu, Z., N. Jiang and Y. You (1993). On the load control of an owc wave power system. In: *Proceedings of the Int. Symp. on Ocean Energy Development*. Hokkaido, Japan.

Yu, Z., N. Jiang and Y. You (1994). Load control method and its realization on an owc wave power converter. In: *Proceedings of the 13th International Conference on Offshore Mechanics and Arctic Engineering*. Houston, USA.

Appendix A

Notation

$\boldsymbol{A}(\omega)$	frequency dependent added mass matrix	(2.20)
$\boldsymbol{B}(\omega)$	frequency dependent damping matrix	(2.21)
$\boldsymbol{A}(\infty), \boldsymbol{M}_A$	added mass at infinite frequency	(2.25)
$\boldsymbol{\eta}$	position vector defined in the n-frame	(2.1)
$\boldsymbol{\nu}$	velocity vector defined in the b-frame	(2.2)
$\boldsymbol{\xi}$	position vector defined in the h-frame	(2.4)
$\boldsymbol{M}_{RB}$	rigid-body system inertia matrix	(2.5)
$\boldsymbol{C}_h$	restoring forces and moments matrix	(2.6)
$\boldsymbol{\tau}_R$	radiation forces and moments	(2.5)
$\boldsymbol{\tau}_{visc}$	viscous forces and moments	(2.5)
$\boldsymbol{\tau}_{ext}$	external forces and moments	(2.5)
$\boldsymbol{\tau}_A$	actuator forces and moments	(2.5)
$\boldsymbol{\tau}_H$	hydrostatic forces and moments	(2.5)
Φ_R	velocity potential	(2.10)
p	hydrodynamic pressure on the surface of the vessel	(2.12)
ρ	water density	(2.12)
$\hat{\boldsymbol{\varphi}}$	frequency domain complex velocity potential	(2.10)
$\boldsymbol{\varphi}_{im}$	imaginary part of the complex velocity potential	(2.16)
$\boldsymbol{\varphi}_{re}$	real part of the complex velocity potential	(2.16)
$\boldsymbol{\psi}$	time domain instantaneous response velocity potential	(2.28)
$\boldsymbol{\chi}$	time domain memory effect velocity potential	(2.28)
$\boldsymbol{k}(t)$	radiation forces memory effect impulse response from velocity to force	(2.36)
$\boldsymbol{K}(j\omega)$	radiation forces memory effect frequency response from velocity to force	(2.55)
SISO	single-input single-output	

Table A.1: Units for Radiation Force Components

	Damping $B_{ij}(\omega)$	Added mass $A_{ij}(\omega)$	Impulse response $k_{ij}(t)$
i=j, j=(1,2,3)	kg/s	kg	kg/s^2
i=j, j=(4,5,6)	kgm^2/s	kgm^2	kgm^2/s^2
i≠j, i,j=(1,...,6)	kgm/s	kgm	kgm/s^2

MIMO	multi-input multi-output	
BIBO	bounded-input bounded-output	
$\boldsymbol{\tau}_{R1}$	instantaneous response of the radiation forces	(3.4)
$\boldsymbol{\tau}_{R2}$	memory effect part of the radiation forces	(3.5)
V	total energy of vessel-water system	(3.32)
$\bar{\boldsymbol{H}}(s)$	radiation forces transfer function from velocity to force	(3.12)
LTI	linear time invariant	
$\begin{array}{c\|c} \boldsymbol{A} & \boldsymbol{B} \\ \hline \boldsymbol{C} & \boldsymbol{D} \end{array}$	LTI system approximating the radiation forces	(3.38)-(3.39)
$\begin{array}{c\|c} \boldsymbol{A} & \boldsymbol{B} \\ \hline \boldsymbol{C} & \end{array}$	linear system matrices with $\boldsymbol{D} = 0$	(3.40)-(3.41)
$\boldsymbol{K}(s)$	radiation forces memory effect transfer function from velocity to force	(3.42)
$\boldsymbol{l}(t)$	radiation forces memory effect impulse response from acceleration to force	(3.76)
$\boldsymbol{L}(j\omega)$	radiation forces memory effect frequency response from acceleration to force	(3.78)
$\hat{\boldsymbol{H}}(s)$	radiation forces transfer function from acceleration to force	(3.87)
$\mathcal{M}$	Markov parameters	(4.14)
SVD	singular value decompositionin	
$\mathcal{H}_{n+1}$	Hankel matrix	(4.16)
$\boldsymbol{\Sigma}$	singular values	(4.17)
$\bar{\boldsymbol{Z}}^N$	frequency response data set	(4.32)
$\bar{K}_{ij}(j\omega_k)$	sample of frequency response in mode ij	(4.32)
$K_{ij}(j\omega)$	parameterized frequency response in mode ij	(4.34)
W	weighting function	(4.35)
$\begin{array}{c\|c} \boldsymbol{A}(\boldsymbol{\theta}) & \boldsymbol{B}(\boldsymbol{\theta}) \\ \hline \boldsymbol{C}(\boldsymbol{\theta}) & \end{array}$	parameterized LTI system	(4.36)-(4.37)
$\boldsymbol{\theta}$	parameters for identification	(4.36)-(4.37)

ε	prediction error	(4.39)
$\boldsymbol{Z}^N$	time domain input-output data set	(4.40)
V_N	cost function	(4.41)
$\hat{\boldsymbol{\theta}}_N$	optimal choice of parameters in $\boldsymbol{\theta}$	(4.42)
$\left\vert\begin{array}{c\vert c}\boldsymbol{A} & \boldsymbol{B}\\ \hline \boldsymbol{C} & \boldsymbol{D}\end{array}\right.$	linear system matrices	(5.1-5.2)
$\boldsymbol{G}(s)$	linear system transfer function	(5.3)
$\left\vert\begin{array}{c\vert c}\boldsymbol{A}_r & \boldsymbol{B}_r\\ \hline \boldsymbol{C}_r & \boldsymbol{D}_r\end{array}\right.$	reduced order linear system matrices	(5.4-5.5)
$\boldsymbol{G}_r(s)$	reduced order linear system transfer function	(5.6)
$\boldsymbol{T}$	coordinate transformation matrix	(5.7)
$\boldsymbol{P}$	controllability gramian	(5.15)
$\boldsymbol{Q}$	observability gramian	(5.16)
$\boldsymbol{\Sigma}$	singular values	(5.20)
$\boldsymbol{\Phi}$	power spectrum	(5.24)
$\boldsymbol{Z}(s)$	phase system	(5.24)
$\left\vert\begin{array}{c\vert c}\boldsymbol{F} & \boldsymbol{G}\\ \hline \boldsymbol{G} & \boldsymbol{H}\end{array}\right.$	phase system $\boldsymbol{Z}(s)$ matrices	
$\boldsymbol{V}(s)$	left spectral factor	(5.24)
$\left\vert\begin{array}{c\vert c}\boldsymbol{F} & \boldsymbol{G}_l\\ \hline \boldsymbol{H} & \boldsymbol{J}_l\end{array}\right.$	left spectral factor $\boldsymbol{V}(s)$ system matrices	(5.36)
$\boldsymbol{W}(s)$	right spectral factor	(5.24)
$\left\vert\begin{array}{c\vert c}\boldsymbol{F} & \boldsymbol{G}\\ \hline \boldsymbol{H}_r & \boldsymbol{J}_r\end{array}\right.$	right spectral factor $\boldsymbol{W}(s)$ system matrices	(5.37)
PR	positive real	
DPR	dual positive real	
V	storage function	(5.49)
s	supply function	(5.49)
V_r	required supply	(5.50)
V_a	available storage	(5.52)
$\boldsymbol{R}$	Required supply gramian	(5.51)
$\boldsymbol{O}$	Available storage gramian	(5.53)
K_x	surge system	(6.13)
$\boldsymbol{K}_{y\psi}$	sway-yaw system	(6.14)
IR	Impulse response	
Ph.	Phase	
Mag.	Magnitude	
NPR	Not positive real system	
R_y^2	Multiple correlation coefficient (squared)	(6.19)
$\boldsymbol{K}_{lat}$	Lateral vessel system	(6.30)

Appendix B

Mathematical Toolbox

Riemann-Lebesgue Lemma:

If $f(x)$ is integrable on $[a, b]$ then

$$\lim_{t\to\infty} \int_a^b f(x) \sin(tx)\ dx = 0 \tag{B.1}$$

and

$$\lim_{t\to\infty} \int_a^b f(x) \cos(tx)\ dx = 0 \tag{B.2}$$

The Fourier Transform:

Consider a continuous-time signal $f(t)$, defined for $-\infty \leq t \leq \infty$. Then the Fourier transform pair associated with $f(t)$ is defined as follows:

$$\mathfrak{F}[f(t)] = F(j\omega) = \int_{-\infty}^{\infty} e^{-j\omega t} f(t)\ dt \tag{B.3}$$

$$\mathfrak{F}^{-1}[F(j\omega)] = f(t) = \frac{1}{2\pi} \int_{-\infty}^{\infty} e^{j\omega t} F(j\omega)\ d\omega \tag{B.4}$$

$F(j\omega)$ is referred to as the Fourier transform of $f(t)$.

The Fourier Cosine Transform:

The Fourier cosine transform is the real part of the Fourier transform. The Fourier cosine transform pair associated with the even function $f(t)$ is defined as follows:

$$\mathfrak{F}_c[f(t)] = F_{re}(j\omega) = \int_0^\infty f(t)\cos\omega t \; dt \tag{B.5}$$

$$\mathfrak{F}_c^{-1}[F_{re}(j\omega)] = f(t) = \frac{2}{\pi}\int_0^\infty F_{re}(j\omega)\cos\omega t \; d\omega \tag{B.6}$$

$F_{re}(j\omega)$ is referred to as the Fourier cosine transform of $f(t)$.

The Fourier Sine Transform:

The Fourier sine transform is the imaginary part of the Fourier transform. The Fourier sine transform pair associated with the odd function $f(t)$ is defined as follows:

$$\mathfrak{F}_s[f(t)] = F_{im}(j\omega) = \int_0^\infty f(t)\sin\omega t \; dt \tag{B.7}$$

$$\mathfrak{F}_s^{-1}[F_{im}(j\omega)] = f(t) = \frac{2}{\pi}\int_0^\infty F_{im}(j\omega)\sin\omega t \; d\omega \tag{B.8}$$

$F_{im}(j\omega)$ is referred to as the Fourier sine transform of $f(t)$.

The Hilbert transform:

The Hilbert transform of the real function $f(t)$ is the imaginary function $\bar{f}(t)$. The Hilbert transform pair associated with $f(t)$ and $\bar{f}(t)$ is defined by

$$\bar{f}(t) = \mathcal{H}\{f(t)\} = \frac{1}{\pi}\int_{-\infty}^\infty \frac{f(u)}{(t-u)} \; du \tag{B.9}$$

$$f(t) = \mathcal{H}^{-1}\left\{\bar{f}(t)\right\} = -\frac{1}{\pi}\int_{-\infty}^\infty \frac{\bar{f}(u)}{(t-u)} \; du \tag{B.10}$$

For a causal function $g(t)$ the following relation is given $g(t) = f(t) - j\bar{f}(t)$.

BIBO stability, Theorem 5.15 in (Antoulas, 2005):

Theorem B.1 *The system described by the convolution integral*

$$\boldsymbol{y}(t) = \int_0^\infty \boldsymbol{h}(t-\tau)\boldsymbol{u}(\tau)d\tau \tag{B.11}$$

is BIBO stable if and only if the $\mathcal{L}_\infty$-induced norm of the convolution operator is finite.

This means that the every element h_{ij} of the impulse response $\boldsymbol{h}$ must be absolutely integrable,

$$\int_0^\infty |h_{ij}(t)|\ dt < \infty \tag{B.12}$$

$\mathcal{L}_p$ input-output stability, Proposition 5.17 in (Antoulas, 2005):

Proposition B.1 *The finiteness of the $\mathcal{L}_1$-norm of the impulse response h implies the $\mathcal{L}_p$ input-output stability of the system $\boldsymbol{\Sigma}$ described by the convolution integral $y(t) = \int_0^\infty h(t-\tau)u(\tau)\ d\tau$ for $1 \le p \le \infty$.*

Relation internal/input-output stability, Theorem 5.18 in (Antoulas, 2005):

Theorem B.2 *Given a dynamical system $\boldsymbol{\Sigma}$ and a finite-dimensional realization $\left(\begin{array}{c|c} \boldsymbol{A} & \boldsymbol{B} \\ \hline \boldsymbol{C} & \boldsymbol{0} \end{array}\right)$ thereof, the following statements are equivalent:*

- $||\Sigma||_1 < \infty$
- $||\Sigma||_2 < \infty$
- *There exist a realization of Σ, with A Hurwitz.*
- *Every minimal realization of Σ has A Hurwitz.*

Passive system (Egeland and Gravdahl, 2002):

Definition B.1 *Consider a system with input $u \in R^n$ and output $y \in R^n$. Suppose that there is a constant $E_0 \geq 0$ so that for all control time histories u and all $T \geq 0$ the integral of $y^T(t)u(t)$ satisfies*

$$\int_0^T y^T(t)u(t)dt \geq -E_0 \tag{B.13}$$

then the system is said to be passive.

Parts of Corollary 2.1 in (Lozano *et al.*, 2000):

Assume that there is a continuously differentiable function $V(t) \geq 0$ and a $d(t)$ such that $\int_0^t d(t)dt \geq 0$ for all $T \geq 0$. Then if

$$\dot{V}(t) \leq y^T(u)u(t) - d(t) \tag{B.14}$$

then the system is said to be passive.

The Laplace Transform:

Consider a continuous-time signal $f(t)$, defined for $0 \leq t \leq \infty$. Then the Laplace transform pair associated with $f(t)$ is defined as follows:

$$\mathcal{L}[f(t)] = F(s) = \int_{0^-}^{\infty} e^{-st} f(t)\ dt \tag{B.15}$$

$$\mathcal{L}^{-1}[F(s)] = f(t) = \frac{1}{2\pi j} \int_{\sigma - j\infty}^{\sigma + j\infty} e^{st} F(s)\ ds \tag{B.16}$$

$F(s)$ is referred to as the Laplace transform of $f(t)$. Some useful properties of the Laplace transform follows.
Final-Value Theorem

$$\lim_{t \to \infty} y(t) = \lim_{s \to 0} sY(s) \tag{B.17}$$

Initial-Value Theorem

$$\lim_{t \to 0^+} y(t) = \lim_{s \to \infty} sY(s) \tag{B.18}$$

Integral Law

$$\mathcal{L}[\int_{0^-}^{t} y(\tau)\ d\tau] = \frac{1}{s} Y(s) \tag{B.19}$$

Relative degree of transfer function (Skogestad and Postlethwaite, 1996):

Definition B.2 *A rational transfer function is given by*

$$G(s) = \frac{N(s)}{D(s)} = \frac{b_n s^n + b_{n-1}s^{n-1} + \cdots + b_1 s + b_0}{s^n + a_{n-1}s^{n-1} + \cdots + a_1 s + a_0} \tag{B.20}$$

The difference in degrees between $N(s)$ and $D(s)$ is called the relative degree of the transfer function. Let the degree of $N(s)$ and $D(s)$ be m and n. Then

1. *$G(s)$ is strictly proper if $G(s) \to 0$ as $s \to \infty$.*
   For a strictly proper system $m < n$.
2. *$G(s)$ is semi-proper or bi-proper if $G(s) \to D \neq 0$ as $s \to \infty$.*
   For a semi-proper system $m = n$.
3. *$G(s)$ is improper if $G(s) \to \infty$ as $s \to \infty$. For a improper system $m > n$.*

Zero-state equivalent (Chen, 1999):

Theorem B.3 *Two linear time-invariant state equations $[A, B, C, D]$ and $\left[\bar{A}, \bar{B}, \bar{C}, \bar{D}\right]$ are zero-state equivalent or have the same transfer matrix if $D = \bar{D}$ and*

$$CA^m B = \bar{C}\bar{A}^m\bar{B}, \qquad m = 0, 1, 2, \ldots \tag{B.21}$$

Stable system (Antoulas, 2005):

Theorem B.4 *A matrix A is Hurwitz; that is $Re(\lambda_i) < 0$ for all eigenvalues of A, if and and only if for any given positive definite symmetric matrix Q there exists a positive definite symmetric matrix P that satisfies the Lyapunov equation*

$$AP + PA^T = -Q \tag{B.22}$$

Moreover if A is Hurwitz, then P is the unique solution of (B.22)